QA: QA

MDL-WIS-PA-000005 REV 00 AD 01

March 2008

Total System Performance Assessment Model/Analysis for the License Application Addendum 01

Volume III

Prepared for:
U.S. Department of Energy
Office of Civilian Radioactive Waste Management
Office of Repository Development
1551 Hillshire Drive
Las Vegas, Nevada 89134-6321

Prepared by:
Sandia National Laboratories
OCRWM Lead Laboratory for Repository Systems
1180 Town Center Drive
Las Vegas, Nevada 89144

Under Contract Number
DE-AC04-94AL85000

DISCLAIMER

This report was prepared as an account of work sponsored by an agency of the United States Government. Neither the United States Government nor any agency thereof, nor any of their employees, nor any of their contractors, subcontractors or their employees, makes any warranty, express or implied, or assumes any legal liability or responsibility for the accuracy, completeness, or any third party's use or the results of such use of any information, apparatus, product, or process disclosed, or represents that its use would not infringe privately owned rights. Reference herein to any specific commercial product, process, or service by trade name, trademark, manufacturer, or otherwise, does not necessarily constitute or imply its endorsement, recommendation, or favoring by the United States Government or any agency thereof or its contractors or subcontractors. The views and opinions of authors expressed herein do not necessarily state or reflect those of the United States Government or any agency thereof.

CONTENTS

Page

8[a]. POSTCLOSURE PERFORMANCE DEMONSTRATION....8-1[a]
8.1[a] CONFORMANCE WITH RADIATION PROTECTION STANDARDS....8-2[a]
8.1.1[a] Individual Protection Standard....8-3[a]
8.1.2[a] Groundwater Protection....8-14[a]
8.1.3[a] Human Intrusion Protection....8-21[a]
8.2[a] PROJECTIONS FOR INDIVIDUAL MODELING CASES....8-27[a]
8.2.1[a] Nominal Modeling Case....8-27[a]
8.2.2[a] Early Failure Scenario Class Modeling Cases....8-29[a]
8.2.3[a] Igneous Scenario Class Modeling Cases....8-32[a]
8.2.4[a] Seismic Scenario Class Modeling Cases....8-34[a]
8.3[a] DESCRIPTION OF MULTIPLE BARRIER CAPABILITY....8-39[a]
8.3.1[a] Radionuclides Selected to Demonstrate Multiple Barrier Capability....8-39[a]
8.3.2[a] Identification of Barriers for Yucca Mountain Repository....8-39[a]
8.3.3[a] Demonstration of Multiple Barrier Capability....8-40[a]
8.4[a] VALIDITY AND DEFENSIBILITY OF PERFORMANCE DEMONSTRATION....8-85[a]
8.4.1[a] Validation of TSPA Model and Component Models....8-85[a]
8.4.2[a] Verification and Validation of TSPA Software and Input Data....8-85[a]
8.4.3[a] Uncertainty Characterization Reviews....8-85[a]
8.4.4[a] Corroboration of TSPA-LA Results....8-85[a]
8.4.5[a] Peer Reviews of YMP TSPA Methodology....8-85[a]

9[a]. INPUTS AND REFERENCES....9-1[a]
9.1[a] DOCUMENTS CITED....9-1[a]
9.2[a] CODES, STANDARDS, REGULATIONS, AND PROCEDURES....9-9[a]
9.3[a] SOFTWARE CODES....9-9[a]
9.4[a] SOURCE DATA LISTED BY DATA TRACKING NUMBER....9-11[a]

APPENDIX B[a] DATA TRACKING NUMBERS FOR THE TSPA-LA MODEL....B-1[a]
APPENDIX C[a] PERFORMANCE MARGIN ANALYSIS....C-1[a]
APPENDIX D[a] PARAMETER LISTING....D-1[a]
APPENDIX H[a] YUCCA MOUNTAIN REVIEW PLAN ACCEPTANCE CRITERIA....H-1[a]
APPENDIX I[a] FEATURES, EVENTS, AND PROCESSES MAPPED TO TSPA-LA MODEL....I-1[a]
APPENDIX J[a] CONCEPTUAL STRUCTURE OF TSPA-LA....J-1[a]
APPENDIX K[a] UNCERTAINTY AND SENSITIVITY ANALYSIS RESULTS....K-1[a]
APPENDIX M[a] COMPARISON WITH ELECTRIC POWER RESEARCH INSTITUTE ANALYSIS....M-1[a]
APPENDIX P[a] IMPACT ASSESSMENTS....P-1[a]

INTENTIONALLY LEFT BLANK

FIGURES

Page

8.1-1[a]. Distribution of Total Expected Annual Dose for 10,000 Years after Repository Closure....F8.1-1[a]

8.1-2[a]. Distribution of Total Expected Annual Dose for 1,000,000 Years after Closure....F8.1-2[a]

8.1-3[a]. Relative Contributions of Modeling Cases to Total Mean Annual Dose for (a) 10,000 Years and (b) 1,000,000 Years after Repository Closure....F8.1-3[a]

8.1-4[a]. Histogram of the Time of Drip Shield Failure for the Nominal and Seismic Ground Motion Modeling Cases....F8.1-4[a]

8.1-5[a]. Fraction of (a) CDSP Waste Packages and (b) CSNF Waste Packages Failed by Seismic Damage as a Function of Time....F8.1-5[a]

8.1-6[a]. Contribution of Individual Radionuclides to Total Mean Annual Dose for 10,000 Years after Repository Closure....F8.1-6[a]

8.1-7[a]. Contribution of Individual Radionuclides to Total Mean Annual Dose for 1,000,000 Years after Repository Closure....F8.1-7[a]

8.1-9[a]. Summary Statistics for Activity Concentrations of Total Radium (^{226}Ra and ^{228}Ra) in Groundwater, Excluding Natural Background, for 10,000 Years after Repository Closure....F8.1-8[a]

8.1-10[a]. Contributions of the Modeling Cases to the Mean Combined ^{226}Ra and ^{228}Ra Activity Concentration in Groundwater, Excluding Natural Background, for 10,000 Years after Repository Closure....F8.1-9[a]

8.1-11[a]. Summary Statistics for Activity Concentration of Gross Alpha and ^{226}Ra (Excluding Radon and Uranium) in Groundwater for 10,000 Years after Repository Closure....F8.1-10[a]

8.1-12[a]. Contributions of the Modeling Cases to the Mean Gross Alpha Activity Concentrations (Including ^{226}Ra but Excluding Radon and Uranium) in Groundwater for 10,000 Years after Repository Closure....F8.1-11[a]

8.1-13[a]. Mean Annual Dose from Beta-Photon Dose for All Organs, Including the Whole Body for (a) 10,000 Years after Repository Closure and (b) Detail for 8,000 to 10,000 Years after Repository Closure....F8.1-12[a]

8.1-14[a]. Summary Statistics for Annual Drinking Water Doses for Combined Beta and Photon Emitting Radionuclides for 10,000 Years after Repository Closure....F8.1-13[a]

8.1-15[a]. Contributions of Modeling Cases to the (a) Whole Body Dose and (b) Thyroid for 10,000 Years after Repository Closure....F8.1-14[a]

8.1-16[a]. Distribution of Expected Annual Doses for the Human Intrusion Scenario for 1,000,000 Years after Repository Closure with Drilling Event at 200,000 Years....F8.1-15[a]

8.1-17[a]. Contribution of Individual Radionuclides to Mean Annual Dose for the Human Intrusion Scenario for 1,000,000 Years after Repository Closure....F8.1-16[a]

FIGURES (Continued)

Page

8.2-1[a]. Distributions of Expected Annual Dose for the Nominal Modeling Case for 1,000,000 Years after Repository Closure ..... F8.2-1[a]

8.2-2[a]. Contribution of Individual Radionuclides to Mean Annual Dose for the Nominal Modeling Case for 1,000,000 Years after Repository Closure ..... F8.2-2[a]

8.2-3[a]. Distributions of Expected Annual Dose for the Drip Shield Early Failure Modeling Case for (a) 10,000 Years and (b) 1,000,000 Years after Repository Closure ..... F8.2-3[a]

8.2-4[a]. Contribution of Individual Radionuclides to Mean Annual Dose for Drip Shield Early Failure Modeling Case for (a) 10,000 Years and (b) 1,000,000 Years after Repository Closure ..... F8.2-4[a]

8.2-5[a]. Distributions of Expected Annual Dose for Waste Package Early Failure Modeling Case for (a) 10,000 Years and (b) 1,000,000 Years after Repository Closure ..... F8.2-5[a]

8.2-6[a]. Contribution of Individual Radionuclides to Mean Annual Dose for Waste Package Early Failure Modeling Case for (a) 10,000 Years and (b) 1,000,000 Years after Repository Closure ..... F8.2-6[a]

8.2-7[a]. Distributions of Expected Annual Dose for the Igneous Intrusion Modeling Case for (a) 10,000 Years and (b) 1,000,000 Years after Repository Closure ..... F8.2-7[a]

8.2-8[a]. Contribution of Individual Radionuclides to Mean Annual Dose for the Igneous Intrusion Modeling Case for (a) 10,000 Years and (b) ,000,000 Years after Repository Closure ..... F8.2-8[a]

8.2-11[a]. Distributions of Expected Annual Dose for the Seismic Ground Motion Modeling Case for (a) 10,000 Years and (b) 1,000,000 Years after Repository Closure ..... F8.2-9[a]

8.2-12[a]. Contribution of Individual Radionuclides to Mean Annual Dose for the Seismic Ground Motion Modeling Case for (a) 10,000 Years and (b) 1,000,000 Years after Repository Closure ..... F8.2-10[a]

8.2-13[a]. Distributions of Expected Annual Dose for the Seismic Fault Displacement Modeling Case for (a) 10,000 Years and (b) 1,000,000 Years after Repository Closure ..... F8.2-11[a]

8.2-14[a]. Contribution of Individual Radionuclides to Mean Annual Dose for the Seismic Fault Displacement Modeling Case for (a) 10,000 Years and (b) 1,000,000 Years after Repository Closure ..... F8.2-12[a]

8.3-1[a]. Mean Radionuclide Activities for Total Repository Inventory as a Function of Time for (a) 10,000 Years and (b) 1,000,000 Years after Repository Closure ..... F8.3-1[a]

8.3-2[a]. Mean Radionuclide Contributions to Total Inventory as a Function of Time for (a) 10,000 Years and (b) 1,000,000 Years after Repository Closure ..... F8.3-2[a]

8.3-3[a]. Upper Natural Barrier Capability to Prevent or Substantially Reduce the Rate of Water Movement to the Waste for the Mean

FIGURES (Continued)

Page

Spatially-Averaged (a) Annual Precipitation, Net Infiltration, and Post-10,000-Year Percolation Rates and (b) Drift Seepage Fluxes for the Combined Nominal/Early Failure Modeling Case and the Seismic Ground Motion Modeling Case – 1,000,000-Year Period ..... F8.3-3[a]

8.3-4[a]. Probability of Drip Shield Failure by General Corrosion for the Nominal Modeling Case Based on 300 Epistemic Realizations of Drip Shield General Corrosion Rates ..... F8.3-4[a]

8.3-5[a]. Summary Statistics for Fraction of Waste Packages Breached for (a) CSNF Waste Packages and (b) CDSP Waste Packages for the Nominal Modeling Case as a Function of Time ..... F8.3-5[a]

8.3-6[a]. Summary Statistics for Fraction of CSNF Waste Packages (a) reached by Stress Corrosion Cracking and (b) Breached by General Corrosion Patches for the Nominal Modeling Case as a Function of Time ..... F8.3-6[a]

8.3-7[a]. Cumulative Distribution Functions of Drip Shield Failure Time for (a) Distributions of Failure Time for 300 Epistemic Sample Elements and (b) Distribution of Expected (Over Aleatory) Failure Time with Confidence Interval for the Seismic Ground Motion Modeling Case ..... F8.3-7[a]

8.3-8[a]. Summary Statistics for Expected Fraction of CSNF WPs (a) Breached by Seismic and Nominal Processes and (b) Breached by Seismic Processes Only; and CDSP WPs (c) Breached by Seismic and Nominal Processes and (d) Breached by Seismic Processes Only for the Seismic Ground Motion Modeling Case as a Function of Time ..... F8.3-8[a]

8.3-9[a]. Summary Statistics for Average Fraction of CSNF Waste Package Surface Breached by Cracks per Breached Waste Package for (a) the Seismic Ground Motion Modeling Case and (b) the Nominal Modeling Case as a Function of Time ..... F8.3-10[a]

8.3-10[a]. Summary Statistics for Fraction of CDSP Waste Package Surface Breached by Cracks per Breached Waste Package for (a) the Seismic Ground Motion Modeling Case and (b) the Nominal Modeling Case as a Function of Time ..... F8.3-11[a]

8.3-11[a]. Summary Statistics for Fraction of CSNF Waste Package Surface Breached by Patches per Breached Waste Package for (a) the Seismic Ground Motion Modeling Case and (b) the Nominal Modeling Case as a Function of Time ..... F8.3-12[a]

8.3-12[a]. Summary Statistics for Fraction of CDSP WP Surface Breached by Patches per Breached Waste Package for (a) the Seismic Ground Motion Modeling Case and (b) the Nominal Modeling Case as a Function of Time ..... F8.3-13[a]

8.3-13[a]. Mean Activity Released from the Engineered Barrier System for the Combined Nominal/Early Failure Modeling Case for (a) 10,000 Years after Repository Closure and (b) Post-10,000-Years after Repository Closure ..... F8.3-14[a]

FIGURES (Continued)

Page

8.3-14[a]. Uncertainty in Activity of ^{99}Tc Released from the Engineered Barrier System for the Combined Nominal/Early Failure Modeling Case for (a) 10,000 Years and (b) 1,000,000 Years after Repository Closure.....F8.3-15[a]

8.3-15[a]. Uncertainty in Activity of ^{239}Pu Released from the Engineered Barrier System for the Combined Nominal/Early Failure Modeling Case for (a) 10,000 Years and (b) 1,000,000 Years after Repository Closure .....F8.3-16[a]

8.3-16[a]. Mean Activity Released from the Engineered Barrier System for the Seismic Ground Motion Modeling Case for (a) 10,000 Years and (b) 1,000,000 Years after Repository Closure .....F8.3-17[a]

8.3-17[a]. Uncertainty in Activity of ^{99}Tc Released from the Engineered Barrier System for the Seismic Ground Motion Modeling Case for (a) 10,000 Years and (b) 1,000,000 Years after Repository Closure.....F8.3-18[a]

8.3-18[a]. Uncertainty in Activity of ^{237}Np Released from the Engineered Barrier System for the Seismic Ground Motion Modeling Case for (a) 10,000 Years and (b) 1,000,000 Years after Repository Closure.....F8.3-19[a]

8.3-19[a]. Uncertainty in Activity of ^{234}U Released from the Engineered Barrier System for the Seismic Ground Motion Modeling Case for (a) 10,000 Years and (b) 1,000,000 Years after Repository Closure.....F8.3-20[a]

8.3-20[a]. Uncertainty in Activity of ^{226}Ra Released from the Engineered Barrier System for the Seismic Ground Motion Modeling Case for (a) 10,000 Years and (b) 1,000,000 Years after Repository Closure.....F8.3-21[a]

8.3-21[a]. Uncertainty in Activity of ^{239}Pu Released from the Engineered Barrier System for the Seismic Ground Motion Modeling Case for (a) 10,000 Years and (b) 1,000,000 Years after Repository Closure.....F8.3-22[a]

8.3-22[a]. Uncertainty in Activity of ^{242}Pu Released from the Engineered Barrier System for the Seismic Ground Motion Modeling Case for (a) 10,000 Years and (b) 1,000,000 Years after Repository Closure.....F8.3-23[a]

8.3-23[a]. Mean Activity Released from the (a) Saturated Zone and (b) Engineered Barrier System for the Combined Nominal/Early Failure Modeling Case for 10,000 Years after Repository Closure.....F8.3-24[a]

8.3-24[a]. Mean Activity Released from the (a) Saturated Zone and (b) Engineered Barrier System for the Combined Nominal/Early Failure Modeling Case for 1,000,000 Years after Repository Closure.....F8.3-25[a]

8.3-25[a]. Mean Activity Released from the (a) Saturated Zone and (b) Engineered Barrier System for the Seismic Ground Motion Modeling Case for 10,000 Years after Repository Closure.....F8.3-26[a]

8.3-26[a]. Mean Activity Released from the (a) Saturated Zone and (b) Engineered Barrier System for the Seismic Ground Motion Modeling Case for 1,000,000 Years after Repository Closure.....F8.3-27[a]

8.3-27[a]. Uncertainty in Activity of ^{99}Tc Released from the Saturated Zone for the Seismic Ground Motion Modeling Case for (a) 10,000 Years and (b) 1,000,000 Years after Repository Closure .....F8.3-28[a]

FIGURES (Continued)

Page

8.3-28[a]. Uncertainty in Activity of ^{237}Np Released from the Saturated Zone for the Seismic Ground Motion Modeling Case for (a) 10,000 Years and (b) 1,000,000 Years after Repository Closure ..... F8.3-29[a]
8.3-29[a]. Uncertainty in Activity of ^{234}U Released from the Saturated Zone for the Seismic Ground Motion Modeling Case for (a) 10,000 Years and (b) 1,000,000 Years after Repository Closure ..... F8.3-30[a]
8.3-30[a]. Uncertainty in Activity of ^{226}Ra Released from the Saturated Zone for the Seismic Ground Motion Modeling Case for (a) 10,000 Years and (b) 1,000,000 Years after Repository Closure ..... F8.3-31[a]
8.3-31[a]. Uncertainty in Activity of ^{239}Pu Released from the Saturated Zone for the Seismic Ground Motion Modeling Case for (a) 10,000 Years and (b) 1,000,000 Years after Repository Closure ..... F8.3-32[a]
8.3-32[a]. Uncertainty in Activity of ^{242}Pu Released from the Saturated Zone for the Seismic Ground Motion Modeling Case for (a) 10,000 Years and (b) 1,000,000 Years after Repository Closure ..... F8.3-33[a]

B-3[a]. Road Map of TSPA-LA Model v5.005 Data Tracking Numbers ..... B-5[a]

K4.5-1[a]. Dose to RMEI (*DOSTOT*, mrem/yr) for all radioactive species under nominal conditions obtained with version 5.005 of the TSPA-LA Model: (a) *DOSTOT* for all (i.e., 300) sample elements, (b) *DOSTOT* for first 50 sample elements, (c) PRCCs for *DOSTOT* for [0; 1,000,000 yr], and (d) PRCCs for *DOSTOT* for [200,000; 1,000,000 yr] ..... FK-1[a]
K4.5-2[a]. Stepwise rank regression analyses and selected scatterplots for dose to RMEI (*DOSTOT*, mrem/yr) for all radioactive species under nominal conditions obtained with version 5.005 of the TSPA-LA Model: (a) regressions for *DOSTOT* at 400,000, 600,000, and 800,000 years, and (b,c,d) scatterplots for *DOSTOT* at 600,000 years ..... FK-2[a]

K5.7.1-1[a]. Expected dose to RMEI (*EXPDOSE*, mrem/yr) over [0, 20,000 yr] for all radioactive species resulting from early DS failure obtained with version 5.005 of the TSPA-LA Model: (a) *EXPDOSE* for all (i.e., 300) sample elements, (b) *EXPDOSE* for first 50 sample elements, and (c) PRCCs for *EXPDOSE* ..... FK-3[a]
K5.7.1-2[a]. Stepwise rank regression analyses and selected scatterplots for expected dose to RMEI (*EXPDOSE*, mrem/yr) over [0, 20,000 yr] for all radioactive species resulting from early DS failure obtained with version 5.005 of the TSPA-LA Model: (a) regressions for *EXPDOSE* at 3,000, 5,000, and 10,000 years, and (b,c,d) scatterplots for *EXPDOSE* at 10,000 years ..... FK-4[a]
K5.7.1-3[a]. Expected dose to RMEI (*EXPDOSE*, mrem/yr) over [0, 1,000,000 yr] for all radioactive species resulting from early DS failure obtained with version 5.005 of the TSPA-LA Model: (a) *EXPDOSE* for all

FIGURES (Continued)

Page

(i.e., 300) sample elements, (b) *EXPDOSE* for first 50 sample elements, and (c) PRCCs for *EXPDOSE* ..... FK-5[a]

K5.7.1-4[a]. Stepwise rank regression analyses and selected scatterplots for expected dose to RMEI (*EXPDOSE*, mrem/yr) over [0, 1,000,000 yr] for all radioactive species resulting from early DS failure obtained with version 5.005 of the TSPA-LA Model: (a) regressions for *EXPDOSE* at 50,000, 200,000, and 500,000 years, and (b,c,d) scatterplots for *EXPDOSE* at 500,000 years ..... FK-6[a]

K5.7.2-1[a]. Expected dose to RMEI (*EXPDOSE*, mrem/yr) over [0, 20,000 yr] for all radioactive species resulting from early WP failure obtained with version 5.005 of the TSPA-LA Model: (a) *EXPDOSE* for all (i.e., 300) sample elements, (b) *EXPDOSE* for first 50 sample elements, and (c) PRCCs for *EXPDOSE* ..... FK-7[a]

K5.7.2-2[a]. Stepwise rank regression analyses and selected scatterplots for expected dose to RMEI (*EXPDOSE*, mrem/yr) over [0, 20,000 yr] for all radioactive species resulting from early WP failure obtained with version 5.005 of the TSPA-LA Model: (a) regressions for *EXPDOSE* at 3,000, 5,000, and 10,000 years, and (b,c,d) scatterplots for *EXPDOSE* at 10,000 years..... FK-8[a]

K5.7.2-3[a]. Expected dose to RMEI (*EXPDOSE*, mrem/yr) over [0, 1,000,000 yr] for all radioactive species resulting from early WP failure obtained with version 5.005 of the TSPA-LA Model: (a) *EXPDOSE* for all (i.e., 300) sample elements, (b) *EXPDOSE* for first 50 sample elements, and (c) PRCCs for *EXPDOSE* ..... FK-9[a]

K5.7.2-4[a]. Stepwise rank regression analyses and selected scatterplots for expected dose to RMEI (*EXPDOSE*, mrem/yr) over [0, 1,000,000 yr] for all radioactive species resulting from early WP failure obtained with version 5.005 of the TSPA-LA Model: (a) regressions for *EXPDOSE* at 50,000, 200,000, and 500,000 years, and (b,c,d) scatterplots for *EXPDOSE* at 500,000 years..... FK-10[a]

K6.3.2-5[a]. Time-dependent release rates (*ESU234*, g/yr) and cumulative (i.e., integrated) releases (*ESU234C*, g) over 1,000,000 years for the movement of dissolved ^{234}U from the EBS to the UZ resulting from an igneous intrusive event at 250 years that destroys all WPs in the repository obtained with version 5.005 of the TSPA-LA Model: (a,b) *ESU234* and *ESU234C* for all (i.e., 300) sample elements, (c,d) *ESU234* and *ESU234C* for first 50 sample elements, and (e,f) PRCCs for *ESU234* and *ESU234C* ..... FK-11[a]

K6.3.2-6[a]. Stepwise rank regression analyses and selected scatterplots for time-dependent release rates (*ESU234*, g/yr) and cumulative (i.e., integrated) releases (*ESU234C*, g) for the movement of dissolved ^{234}U from the EBS to the UZ resulting from an igneous intrusive event at 250 years that destroys all WPs in the repository obtained with

FIGURES (Continued)

Page

version 5.005 of the TSPA-LA Model: (a,b) regressions for *ESU234* and *ESU234C* at 50,000, 200,000, and 500,000 years, and (c-h) scatterplots for *ESU234* and *ESU234C* at 500,000 years ..... FK-12[a]

K6.3.2-7[a]. Time-dependent release rates (*ESTH230*, g/yr) and cumulative (i.e., integrated) releases (*ESTH230C*, g) over 1,000,000 years for the movement of dissolved ^{230}Th from the EBS to the UZ resulting from an igneous intrusive event at 250 years that destroys all WPs in the repository obtained with version 5.005 of the TSPA-LA Model: (a,b) *ESTH230* and *ESTH230C* for all (i.e., 300) sample elements, (c,d) *ESTH230* and *ESTH230C* for first 50 sample elements, and (e,f) PRCCs for *ESTH230* and *ESTH230C*..... FK-14[a]

K6.3.2-8[a]. Stepwise rank regression analyses and selected scatterplots for time-dependent release rates (*ESTH230*, g/yr) and cumulative (i.e., integrated) releases (*ESTH230C*, g) for the movement of dissolved ^{230}Th from the EBS to the UZ resulting from an igneous intrusive event at 250 years that destroys all WPs in the repository obtained with version 5.005 of the TSPA-LA Model: (a,b) regressions for *ESTH230* and *ESTH230C* at 50,000, 200,000, and 500,000 years, and (c-h) scatterplots for *ESTH230* and *ESTH230C* at 200,000 years ..... FK-15[a]

K6.3.2-9[a]. Time-dependent release rates (*ESRA226*, g/yr) and cumulative (i.e., integrated) releases (*ESRA226C*, g) over 1,000,000 years for the movement of dissolved ^{226}Ra from the EBS to the UZ resulting from an igneous intrusive event at 250 years that destroys all WPs in the repository obtained with version 5.005 of the TSPA-LA Model: (a,b) *ESRA226* and *ESRA226C* for all (i.e., 300) sample elements, (c,d) *ESRA226* and *ESRA226C* for first 50 sample elements, and (e,f) PRCCs for *ESRA226* and *ESRA226C* ..... FK-17[a]

K6.3.2-10[a]. Stepwise rank regression analyses and selected scatterplots for time-dependent release rates (*ESRA226*, g/yr) and cumulative (i.e., integrated) releases (*ESRA226C*, g) for the movement of dissolved ^{226}Ra from the EBS to the UZ resulting from an igneous intrusive event at 250 years that destroys all WPs in the repository obtained with version 5.005 of the TSPA-LA Model: (a,b) regressions for *ESRA226* and *ESRA226C* at 50,000, 200,000, and 500,000 years, and (c-h) scatterplots for *ESRA226* and *ESRA226C* at 50,000 years..... FK-18[a]

K6.4.2-1[a]. Time-dependent release rates (*UZU234*, g/yr) and cumulative (i.e., integrated) releases (*UZU234C*, g) over 1,000,000 years for the movement of dissolved ^{234}U from the UZ to the SZ resulting from an igneous intrusive event at 250 years that destroys all WPs in the repository obtained with version 5.005 of the TSPA-LA Model: (a,b) *UZU234* and *UZU234C* for all (i.e., 300) sample elements, (c,d) *UZU234* and *UZU234C* for first 50 sample elements, and (e,f) PRCCs for *UZU234* and *UZU234C*..... FK-20[a]

FIGURES (Continued)

Page

K6.4.2-2[a]. Stepwise rank regression analyses and selected scatterplots for time-dependent release rates (*UZU234*, g/yr) and cumulative (i.e., integrated) releases (*UZU234C*, g) for the movement of dissolved ^{234}U from the UZ to the SZ resulting from an igneous intrusive event at 250 years that destroys all WPs in the repository obtained with version 5.005 of the TSPA-LA Model: (a,b) regressions for *UZU234* and *UZU234C* at 50,000, 200,000, and 500,000 years, and (c-h) scatterplots for *UZU234* and *UZU234C* at 500,000 years ..... FK-21[a]

K.6.4.2-3[a]. Comparison of cumulative releases of dissolved ^{234}U into the UZ (*ESU234C*, g) and out of the UZ (*UZU234C*, g) obtained with version 5.005 of the TSPA-LA Model at (a) 50,000, (b) 100,000, (c) 200,000, and (d) 600,000 years for an igneous intrusive event at 250 years that destroys all WPs in the repository ..... FK-23[a]

K6.4.2-4[a]. Time-dependent release rates (*UZTH230*, g/yr) and cumulative (i.e., integrated) releases (*UZTH230C*, g) over 1,000,000 years for the movement of dissolved ^{230}Th from the UZ to the SZ resulting from an igneous intrusive event at 250 years that destroys all WPs in the repository obtained with version 5.005 of the TSPA-LA Model: (a,b) *UZTH230* and *UZTH230C* for all (i.e., 300) sample elements, (c,d) *UZTH230* and *UZTH230C* for first 50 sample elements, and (e,f) PRCCs for *UZTH230* and *UZTH230C* ..... FK-24[a]

K6.4.2-5[a]. Stepwise rank regression analyses and selected scatterplots for time-dependent release rates (*UZTH230*, g/yr) and cumulative (i.e., integrated) releases (*UZTH230C*, g) for the movement of dissolved ^{230}Th from the UZ to the SZ resulting from an igneous intrusive event at 250 years that destroys all WPs in the repository obtained with version 5.005 of the TSPA-LA Model: (a,b) regressions for *UZTH230* and *UZTH230C* at 50,000, 200,000, and 500,000 years, and (c-h) scatterplots for *UZTH230* and *UZTH230C* at 200,000 years..... FK-25[a]

K.6.4.2-6[a]. Comparison of cumulative releases of dissolved ^{230}Th into the UZ (*ESTH230C*, g) and out of the UZ (*UZTH230C*, g) obtained with version 5.005 of the TSPA-LA Model at (a) 50,000, (b) 100,000, (c) 200,000, and (d) 600,000 years for an igneous intrusive event at 250 years that destroys all WPs in the repository ..... FK-27[a]

K6.4.2-7[a]. Time-dependent release rates (*UZRA226*, g/yr) and cumulative (i.e., integrated) releases (*UZRA226C*, g) over 1,000,000 years for the movement of dissolved ^{226}Ra from the UZ to the SZ resulting from an igneous intrusive event at 250 years that destroys all WPs in the repository obtained with version 5.005 of the TSPA-LA Model: (a,b) *UZRA226* and *UZRA226C* for all (i.e., 300) sample elements, (c,d) *UZRA226* and *UZRA226C* for first 50 sample elements, and (e,f) PRCCs for *UZRA226* and *UZRA226C* ..... FK-28[a]

FIGURES (Continued)

Page

K6.4.2-8[a]. Stepwise rank regression analyses and selected scatterplots for time-dependent release rates (*UZRA226*, g/yr) and cumulative (i.e., integrated) releases (*UZRA226C*, g) for the movement of dissolved ^{226}Ra from the UZ to the SZ resulting from an igneous intrusive event at 250 years that destroys all WPs in the repository obtained with version 5.005 of the TSPA-LA Model: (a,b) regressions for *UZRA226* and *UZRA226C* at 50,000, 200,000, and 500,000 years, and (c-h) scatterplots for *UZRA226* and *UZRA226C* at 50,000 years ..... FK-29[a]

K.6.4.2-9[a]. Comparison of cumulative releases of dissolved ^{226}Ra into the UZ (*UZRA226C*, g) and out of the UZ (*UZRA226C*, g) obtained with version 5.005 of the TSPA-LA Model at (a) 50,000, (b) 100,000, (c) 200,000, and (d) 600,000 years for an igneous intrusive event at 250 years that destroys all WPs in the repository ..... FK-31[a]

K6.5.2-5[a]. Time-dependent release rates (*SZU234*, g/yr) and cumulative (i.e., integrated) releases (*SZU234C*, g) over 1,000,000 years for the movement of dissolved ^{234}U across a subsurface plane at the location of the RMEI resulting from an igneous intrusive event at 250 years that destroys all WPs in the repository obtained with version 5.005 of the TSPA-LA Model: (a,b) *SZU234* and *SZU234C* for all (i.e., 300) sample elements, (c,d) *SZU234* and *SZU234C* for first 50 sample elements, and (e,f) PRCCs for *SZU234* and *SZU234C*..... FK-32[a]

K6.5.2-6[a]. Stepwise rank regression analyses and selected scatterplots for time-dependent release rates (*SZU234*, g/yr) and cumulative (i.e., integrated) releases (*SZU234C*, g) for the movement of dissolved ^{234}U across a subsurface plane at the location of the RMEI resulting from an igneous intrusive event at 250 years that destroys all WPs in the repository obtained with version 5.005 of the TSPA-LA Model: (a,b) regressions for *SZU234* and *SZU234C* at 50,000, 200,000, and 500,000 years, and (c-h) scatterplots for *SZU234* and *SZU234C* at 500,000 years ..... FK-33[a]

K.6.5.2-7[a]. Comparison of cumulative releases of dissolved ^{234}U into the SZ (*UZU234C*, g) and across a subsurface plane at the location of the RMEI (*SZU234C*, g) obtained with version 5.005 of the TSPA-LA Model at (a) 50,000, (b) 100,000, (c) 200,000, and (d) 600,000 years for an igneous intrusive event at 250 years that destroys all WPs in the repository ..... FK-35[a]

K6.5.2-8[a]. Time-dependent release rates (*SZTH230*, g/yr) and cumulative (i.e., integrated) releases (*SZTH230C*, g) over 1,000,000 years for the movement of dissolved ^{230}Th across a subsurface plane at the location of the RMEI resulting from an igneous intrusive event at 250 years that destroys all WPs in the repository obtained with version 5.005 of the TSPA-LA Model: (a,b) *SZTH230* and *SZTH230C* for all (i.e., 300)

FIGURES (Continued)

Page

sample elements, (c,d) *SZTH230* and *SZTH230C* for first 50 sample elements, and (e,f) PRCCs for *SZTH230* and *SZTH230C* ..... FK-36[a]

K6.5.2-9[a]. Stepwise rank regression analyses and selected scatterplots for time-dependent release rates (*SZTH230*, g/yr) and cumulative (i.e., integrated) releases (*SZTH230C*, g) for the movement of dissolved ^{230}Th across a subsurface plane at the location of the RMEI resulting from an igneous intrusive event at 250 years that destroys all WPs in the repository obtained with version 5.005 of the TSPA-LA Model: (a,b) regressions for *SZTH230* and *SZTH230C* at 50,000, 200,00, and 500,000 years, and (c-h) scatterplots for *SZTH230* and *SZTH230C* at 500,000 years ..... FK-37[a]

K.6.5.2-10[a]. Comparison of cumulative releases of dissolved ^{230}Th into the SZ (*UZTH230C*, g) and across a subsurface plane at the location of the RMEI (*SZTH230C*, g) obtained with version 5.005 of the TSPA-LA Model at (a) 50,000, (b) 100,000, (c) 200,000, and (d) 600,000 years for an igneous intrusive event at 250 years that destroys all WPs in the repository ..... FK-39[a]

K6.5.2-11[a]. Time-dependent release rates (*SZRA226*, g/yr) and cumulative (i.e., integrated) releases (*SZRA226C*, g) over 1,000,000 years for the movement of dissolved ^{226}Ra across a subsurface plane at the location of the RMEI resulting from an igneous intrusive event at 250 years that destroys all WPs in the repository obtained with version 5.005 of the TSPA-LA Model: (a,b) *SZRA226* and *SZRA226C* for all (i.e., 300) sample elements, (c,d) *SZRA226* and *SZRA226C* for first 50 sample elements, and (e,f) PRCCs for *SZRA226* and *SZRA226C*..... FK-40[a]

K6.5.2-12[a]. Stepwise rank regression analyses and selected scatterplots for time-dependent release rates (*SZRA226*, g/yr) and cumulative (i.e., integrated) releases (*SZRA226C*, g) for the movement of dissolved ^{226}Ra across a subsurface plane at the location of the RMEI resulting from an igneous intrusive event at 250 years that destroys all WPs in the repository obtained with version 5.005 of the TSPA-LA Model: (a,b) regressions for *SZRA226* and *SZRA226C* at 50,000, 200,000, and 500,000 years, and (c-h) scatterplots for *SZRA226* and *SZRA226C* at 50,000 years ..... FK-41[a]

K.6.5.2-13[a]. Comparison of cumulative releases of dissolved ^{226}Ra into the SZ (*UZRA226C*, g) and across a subsurface plane at the location of the RMEI (*SZRA226C*, g) obtained with version 5.005 of the TSPA-LA Model at (a) 50,000, (b) 100,000, (c) 200,000, and (d) 600,000 years for an igneous intrusive event at 250 years that destroys all WPs in the repository ..... FK-43[a]

K.6.6.2-5[a]. Time-dependent dose to the RMEI (*DOU234*, mrem/yr) over 1,000,000 years for the movement of dissolved ^{234}U across a subsurface plane at the location of the RMEI resulting from an igneous

FIGURES (Continued)

Page

intrusive event at 250 years that destroys all WPs in the repository obtained with version 5.005 of the TSPA-LA Model: (a) *DOU234* for all (i.e., 300) sample elements, (b) *DOU234* for first 50 sample elements, and (c) PRCCs for *DOU234* ..... FK-44[a]

K.6.6.2-6[a]. Stepwise rank regression analyses and selected scatterplots for time-dependent dose to the RMEI (*DOU234*, mrem/yr) for the movement of dissolved ^{234}U across a subsurface plane at the location of the RMEI (*SZU234*, g/yr) resulting from an igneous intrusive event at 250 years that destroys all WPs in the repository obtained with version 5.005 of the TSPA-LA Model: (a) regressions for *DOU234* at 50,000, 200,000, and 500,000 years, (b,c,d) scatterplots for *DOU234* at 500,000 years, and (e) scatterplot comparing *SZU234* and *DOU234* at 500,000 years ..... FK-45[a]

K.6.6.2-7[a]. Time-dependent dose to the RMEI (*DOTH230*, mrem/yr) over 1,000,000 years for the movement of dissolved ^{230}Th across a subsurface plane at the location of the RMEI resulting from an igneous intrusive event at 250 years that destroys all WPs in the repository obtained with version 5.005 of the TSPA-LA Model: a) *DOTH230* for all (i.e., 300) sample elements, (b) *DOTH230* for first 50 sample elements, and (c) PRCCs for *DOTH230* ..... FK-46[a]

K.6.6.2-8[a]. Stepwise rank regression analyses and selected scatterplots for time-dependent dose to the RMEI (*DOTH230*, mrem/yr) for the movement of dissolved ^{230}Th across a subsurface plane at the location of the RMEI (*SZTH230*, g/yr) resulting from an igneous intrusive event at 250 years that destroys all WPs in the repository obtained with version 5.005 of the TSPA-LA Model: (a) regressions for *DOTH230* at 50,000, 200,000, and 500,000 years, (b,c,d) scatterplots for *DOTH230* at 500,000 years, and (e) scatterplot comparing *SZTH230* and *DOTH230* at 500,000 years..... FK-47[a]

K.6.6.2-9[a]. Time-dependent dose to the RMEI (*DORA226*, mrem/yr) over 1,000,000 years for the movement of dissolved ^{226}Ra across a subsurface plane at the location of the RMEI resulting from an igneous intrusive event at 250 years that destroys all WPs in the repository obtained with version 5.005 of the TSPA-LA Model: (a) *DORA226* for all (i.e., 300) sample elements, (b) *DORA226* for first 50 sample elements, and (c) PRCCs for *DORA226* ..... FK-48[a]

K.6.6.2-10[a]. Stepwise rank regression analyses and selected scatterplots for time-dependent dose to the RMEI (*DORA226*, mrem/yr) for the movement of dissolved ^{226}Ra across a subsurface plane at the location of the RMEI (*SZRA226*, g/yr) resulting from an igneous intrusive event at 250 years that destroys all WPs in the repository obtained with version 5.005 of the TSPA-LA Model: (a) regressions for *DORA226* at 50,000, 200,000, and 500,000 years, (b,c,d) scatterplots for

FIGURES (Continued)

Page

DORA226 at 50,000 years, and (e) scatterplot comparing *SZRA226* and *DORA226* at 50,000 years..... FK-49[a]

K6.7.1-1[a]. Expected dose to RMEI (*EXPDOSE*, mrem/yr) over [0, 20,000 yr] for all radioactive species resulting from igneous intrusion obtained with version 5.005 of the TSPA-LA Model: (a) *EXPDOSE* for all (i.e., 300) sample elements, (b) *EXPDOSE* for first 50 sample elements, and (c) PRCCs for *EXPDOSE* ..... FK-50[a]

K6.7.1-2[a]. Stepwise rank regression analyses and selected scatterplots for expected dose to RMEI (*EXPDOSE*, mrem/yr) over [0, 20,000 yr] for all radioactive species resulting from igneous intrusion obtained with version 5.005 of the TSPA-LA Model: (a) regressions for *EXPDOSE* at 3,000, 5,000, and 10,000 years, and (b,c,d) scatterplots for *EXPDOSE* at 10,000 years..... FK-51[a]

K.6.7.2-1[a]. Expected dose to RMEI (*EXPDOSE*, mrem/yr) over [0, 1,000,000 yr] for all radioactive species resulting from igneous intrusion obtained with version 5.005 of the TSPA-LA Model: (a) *EXPDOSE* for all (i.e., 300) sample elements, (b) *EXPDOSE* for first 50 sample elements, and (c) PRCCs for *EXPDOSE* ..... FK-52[a]

K.6.7.2-2[a]. Stepwise rank regression analyses and selected scatterplots for expected dose to RMEI (*EXPDOSE*, mrem/yr) over [0, 1,000,000 yr] for all radioactive species resulting from igneous intrusion obtained with version 5.005 of the TSPA-LA Model: (a) regressions for *EXPDOSE* at 50,000, 200,000, and 500,000 years, and (b,c,d) scatterplots for *EXPDOSE* at 500,000 years..... FK-53[a]

K7.7.1-1[a]. Expected dose to RMEI (*EXPDOSE*, mrem/yr) over [0, 20,000 yr] for all radioactive species resulting from seismic ground motion obtained with version 5.005 of the TSPA-LA Model: (a) *EXPDOSE* for all (i.e., 300) sample elements, (b) *EXPDOSE* for first 50 sample elements, and (c) PRCCs for *EXPDOSE* ..... FK-54[a]

K7.7.1-2[a]. Stepwise rank regression analyses and selected scatterplots for expected dose to RMEI (*EXPDOSE*, mrem/yr) over [0, 20,000 yr] for all radioactive species resulting from seismic ground motion obtained with version 5.005 of the TSPA-LA Model: (a) regressions for *EXPDOSE* at 3,000, 5,000, and 10,000 years, and (b,c,d) scatterplots for *EXPDOSE* at 10,000 years..... FK-55[a]

K7.7.2-1[a]. Expected dose to RMEI (*EXPDOSE*, mrem/yr) over [0, 1,000,000 yr] for all radioactive species resulting from seismic ground motion obtained with version 5.005 of the TSPA-LA Model: (a) *EXPDOSE* for all (i.e., 300) sample elements, (b) *EXPDOSE* for first 50 sample elements, and (c) PRCCs for *EXPDOSE* ..... FK-56[a]

K7.7.2-2[a]. Stepwise rank regression analyses and selected scatterplots for expected dose to RMEI (*EXPDOSE*, mrem/yr) over [0, 1,000,000 yr]

FIGURES (Continued)

Page

for all radioactive species resulting from seismic ground motion obtained with version 5.005 of the TSPA-LA Model: (a) regressions for *EXPDOSE* at 50,000, 200,000, and 500,000 years, and (b,c,d) scatterplots for *EXPDOSE* at 500,000 years ..... FK-57[a]

K7.8.1-1[a]. Expected dose to RMEI (*EXPDOSE*, mrem/yr) over [0, 20,000 yr] for all radioactive species resulting from seismic fault displacement: (a) *EXPDOSE* for all (i.e., 300) sample elements, (b) *EXPDOSE* for first 50 sample elements, and (c) PRCCs for *EXPDOSE* ..... FK-58[a]

K7.8.1-2[a]. Stepwise rank regression analyses and selected scatterplots for expected dose to RMEI (*EXPDOSE*, mrem/yr) over [0, 20,000 yr] for all radioactive species resulting from seismic fault displacement: (a) regressions for *EXPDOSE* at 3,000, 5,000, and 10,000 years, and (b,c,d) scatterplots for *EXPDOSE* at 10,000 years ..... FK-59[a]

K7.8.2-1[a]. Expected dose to RMEI (*EXPDOSE*, mrem/yr) over [0, 1,000,000 yr] for all radioactive species resulting from seismic fault displacement: (a) *EXPDOSE* for all (i.e., 300) sample elements, (b) *EXPDOSE* for first 50 sample elements, and (c) PRCCs for *EXPDOSE* ..... FK-60[a]

K7.8.2-2[a]. Stepwise rank regression analyses and selected scatterplots for expected dose to RMEI (*EXPDOSE*, mrem/yr) over [0, 1,000,000 yr] for all radioactive species resulting from seismic fault displacement: (a) regressions for *EXPDOSE* at 50,000, 200,000, and 500,000 years, and (b,c,d) scatterplots for *EXPDOSE* at 500,000 years..... FK-61[a]

K8.1-1[a]. Expected dose to RMEI (*EXPDOSE*, mrem/yr) over [0, 20,000 yr] for all scenario classes obtained with version 5.005 of the TSPA-LA Model: (a) *EXPDOSE* for all (i.e., 300) sample elements, (b) *EXPDOSE* for first 50 sample elements, and (c) PRCCs for *EXPDOSE* .. FK-62[a]

K8.1-2[a]. Stepwise rank regression analyses and selected scatterplots for expected dose to RMEI (*EXPDOSE*, mrem/yr) over [0, 20,000 yr] for all scenario classes obtained with version 5.005 of the TSPA-LA Model: (a) regressions for *EXPDOSE* at 3,000, 5,000, and 10,000 years, and (b,c,d) scatterplots for *EXPDOSE* at 10,000 years ..... FK-63[a]

K8.2-1[a]. Expected dose to RMEI (*EXPDOSE*, mrem/yr) over [0, 1,000,000 yr] for all scenario classes obtained with version 5.005 of the TSPA-LA Model: (a) *EXPDOSE* for all (i.e., 300) sample elements, (b) *EXPDOSE* for first 50 sample elements, and (c) PRCCs for *EXPDOSE* .. FK-64[a]

K8.2-2[a]. Stepwise rank regression analyses and selected scatterplots for expected dose to RMEI (*EXPDOSE*, mrem/yr) over [0, 1,000,000 yr] for all scenario classes obtained with version 5.005 of the TSPA-LA Model: (a) regressions for *EXPDOSE* at 50,000, 200,000, and 500,000 years, and (b,c,d) scatterplots for *EXPDOSE* at 500,000 years ..... FK-65[a]

FIGURES (Continued)

Page

K10-1[a]. Expected dose to RMEI (*EXPDOSE*, mrem/yr) over [200,000, 220,000 yr] resulting from human intrusion at 200,000 years obtained with version 5.005 of the TSPA-LA Model: (a) *EXPDOSE* for all (i.e., 300) sample elements, (b) *EXPDOSE* for first 50 sample elements, and (c) PRCCs for *EXPDOSE* ..... FK-66[a]

K10-2[a]. Stepwise rank regression analyses and selected scatterplots for expected dose to RMEI (*EXPDOSE*, mrem/yr) over [200,000, 220,000 yr] resulting from human intrusion at 200,000 years obtained with version 5.005 of the TSPA-LA Model: (a) regressions for *EXPDOSE* at 201,000, 203,000, and 205,000 years, (b,c,d) scatterplots for *EXPDOSE* at 201,000 years, and (e,f,g) scatterplots for *EXPDOSE* at 205,000 years ..... FK-67[a]

K10-3[a]. Expected dose to RMEI (*EXPDOSE*, mrem/yr) over [220,000, 1,000,000 yr] resulting from human intrusion at 200,000 years obtained with version 5.005 of the TSPA-LA Model: (a) *EXPDOSE* for all (i.e., 300) sample elements, (b) *EXPDOSE* for first 50 sample elements, and (c) PRCCs for *EXPDOSE*. ..... FK-69[a]

K10-4[a]. Stepwise rank regression analyses and selected scatterplots for expected dose to RMEI (*EXPDOSE*, mrem/yr) over [220,000, 1,000,000 yr] resulting from human intrusion at 200,000 years obtained with version 5.005 of the TSPA-LA Model: (a) regressions for *EXPDOSE* at 240,000, 500,000, and 760,000 years, and (b,c,d,e) scatterplots for *EXPDOSE* at 500,000 years..... FK-70[a]

K10-5[a]. Comparison of expected dose to RMEI (*EXPDOSE*, mrem/yr) over [200,000, 1,000,000 yr] resulting from human intrusion at 200,000 years obtained with versions 5.000 and 5.005 of the TSPA-LA Model at (a) 201,000, (b) 205,000, (c) 500,000, and (d) 1,000,000 years ..... FK-71[a]

K10-6[a]. Comparison of summary curves (i.e., mean and 0.05, 0.5, and 0.95 quantile) for expected dose to RMEI (*EXPDOSE*, mrem/yr) over [200,000, 1,000,000 yr] resulting from human intrusion at 200,000 years obtained with versions 5.000 and 5.005 of the TSPA-LA Model.... FK-72[a]

P-20[a]. Expected Annual Dose versus Average Seepage Fraction for the Nominal Modeling Case for 1,000,000 Years after Repository Closure.... FP-23[a]

P-21[a]. Expected Annual Dose versus Average Seepage Fraction for the Seismic Ground Motion Modeling Case for (a) 10,000 Years and (b) 1,000,000 Years after Repository Closure ..... FP-24[a]

TABLES

8.1-1[a]. Performance Demonstration Results for Individual Protection Standard ..... 8-25[a]
8.1-2[a]. Performance Demonstration Results for the Separate Standards for the Protection of Groundwater ..... 8-25[a]
8.1-3[a]. Performance Demonstration Results for the Individual Protection Standard for Human Intrusion ..... 8-25[a]
8.1-4[a]. Uncertainty in Projections of Maximum Total Mean and Median Annual Dose (mrem) for the Individual Protection Standard ..... 8-26[a]
8.1-5[a]. Inventories and Biosphere Dose Conversion Factors for Radionuclides Important to Total Mean Annual Dose for 10,000 Years ..... 8-26[a]
8.1-6[a]. Uncertainty Importance Ranking as a Function of Time for Four Key TSPA-LA Model Parameters ..... 8-26[a]

8.3-2[a]. Seepage Fractions for CDSP and CSNF Waste Packages for Combined Nominal/Early Failure Modeling Case for Glacial-Transition Climate, 2,000 to 10,000 Years ..... 8-81[a]
8.3-3[a]. Seepage Fractions for CDSP and CSNF Waste Packages for Combined Nominal/Early Failure Modeling Case for Post-10,000-Year Period ..... 8-81[a]
8.3-4[a]. Seepage Fractions for CDSP and CSNF Waste Packages for Seismic Ground Motion Modeling Case for Glacial-Transition Climate, 2,000 to 10,000 Years ..... 8-82[a]
8.3-5[a]. Seepage Fractions for CDSP and CSNF Waste Packages for Seismic Ground Motion Modeling Case for Post-10,000-Year Period ..... 8-82[a]
8.3-6[a]. Drift Wall Condensation for CSNF Waste Packages for Stage 2 and Stage 3 Condensation ..... 8-83[a]
8.3-7[a]. Drift Wall Condensation for CDSP Waste Packages for Stage 2 and Stage 3 Condensation ..... 8-84[a]
8.3-8[a]. Mean Seepage Rates for Waste Packages during Stage 2 and Stage 3 Condensation ..... 8-84[a]

C9-1[a]. Impact Assessment Summary Table ..... C-3[a]

H-1[a]. Applicable Regulatory Requirements of 10 CFR Part 63 and NUREG-1804 Acceptance Criteria Addressed in this Document ..... H-3[a]

I-2[a]. Model Implementation for Included Features, Events, and Processes ..... I-3[a]

K9-1[a]. Summary of Selected Sensitivity Analysis Results ..... K-35[a]

P-6[a]. Discussion of Other Minor Implementation Errors ..... P-11[a]
P-7[a]. Impact Assessment Summary Table ..... P-20[a]

INTENTIONALLY LEFT BLANK

8[a]. POSTCLOSURE PERFORMANCE DEMONSTRATION

Section 8[a] of this addendum contains the updated results for the Total System Performance Assessment for the License Application (TSPA-LA) Model performance analyses used for evaluating the postclosure performance of the repository and its compliance with U.S. Nuclear Regulatory Commission (NRC) Proposed Rule 10 CFR 63.113 [DIRS 180319] and the performance measures defined in proposed 10 CFR 63.303 [DIRS 178394] for the individual protection standard after permanent closure in proposed 10 CFR 63.311(a)(1) and (2) [DIRS 178394], the individual protection standard for human intrusion in 10 CFR 63.321(a)(1) and (2) [DIRS 178394], and the separate standards for protection of groundwater in 10 CFR 63.331 ([DIRS 180319], Table 1). The probabilistic TSPA-LA analyses account for uncertainty and address features, events and processes (FEPs) that could affect total system performance. Volume III presents the updated results of analyses and calculations in the following areas:

- Comparison of TSPA-LA Model analyses with the performance measures defined in proposed 10 CFR 63.303 [DIRS 178394] for the individual protection standard after permanent closure in 10 CFR 63.311(a)(1) and (2) [DIRS 178394], the individual protection standard for human intrusion in 10 CFR 63.321(a)(1) and (2) [DIRS 178394], and the separate standards for protection of groundwater in 10 CFR 63.331 ([DIRS 180319], Table 1)

- System and subsystem performance analyses for the Nominal Scenario Class, including the Nominal Modeling Case; the Early Failure Scenario Class, including the Drip Shield Early Failure (EF) and Waste Package EF Modeling Cases; the Igneous Scenario Class, including Igneous Intrusion Modeling Case; and the Seismic Scenario Class, including the Seismic Ground Motion (GM) and Fault Displacement (FD) Modeling Cases

- Analyses of the capabilities and importance of the upper and lower natural barriers and the engineered barrier system (EBS) that have been identified as contributing to repository performance.

The results presented in this addendum represent an iterative process that reflects a rigorous model verification and implementation cycle.

As used in this addendum, the designator “no change” means that the reader should refer to the original text for that section or subsection of the parent TSPA-LA document. Documentation provided in this addendum consists of a combination of supplemental and revised information for the postclosure performance demonstration. In the case of revised information, the documentation presents the revised plots, tables, and discussion of the revised TSPA-LA results. The organization of the sections and subsections parallel those of the parent document. Also, section numbers, figure numbers and table numbers cited in the text with [a] refer to this addendum, while those without it refer to the section, figure or table number in the parent document. It should be noted, that some of the important aspects of the performance requirements are restated from the parent document. The material from the parent document is reproduced in this addendum to provide clarity in the presentation.

The primary output DTNs are presented in Section 8 of the parent document and in Section 8[a] of this addendum. However, for a complete listing of the output DTNs associated with the parent document and this addendum, see Appendix B and Appendix B[a].

8.1[a] CONFORMANCE WITH RADIATION PROTECTION STANDARDS

The U.S. Environmental Protection Agency (EPA) and NRC regulations for a high-level radioactive waste (HLW) repository at Yucca Mountain require that the U.S. Department of Energy (DOE) demonstrate a reasonable expectation of compliance with the applicable radiation protection standards. The proposed EPA regulation, 40 CFR Part 197 (2005 [DIRS 175755]), establishes three separate and distinct radiation protection standards for the Yucca Mountain repository. As the licensing agency, the NRC adopted the following three radiation protection standards:

- Individual Protection Standard after Permanent Closure (10 CFR 63.311 [DIRS 178394]), which considers the required characteristics of the reasonably maximally exposed individual (RMEI) as described in 10 CFR 63.312 [DIRS 180319].
- Individual Protection Standard for Human Intrusion (10 CFR 63.321 [DIRS 178394]) according to the Human Intrusion Scenario described in 10 CFR 63.322 [DIRS 180319].
- Separate Standards for Protection of Ground Water (10 CFR 63.331 [DIRS 180319]) using the representative volume specified in 10 CFR 63.332 [DIRS 180319].

The EPA and NRC proposed regulations for Individual Protection and Human Intrusion establish standards for annual doses to the RMEI corresponding to: (1) the time period of 10,000 years after closure, and (2) the time period after 10,000 years but within the period of geologic stability, defined as 1,000,000 years in 10 CFR 63.302 [DIRS 178394]. In contrast, the Separate Standards for Protection of Ground Water sets limits for annual dose and activity concentrations (i.e., radionuclide activity per unit volume) for only the 10,000-year period following repository closure. For the purpose of making performance projections for these time periods, the characteristics of the RMEI are defined in 10 CFR 63.312 [DIRS 180319], and the RMEI is taken to reside approximately 18 km (11 mi) downgradient of the repository (66 FR 55732 [DIRS 156671], III Public Comments and Responses, 3.5, p. 55750).

Detailed probabilistic projections developed for this postclosure performance demonstration are presented and explained in the subsequent sections. Tables 8.1-1[a] through 8.1-3[a] present tabulations of the maximum of total mean and median annual doses and mean activity concentrations for direct comparisons with the three radiation protection standards. The times at which the maximum total annual doses occur are also shown in Tables 8.1-1[a]. To highlight the spread in the computed distribution of expected annual doses, additional statistics are presented in Table 8.1-4[a] to better clarify the comparison with the limits of the Individual Protection Standard. Comparisons of these updated results with the results reported in the parent document are provided in Sections 8.1.1[a], 8.1.2[a], and 8.1.3[a] as part of the discussion for each radiation protection standard.

As shown in the tabular comparisons, the numerical limits prescribed in all three standards are met, with the maximum total annual doses and activity concentrations falling well below the

limits. These numerical comparisons, however, represent only a part of the postclosure performance demonstration and many detailed calculations and graphical outputs are presented in Section 8.2[a] to elucidate the comparisons with the regulatory requirements. For the purpose of explaining the basis for a reasonable expectation of compliance, the performance demonstration for each radiation protection standard addresses the following fundamental questions regarding the TSPA of the repository and the projections of the regulatory metrics:

1. What scenario classes are considered to make performance projections, and what contribution does each scenario class make to the performance metrics?

2. What events, processes, or site characteristics modeled in the scenario classes are most important to the projections of each performance metric?

3. What barrier attributes and/or characteristics are most influential in reducing the radionuclide release rates, rate of water, or radionuclide movement?

4. What radionuclides in the nuclear waste inventory contribute the most to the annual doses and why?

5. Which uncertain input variables are most dominant in determining the uncertainty in the projected performance metrics and why?

In addition, the effect on the performance assessment of the conservatisms incorporated into the TSPA-LA Model is summarized in Section 7.7.4[a]; Section 8.4[a] summarizes the activities performed to ensure that the TSPA-LA Model and the results obtained from the model are technically sound and defensible.

The next sections describe and explain the projections that constitute the postclosure performance demonstration for the three radiation protection standards. Section 8.1.1[a] summarizes the results relevant to the Individual Protection Standard after permanent closure, Section 8.1.2[a] presents the results relevant to the Standards for the Protection of Groundwater, and Section 8.1.3[a] addresses the Individual Protection Standard for Human Intrusion. The exposure models and conversion factors used to calculate annual dose and activity concentrations in groundwater are summarized in the Biosphere Submodel description (Section 6.3.11). Conversion factors for dose to the RMEI are calculated for two general exposure scenarios, namely, groundwater and volcanic ash (SNL 2007 [DIRS 177399], Section 6.1.3).

8.1.1[a] Individual Protection Standard

No change.

8.1.1.1[a] Scenario Classes Considered and Calculation of Total Annual Doses

No change.

8.1.1.2[a] Projected Annual Doses and Major Observations

Projections of postclosure performance for comparison with the Individual Protection Standard were developed using the Monte Carlo simulation methodology, which is described in

Appendix J of the parent document. This methodology incorporates aleatory and epistemic uncertainties into the projections in two separate computational loops: (1) an outer loop that samples probability distributions for model parameters with epistemic uncertainty using the Latin hypercube sampling technique (Helton and Davis 2002 [DIRS 163475]), and (2) an inner loop that evaluates expected annual dose for each epistemic sample element by integrating over probability distributions that represent aleatory uncertainties. The methodology produces an ensemble of expected annual dose histories for each scenario class, which are then combined to obtain an ensemble of total expected annual doses. This is described by Equation 8.1.1-1 of the parent document, using the separate terms $\bar{D}_N(\tau \mid \mathbf{e})$ and $\bar{D}_S(\tau \mid \mathbf{e})$ for 10,000-year results and including the combined term $\bar{D}_N(\tau \mid \mathbf{e}) + \bar{D}_S(\tau \mid \mathbf{e})$ for post-10,000-year results.

The expected annual dose histories for the RMEI are generally plotted in the form of a multi-realization plot. The mean and median values of this ensemble of total expected annual doses are termed the total mean annual dose and total median annual dose, respectively, and are the performance metrics for comparison with the Individual Protection Standard. The revised projections of postclosure performance for the 10,000-year and 1,000,000-year compliance periods were developed using TSPA-LA Model v5.005, and the results are shown on Figure 8.1-1[a] and Figure 8.1-2[a]; the plots in these figures show the multi-realization dose histories and include curves for the mean, median, 5th and 95th percentiles. For 10,000 years after closure, the maximum total mean and median annual doses to the RMEI are estimated to be about 0.24 mrem and 0.13 mrem, respectively, well below the individual protection limit of 15 mrem. Similarly, for the post-10,000-year period over the period of geologic stability, the maximum total mean and median annual doses to the RMEI are estimated to be about 2.0 mrem and 0.96 mrem, respectively. The projected maximum total median annual dose for the post-10,000 year time period is well below the proposed individual protection limit of 350 mrem.

In the parent document, results from TSPA-LA Model v5.000 showed the maximum total mean annual doses to the RMEI for 10,000 years of 0.24 mrem, and maximum total median annual doses to the RMEI for 1,000,000 years of 0.99 mrem. Thus, the corrections and changes to the TSPA-LA Model from v5.000 to v5.005 (detailed in Appendix P[a]) result in only minor changes to these performance metrics. Additional comparison of the maximum total annual doses between the two model versions is provided in Sections 7.3.1.5.8[a] and 7.3.1.5.9[a].

Contribution to Total Annual Doses by Modeling Case

To show the relative contribution of each of the four scenario classes to total mean annual dose, the total mean annual dose is disaggregated into the mean annual dose histories for the individual modeling cases. The four scenario classes include Nominal, Early Failure, Igneous, and Seismic. As described in the parent document, the Nominal Scenario Class (Section 6.3) is composed of one modeling case, while Early Failure (Section 6.4), Igneous (Section 6.5), and Seismic (Section 6.6) Scenario Classes each have two modeling cases. The Early Failure Scenario Class consists of the Drip Shield and Waste Package EF Modeling Cases. The Igneous Scenario Class is composed of Igneous Intrusion and Volcanic Eruption Modeling Cases. Finally, the Seismic Scenario Class is made up of the Seismic GM and Seismic FD Modeling Cases.

Projections of the expected annual doses to the RMEI for each of these modeling cases are shown on Figure 8.1-3[a]. These annual dose history curves demonstrate that:

- Total mean annual doses for both the 10,000-year and post-10,000-year compliance periods are dominated by contributions from the Seismic GM and Igneous Intrusion Modeling Cases, which are on the order of 10^{-1} mrem for the 10,000-year period and 1 mrem for the post-10,000-year compliance period.

- Mean annual doses for the Waste Package EF and Seismic FD Modeling Cases are relatively small and are estimated to be on the order of 10^{-2} mrem or less for both the 10,000-year and post-10,000-year time periods.

- Mean annual doses projected for Drip Shield EF and Volcanic Eruption Modeling Cases are on the order of 10^{-3} mrem or less for both the 10,000-year and post-10,000-year time periods.

For each modeling case, the expected annual dose at a time τ can be conceptualized as the sum (over all possible events represented by a modeling case) of the annual dose at time τ from each event weighted by the probability of each event's occurrence (Section 6.1.2.4 of the parent document). Thus, the relative influence on total mean annual dose of each modeling case stems from one or both of the factors involved: the dose resulting from an event and the probability of an event's occurrence.

For the 10,000-year period after closure, the Seismic GM Modeling Case (Section 6.6.1 of the parent document) provides the majority of the total mean annual dose, with a smaller contribution from the Igneous Intrusion Modeling Case (Section 6.5.1 of the parent document). The Seismic GM Modeling Case estimates the expected annual dose resulting from the occurrence of seismic ground motion events that could damage waste packages (WPs). The dominant effect of ground motion events in the first 10,000-years after repository closure is stress-corrosion cracks of co-disposed (CDSP) WPs (Section 7.3.2.6.1.3). Within 10,000 years, the probability of a seismic event that results in damage to CDSP WPs ranges between 0 and 0.2 with a mean value of 0.07 (output DTN: MO0708CDSPSEIS.000 [DIRS 183007], *FreqDamageCDSP_v5.pdf*). This probability depends on the sampled value for the parameter *SCCTHRP* (residual stress threshold [RST] for stress corrosion cracking [SCC] nucleation of Alloy 22 as a percentage of yield strength; see Section 8.1.1.6[a]). The dose resulting from a damaging seismic event includes releases from all 3,416 CDSP WPs (Section 6.6.1.2.2.2 of the parent document). However, the ensuant radionuclide releases are moderated by the relatively small damaged area on each of the WPs (Figure 6.6-13a of the parent document), which limits the radionuclide release rates from the WPs (Section 6.3.8.1 of the parent document). Appendix J, Figure J8.3-1 of the parent document, illustrates the distribution of annual doses that are projected after the occurrence of a seismic ground motion event.

In contrast, the mean probability of an igneous event is estimated to be $1.69 \times 10^{-4} = (1.69 \times 10^{-8}\ /\text{yr}) \times (10^{4}\ \text{yr})$ (Table 6.5-2 of the parent document) much less than the probability of occurrence of a seismic event. The annual dose that results after an igneous event (Appendix J, Figure J7.2-1 of the parent document) is much larger than the annual dose from a seismic ground motion event, because: (1) an igneous intrusion affects all WPs (Section 6.5.1.1

of the parent document) and (2) after the intrusion, neither the drip shields (DSs) nor the WPs present any barrier to radionuclide mobilization and transport. However, as illustrated by the curves on Figure 8.1-3a[a], the lower probability of occurrence of an igneous event offsets the larger annual dose from an igneous event, which explains why the expected annual dose from igneous events is less than that from seismic ground motion events.

For the post-10,000-year time period, the Igneous Intrusion Modeling Case (Section 6.5.1 of the parent document) dominates the total mean annual dose history for about 725,000 years. After that time and up to 1,000,000 years, the Igneous Intrusion and Seismic GM Modeling Cases contribute almost equally to the total mean annual dose. The probability of an igneous event remains below 0.02 before 1,000,000 years. However, as discussed in Section 8.2.4.1[a], for the post-10,000-year period, the Seismic GM Modeling Case includes the combined effects of seismic events and nominal corrosion processes on all DSs and WPs in the repository. Additional discussion of the occurrence of damage to DSs and WPs from corrosion and seismic events is provided in Section 8.3.3.2[a] and in Section 8.1.1.3[a], respectively.

The remaining four modeling cases (i.e., Drip Shield EF, Waste Package EF, Seismic FD, and Volcanic Eruption) address events that occur with varying probabilities but result in radionuclide releases from only a small number of WPs. Fault displacement events, for example, are estimated to occur with annual frequencies in the range of 10^{-7} yr^{-1}, and involve on average at most a few tens of WPs (Table 6.6-1 of the parent document). The probability that at least one WP experiences an early failure is 0.442 (Section 8.2.2 of the parent document), while the expected number of early failed WPs (given that at least one early failure occurs) is estimated to be 2.46 (Section 8.2.2 of the parent document) out of 11,629 WPs (3,416 CDSPs and 8,213 CSNFs). The probability of at least one or more DS early failures is 0.017 (Section 8.2.2), and the expected number of early failed DSs (given that at least one early failure occurs) is only 1.09 (Section 8.2.2 of the parent document). Potential volcanic eruptions occur within 10,000 years with a mean probability of $(0.083) \times (1.69 \times 10^{-8}/yr) \times (10^{4}\ yr) = 1.4 \times 10^{-6}$ (Appendix J, Section J7.5 of the parent document) and are projected to induce releases from seven WPs or less (Table 6.5-3 of the parent document). Additional discussion and explanation of the results for each modeling case is presented in Section 8.2[a].

8.1.1.3[a] Disruptive Events Important to Postclosure Performance

As noted in Section 8.1.1.2[a], the most important events potentially affecting releases from the WPs were found to be seismic ground motion and igneous intrusion (i.e., a magmatic dike rising through the earth's crust and intersecting the repository). Based on the FEPs screening process, the seismic and igneous events only affect the EBS. In the case of seismic or vibratory ground motion, it is possible that extensive damage and failure of the WPs and DSs could be caused by a single extreme ground motion event. More commonly, however, damage would accumulate from a sequence of small to moderate vibratory ground motions over a period of time (Section 6.6.1.2.2.2 of the parent document). However, not all WPs that experience small to moderate ground motion events are breached. In contrast, a potential igneous intrusion into the repository area is assumed to cause complete failure of all WPs and DSs in a single discrete event (Section 6.5.1.1 of the parent document).

Vibratory ground motion events can cause damage to WPs, in the form of stress corrosion cracks, ruptures or punctures of the WP outer corrosion barrier (OCB) (Section 6.6.1.1.2 of the parent document) whereas for the DS, failure occurs as the result of loading from seismic induced rock fall. In the first 10,000 years after repository closure, the primary damage caused by ground motion events is stress corrosion cracks of CDSP WPs (Section 7.3.2.6.1.3 of the parent document). The probability of a seismic event that results in damage to CDSP WPs has a mean value of about 0.07 (based on λD_CDSPi23 = 7.484×10^{-6} yr^{-1} for 10,000 years), with a maximum value of about 0.2 (based on λD_CDSPi23r90 = 2.181×10^{-5} yr^{-1} for 10,000 years) (output DTN: MO0708CDSPSEIS.000 [DIRS 183007], FreqDamageCDSP_v5.pdf). The probability of seismic induced DS failure before 10,000 years is approximately 1.8×10^{-4} (DTN: MO0712PBANLNWP.000 [DIRS 184664], Lith Probability of DS Failure.pdf). Rupture and puncture of WPs are not considered because the probability that these events occur within 10,000 years is low enough and the consequence in terms of expected annual dose to the RMEI has been shown to be small enough that the contribution to the expected annual dose for the Seismic GM Modeling Case from these events is also low (Section 7.3.2.6.1.3). For this reason, the projections of mean annual dose from seismic ground motion events before 10,000 years is approximated by considering only SCC damage to CDSP WPs.

For the time period out to 1,000,000 years, seismic ground motion events have a variety of effects on the DSs and WPs. Ground motion events can lead to drift degradation and rockfall accumulation on the DS (Section 6.6.1.1 of the parent document). Subsequent failure of the DS can occur as a result of dynamic loading and deformation and/or by static loading due to accumulated rockfall. The ability of the DS to withstand the dynamic and static loading diminishes with time because general corrosion reduces the thickness of the titanium DS plate and framework. Ultimately, the DSs will fail as a result of load-induced buckling or rupture. A histogram of the time of DS plate failure for the Seismic GM Modeling Case is shown on Figure 8.1-4[a]; DS failure times for the Nominal Modeling Case (described in Section 6.3.5 of the parent document), in which DS plate failure occurs only due to general corrosion, are also shown for the purposes of comparison. As shown, the projected times of DS plate failure for the Seismic GM Modeling case are largely distributed between 100,000 years and about 300,000 years. In contrast, for the Nominal Modeling Case, DS plate failure times are distributed between 270,000 years and 340,000 years. A cumulative distribution function (CDF) for DS failure times is presented later in Section 8.3.3.2[a], along with discussion of the uncertainty in the time of DS failure. These updated histograms of DS plate failure times are nearly identical to those presented in the parent document.

As presented in Section 6.6 of the parent document, seismically induced damage of the WPs is most likely to occur from deformation or denting of the WP OCB. These localized areas of deformation or denting develop residual stresses that are susceptible to SCC. Rupture of a WP could potentially occur as a result of kinematic loading caused by package-to-pallet and/or package-to-package impacts, and a severely deformed OCB may be punctured by the sharp edges of fractured or partly degraded internal components. Generally, seismic crack damage is more likely to occur than either rupture or puncture, and CDSP WPs are more likely to be damaged than are CSNF WPs. Figure 8.1-5[a] shows summary statistics for the distribution of the probability of occurrence of seismic damage to (a) CDSP WPs and (b) CSNF WPs, estimated as the fraction of aleatory samples (futures) in which seismic damage occurs to all WPs, for each epistemic sample element. The probability of occurrence of seismic damage to CSNF WP is

zero at and below the 5th percentile (Figure 8.1-5b[a]). The distribution summarized on Figure 8.1-5a[a] results from epistemic uncertainty in the RST for Alloy 22 (*SCCTHRP,* RST for SCC nucleation of Alloy 22 as a percentage of yield strength; see Section 8.1.1.6[a]); the spread between the quantiles indicates the strong dependence of the occurrence of seismic damage on this uncertain parameter. Section 8.1.1.6[a] provides a summary of sensitivity analyses that further illustrate this dependence.

Figure 8.1-5[a] illustrates that CSNF WPs are far less likely to be damaged by seismic events than are CDSP WPs, due to the use of the transportation, aging, and disposal (TAD) canister for CSNF, which enhances the structural integrity of these WPs. Finally, the probability that seismic events have damaged CDSP WPs increases until around 200,000 years, when DSs fail, after which only slight increases are observed. While the DSs are intact, WP damage from seismic events is determined by abstractions in which the WPs move freely beneath the DSs. In contrast, after DS failure, rubble is assumed to surround the WPs (Section 6.6.1.2.2.1 of the parent document), resulting in a significant reduction in the probabilities of damage from seismic events (output DTN: MO0708FREQCALC.000 [DIRS 183006], compare files: *Rubble_Damage.pdf* and DTN: MO0708CDSPSEIS.000 [DIRS 183007] *FreqDamageCDSP_v5.pdf*). The effects of seismic events on EBS components are described and explained in more detail in Section 8.3.3.2[a]. The revised projections of expected fraction of WPs breached by SCC are shown on Figure 8.1-5[a]; these plots reflect the corrections made to address implementation errors in two model abstractions (Appendix P, Table P-7, issues P3 and P4 in the parent document).

8.1.1.4[a] Multiple Barrier Processes that Contribute to Postclosure Performance

Many of the multiple barrier processes that are important to postclosure performance have been identified in previous TSPAs of the Yucca Mountain repository (Williams 2001 [DIRS 157307]). The modeling studies conducted in support of this TSPA-LA have provided additional insights and understanding, particularly with regard to individual features of natural and engineered barriers. Some of the fundamental barrier processes and characteristics that are typically influential in determining how well the system of multiple barriers isolates (i.e., contains and confines) the nuclear waste are:

- Net infiltration into the unsaturated zone (UZ) (Section 6.3.1 of the parent document) and seepage into the drifts (Section 6.3.3 of the parent document)
- Mechanical strength and corrosion rates of the WPs and DSs (Section 6.3.5 of the parent document)
- Solubilities for key radionuclides such as neptunium, uranium, and plutonium (Section 6.3.7 of the parent document)
- Radionuclide sorption onto corrosion products inside the WPs (Section 6.3.8 of the parent document)

- Diffusion-limited radionuclide releases from failed WPs (Section 6.3.8 of the parent document)

- Sorption and matrix diffusion properties of the UZ and saturated zone (SZ) underlying the repository (Sections 6.3.9 and 6.3.10 of the parent document).

With regard to infiltration and seepage, these attributes are important because they determine: (1) fraction of WPs and DSs in seeping and non-seeping environments, and (2) water flow into a failed WP and the ensuant mobilization and release of radionuclides. The strength properties of the WP OCB (i.e., Alloy 22 [UNS N06022]) and DS plate (i.e., Titanium Grade 7) and frame (i.e., Titanium Grade 29) determine their capability to withstand dynamic and static loads induced by vibratory ground motion (Section 6.6.1.2 of the parent document). General corrosion and SCC are important processes affecting WP structural integrity because they progressively reduce metal barrier thickness over a period of time. The general corrosion rate of the WP OCB is temperature-dependent, which makes the WP surface temperature an important factor. The importance of radionuclide solubilities is derived from the fact that they limit the release rates from the WPs. Solubilities of such radionuclides as neptunium, uranium, and plutonium are particularly important because they have relatively large initial inventories and produce radionuclide species that have very long half-lives. Corrosion of the WP internals produces metal oxides that provide sorption sites for a variety of fission products and actinide elements (Section 6.3.8 of the parent document). Diffusional release of radionuclides from a failed WP is a function of the breach geometry (e.g., cracks and patches) and effectively limits the rate of release to the natural barrier. The sorption properties of the volcanic tuff and alluvium layers in the UZ and SZ influence the rate of subsurface migration to the RMEI location.

Analyses of single realizations from the TSPA-LA Model (presented in Section 7.7.1[a]) illustrate these important processes and their role in isolating the nuclear waste. Although these analyses are conducted on individual modeling cases, the results for modeling cases that are important to total mean annual dose (Figure 8.1-3[a]) provide useful insights into processes and their relationships with dose outcomes. For example, the single realization analyses of the Seismic GM Modeling Case for 10,000 years (Section 7.7.1.7[a]) provide insights about impacts on repository performance for 10,000 years after closure; whereas the analyses of the Igneous Intrusion Modeling Case (Section 7.7.1.3[a]) and Seismic GM Modeling Case for 1,000,000 years (Section 7.7.1.4[a]) illustrate processes that dominate performance over 1,000,000 years. Additional discussion and interpretation of the simulation results for each of these modeling cases is provided in Section 8.2[a]. Section 8.3.3[a] provides further insight into the processes important within each of the three primary barriers.

8.1.1.5[a] Radionuclides Important to Postclosure Performance

In general, the radionuclides in the nuclear waste that dominate the calculation of annual doses typically have one or more of the following characteristics: (1) large initial inventories in the nuclear waste, (2) moderate to high solubilities, (3) very long half-lives (e.g., $\geq 10^5$ years), and (4) low to non-sorbing properties. The radionuclides that become important to dose also depend on the time frame considered (i.e., 10,000 years or 1,000,000 years after closure), because of the effect of radionuclide decay on the activity concentrations. Ingrowth of radionuclides via chain decay (Figure 6.3.7-4 of the parent document) can also be an important process that determines

the role and importance of actinide elements in the actinium, uranium, neptunium, and thorium series. For groundwater releases, the basic transport processes of advection, dispersion, matrix diffusion, and sorption play an important role, as illustrated in the analyses documented in Section 7.7.1[a]. Moreover, the specific modes (e.g., dissolved and colloidal phases) of transport can also be important; the modes analyzed for each radionuclide are listed in Table 6.3.7-6[a].

The contributions of the individual radionuclides to the maximum total mean annual dose are shown on Figures 8.1-6[a] and 8.1-7[a] for 10,000 years and post-10,000 years, respectively. The relative contribution of each radionuclide is determined by its mass in the initial inventory, the intrinsic properties of each radionuclide, as well as the relative importance of the events (i.e., seismic and igneous), which lead to release of radionuclides. The radionuclide half-lives quoted in the following discussion can be found in Table 6.3.9-1[a].

Important Radionuclides for 10,000-Year Performance Projection—The total mean annual dose curves for individual radionuclides on Figure 8.1-6[a] show that the principal contributors to the total mean annual dose, ranked from highest to lowest, are: ^{99}Tc (half-life 2.13×10^5 yrs), ^{14}C (half-life 5.72×10^3 yrs), ^{239}Pu (half-life 2.41×10^4 yrs), and ^{129}I (half-life 1.57×10^7 yrs). Collectively, these four radionuclides account for about 87 percent of the maximum of the total mean annual dose, which occurs at 10,000 years postclosure. The dominant contributor is ^{99}Tc, which accounts for about 51 percent of the total. Other radionuclides, notably ^{36}Cl, ^{240}Pu, ^{79}Se, and ^{237}Np, make up the remaining 13 percent of the total mean annual dose.

The fission products, ^{99}Tc and ^{129}I, and the activation product, ^{14}C, collectively represent about 75 percent of the total mean annual dose. These three radionuclides are important because they are very soluble in water, do not sorb in earth materials, and in the case of ^{99}Tc and ^{129}I have very long half-lives relative to the 10,000-year time frame. Because technetium, iodine, and carbon radionuclides are very soluble, their release rates from the nuclear waste are limited only by: (1) the waste form degradation rates, (2) rate and extent of water saturation inside WPs, and (3) mass transport mechanisms (i.e., diffusion and/or advection) out of the WPs. The non-sorbing property is important because these radionuclides are transported from the EBS, through the natural barrier, and to the RMEI at the rate at which the groundwater naturally travels (i.e., no delay by chemical retardation). The relatively long half-lives of ^{99}Tc and ^{129}I, compared to 10,000 years, means that decay would not appreciably reduce their activity level.

The rate of transport of radionuclides from WPs depends on the nature and extent of damage to DSs and WPs resulting from disruptive events, the most important of which are seismic ground motion and igneous intrusion events. Before 10,000 years, roughly 70 percent of the total mean annual dose is attributable to the mean annual dose for the Seismic GM Modeling Case (Figure 8.1-3[a]), which in turn consists almost entirely of the highly soluble radionuclides ^{99}Tc, ^{14}C, ^{129}I, ^{36}Cl, and ^{79}Se (Figure 8.2-12a[a]). The predominant damage caused by vibratory ground motion is SCC of CDSP WPs (Section 7.3.2.6.1.3 of the parent document), which permits diffusion of radionuclides from WPs but not advection. In these circumstances, highly soluble radionuclides are more readily transported from the damaged WPs than are solubility-limited radionuclides such as plutonium.

The dominance of ^{99}Tc, compared to ^{14}C and ^{129}I, largely stems from its WP inventory (Table 8.1-5[a]) and the fact that the predominant damage caused by vibratory ground motion is

SCC of CDSP WPs (Section 7.3.2.6.1.3 of the parent document). In CDSP WPs, the total of ^{99}Tc inventory on a curie per package basis is about 1,000 times that of ^{129}I and about 2.5 times that of ^{14}C. Although ^{14}C has a larger biosphere dose conversion factor (BDCF) (Table 8.1-5[a]) than ^{99}Tc and ^{129}I, it also has a relatively short half-life (5,715 years) and will experience some decay in transport. Thus, due to the larger inventory of ^{99}Tc and it's very long half-life (2.13×10^5), it is reasonable and consistent that ^{99}Tc would have greater influence than ^{14}C and ^{129}I on total mean annual dose to the RMEI.

In contrast, the Igneous Intrusion Modeling Case contributes roughly 30 percent of the total mean annual dose before 10,000 years (Figure 8.1-3[a]). The highly soluble, non-sorbing radionuclides, ^{99}Tc, ^{14}C, and ^{129}I, are important to the mean annual dose for this modeling case (Figure 8.2-8a[a]) for the first 4,000 years. However, after 8,000 years, ^{239}Pu becomes the dominant radionuclide with ^{99}Tc, ^{240}Pu, and ^{129}I contributing to mean annual dose from igneous intrusions. Because an igneous intrusion causes complete failure of all DSs and WPs at the time of the event, radionuclides are transported from the WPs by advection as well as diffusion, resulting in the emerging importance of ^{239}Pu. The time that ^{239}Pu becomes important is determined by the processes that govern the mobilization and transport of this radionuclide. The mean annual dose between 4,000 and 6,000 years shows both ^{239}Pu and ^{240}Pu emerging as dominant dose contributors (Figure 8.2-8a[a]). The comparison of Figure 8.2-8a[a] to Figure 8.1-6[a] shows that the contribution of ^{239}Pu to total mean annual dose at 10,000 years is due to its contribution to mean annual dose from the Igneous Intrusion Modeling Case. Thus, although the actinide ^{239}Pu has a relatively large initial inventory (Table 6.3.7-5 of the parent document), its contribution to total mean annual dose is limited due to the low probability of an event that can lead to its release, as well as the hydrologic and chemical processes that determine the rate of plutonium transport through the EBS and lower natural barrier. Additional discussion of these processes is provided in Sections 6.3.7 through 6.3.10 of the parent document.

Important Radionuclides for Post-10,000-Year Performance Projection—Figure 8.1-7[a] shows the mean annual dose for individual radionuclides for 1,000,000 years after repository closure. Between 10,000 years and 20,000 years, the dominant radionuclides are the same as those listed for the 10,000-year performance projection, namely, ^{99}Tc, ^{14}C, ^{239}Pu, and ^{129}I; however, ^{239}Pu becomes increasingly important with time. Between about 20,000 years until 200,000 years, the radionuclides with largest contributions to total mean annual dose are ^{239}Pu and ^{99}Tc, with ^{242}Pu (half-life 3.75×10^5 yrs) overtaking ^{99}Tc around 150,000 years. Beyond 200,000 years, ^{242}Pu is the largest contributor, with secondary contributions from ^{99}Tc, ^{129}I, ^{237}Np (half-life 2.14×10^6 yrs), and ^{226}Ra (half-life 1,600 yrs). The maximum of the total mean annual dose occurs at 1,000,000 years; the radionuclides contributing to total mean annual dose, ranked from highest to lowest, are: ^{242}Pu, ^{237}Np, ^{226}Ra, and ^{129}I. These four radionuclides account for about 77 percent of the total. The actinides ^{242}Pu and ^{237}Np together represent about 52 percent of the total annual dose with ^{226}Ra and ^{129}I contributing about 25 percent.

At 1,000,000 years, the primary difference between the projections presented in this addendum (TSPA-LA Model v5.005) and the original projections documented in the parent document (TSPA-LA Model v5.000) is that ^{226}Ra is ranked third in the addendum projections instead of first for the post-10,000-year compliance period. This change is attributed to the correction to longitudinal dispersivity distribution, which is described in Appendix P, Section P15, of the

parent document. The explanation for persistence of the ^{226}Ra at 1,000,000 years is due to chain decay, which is described in the parent document.

The persistent importance of ^{99}Tc and ^{129}I to total mean annual dose throughout the 1,000,000-year time period is derived from their contributions to mean annual dose in the Seismic GM Modeling Case (Figure 8.2-12b[a]). This modeling case includes the combined effects of seismic events and nominal corrosion processes on all DSs and WPs in the repository. Because of the relatively low probability that seismic events have damaged all WPs (Figure 8.1-5[a]), it is likely that some WPs remain intact until failure occurs by nominal corrosion processes, most commonly as SCC of lid welds. As the intact WPs fail, additional quantities of ^{99}Tc and ^{129}I are released from the EBS, which results in continual releases of these radionuclides from the repository system throughout the 1,000,000 period. Additional discussion of the Seismic GM Modeling Case is provided in Section 8.2.4.1[a].

Beyond 20,000 years, two plutonium species, ^{239}Pu and ^{242}Pu, are the dominant contributors to total mean annual dose, with ^{242}Pu supplanting ^{239}Pu at about 200,000 years due to radioactive decay of the latter. The contribution of these two plutonium species to total mean annual dose is due primarily to their importance in the Igneous Intrusion Modeling Case (Figure 8.2-8b[a]), where these two species comprise the dominant contributors to mean annual dose. In the Seismic GM Modeling Case, these radionuclides are minor contributors to mean annual dose until about 600,000 years, when WPs begin to fail by general corrosion. After general corrosion failures begin, seepage waters can flow through WPs with general corrosion failures, thereby increasing the quantity of plutonium released from the EBS and into the lower natural barrier. The processes that govern the mobilization and transport of plutonium are discussed in Sections 6.3.7 through 6.3.10 of the parent document.

Plutonium from degraded waste forms can be transported through the EBS either in dissolved phase, as well as sorbed reversibly or irreversibly to colloids. Plutonium releases from the EBS are moderated by sorption onto the corrosion products inside the WP (Section 6.3.8). Plutonium species are transported through groundwater in dissolved phase and reversible colloids, as well as fast (i.e., not retarded by matrix diffusion or attachment/detachment process) and slow irreversible colloids (Table 6.3.7-6), with a broad range of transport times in the SZ. Detailed probabilistic simulations of plutonium transport through the SZ in dissolved phase and as reversible colloids, neglecting effects of decay, indicate median transport times ranging from 3,000 years to greater than 1,000,000 years, with a median among all realizations of about 95,000 years (SNL 2008 [DIRS 183750], Table 6-10[a]). Simulations for the fast irreversible plutonium colloids show transport times ranging from 10 years to about 1,800 years, with a median among all realizations of about 60 years (SNL 2008 [DIRS 183750], Table 6-10[a]). However, the fast irreversible colloids represent less than one percent of all irreversible colloids (BSC 2004 [DIRS 170006], Section 6.6, Table 6-4). In contrast, for slow irreversible colloids, transport times range from 100 years to about 500,000 years, with a median among all realizations of about 4,500 years (SNL 2008 [DIRS 183750], Table 6-10[a]). The TSPA-LA Model projections indicate that the dissolved phase and reversible colloids account for the larger fraction of the contribution of plutonium to total mean annual dose.

In contrast, neptunium has higher solubilities than plutonium (compare Table 6.3.7-35 and Table 6.3.7-36 to Table 6.3.7-37 of the parent document) and travels relatively more rapidly

through the SZ; transport simulations for neptunium (neglecting effects of decay) indicate median transport times ranging from 100 years to 455,000 years, with a median among all realizations of about 3,700 years (SNL 2008 [DIRS 183750], Table 6-10[a]). However, neptunium is more retarded by sorption to corrosion products inside the WPs than is plutonium (Figure 7.7.1-8[a]), thus limiting the rate of release of neptunium from the EBS as compared to plutonium. Transport of radium is discussed in Section 8.1.2.1[a] with the presentation of results for the Groundwater Protection Standard.

8.1.1.6[a] Model Parameters Influencing Uncertainty in Expected Annual Doses

Uncertainty and sensitivity analyses were conducted to identify the TSPA-LA Model parameters that were most influential in determining the spread in the total expected annual dose projections (Appendix K[a], Section K8[a]). Those analyses identify four model parameters as having the largest influence on the overall uncertainty in the expected annual doses to the RMEI. These four parameters are: (1) occurrence rate of igneous events, *IGRATE*; (2) RST for Alloy 22, *SCCTHRP*; (3) temperature dependence parameter for Alloy 22 general corrosion rate, *WDGCA22*; and (4) the SZ ground water specific discharge, *SZGWSPDM*. The importance ranking of these four model parameters varies with time, which is illustrated in Table 8.1-6[a]. Appendix K[a], Figure K8.1-2[a], provides information for times prior to 20,000 years, and Figure K8.2-2[a] provides information for times after 20,000 years. These model parameters are described below; Table K3-1 of the parent document provides additional details and references for each parameter. These results are very similar to that presented in the parent document.

IGRATE—This parameter is the estimated annual frequency of an igneous dike intersecting the repository, which is characterized as an epistemic uncertain quantity. The annual frequency of an igneous event intersecting the repository ranges from approximately 7.4×10^{-10}/yr to 5.5×10^{-8}/yr for the 5th and 95th percentiles, respectively, with a mean annual frequency of 1.7×10^{-8}/yr (Table 6.5-2 of the parent document). In a given epistemic realization, the annual frequency of an igneous event is sampled from the CDF for *IGRATE*, and is used to determine the probability that an igneous event occurs.

SCCTHRP—This parameter is the RST for the Alloy-22 WP OCB, which is represented as an epistemically uncertain value. When the residual stress in the OCB of a WP exceeds this threshold, then SCC is presumed to occur. As explained in Section 6.3.5, residual stresses in the WP OCB result primarily from seismic ground motions that cause impacts between WPs and other WPs, emplacement pallets, or DSs; these impacts could potentially cause dynamic loads that dent the OCB, which could result in creation of residual stresses. The uncertainty in this model parameter is represented using a uniform distribution.

WDGCA22—This parameter relates to the temperature dependence for the general corrosion rate of the Alloy 22 WP OCB, which is characterized as an epistemically uncertain quantity. As explained in Section 6.3.5, this parameter determines the magnitude of this temperature dependence and directly influences the short-term and long-term general corrosion rates of the Alloy 22. Larger values of this parameter correspond to higher general corrosion rates while WP temperatures are above 60ºC, and to lower general corrosion rates when WP temperatures are below 60ºC. This parameter is sampled from a truncated normal distribution.

SZGWSPDM—This SZ flow and transport parameter is the logarithm of the scale factor for the groundwater specific discharge multiplier. The parameter accounts for the epistemic uncertainty in the discharge flow rate, which is used to compute advective radionuclide transport. As explained in Section 6.3.10, this uncertainty parameter is applied to all of the climate states. Values for this parameter are sampled from an empirical CDF; the technical basis for that distribution is documented in *Saturated Zone Flow and Transport Model* (SNL 2008 [DIRS 183750], Section 6.5.2.1).

More detailed discussion of the importance of these and other model parameters is given in Appendix K[a], Section K8[a].

8.1.2[a] Groundwater Protection

No change.

8.1.2.1[a] Projections for Combined ^{226}Ra and ^{228}Ra

The performance demonstration for this first metric of the Separate Standards for the Protection of Groundwater is based on the combined activity concentration for ^{226}Ra and ^{228}Ra (NRC Proposed Rule 10 CFR 63.331 [DIRS 180319], Table 1). The revised probabilistic projections of the activity concentrations are presented on Figure 8.1-9[a]. The curves shown in this figure include the estimated background level, projected mean, and 95th percentile activity concentrations of combined radium species; both the mean and 95th percentile curves exclude background. From these plots, the maximum mean groundwater concentration of combined radium at the RMEI location is estimated to be about 1.3×10^{-7} pCi/L, or less than 10^{-6} pCi/L. This maximum mean activity concentration is well below the 5 pCi/L limit specified in 10 CFR 63.331 ([DIRS 180319], Table 1). This maximum activity concentration is about one order of magnitude lower than the projection presented in the parent document. This difference is primarily due to the change to the uncertainty distribution for longitudinal mass dispersivity; the description of this change is documented in Section 6.3.10.2[a].

Figure 8.1-10[a] shows the contributions of the modeling cases to the projected mean of combined radium activity concentration in groundwater, excluding natural background, for 10,000 years after closure (with the natural background level included in the graph). From the curves in this figure, it is evident that the mean of the combined radium concentration is dominated by the contribution from the Waste Package EF Modeling Case (Section 6.4.2) until 4,500 years, after which the contribution from the Seismic GM Modeling Case dominates. At 10,000 years, when the mean radium concentration obtains its maximum value, roughly 90 percent of the mean radium concentration is attributable to the Seismic GM Modeling Case. The contributions to the mean radium concentration from each modeling case parallel the importance of these modeling cases to the total mean annual dose (Section 8.1.1.2[a]). In particular, the Seismic GM Modeling Case is the dominant contributor to mean radium concentrations because this modeling case represents the potential radionuclide releases from many WPs that may be damaged by seismic events, whereas the early failure modeling cases represent radionuclide releases from the relatively few WPs that may be affected by early failures of either DSs or WPs. In both the Seismic GM and Waste Package EF Modeling Cases, radionuclide transport from the WP occurs primarily by diffusion. In contrast, early failure of DSs allows seepage waters to flow through the underlying WPs (Section 6.4.1.3 of the parent

document), which could result in greater quantity of radionuclides mobilized from each affected WPs. However, this potential for greater releases is offset by the lower expected number of affected WPs, resulting in a relatively minor contribution to the mean radium concentration from the Drip Shield EF Modeling Case.

The fundamental reasons for the very low mean radium concentrations at the RMEI location are: the relatively short half-lives of the two radium isotopes compared to their transport times in the lower natural barrier; the limited release of thorium (a parent of radium) from the EBS; and the lengthy transport time of thorium in the lower natural barrier. Both ^{228}Ra and ^{226}Ra are discussed below.

^{228}Ra Activity Concentration—The chemical and nuclear properties of ^{228}Ra, together with its very small inventory, largely explain its small contribution to the total radium activity concentrations. The radionuclide radium sorbs very strongly in the geologic media (Tables 6.3.9-2 and 6.3.10-2 of the parent document), resulting in very long transport times for ^{228}Ra through the lower natural barrier. Travel times for radium through the SZ alone are predominantly greater than 10,000 years (SNL 2008 [DIRS 183750], Figure 6-14[a]). However, if radium was released from WPs into the lower natural barrier, and if one postulates an unlikely hypothetical pathway with a very fast transport time, for example, of 500 years, then ^{228}Ra, with a half-life of 5.8 years, would still experience about 86 half-lives of decay before reaching the RMEI location. This would reduce its activity by a factor of $(1/2)^{86} \sim 10^{-26}$. The initial total inventory of ^{228}Ra is almost entirely in the CDSP WPs (Table 6.3.7-5 of the parent document). The total activity of ^{228}Ra can be estimated by multiplying its initial activity per WP with the total number of CDSP WPs (Table 6.3.7-1) ($(2.39 \times 10^{-3}$ Ci/pkg from DOE spent nuclear fuel [DSNF] + 3.27×10^{-3} Ci/pkg from HLW) × 3416 pkg = 19.3 Ci). After 86 half-lives of decay, the original quantity of ^{228}Ra would be reduced to about 2×10^{-13} pCi. After mixing this activity in the representative volume of 3,000 acre-ft, the ^{228}Ra activity concentration in the groundwater would be undetectable.

^{228}Ra could also potentially reach the RMEI location via transport of its precursor ^{232}Th and subsequent ingrowth. The relevant part of the decay chain is:

$$^{232}\text{Th (half-life } 1.4 \times 10^{10} \text{ years)} \rightarrow {}^{228}\text{Ra}$$

Because of its extraordinarily long half-life, the ^{232}Th is for all practical purposes a stable element for time periods of 10,000 years. For this reason, it is conservatively assumed that ^{228}Ra and ^{232}Th are in secular equilibrium. The total initial activity of ^{232}Th is about the same as that of ^{228}Ra, about 20 Ci (Table 6.3.7-5 of the parent document). However, in the Seismic GM Modeling Case, transport of thorium from the EBS to the lower natural barrier is significantly constrained by (1) the relatively small damaged area on WP surfaces with stress corrosion cracks, which limits the quantity of water available to dissolve thorium; (2) sorption of thorium onto stationary iron oxyhydroxide corrosion products within the WP; and (3) diffusion of thorium through the WP OCB. For other radionuclides (i.e., uranium and plutonium) affected by these same processes, the mean mass of these radionuclides released from the EBS over 10,000 years is only a minute fraction of the inventory (Figure 8.3-19a[a] for uranium, and Figure 8.3-21a[a] for plutonium). Once in the lower natural barrier, thorium is retarded more by sorption in the geologic media than is radium (Tables 6.3.9-2 and 6.3.10-2 of the parent

document). Simulations of thorium transport through the SZ show that (neglecting effects of decay) the median transport times (through the SZ) for thorium range from about 1,000 years to over 1,000,000 years, with the 50th percentile of the median transport times among all realizations being greater than 1,000,000 years (SNL 2008 [DIRS 183750], Table 6-10[a]).

Thus, due to the short half-life of ^{228}Ra, the processes constraining the release of its parent, ^{232}Th, from the EBS, and the long travel time of thorium through the lower natural barrier, it is reasonable to expect the activity concentrations for ^{228}Ra to show effectively undetectable levels for 10,000 years after disposal.

^{226}Ra Activity Concentration—The explanation for the projected low ^{226}Ra activity concentrations is similar to that for ^{228}Ra. More specifically, ^{226}Ra is initially present in the nuclear waste, and it may also be produced as a result of the decay of uranium and thorium (Figure 6.3.7-4). The relevant part of that decay chain consists of the following:

$$^{234}\text{U (half-life 246,000 yrs)} \rightarrow {}^{230}\text{Th (half-life 75,400 yrs)} \rightarrow {}^{226}\text{Ra (half-life 1,600 yrs)}.$$

This decay chain is significant because it means that, even after ^{226}Ra depletes its initial inventory, it will be continuously replenished so long as there is a source of ^{230}Th and ^{234}U. While both ^{226}Ra and ^{230}Th have relatively small initial inventories in the nuclear waste, the precursor ^{234}U has a significant initial inventory. Also, the large contrast in half-lives between ^{226}Ra and ^{230}Th means that ^{226}Ra will ultimately reach a state of secular equilibrium with ^{230}Th. Similarly, after ^{230}Th depletes its initial inventory, its activity will be in secular equilibrium with its precursor ^{234}U. The net effect is that ^{226}Ra will persist in the waste form for potentially millions of years.

In the Seismic GM Modeling Case, only a minute fraction of the radium present in the WP is released from the EBS (Figure 8.3-20a[a]). Radium that is released from the EBS is unlikely to reach the RMEI location in any significant quantity. As mentioned above, radium exhibits high sorption in the unsaturated tuff layers, particularly in the Zeolitic and devitrified tuff (Table 6.3.9-2 of the parent document), as well as in the volcanic units and alluvium of the SZ (Table 6.3.10-2 of the parent document). These sorption properties have the effect of greatly slowing the ^{226}Ra rate of migration through the lower natural barrier, to the extent that the activity concentrations of ^{226}Ra would diminish by simple decay before reaching the RMEI location. The breakthrough curves for radium transport through the SZ are reproduced on Figure 8.1-8; additional information is provided in *Saturated Zone Flow and Transport Model Abstraction* (SNL 2008 [DIRS 183750], Figure 6-14[a]). It is important to note that the breakthrough curves shown on Figure 8.1-8 do not account for decay during transport; rather, the decay is accounted for when the time-dependent releases of ^{226}Ra from the UZ are computed (SNL 2008 [DIRS 183750], Section 6.5). Figure 8.1-8 shows that (neglecting effects of decay) the majority of the ^{226}Ra transport times at the RMEI location are much greater than 10,000 years; more specifically, for individual realizations the median transport times (i.e., the times when relative mass equals 0.5 on the upper plot on Figure 8.1-8 of the parent document) in the SZ range from 18,000 years to more than 1,000,000 years (SNL 2008 [DIRS 183750], Table 6-10[a]). The 50th percentile of the median ^{226}Ra transport times among all realizations is estimated to be about 731,000 years (SNL 2008 [DIRS 183750], Table 6-10[a]). Due to the magnitude of these transport times, ^{226}Ra would experience from about 11 to more than

600 half-lives of decay before reaching the RMEI, thus reducing the activity concentration by factors $(1/2)^{11}$ to $(1/2)^{600}$. These decay factors suggest that any ^{226}Ra released from the EBS would contribute negligibly to radium activity concentrations at the RMEI location.

^{226}Ra could also potentially reach the RMEI location via transport of ^{230}Th and ^{234}U. Release of uranium from the EBS is constrained by the same processes described in the previous section for thorium. Due to the relatively long transport times for thorium (median greater than 1,000,000 years, see previous section) compared to the half-life of ^{230}Th (75,400 years), any ^{230}Th entering the SZ will likely experience significant decay before exiting the SZ. Any ^{226}Ra produced in the SZ will be subject to chemical sorption in the geologic media, as discussed, and will also likely decay. Because of these factors, it is reasonable to expect insignificant levels of ^{226}Ra activity at the RMEI location from transport and decay of its precursors.

Figure 8.3-30a[a] shows that for the Seismic GM Modeling Case at 10,000 years, the repository system retains all but a minute fraction (mean of 10^{-10}) of all ^{226}Ra in the initial inventory or produced by chain decay over 10,000 years. This performance is due to the relatively short half-life of ^{226}Ra compared to its transport time in the SZ, the processes constraining the release of ^{234}U and ^{230}Th from the EBS, and the long travel time of thorium through the lower natural barrier. Thus, it is reasonable to expect the activity concentrations for ^{226}Ra to show effectively undetectable levels for 10,000 years after disposal.

Uncertainty in Radium Activity Concentrations—The combined activity concentration for ^{226}Ra and ^{228}Ra are computed probabilistically using the TSPA-LA Model described in Section 6.0. Conceptually, a combined ^{226}Ra and ^{228}Ra activity concentration is computed for each combination of an epistemic sample element with values for aleatory parameters; an overall mean activity concentration is determined analogous to the computation of total mean dose to the RMEI (Section 8.1.1.1), although the calculation of mean activity concentration considers only a subset of the scenario classes. Thus, in principle, the calculation of a combined ^{226}Ra and ^{228}Ra activity concentration yields an ensemble of expected activity concentrations (where the expectation averages over aleatory uncertainty), and the relationship between epistemically uncertain variables and expected activity concentrations can be explored through sensitivity analyses.

However, for most epistemic sample elements, the expected activity concentration is effectively zero. Only a few sample elements yield numerically meaningful values, which can be observed by noting that the mean activity concentration at 10,000 years is greater than the 95th percentile (Figure 8.1-9[a]). Consequently, no sensitivity analyses are conducted for the expected activity concentration. The uncertain variables most likely to influence the uncertainty in activity concentration are those that determine the occurrence and extent of failure of WPs and the rate of radium and thorium transport through the SZ. The most important of these variables are the RST for Alloy 22 (*SCCTHRP*), which is important in the Seismic GM Modeling Case (Section 8.2.4.1[a]), the probability of early failure of WPs (*PROBWPEF*) which is important in the Waste Package EF Modeling Case (Section 8.2.2.2[a]), and the logarithm of the scale factor for the SZ groundwater specific discharge (*SZGWSPDM*). Additionally, sensitivity analyses of the movement of ^{234}U, ^{230}Th, and ^{226}Ra through the EBS and lower natural barrier are presented in Appendix K[a], Section K.6, for the Igneous Intrusion Modeling Case. Although the Igneous Scenario Class is not considered in the calculation of mean activity concentration, results of

these analyses are informative about the influence of uncertain variables on the transport of these radionuclides. Additional discussion of the capability of the EBS and lower natural barrier to retain these radionuclides is presented in Section 8.3.3.2[a] and Section 8.3.3.3[a].

In summary, the projections for the mean activity concentrations of combined radium demonstrate with a high level of confidence that the projected level of radioactivity in a representative volume of groundwater would not exceed the numerical limit of 5 pCi/L for the combined ^{226}Ra and ^{228}Ra for the separate standards for the Protection of Groundwater (10 CFR 63.331 [DIRS 180319], Table 1).

8.1.2.2[a] Projections for Gross Alpha Activity Concentration

The performance demonstration for this metric of the Groundwater Protection Standard is based on a calculation of the mean of the gross alpha activity concentration, including ^{226}Ra but excluding ^{222}Rn and the uranium species (10 CFR 63.331 [DIRS 180319]). The TSPA Biosphere Component Model, documented in DTN: MO0702PAGWPROS.001_R0 [DIRS 179328], identifies 15 primary radionuclides that have one or more alpha emitters in their decay chain to the next tracked radionuclide. The specific alpha emitting radionuclides considered in estimating the gross alpha activity concentrations are:

- ^{210}Pb (half-life 22.3 years)
- ^{226}Ra (half-life 1,600 years)
- ^{227}Ac (half-life 21.8 years)
- ^{228}Th (half-life 1.913 years)
- ^{229}Th (half-life 7,300 years)
- ^{230}Th (half-life 75,400 years)
- ^{232}Th (half-life 1.4×10^{10} years)
- ^{231}Pa (half-life 32,800 years)
- ^{237}Np (half-life 2.14×10^{6} years)
- ^{238}Pu (half-life 87.7 years)
- ^{239}Pu (half-life 24,100 years)
- ^{240}Pu (half-life 6,560 years)
- ^{242}Pu (half-life 3.75×10^{5} years)
- ^{241}Am (half-life 433 years)
- ^{243}Am (half-life 7,370 years).

In the calculation for gross alpha, the concentration of ^{210}Pb is not calculated in the TSPA-LA Model instead one alpha particle for ^{210}Pb has been added to that for ^{226}Ra resulting in a total of four alpha particles for ^{226}Ra Likewise, four alpha particles for ^{228}Th have been added to ^{232}Th resulting in a total of five alpha particles for ^{232}Th.

The revised probabilistic projections for gross alpha activity concentrations over the 10,000-year time period are shown on Figure 8.1-11[a]; the activity concentration for gross alpha was calculated based on the annual mass flux of the alpha emitting radionuclides across the boundary of the accessible environment and collected in the representative groundwater volume of 3,000 acre-ft/yr. The plot in this figure shows curves for the mean and 95th percentile for gross alpha activity concentration as well as the background concentration. From the plot, the

maximum of the mean activity concentration is estimated to be 6.70×10^{-5} pCi/L (excluding background), or effectively less than 10^{-4} pCi/L. This maximum value is well below the 10 CFR 63.331 ([DIRS 180319], Table 1) limit for gross alpha activity of 15 pCi/L. This revised projection is higher than the maximum activity concentration documented in the parent document by about 26 percent. This increase in projected activity concentration is due to the correction of several of the errors documented in Appendix P of the parent document; in particular, correction of the error involving iron oxyhydroxide colloid concentrations (Appendix P, Table P-7, item P18) affects the release of americium in the Drip Shield EF Modeling Case (Section 7.3.1.5.2[a]).

Figure 8.1-12[a] shows the contributions of the individual modeling cases to the mean curve for the gross alpha activity, for 10,000 years after closure (with the background level shown in the graph). Figure 8.1-12[a] shows that the mean gross alpha activity concentration is dominated by the Drip Shield EF Modeling Case until approximately 7,000 years postclosure. From 7,000 to 8,000 years, the Waste Package EF, the Drip Shield EF, and Seismic GM Modeling Case contribute approximately equally to the projected gross alpha activity concentration. Over the remaining 2,000 years, the releases from the Seismic GM modeling case become the dominant factor in the projected gross alpha activity concentration.

The primary radionuclides contributing to the mean gross alpha are solubility controlled species. The advective water flux through the WPs in the Drip Shield EF Modeling Case accounts for the early dominance of this modeling case. Both the Waste Package EF and Seismic GM Modeling Cases have intact DSs and therefore exhibit only diffusive releases from the WPs. The diffusive release mechanism in these two cases, combined with the solubility control and sorption of the alpha emitting radionuclides, accounts for the delay in their contributions to the projected gross alpha activity concentration history. Additional discussion of these modeling cases, including discussion of important radionuclides and uncertain variables, is provided in Section 8.2[a].

In summary, the projections for the mean activity concentrations of gross alpha demonstrate with a high level of confidence that the level of radioactivity in a representative volume of groundwater would not exceed the numerical limit of 15 pCi/L for the gross alpha activity (including ^{226}Ra but excluding radon and uranium isotopes) for the Separate Standards for the Protection of Groundwater (10 CFR 63.331 [DIRS 180319], Table 1).

8.1.2.3[a] Projections for Combined Beta- and Photon-Emitting Radionuclides

The performance demonstration for this metric of the Separate Standards for Protection of Groundwater is based on combined beta- and photon-emitting radionuclides; both the primary beta emitters and any daughter products that decay by beta-emission are considered. The annual doses from exposure to beta-photon emitters are quantified in terms of both whole body and organ dose. The TSPA Biosphere Component Model documented in the *Biosphere Model Report* (SNL 2007 [DIRS 177399], Table 6.15-2), identifies a total of 19 primary radionuclides that are used to compute this groundwater protection metric.

Some of the more prominent beta emitters are: ^{14}C, ^{36}Cl, ^{79}Se, ^{90}Sr, ^{99}Tc, ^{129}I, ^{135}Cs, and ^{137}Cs. Of this set, only ^{90}Sr and ^{137}Cs have short half-lives (~ 30 years) relative to the 10,000-year time period. Some of the beta-photon emitters are daughter products of alpha and beta emitters (SNL 2007 [DIRS 177399], Table 6.15-2) such as ^{137m}Ba (half-life 2.55 m), ^{228}Ac (half-life

6.15 h), ^{212}Pb (10.64 h), and ^{208}Tl (half-life 3.05 m). Because these radioisotopes have half-lives ranging from minutes to several hours, they are not included in radionuclide transport calculations; however, the associated conversion factors are included in the calculation of the beta-photon dose (SNL 2007 [DIRS 177399], Section 6.15.1.2). The projections of annual doses for beta-photon emitting radionuclides are evaluated as a function of the release rates from the repository, in-growth, and groundwater transport to the accessible environment.

The revised mean annual doses to the major organs and whole body are shown on Figure 8.1-13[a] for the 10,000-year compliance period. Mean annual doses are calculated by summing the expected annual doses from each beta- and photon-emitting radionuclide and averaging over all epistemic sample elements, analogous to the calculation of total mean annual dose for the Individual Protection Standard (Section 8.1.1.1[a]). As shown on Figure 8.1-13b[a], the mean annual dose curves for the thyroid and lower large intestine overlay one another; the maximum mean annual dose for the thyroid is estimated to be 0.26 mrem and for the lower large intestine about 0.25 mrem. These maximum doses from beta-photon emitters are well below the 10 CFR 63.331 ([DIRS 180319], Table 1) limit of less than or equal to 4 mrem. The mean annual doses for the thyroid and whole body are higher than the original results presented in the parent document by 35 and 38 percent respectively, due primarily to the inclusion of ^{36}Cl and ^{79}Se in the revised calculations (Appendix P[a], Table P-7[a], item P2). Plots of the revised projected mean and 95th percentile curves are shown on Figure 8.1-14[a], which illustrate the uncertainties in the whole body and thyroid annual dose curves.

As can be seen on Figure 8.1-15[a], the largest contributions to mean annual doses to the thyroid and whole body are attributable to the Seismic GM Modeling Case. The dominance of this modeling case for the mean annual doses to the thyroid and whole body is similar to its dominance in the total mean annual dose to the RMEI, and is explained by the fact that the Seismic GM Modeling Case represents a larger expected number of breached WPs and therefore larger radionuclide releases (Section 8.1.1.2[a]). The important radionuclides for these performance metrics are similar to those for the Seismic GM Modeling Case (Section 8.2.4.1[a]). In particular, dose to the thyroid is largely attributable to ^{129}I; while, ^{99}Tc contributes primarily to the alimentary tract organs, with the lower large intestine and the stomach receiving the highest doses (EPA 2002 [DIRS 175544], CD-ROM, ingestion dose coefficients for ^{99}Tc and ^{129}I). Whole body dose is calculated as a weighted sum of doses to the individual organs. In this calculation, the alimentary tract organs, in particular the colon (lower large intestine) and the stomach, have large tissue weighting factors relative to other organs (proposed 40 CFR Part 197 (70 FR 49014 [DIRS 177357], Appendix A, Table A.2)). The ingestion of ^{99}Tc largely contributes to the dose to these organs (EPA 2002 [DIRS 175544], CD-ROM, ingestion dose coefficient for ^{99}Tc). Thus, most of the whole body dose can be attributed to the dose from ^{99}Tc to the lower large intestine and the stomach, and to the dose from ^{129}I to the thyroid.

Because the largest contributions to the mean annual doses to the thyroid and whole body are attributable to the Seismic GM Modeling Case and result from two radionuclides that are important to the mean annual dose to the RMEI for this modeling case, the uncertain inputs important to uncertainty in organ and whole body doses are the same as those important to the mean annual dose to the RMEI. Specifically, the most important uncertain input is the RST for the Alloy-22 WP OCB (*SCCTHRP*), which largely determines the probability of WP failure from

seismic events. Additional discussion of important uncertain inputs for the Seismic GM Modeling Case is provided in Section 8.2.4.1[a].

In summary, the projections of mean annual beta-photon dose demonstrate with a high level of confidence that the annual doses to the whole body or any organ would not exceed the numerical limit of 4 mrem for groundwater protection for the combined beta- and photon-emitting doses for the separate standards for the Protection of Groundwater (10 CFR 63.331 [DIRS 180319], Table 1).

8.1.3[a] Human Intrusion Protection

No change.

8.1.3.1[a] Determination of Earliest Time for Drilling Intrusion

No change.

8.1.3.2[a] Projections of Annual Doses for Human Intrusion

To address the requirements of the Individual Protection Standard for Human Intrusion (10 CFR 63.321 [DIRS 178394]), a probabilistic TSPA methodology, analogous to that used to demonstrate performance with the Individual Protection Standard after Permanent Closure and the Separate Standards for Protection of Groundwater, was used to make projections of the annual dose following a human intrusion. The calculations of expected annual dose account for only the radionuclides released into groundwater as a consequence of the intrusion, as specified in 10 CFR 63.322(f and g) [DIRS 180319]. Based on the analysis described in Section 8.1.3.1 of the parent document, the earliest time after disposal for the drilling intrusion was taken to be 200,000 years.

As described in Section 6.1.2.5 of the parent document, a separate scenario, the Human Intrusion Scenario, is used to estimate projections of annual dose resulting from a human intrusion. This scenario considers aleatory uncertainty in the type of WP assumed to be penetrated and the location of the penetration, both within the repository footprint and in the underlying SZ. For each epistemic sample element, expected annual dose is computed by averaging over these aleatory uncertainties.

The revised probabilistic projections of expected annual dose for the Human Intrusion Scenario are presented on Figure 8.1-16[a]. The plots show the curves for the mean, median, and 5th and 95th percentiles of the distribution of expected annual doses for the period of geologic stability. The maximum of the mean annual dose to the RMEI occurs within a few thousand years after the intrusion. The maximum values of the mean and median are projected to be less than 0.013 mrem and 0.011 mrem, respectively, well below the regulatory limit of 350 mrem (10 CFR 63.321(b)(2) [DIRS 178394]). The maximum of the median annual dose, which occurs about 2500 years after the intrusion, is about 70 percent higher than the results presented in the parent document. This change is the result of correcting several implementation errors affecting this modeling case (Appendix P[a], Table P-6[a], items 6, 9, and 13) and of refining the temporal discretization for this modeling case (Section 7.3.3.6[a]). The spread of values about the median annual dose is reflected in the 5th and 95th percentiles, which are approximately

1.24×10^{-3} mrem and 2.86×10^{-2} mrem, respectively, at the time when the median achieves its maximum value.

The contribution of individual radionuclides to the total mean annual dose for the Human Intrusion Scenario for 1,000,000 years after repository closure is shown on Figure 8.1-17[a]. The Human Intrusion Modeling Case conservatively assumes that the intruded WP is intact until the intrusion. Following the intrusion, the long-lived fission products that are highly soluble and non-sorbing, such as ^{99}Tc (half-life 2.13×10^5 yrs) and ^{129}I (half-life 1.57×10^7 yrs), dominate the annual dose for about 50,000 years after the intrusion while the waste form is degrading, and account for about 99 percent of the maximum median annual dose. After ^{99}Tc and ^{129}I inventory is depleted, the long-term dose to the RMEI occurs from long-lived radionuclides that undergo sorption, primarily ^{242}Pu (half-life 3.75×10^5 yrs) with secondary contributions from ^{135}Cs (half-life 2.3×10^6 yrs), and ^{237}Np (half-life 2.14×10^6 yrs). The annual dose from radionuclides that are not solubility limited, such as ^{99}Tc, ^{129}I, and ^{135}Cs, is similar to those in the Waste Package EF Modeling Case because the expected number of early failed waste packages is approximately equal to 1 (Section 6.4.2.2 of the parent document) and the releases for these radionuclides out of the WP are primarily diffusive. (Note that in the Waste Package EF Modeling Case, most of the mass for these radionuclides is released prior to DS failure and thus remains primarily diffusive.) It is not feasible to compare the magnitude of ^{242}Pu dose between the two modeling cases due to differences in transport through the EBS and UZ. For example, following DS failure in the Waste Package EF Modeling Case, the advective releases of ^{242}Pu dominate over diffusive releases, which is not the case in the Human Intrusion Modeling Case where the diffusive releases remain dominant for the simulated time period (Section 7.7.1.6[a]). In addition, more retardation of dissolved ^{242}Pu mass occurs in the Human Intrusion Modeling Case due to matrix diffusion along UZ borehole pathway (Section 7.7.1.6[a]).

Sensitivity analyses of the expected annual dose to the RMEI resulting from a human intrusion are presented in Appendix K[a], Section K10[a]. Due to the highly transient nature of the pulse of ^{99}Tc and ^{129}I, sensitivity analyses are performed within a few thousand years of the intrusion (Figures K10-1[a] and K10-2[a]) as well as many thousands of years after the intrusion (Figures K10-3[a] and K10-4[a]). The uncertain inputs that influence the uncertainty in expected annual dose during the initial pulse of ^{99}Tc and ^{129}I are those that influence (1) the time of arrival of the pulse (i.e., *SZGWSPDM* (logarithm of scale factor that characterizes uncertainty in groundwater specific discharge) and *INFIL* (pointer variable for determining infiltration condition)), (2) the effect of these radionuclides on the RMEI (i.e., *MICTC99* (BDCF for technetium)) and (3) the total mass of these radionuclides in the nuclear waste (i.e., *CSNFMASS* (uncertainty in radionuclide content of CSNF)). After the initial pulse of ^{99}Tc and ^{129}I, sensitivity analyses identify several variables with influence on the uncertainty in the long-term expected annual dose, although the analyses do not produce regression models with large R^2 values (Figure K10-4a[a]). These variables are primarily related to the mobilization of plutonium from the waste, and to the rate of plutonium transport through the lower natural barrier. Additional discussion is provided in Appendix K[a], Section K10[a].

In summary, these projections demonstrate with a high level of confidence that the mean annual doses to the RMEI would be well below the limits for the Individual Protection Standard for Human Intrusion (10 CFR 63.321 [DIRS 178394]). Moreover, the projections indicate that the system of multiple barriers would be sufficiently robust and resilient to limit annual doses for the prescribed Human Intrusion Scenario.

INTENTIONALLY LEFT BLANK

Table 8.1-1[a]. Performance Demonstration Results for Individual Protection Standard

Time After Closure (yrs)	Maximum Total Mean Annual Dose (mrem)	Time of Maximum Total Mean Annual Dose (yr)	Maximum Total Median Annual Dose (mrem)	Time of Maximum Total Median Annual Dose (yr)	Limit for Annual Dose (mrem)
10,000	0.24	10,000	0.13	~ 9,900	15 (mean)
1,000,000	2.00	1,000,000	0.96	~ 720,000	350 (median)

Source: Output DTN: MO0710PLOTSFIG.000 [DIRS 185207],
Files: LA_v5.005_10kyr_Total_Dose_Calcs_Rev01.gsm and LA_v5.005_1Myr_Total_Dose_Calcs_Rev00.gsm.
Numerical Limits from 10 CFR 63.311(a) [DIRS 178394]

Table 8.1-2[a]. Performance Demonstration Results for the Separate Standards for the Protection of Groundwater

Type of Limit	Maximum of Mean Activity Concentration or Annual Dose	Natural Background Level	Limit for Activity Concentration or Annual Dose
Combined ^{226}Ra and ^{228}Ra	$<10^{-6}$ pCi/L	0.5 pCi/L	5 pCi/L
Gross Alpha Activity	$<10^{-4}$ pCi/L	0.5 pCi/L	15 pCi/L
Dose from Combined Beta & Photon Emitting Radionuclides	Whole Body ~ 0.06 mrem Thyroid ~ 0.26 mrem	Background level excluded in regulatory requirement	4 mrem

Source: Output DTN: MO0710PLOTSFIG.000 [DIRS 185207],
Files: LA_v5.005_10k_Ra_Mean_Contributions_Rev00.JNB, LA_v5.005_10Kyr_Alpha_Mean_Contributions_Rev00.JNB, and LA_v5.005_10kyr_Thyroid_Whole_Body_Rev00.JNB.
Numerical Limits from 10 CFR 63.331 [DIRS 180319]

Table 8.1-3[a]. Performance Demonstration Results for the Individual Protection Standard for Human Intrusion

Time After Closure (yrs)	Projected Maximum Annual Dose (mrem)	Limit for Annual Dose (mrem)
10,000	0	15 (mean)
1,000,000	0.01 (median)	350 (median)

Source: Output DTN: MO0710ADTSPAWO.000 [DIRS 185207],
File: LA_v5.005_HI_009000_000.gsm.
Numerical Limits from 10 CFR 63.321(b) [DIRS 178394]

Table 8.1-4[a]. Uncertainty in Projections of Maximum Total Mean and Median Annual Dose (mrem) for the Individual Protection Standard

Time After Closure (yrs)	Total Mean Annual Dose	Total Median Annual Dose	5th Percentile Total Expected Annual Dose	95th Percentile Total Expected Annual Dose
10,000	0.24	0.13	6.67×10^{-3}	0.67
720,000	1.55	0.96	0.09	4.62
1,000,000	2.00	0.86	0.14	9.06

Source: Output DTN: MO0710PLOTSFIG.000 [DIRS 185207], Files: LA_v5.005_10kyr_Total_Dose_Calcs_Rev01.gsm and LA_v5.005_1Myr_Total_Dose_Calcs_Rev00.gsm.

Table 8.1-5[a]. Inventories and Biosphere Dose Conversion Factors for Radionuclides Important to Total Mean Annual Dose for 10,000 Years

Radionuclide	Radionuclide Activity (Ci per Waste Package)			Mean BDCF (Sv/yr) / (Bq / m^3)
	CSNF	CDSP-DSNF	CDSP-HLW	
^{99}Tc	1.30×10^{2}	2.69	17.2	1.12×10^{-9}
^{14}C	6.09	7.98	0.00	1.93×10^{-9}
^{129}I	3.12×10^{-1}	6.30×10^{-3}	1.29×10^{-2}	1.29×10^{-7}

Sources: Table 6.3.7-5 and SNL 2007 [DIRS 177399], Table 6.11-12.

NOTE: Activity is estimated at time of closure and does not include uncertainty in waste inventory (Section 6.3.7.1.2).

Table 8.1-6[a]. Uncertainty Importance Ranking as a Function of Time for Four Key TSPA-LA Model Parameters

Time After Closure (yrs)	Two Most Important Parameters	
3,000	*SCCTHRP*	*IGRATE*
5,000	*SCCTHRP*	*IGRATE*
10,000	*SCCTHRP*	*IGRATE*
125,000	*IGRATE*	*SZGWSPDM*
250,000	*IGRATE*	*SZGWSPDM*
500,000	*IGRATE*	*WDGCA22*
1,000,000	*IGRATE*	*WDGCA22*

Sources: Appendix K[a], Figure K8.1-2[a] and Figure K8.2-2[a]; and output DTN: MO0801TSPAMVAC.000 [DIRS 185080]

NOTE: *IGRATE* = occurrence rate of igneous events

SCCTHRP = RST for Alloy 22

SZGWSPDM = logarithm of scale factor for SZ groundwater-specific discharge

WDGCA22 = temperature dependence parameter for Alloy 22 general corrosion rate

8.2[a] PROJECTIONS FOR INDIVIDUAL MODELING CASES

This section presents the probabilistic projections for the set of modeling cases used in developing the performance demonstration for the Individual Protection Standard After Permanent Closure (10 CFR 63.311 [DIRS 178394]). A subset of these modeling cases was also used for the performance demonstration for the Separate Standards for the Protection of Groundwater (NRC Proposed Rule 10 CFR 63.331, Table 1 [DIRS 180319]) (Section 8.2.1[a]). Six modeling cases are presented and explained, including: (1) Nominal (Section 6.3), (2) Waste Package EF (Section 6.4.2), (3) Drip Shield EF (Section 6.4.1), (4) Igneous Intrusion (Section 6.5.1), (5) Seismic GM (Section 6.6.1), and (6) Seismic FD (Section 6.6.1). Because the changes from TSPA-LA Model v5.000 to v5.005 only affect the analysis of the groundwater pathway, the Volcanic Eruption Modeling Case was not recalculated. Thus, the discussion presented for the Igneous Scenario Class, Section 8.2.3[a], only addresses the results of the Igneous Intrusion Modeling Case. These analyses are presented supplemental to the analyses documented in Section 8.2 of the parent document.

As noted in Section 8.1.1.2[a], the revised projections of total mean annual doses to the RMEI are largely dominated by two modeling cases: (1) Seismic GM and (2) Igneous Intrusion—as shown on Figure 8.1-3[a]. This observation is consistent with the original projections in the parent document. For the 10,000-year period, the Seismic GM Modeling Case contributed about 70 percent and the Igneous Intrusion Modeling Case contributed about 27 percent of the maximum of the total mean annual dose (i.e., 0.24 mrem). In contrast, for the post-10,000-year period, the Igneous Intrusion Modeling Case is the primary contributor with the Seismic GM Modeling Case increasing in importance as the second highest contributor to the total mean and median annual doses until approximately 750,000 years after closure. After approximately 750,000 years postclosure, the Seismic GM and Igneous Intrusion Modeling Cases contributed almost equally to the maximum median of the total annual dose (i.e., 0.96 mrem) for the post-10,000 year period.

8.2.1[a] Nominal Modeling Case

The revised projections for the Nominal Modeling Case (Section 6.3) are shown on Figure 8.2-1[a]. There is no annual dose to the REMI in the first 10,000 years, with earliest occurrence of dose around 21,000 years. In the parent document, there were no doses until about 120,000 years after closure. This change in projected doses is due to correcting the implementation error documented in Appendix P, Section P6, of the parent document. That section of the parent document describes the implementation error in the weld volume calculation, which caused an underestimation of the volume for stress corrosion cracks. Correcting this error increased the median probability of SCC occurring by a factor of about 3 for both the CDSP and CSNF WPs (Appendix P, Section P6 of the parent document). As a result, the probabilistic projections of WP breaches now exhibit a few realizations with a SCC crack penetrating the WP OCB well before 100,000 years. In particular, crack penetration occurred in less than 10,000 years in one WP in one realization because of a combination of sampled values for SCC in the closure-lid weld resulting in large initial crack length and high crack propagation velocity (output DTN: MO0801TSPAWPDS.000 [DIRS 185077] files: LA_v5.005_NC_000300_005_Conceptual_Description.doc, v5.005_rlz_182_initial_crack_length_estimate.xls]). Further comparison of the TSPA-LA Model v5.005 results to the

TSPA-LA Model v5.000 results for the Nominal Modeling Case is provided in Section 7.3.1.5.1[a].

The revised maximum mean and median annual doses for the post-10,000-year period are 0.55 mrem and 0.28 mrem, respectively. The maximum mean and median annual doses to the RMEI occur at about 730,000 and 850,000 years, respectively. The two radionuclides dominating the maximum annual dose are the very soluble, long-lived, and mobile radionuclide species ^{129}I and ^{99}Tc. Other second order contributors to this maximum dose value are ^{135}Cs, ^{242}Pu, ^{79}Se, and ^{237}Np (Figure 8.2-2[a]).

As discussed in Section 6.1.2.4, expected annual dose from WPs in the Nominal Modeling Case is computed directly by the GoldSim component of the TSPA-LA Model. Aleatory uncertainty in the time and location of WP breaches, as well as the degree of damage to each WP, is implicitly accounted for in the averaging performed by the WAPDEG software and in the partitioning of WPs into representative groups (Appendix N of the parent document). The expected dose histories on Figure 8.2-1[a] are the result of a succession of three phases for releases from WPs. First, a few WP breaches may occur early, which generally consist of SCC occurring in the WP OCB closure lid welds. SCC may initiate in the lid welds once general corrosion processes have removed the layer of compressive stress produced by low plasticity burnishing (Section 6.3.5.1.2). No releases are observed before about 20,000 years after repository closure (Figure 7.7.1-74b[a]). Because infiltration rates and temperatures vary across the repository footprint, the time at which a continuous thin film of adsorbed water required for diffusive radionuclide transport begins also varies (Section 6.3.8.1 of the parent document). The second phase begins at approximately 200,000 years and dominates until roughly 800,000 years, at which time SCC breaches in the WP lid welds have occurred in most realizations (Figure 8.3-6a[a]). The third phase starts around 500,000 years when WPs begin to fail by general corrosion (i.e., begin to have patch openings in the WP OCB (Figure 8.3-6b[a])). When patch openings occur, seepage waters can flow through the waste, generally resulting in larger releases of radionuclides. However, general corrosion patch penetrations occur in only a minority of WPs, and in a few realizations. Section 7.7.1.5[a] provides additional analyses of individual realizations in the Nominal Modeling Case. Finally, the step-wise increases in the annual dose curves at around 200,000 years, 300,000 years, 500,000 years and 700,000 years are due to immediate increases in the number of WP failures from SCC. These immediate increases in WP failure are caused by the coarse temporal discretization used by WAPDEG V4.07 past 100,000 years (Section 7.3.3.7[a]).

Appendix K[a] presents sensitivity analyses that determine the contribution to the uncertainty in expected annual dose that derives from individual uncertain inputs. These analyses identify the temperature dependence parameter for the Alloy 22 general corrosion rate, *WDGCA22*, as the uncertain input that largely explains the uncertainty in the expected annual dose for the Nominal Modeling Case (Figure K4.5-1[a] and Figure K4.5-2[a]). Higher values of *WDGCA22* lead to lower general corrosion rates throughout most of the 1,000,000-year performance period. In turn, lower general corrosion rates lead to later WP failures by SCC, and to fewer WP failures by general corrosion. Several other uncertain inputs, such as the deviation from median yield strength range for the WP outer lid, *WDZOLID*, are identified as having additional, lesser effects. The effects of these other inputs are discussed in Appendix K[a], Section K4.5[a].

Sensitivity analyses for intermediate model outputs, such as the number of failed WPs, environmental and chemical conditions within the EBS, and the movement of an important radionuclide (^{237}Np), are presented in Appendix K, Section K4. Although these analyses are performed using results from TSPA-LA Model v5.000, the conclusions of these analyses also apply to results from TSPA-LA Model v5.005, due to the similarity in the results for the two model versions (Section 7.3.1.5.1[a]).

8.2.2[a] Early Failure Scenario Class Modeling Cases

No change.

8.2.2.1[a] Drip Shield Early Failure Modeling Case

Revised projections for the Drip Shield EF Modeling Case (Section 6.4.1) are shown on Figure 8.2-3[a] for both the (a) 10,000-year period after closure and (b) post-10,000 year time period. The expected annual dose to the RMEI for the first 10,000 years shows a maximum mean value of about 2.8×10^{-4} mrem and maximum median of 3.8×10^{-5} mrem; these maximum values occur at approximately 2,000 years and 2,200 years, respectively. Comparing these revised maximum doses with those reported in the parent document, the differences are very small. The only observable difference between the original and revised projections is that the 5th percentile curve in the revised results is slightly below 10^{-6} mrem level and thus does not appear on Figure 8.2-3[a]. Similarly, the maximum doses for the post-10,000-year period are also nearly identical to the original results in the parent document, including the timing of the maximums. Further comparison of the results of this modeling case is provided in Section 7.3.1.5.2[a].

The primary radionuclides that contribute to the mean annual dose for the Drip Shield EF Modeling Case are shown on Figure 8.2-4[a]. In the first 4,000 years after repository closure, three soluble and mobile radionuclides dominate dose; these radionuclides are ^{99}Tc, ^{129}I, and ^{14}C. Between 4,000 and 7,000 years the contribution of ^{239}Pu becomes increasingly important. After 7,000 years, ^{239}Pu is the dominant contributor. The mean annual dose from ^{239}Pu continues to increase from 7,000 years until about 40,000, creating a secondary peak in the mean annual dose curve of about 1.5×10^{-4} mrem. The ^{239}Pu continues to dominate but its contribution declines until about 200,000 years, at which point ^{242}Pu and ^{237}Np become dominant. This pattern of dominant radionuclides and timing of the maximums are nearly identical to those discussed in Section 8.2.2.1 of the parent document.

As discussed in Section 6.1.2.4, expected annual dose from early-failed DSs is computed as a weighted average of the dose resulting from early failure of DSs overlying CDSP and CSNF WPs that may occur in different percolation subregions. Additional discussion of the processes important in determining radionuclide releases from early-failed DSs is provided in the analyses of single realizations (Section 7.7.1.2[a]).

Appendix K[a] presents sensitivity analyses that determine the contribution to the uncertainty in expected annual dose that derives from individual uncertain inputs. These analyses identify the probability for undetected defects in DSs, *PROBDSEF*, as the uncertain input that for the most part explains the uncertainty in the expected annual dose for the Drip Shield EF Modeling Case (Figure K5.7.1-1[a] and Figure K5.7.1-2[a] for 20,000 years; and Figure K5.7.1-3[a] and Figure K5.7.1-4[a] for 1,000,000 years). Higher values of *PROBDSEF* lead to a greater

expected number of early-failed DSs, which in turn exposes a larger number of WPs to seepage waters. At early times, other uncertain inputs that determine the extent and rate of seepage are identified as having lesser effects, namely, *SEEPUNC* (uncertainty factor accounting for small-scale heterogeneity in fracture permeability) and *SEEPPRM* (logarithm of mean fracture permeability in the lithophysal rock units). At later times, *INFIL* (pointer variable for determining infiltration condition) is also important. The effects of these and other inputs are discussed in Appendix K[a], Section K5.7.1[a].

Sensitivity analyses for intermediate model outputs, such as the movement of several important radionuclides (^{239}Pu, ^{237}Np, and ^{99}Tc) through the repository system, are presented in Appendix K, Section K5. Although these analyses are performed using results from TSPA-LA Model v5.000, the conclusions of these analyses also apply to results from TSPA-LA Model v5.005, due to the similarity in the results for the two model versions (Section 7.3.1.5.2[a]).

8.2.2.2[a] Waste Package Early Failure Modeling Case

Revised projections for the Waste Package EF Modeling Case (Section 6.4.2) are shown on Figure 8.2-5[a] for both the (a) 10,000-year period after closure and (b) post-10,000 years. For the first 10,000 years after repository closure, the maximum mean and median annual doses are estimated to be about 3.7×10^{-3} mrem and 6.2×10^{-4} mrem; the maximum values occur between 9,000 to 10,000 years for the mean and at 2,000 years for the median. These maximum dose values are slightly higher than those reported in the parent document. The higher doses are attributed to the correction for ^{36}Cl, ^{79}Se, and ^{126}Sn, which were omitted in the analyses for the parent document; the effect of the error is documented in Appendix P, Section P2.1, of the parent document. For the post-10,000-year period, the maximum mean and median annual doses reach levels of approximately 2.1×10^{-2} mrem and 6.1×10^{-3} mrem, respectively. The maximum mean annual dose occurs at about 12,500 years, while the maximum median annual dose occurs at about 13,500 years. The dose curves gradually decline until about 250,000 years, then increase slightly as a result of the timing of nominal failures of the DSs. When the DSs fail due to general corrosion and seepage waters begin to flow through the failed WPs, advective flow through the WPs will result in additional radionuclide mobilization and transport. By the end of the 1,000,000-year period, the projected mean annual dose falls below 10^{-3} mrem. These patterns and trends are nearly identical to those documented in Section 8.2.2.2 of the parent document. Further comparison of the results of this modeling case is provided in Section 7.3.1.5.3[a].

The major radionuclides that contribute to the mean annual dose for the Waste Package EF Modeling Case are shown on Figure 8.2-6[a]. In the first 10,000 years postclosure, soluble and mobile radionuclides, in particular ^{99}Tc, ^{14}C, and ^{129}I, dominate the estimate of mean annual dose. In the post-10,000-year period, the maximum mean annual dose is dominated by ^{99}Tc, ^{129}I, and ^{239}Pu until approximately 50,000 years, then ^{239}Pu dominates up to about 200,000 years; thereafter, ^{242}Pu, ^{226}Ra, and ^{237}Np are the primary contributors to the maximum mean annual dose. This pattern of dominant radionuclides is identical to that documented in Section 8.2.2.2 of the parent document.

As discussed in Section 6.1.2.4, expected annual dose from early-failed WPs is computed as a weighted average of the dose resulting from early failures of CDSP and CSNF WPs that may occur in different percolation subregions and that may or may not experience seepage. The

expected dose histories on Figure 8.2-5[a] are the result of a succession of four phases for releases from early-failed WPs. During the first phase, no releases are observed before about 500 years after repository closure, because WP temperatures are high enough during the first few hundred years after repository closure that insufficient water is present in the failed WPs to allow diffusive transport of radionuclides. The second phase starts when CDSP WPs begin to cool sufficiently to allow diffusion of radionuclides from the waste to the invert. Between about 500 years and 2000 years, radionuclide concentrations begin to be observed in the groundwater at the RMEI location.

The third phase begins when CSNF WPs begin to cool sufficiently that radionuclides begin to diffuse from these WPs. The initiation of release from these WPs causes the sharp increase in expected annual dose indicated on Figure 8.2-5[a] just prior to 10,000 years; additional detail is shown on Figure 7.7.1-1[a]. Because CSNF WP temperatures vary spatially in the repository, diffusive releases from these WPs begin at different times, resulting in the sequence of increases in expected annual dose. The third phase lasts until about 300,000 years, when the DSs fail due to general corrosion, and seepage waters begin to flow through the failed WPs. These advective flows result in additional radionuclide mobilization and transport, as shown by the increase in expected dose around 300,000 years. Further information about the important processes that result in radionuclide releases from early-failed WPs is provided in the analysis of single realizations in Section 7.7.1.1[a].

Appendix K[a] presents sensitivity analyses that determine the contribution to the uncertainty in expected annual dose that derives from individual uncertain inputs. These analyses identify the probability for undetected defects in WPs, *PROBWPEF*, as the uncertain input that predominately explains the uncertainty in the expected annual dose for the Waste Package EF Modeling Case (Figure K5.7.2-1[a] and Figure K5.7.2-2[a] for 20,000 years, and Figure K5.7.2-3[a] and Figure K5.7.2-4[a] for 1,000,000 years). Higher values of *PROBWPEF* lead to a greater expected number of early-failed WPs. Other uncertain inputs are identified as having lesser effects on expected annual dose, depending on the time after repository closure. In particular, at early times, the analysis identifies *INFIL* (pointer variable for determining infiltration condition) and *THERMCON* (selector variable for host-rock thermal conductivity) as important, because these variables significantly influence the time at which humidity in the WP allows diffusion to begin. Before DS failure at 300,000 years, the analysis indicates an effect from *ISCSNS* (pointer variable that determines ionic strength for CSNF under vapor influx conditions) because this variable affects the solubility of many radionuclides. After DS failure, the analysis identifies as important several variables that determine the rate of water flow through the WPs (*INFIL*, *SEEPPRM* (logarithm of mean fracture permeability in the lithophysal rock units), and *SEEPUNC* (uncertainty factor accounting for small-scale heterogeneity in fracture permeability)) as well as variables that determine the solubility of plutonium (*EP1LOWPU* (logarithm of scale factor used to characterize uncertainty in plutonium solubility)) and uranium (*EP1LOWNU* (logarithm of scale factor used to characterize uncertainty in uranium solubility)). The effects of these and other inputs are discussed in Appendix K[a], Section K5.7.2[a].

Sensitivity analyses for intermediate model outputs, such as the movement of several important radionuclides (^{239}Pu, ^{237}Np, and ^{99}Tc) through the repository system, are presented in Appendix K, Section K5. Although these analyses are performed using results from TSPA-LA

Model v5.000, the conclusions of these analyses also apply to results from TSPA-LA Model v5.005 due to the similarity in the results for the two model versions (Section 7.3.1.5.3[a]).

8.2.3[a] Igneous Scenario Class Modeling Cases

As described in Section 6.5 of the parent document, the Igneous Scenario Class consists of two modeling cases: (1) the Igneous Intrusion Modeling Case that represents the interaction of a hypothetical magmatic dike with the repository and ensuant release of radionuclides to the groundwater pathway, and (2) the Volcanic Eruption Modeling Case that represents a hypothetical volcanic eruption at the land surface and the release of radionuclides to the atmospheric pathway. Because the changes from TSPA-LA Model v5.000 to v5.005 only affect the analysis of the groundwater pathway, the Volcanic Eruption Modeling Case was not recalculated. Thus, the discussion below only addresses the results of the Igneous Intrusion Modeling Case.

8.2.3.1[a] Igneous Intrusion Modeling Case

The revised projections of expected annual dose for the Igneous Intrusion Modeling Case (Section 6.5.1) are shown on Figure 8.2-7[a] for both the (a) 10,000-year period after closure and (b) post-10,000 years time period. For the first 10,000 years after repository closure, the maximum mean and median annual doses are estimated to be about 6.6×10^{-2} mrem and 1.8×10^{-2} mrem; both maximum values occur at the end of the 10,000 time period. These values are comparable with those documented in the parent document. For the post-10,000-year period, the maximum mean and median annual doses are estimated to be about 0.89 mrem and 0.32 mrem, respectively; both the maximum annual doses occur at 1,000,000 years. These maximum values are lower but comparable to those presented in Section 8.2.3.1 of the parent document. Further comparison of the results of this modeling case is provided in Section 7.3.1.5.4[a].

The radionuclides that contribute most to the mean annual dose are shown on Figure 8.2-8[a]. Figure 8.2-8a[a] shows that radionuclides ^{99}Tc and ^{129}I dominate the estimate of the mean for the first 4,000 years, and ^{239}Pu and ^{99}Tc dominate the estimate of the mean for the remainder of the 10,000 years postclosure period with a significant contribution from ^{240}Pu starting from about 6,000 years. Figure 8.2-8b[a] shows that ^{239}Pu, which is transported both in dissolved and colloidal form, dominates the maximum mean annual dose for the first 200,000 years and radionuclides ^{242}Pu, ^{237}Np, and ^{226}Ra dominate the estimate of the mean for the remainder of the post-10,000-year time period. These patterns of radionuclide dominance are identical to those documented in Section 8.2.3.1 of the parent document.

As discussed in Section 6.1.2.4, the expected annual dose at time τ is computed as the sum of the contributions to dose from all possible preceding igneous events, where the dose from each event is weighted by the probability of the event's occurrence. The results of this expectation can be seen in the different shapes of the individual radionuclide mean dose curves on Figure 8.2-8b[a]. The ^{129}I dose curve is relatively flat and stable for the entire 1,000,000-year period (and essentially unaffected by radioactive decay because of its long half-life), whereas the dose curves for actinides with long half-lives, such as ^{235}U, ^{238}U, and ^{237}Np (and their decay products) are steadily increasing. These two differing behaviors are a result of the Poisson nature of igneous activity at the repository in which the probability of an igneous event increases linearly through

time at the annual occurrence rate, with a mean of 1.7×10^{-8} yr^{-1}. The steadily increasing probability of occurrence of an igneous event, combined with: (1) nearly instantaneous release of a highly soluble, non-sorbing radionuclide such as ^{129}I, and (2) nearly constant continuous release of a solubility-limited, sorbing radionuclide such as ^{237}Np, results in a relatively constant mean annual dose for the instantaneous release radionuclide (^{129}I) and an approximately linearly increasing mean annual dose for the constant release radionuclide (^{237}Np). The mean annual dose curve for ^{129}I is not perfectly flat through time, as would be expected for a Poisson process, but rather begins to show a decreasing tendency in mean annual dose beginning between 200,000 and 400,000 years after repository closure because, as mentioned in Section 6.1.4.2 of the parent document, nominal corrosion processes are not included in the igneous intrusion modeling case to avoid double-counting the inventory in the calculation of total dose. Consequently, ^{129}I that is released from the WPs due to nominal SCC and general corrosion patches is not included in the calculation of expected annual dose due to igneous intrusions, which results in lower expected annual dose at later times.

Section 7.7.1.3[a] presents analyses of individual realizations of expected annual dose, and illustrates the computation of expected annual dose from the results of simulations of single igneous intrusion events. The analyses presented in Section 7.7.1.3[a] also describe processes that determine the release of radionuclides after an intrusion, and the movement of these radionuclides through the barriers of the repository. Analyses are presented for a realization for which the expected annual dose is similar to the mean annual dose, and for a realization that has the largest value of expected annual dose, and hence significantly influences the mean annual dose.

Appendix K[a] presents sensitivity analyses that determine the contribution to the uncertainty in expected annual dose that derives from individual uncertain inputs. These analyses identify the frequency of occurrence of igneous events, *IGRATE*, as the uncertain input that primarily explains the uncertainty in the expected annual dose for the Igneous Intrusion Modeling Case (Figure K6.7.1-1[a] and Figure K6.7.1-2[a] for 20,000 years, and Figure K6.7.2-1[a] and Figure K6.7.2-2[a] for 1,000,000 years). Higher values of *IGRATE* lead to a greater probability of occurrence of igneous events. The strong and consistent correlation between uncertainty in expected annual dose and *IGRATE* also indicates that the uncertainty in dose resulting from igneous intrusions does not change significantly over time. Other uncertain inputs are identified as having lesser effects on expected annual dose. In particular, the analysis identifies *SZGWSPDM* (logarithm of scale factor that characterizes uncertainty in groundwater specific discharge) and *INFIL* (pointer variable for determining infiltration condition), because these variables significantly influence the rate of water flow through the natural barriers and hence influence the rate of radionuclide transport. Also, before 10,000 years, the analysis identifies the BDCF for technetium (*MICTC99*) as important because ^{99}Tc is a large contributor to dose before 10,000 years. Similarly after 10,000 years, the variable *EP1LOWPU* (logarithm of scale factor used to characterize uncertainty in plutonium solubility) is important because plutonium is the dominant contributor to dose after 10,000 years. The effects of these and other inputs are discussed in Appendix K[a], Section K6.7.1[a] and Section K6.7.2[a].

Sensitivity analyses for intermediate model outputs, such as the movement of several important radionuclides (^{239}Pu, ^{237}Np, and ^{99}Tc) through the repository system, are presented in Appendix K, Section K6. Although these analyses are performed using results from TSPA-LA

Model v5.000, the conclusions of these analyses also apply to results from TSPA-LA Model v5.005 due to the similarity in the results for the two model versions (Section 7.3.1.5.4[a]).

8.2.3.2[a] Volcanic Eruption Modeling Case

No change.

8.2.4[a] Seismic Scenario Class Modeling Cases

As described in Section 6.6 of the parent document, the Seismic Scenario Class consists of two modeling cases: (1) Seismic GM Modeling Case and (2) Seismic FD Modeling Case. The following sections present and explain the revised projections for these two modeling cases.

8.2.4.1[a] Seismic Ground Motion Modeling Case

Summary of Results—The expected annual dose for the Seismic GM Modeling Case is shown on Figure 8.2-11[a]; plots are presented for both the (a) 10,000-year period and (b) post-10,000-year period. The projections of annual dose take into account aleatory uncertainty associated with characteristics of future events, such as number of events, times of events, and the event's peak ground velocity. The mean, median, and 5th and 95th percentile curves on Figure 8.2-11[a] show uncertainty in the value of the expected annual dose, taking into account epistemic uncertainty associated with incomplete knowledge of the behavior of the physical system during and after the disruptive event. The maximum mean and median annual dose for the 10,000 year period are about 0.17 mrem and 0.07 mrem, respectively; both the maximum annual doses occur at the end of the 10,000 year time period. For the post-10,000-year period, the maximum mean and median annual doses are 1.1 mrem and 0.37 mrem, respectively; the maximum annual doses occur at 1,000,000 years and at 875,000 years, respectively. The maximum values for the 10,000 year time period are slightly lower but comparable to those documented in the parent document; however, those for the post-10,000 year period are lower by about 50 percent. The occurrence and timing of intermediate maximums in the dose curves are also different. These differences are largely attributed to the implementation correction documented in Appendix P, Sections P3 and P4, of the parent document. Further comparison of the results of this modeling case is provided in Section 7.3.1.5.6[a].

The radionuclides that contribute most to the estimate of mean annual dose are presented on Figure 8.2-12[a]. The mean dose curves on Figure 8.2-12a[a] illustrate that four radionuclides, ^{99}Tc, ^{14}C, ^{129}I, and ^{36}Cl, contribute the most to the maximum mean annual dose for the 10,000-year time period. One of these species, ^{36}Cl, was not listed in the parent document as important due to an implementation error, as documented in Appendix P, Section P2, of the parent document. As can be seen from Figure 8.2-12b[a], the dominant radionuclides for the post-10,000 years are ^{99}Tc, ^{129}I, ^{242}Pu, and ^{237}Np. Two dominant radionuclide species, ^{226}Ra and ^{79}Se, listed in the parent document do not significantly influence the expected annual dose results presented in this addendum. The reduction of the importance of these two radionuclides in the analyses presented in this addendum can be attributed to correction for the longitudinal dispersivity used in the SZ Flow and Transport Submodel documented in Section 6.3.10[a] and Appendix P, Section P15, of the parent document.

Expected Annual Dose for 10,000 Years—As summarized in Section 6.1.2.4, for the first 10,000 years after repository closure, the expected annual dose at time τ is computed as the sum of the contributions to dose from all possible preceding seismic ground motion events, where the dose from each event is weighted by the probability of the event's occurrence. The integration-based procedure used to calculate expected annual dose results in the relatively smooth results evident on Figure 8.2-11a[a]. Section 7.7.1.7[a] presents analyses of an individual realization of expected annual dose for the 10,000-year period. Appendix J, Figure J8.3-3, illustrates the computation of expected annual dose from the results of simulations of single seismic events, using the simplifications to the seismic damage abstractions that are justified in Section 7.3.2.6.1.

The analyses presented in Section 7.7.1.7[a] also describe processes that determine the release of radionuclides after a damaging seismic event in the first 10,000 years, and the movement of these radionuclides through the barriers of the repository. Analyses are presented for a realization for which the expected annual dose is relatively large, and thus has a significant influence on the mean annual dose. The analyses focus on two radionuclides (^{99}Tc and ^{79}Se) that are representative of radionuclides important to the expected annual dose for this modeling case. These radionuclides are dominant contributors to the expected annual dose because they are highly soluble and thus diffuse relatively rapidly through SCC in the WP OCB, and they transport relatively rapidly through the UZ and SZ.

Appendix K[a] presents sensitivity analyses that determine the contribution to the uncertainty in expected annual dose that derives from individual uncertain inputs. These analyses identify the RST for Alloy 22, *SCCTHRP*, as the uncertain input that predominately explains the uncertainty in the expected annual dose for the Seismic GM Modeling Case for 10,000 years (Figure K7.7.1-1[a] and Figure K7.7.1-2[a]). Lower values of *SCCTHRP* lead to a greater probability of damage occurring from seismic events, which in turn increases the expected value of the dose resulting from seismic events. Aside from *SCCTHRP*, other uncertain inputs are identified as having lesser effects on expected annual dose, although the correlations with these other inputs are not strong. At 10,000 years, the analysis identifies the BDCF for technetium (*MICTC99*) as important because ^{99}Tc is the largest contributor to dose at 10,000 years. Other variables with minor contributions to uncertainty include *DSNFMASS* (scale factor characterizing uncertainty in radionuclide content of DSNF) and *HLWDRACD* (effective rate coefficient for the dissolution of HLW glass), because of the effect these variables have on the mass of ^{99}Tc and its release from the waste form. The effects of these and other inputs are discussed in Appendix K[a], Section K7.7.1[a].

Sensitivity analyses for intermediate model outputs, such as the movement of several important radionuclides (^{239}Pu, ^{237}Np, and ^{99}Tc) through the repository system, are presented in Appendix K, Section K7.3 of the parent document. Although these analyses are performed using results from TSPA-LA Model v5.000, the conclusions of these analyses also apply to results from TSPA-LA Model v5.005 due to the similarity in the results for the two model versions (Sections 7.3.1.5.6[a], and 7.3.1.5.8[a]).

Expected Annual Dose for 1,000,000 Years—For the time period out to 1,000,000 years after repository closure, the expected annual dose at time τ is computed by a Monte Carlo simulation employing the full detail of the seismic consequences abstraction. As explained in Section 6.1.2.4, this numerical treatment is used due to the complexity of the seismic

consequences abstraction and the necessity to combine nominal corrosion processes with the effects of seismic ground motion events in this modeling case. The use of the Monte Carlo technique produces relatively noisy results as shown on Figure 8.2-11b[a]. Appendix J, Figure J8.4-1, illustrates the computation of expected annual dose from the results of simulations of single seismic events for a few epistemic sample elements, and the variability in annual dose that can result from aleatory uncertainty in the seismic events and from epistemic uncertainty in the model inputs.

The expected dose histories shown on Figure 8.2-11b[a] display two phases for the occurrence of damage to WPs. First, prior to DS failure at roughly 200,000 years (Figure 8.1-4[a]), WPs experience damage primarily from seismic events. Moreover, CDSP WPs are damaged far more frequently than are CSNF WPs (compare Figure 8.3-8a[a] for CSNF WPs and Figure 8.3-8c[a] for CDSP WPs). However, as indicated by Appendix K[a], Figure K7.7.2-2[a], the occurrence of damage to WPs in the first 200,000 years is strongly affected by the uncertainty in the RST for Alloy 22 (*SCCTHRP*). In particular, in sample elements with a large value of *SCCTHRP*, the probability of damage to CDSP WPs can be quite small (output DTN: MO0708CDSPSEIS.000 [DIRS 183007], *FreqDamageCDSP_v5.pdf*).

A second phase begins when the DS fails and the drifts are conceptualized to be filled with rubble. The presence of rubble significantly reduces the probability of further damage to WPs from seismic events (output DTN: MO0708FREQCALC.000 [DIRS 183006], *Rubble_Damage.pdf*). After DS failure, nominal corrosion processes are generally the cause of further damage to WPs, first as SCC failures of lid welds, and at much later times, as patch openings caused by general corrosion. As a consequence, at later times, the expected dose from the combination of nominal corrosion processes and seismic ground motion events (Figure 8.2-11b[a]) resembles the expected dose for the Nominal Modeling Case (Figure 8.2-1[a]). The step-wise increases in the annual dose curves at around 200,000 years, 300,000 years, 500,000 years and 700,000 years are due to immediate increases in the number of WP failures from SCC. These immediate increases in WP failure are caused by the coarse temporal discretization used by WAPDEG v4.07 past 100,000 years (Section 7.3.3.7[a]). Additional discussion of these failures is provided with the Nominal Modeling Case in Section 8.2.1[a].

Section 7.7.1.4[a] presents an analysis of a single realization of expected annual dose for the post-10,000-year period, and illustrates the progression of damage to EBS components as seismic events occur, as well as the effects of nominal corrosion processes on EBS components. Figures 8.3-7[a] through 8.3-12[a] summarize the performance of DS and WP components of the EBS subjected to ground motion and nominal corrosion processes; these results should be contrasted with Figures 8.3-4[a] through 8.3-6[a], which summarize the effects of only the nominal corrosion processes on EBS components.

Appendix K[a] presents sensitivity analyses that determine the contribution to the uncertainty in expected annual dose that derives from individual uncertain inputs. At early times, before DS failure, these analyses identify the RST for Alloy 22, *SCCTHRP*, as the uncertain input that predominantly explains the uncertainty in the expected annual dose (Figure K7.7.2-1[a] and Figure K7.7.2-2[a]). At later times, the temperature dependence parameter for Alloy 22 general corrosion rate, *WDGCA22*, is dominant. Beyond *SCCTHRP* and *WDGCA22*, the analysis identifies a number of other variables with minor contributions to uncertainty in expected annual

dose. However, the lack of smoothness in the expected annual dose results due to the use of the Monte Carlo method inhibits the sensitivity analysis' resolution of the importance of these minor contributors. In addition, the use of the Monte Carlo method precludes sensitivity analyses for intermediate model outputs, such as the movement of several important radionuclides (^{239}Pu, ^{237}Np, and ^{99}Tc) through the repository system, as explained in Appendix K[a], Section K7.7.2[a].

8.2.4.2[a] Seismic Fault Displacement Modeling Case

The revised projections of expected mean annual dose for the Seismic FD Modeling Case are shown on Figure 8.2-13[a]; the figure shows plots for both the (a) 10,000-year period and (b) post-10,000-year period. The expected annual dose takes into account aleatory uncertainty associated with characteristics associated with the number, type and location of DSs and WPs disrupted. The mean, median, and 5th and 95th percentile curves on Figure 8.2-13[a] show uncertainty in the value of the expected annual dose, taking into account epistemic uncertainty associated with incomplete knowledge of the behavior of the physical system during and after the disruptive event. For the 10,000-year postclosure period, the revised maximum mean annual dose is about 1.5×10^{-3} mrem, which is slightly lower than the original projection of 1.8×10^{-3} mrem. Similarly, for the post-10,000-year period, the revised maximum median annual dose is about 1.1×10^{-2} mrem, whereas the original projection was 1.5×10^{-2} mrem. Further comparison of the results of this modeling case is provided in Section 7.3.1.5.7[a].

The individual radionuclide contributions to mean annual dose are shown in the results presented on Figure 8.2-14[a] for both the 10,000-year and post-10,000-year period after closure. The plot for the 10,000-year period (Figure 8.2-14a[a]) shows that ^{99}Tc and ^{129}I dominate the dose for approximately the first 5,000 years after closure and ^{99}Tc and ^{239}Pu dominate the dose for the subsequent 5,000 years. Figure 8.2-14b[a] shows that ^{239}Pu dominates the mean annual dose for the post-10,000-year time period until approximately 200,000 years postclosure. After approximately 200,000 years and until 1,000,000 years postclosure, the radionuclides contributing most to the mean annual dose are ^{242}Pu, ^{237}Np, and ^{226}Ra. These patterns of radionuclide contribution and dominance are identical to those documented in Section 8.2.4.2 of the parent document.

Analyses of single realizations from the Seismic FD Modeling Case are not presented in Section 7.7.1, because this modeling case is a relatively low contributor to the total expected dose (Figure 8.1-3[a]), and because the processes important to radionuclide releases are examined in the analyses for the Waste Package EF Modeling Case (Section 7.7.1.1[a]) and Drip Shield EF Modeling Case (7.7.1.2[a]). The expected annual dose at time τ is computed as the sum of the contributions to dose from all possible preceding fault displacement events, where the dose from each event is weighted by the probability of the event's occurrence (Section 6.1.2.4). As indicated by Equation 6.1.2-25, each realization of expected annual dose is implicitly averaged over the aleatory uncertainty in the number, type and location of WPs damaged by fault displacement. Specifically, the GoldSim component of the TSPA-LA Model computes the dose resulting from fault displacement damage to 100 WPs of each type distributed proportionally among the percolation subregions, and within each subregion, into either seeping or non-seeping conditions. The EXDOC component (EXDOC_LA V2.0, STN: 11193-2.0-00 [DIRS 182102]) of the TSPA-LA Model computes expected annual dose by scaling these results to the expected number of WPs of each type. This implementation is chosen for numerical efficiency. Because

of this implementation, each annual dose history computed by the GoldSim component involves WPs placed in both seeping and non-seeping conditions. Therefore, the analyses presented in Section 7.7.1.2[a] for the Drip Shield EF Modeling Case provide insight into the processes important to radionuclide releases from WPs affected by fault displacement that are in seeping conditions. Similarly, the analyses presented in Section 7.7.1.1[a] for the Waste Package EF Modeling Case provide insight into the processes important to radionuclide releases from WPs affected by fault displacement that are in non-seeping conditions.

Appendix K[a] presents sensitivity analyses that determine the contribution to the uncertainty in expected annual dose that derives from individual uncertain inputs. These analyses identify several variables with moderate influence on the uncertainty in the expected annual dose for the Seismic FD Modeling Case (Figure K7.8.1-1[a] and Figure K7.8.1-2[a] for 10,000 years; and Figure K7.8.2-1[a] and Figure K7.8.2-2[a] for 1,000,000 years). For the first 10,000 years after repository closure, the uncertain inputs with the strongest influence on the uncertainty in expected annual dose are variables that influence the rate of water flow and the dose from ^{99}Tc. In particular, the analysis identifies *SZGWSPDM* (logarithm of scale factor that characterizes uncertainty in groundwater specific discharge) and *INFIL* (pointer variable for determining infiltration condition) as important, because these variables significantly influence the rate of water flow through the natural barriers and, hence, influence the rate of radionuclide transport. Also, before 10,000 years, the analysis identifies the BDCF for technetium (*MICTC99*) as important because ^{99}Tc is a large contributor to dose before 10,000 years. However, the regression model (Figure 7.8.1-2a[a]) that results from considering these three variables explains only part of the uncertainty in expected annual dose; a number of other uncertain inputs are identified as having lesser effects and incrementally improving the regression model.

After 10,000 years, the uncertain inputs with the strongest influence on the uncertainty in expected annual dose are variables that influence the rate of water flow, along with uncertainty in plutonium solubility. In particular, the analysis again identifies the variables *SZGWSPDM* and *INFIL*, along with *WPFLUX* (WP flux splitting factor) and *SEEPPRM* (logarithm of mean fracture permeability in the lithophysal rock units) as important due to the effects that these variables have on water flow through the EBS and natural barriers. Also, the variable *EP1LOWPU* (logarithm of scale factor used to characterize uncertainty in plutonium solubility) is important because plutonium is the dominant contributor to dose after 10,000 years. However, the regression model (Figure K7.8.2-2a[a]) that results from considering these variables explains only part of the uncertainty in expected annual dose; a number of other uncertain inputs are identified as having lesser effects and incrementally improving the regression model.

Sensitivity analyses for intermediate model outputs, such as the movement of radionuclides through the repository system, are not presented for the Seismic FD Modeling Case. Insight into the processes important to radionuclide movement can be obtained from the analyses of radionuclide movement for early failure modeling cases, presented in Appendix K, Section K5. Although these analyses are performed using results from TSPA-LA Model v5.000, the conclusions of these analyses also apply to results from TSPA-LA Model v5.005 due to the similarity in the results for the two model versions (Section 7.3.1.5.7[a]).

8.3[a] DESCRIPTION OF MULTIPLE BARRIER CAPABILITY

As shown on Figure 8-1 of the parent document, the repository system is composed of three primary barriers that include: (1) upper natural barrier (Section 8.3.2.1), (2) engineered barrier system (EBS) (Section 8.3.2.2), and (3) lower natural barrier (Section 8.3.2.3). In this section, both qualitative and quantitative descriptions are presented to explain the performance capabilities of the multiple barriers. As used here, barrier capability is defined as the extent to which a barrier performs its functions. Barrier functions are two-fold: (1) prevent or substantially reduce the water from contacting the waste, and (2) prevent or substantially reduce the release of radionuclides from the repository to the accessible environment.

The analyses presented in this section are intended to address the NRC requirements of 10 CFR 63.115 [DIRS 180319] for multiple barriers. Section 8.3.3[a] of this addendum has been added to the material presented in the parent document. Section 8.3.3[a] contains a quantitative discussion of the capabilities of the individual barriers. This section should be utilized with the material in Section 8.3 of the parent document to provide a complete discussion of the performance characteristics and capabilities of the individual barriers.

8.3.1[a] Radionuclides Selected to Demonstrate Multiple Barrier Capability

As described in Section 8.3.1 of the parent document, twelve radionuclides were selected for analysis in the demonstration of barrier capability. The radionuclides were grouped into the five categories shown below (descriptions slightly modified from parent document):

1. Large initial inventory and short half-life: ^{137}Cs, ^{90}Sr, ^{241}Am, and ^{240}Pu
2. Highly soluble, non-sorbing, long half-life, and major contributor to dose: ^{99}Tc
3. Solubility limited, moderately to strongly sorbing, long half-life, transported in dissolved and colloidal phases, and important contributor to dose: ^{239}Pu and ^{242}Pu
4. Moderately soluble, weakly sorbing in the lower natural barrier, very long half-life, and transported in dissolved phase: ^{237}Np and ^{234}U
5. Strongly sorbed, and contributes to or is produced by decay chain ingrowth: ^{243}Am, ^{230}Th, and ^{226}Ra.

These twelve radionuclides represent a broad range of radioactive decay properties, geochemical behavior, BDCFs, and transport characteristics in geologic media. Because of these diverse properties, these twelve radionuclides provide a means of examining the performance characteristics of the natural and engineered barriers. The inventory decay histories for these twelve radionuclides are shown on Figure 8.3-1[a] for the two compliance periods (i.e., 10,000 years and post-10,000 years); Figure 8.3-2[a] shows the fraction of total activity attributed to each radionuclide.

8.3.2[a] Identification of Barriers for Yucca Mountain Repository

No change.

8.3.2.1[a] Upper Natural Barrier

No change.

8.3.2.2[a] Engineered Barrier System

No change.

8.3.2.3[a] Lower Natural Barrier

No change.

8.3.3[a] Demonstration of Multiple Barrier Capability

While the applicable NRC regulation (10 CFR 63.115 [DIRS 180319]) does not require performance analyses of individual barriers, a model-based demonstration of barrier capability was considered central to explaining and supporting the compliance demonstrations presented earlier in Section 8.1 of the parent document, as well as the revised results in Section 8.1[a]. In the case of the upper natural barrier, the performance characteristics have been analyzed using detailed process-level models (SNL 2007 [DIRS 182145] and SNL 2007 [DIRS 184614]). Performance analyses of the EBS and the lower natural barrier, however, were conducted using the TSPA-LA Model, which is described in Section 6 of the parent document.

In this section, TSPA-LA Model simulation results are presented that provide insights to the intrinsic characteristics of individual barriers that would contribute significantly to the isolation (i.e., containment and confinement) of the nuclear waste. Probabilistic projections for fundamental barrier performance and characteristics are presented that clearly illustrate effectiveness of three principal barriers. As described in Section 8.3 of the parent document, two demonstration modeling cases are used to quantify the capability for the three primary barriers. These demonstration modeling cases are: (1) combined Nominal/Early Failure Modeling Case (representative of the absence of disruptive events), and (2) Seismic GM Modeling Case (representative of the presence of disruptive events). With regard to the combined Nominal/Early Failure Modeling Case, the early failures include both DSs and WPs (Section 6.4.1 and 6.4.2 of the parent report). Because nominal corrosion processes alter the response of the engineered barrier components to seismic events, nominal corrosion processes are also included in the Seismic GM Modeling Case calculation.

8.3.3.1[a] Upper Natural Barrier

The hydrologic effectiveness of the Yucca Mountain upper natural barrier has been evaluated in recent modeling studies of: (1) net infiltration through the surficial soil, (2) three-dimensional flow and deep percolation, and (3) local flow processes determining drift seepage. The recent study of net infiltration (SNL 2008 [DIRS 182145]) provided boundary conditions for the study of three-dimensional (3-D) flow (SNL 2007 [DIRS 184614]) in the unsaturated tuff unit overlying the repository. Based on the UZ flow fields, probabilistic analyses of drift seepage were conducted to study the processes determining drift seepage and to project drift seepage for intact and collapsed drift conditions (SNL 2007 [DIRS 181244]). Collectively, these flow modeling studies and projections provide the basis to describe how well the upper natural barrier

prevents or substantially reduces the rate of water flow through the UZ and to the repository. The effectiveness of the upper natural barrier is described using the following three relative metrics:

1. Net infiltration into the bedrock as a percentage of precipitation rate for the 10,000-year compliance period

2. Spatially averaged drift seepage rate as a percentage of percolation flux (percolation rates are prescribed for the post-10,000-year compliance period in NRC Proposed Rule 10 CFR 63.342(c)(2) [DIRS 178394])

3. Seepage fraction for each percolation subregion for the 10,000-year and post-10,000-year compliance periods.

The first barrier capability metric provides a quantitative demonstration of the effectiveness of the topography and surficial soils. The second and third metrics focus on the effectiveness of the UZ tuff units above and inclusive of the repository horizon. The quantification of these relative metrics is presented for each of the three climate states (BSC 2004 [DIRS 170002], Section 7.1) of the 10,000-year compliance period, namely: (1) present-day (from 0 to 600 years), (2) monsoon (from 600 to 2,000 years), and (3) glacial-transition (from 2,000 to 10,000 years). For the post-10,000-year period, net infiltration and precipitation are not used because the percolation rates are prescribed in NRC Proposed Rule 10 CFR 63.342(c)(2) [DIRS 178394].

In the case of the first metric, net infiltration is the same for the two demonstration modeling cases because the barrier function of surficial soils is independent of the repository conditions. In contrast, the drift seepage (i.e., flow of liquid water into a drift per unit of time per unit area) and seepage fractions (i.e., ratio of WPs experiencing seepage to all WPs in a percolation subregion) are direct functions of hydrologic, thermal, drift degradation, and other repository conditions that depend on modeling cases; thus, these two metrics will have different values for the combined Nominal/Early Failure and Seismic GM Modeling Cases.

Basis for Net Infiltration Metric—To ensure a defensible basis for estimates of net infiltration (i.e., water flux across the soil/bed rock interface), a technical work plan (BSC 2006 [DIRS 177492]) was developed for independent evaluations of the available field data, software, and documentation. Those evaluations confirmed that the field data and supporting information used for the TSPA-LA conformed to appropriate quality assurance requirements. In addition, a new infiltration model, Mass Accounting System for Soil Infiltration and Flow (MASSIF) (SNL 2008 [DIRS 182145], Section 6.5.7), was developed and validated in accordance with SCI-PRO-006, *Models*. This new model of infiltration processes was used to develop projections of net infiltration into the bedrock. These projections were compared with published estimates of net infiltration and recharge efficiencies for other Nevada hydrographic areas/subareas (SNL 2008 [DIRS 182145], Section 7.2.1.2[a] and Figure 7.2.1.2-2[a]). The full technical basis for the model and revised assessment of net infiltration at Yucca Mountain is documented in *Simulation of Net Infiltration for Present-Day and Potential Future Climates* (SNL 2008 [DIRS 182145]). The estimates of precipitation and other meteorological data used are documented in *Data Analysis for Infiltration Modeling: Extracted Weather Station Data*

Used to Represent Present-Day and Potential Future Climate Conditions in the Vicinity of Yucca Mountain (SNL 2006 [DIRS 177081]).

Basis for Drift Seepage Metric—The scientific basis for the projections of three-dimensional UZ flow fields, deep percolation flow, and drift seepage are the end products of more than a decade of studies, including field testing and data collection. The modeling studies have been largely conducted using the well established TOUGH2 family of codes (i.e., TOUGH2 (STN: 10007-1.6-01 [DIRS 161491]), T2R3D (STN: 10006-1.4-00 [DIRS 146654]), and TOUGHREACT (STN: 10396-3.0-00 [DIRS 161256])), which have been subjected to a rigorous validation process using a wide variety of field data from the Yucca Mountain site. More specifically, the UZ flow model and submodels have been tested and corroborated using: (1) water-potential data from the Enhanced Characterization of Repository Block; (2) chloride data from the Exploratory Studies Facility (ESF), Enhanced Characterization of Repository Block, and boreholes; (3) perched water data and pneumatic data from boreholes; (4) carbon-14 data from gas samples; (5) strontium concentrations; and (6) calcite coating (SNL 2007 [DIRS 184614]). Most of the results of the model validation and corroboration studies are published in refereed scientific journals. The full technical basis for the deep percolation flow models and drift seepage is documented in *UZ Flow Models and Submodels* (SNL 2007 [DIRS 184614]) and *Abstraction of Drift Seepage* (SNL 2007 [DIRS 181244]).

Basis for Drift Seepage Fraction Metric—The TSPA-LA Model utilizes an abstraction of UZ flow to determine the percolation flux at the top of the repository horizon. Drift seepage flux is then computed as a function of the local percolation flux (defined as the percolation flux times the flow focusing factor), host rock permeability, and capillary strength (Figure 6.3.3-5 of the parent document). The drift seepage flux calculation is also adjusted to account for drift degradation and a thermal-hydrologic (TH) environment. The seepage fraction is calculated as the ratio of WPs experiencing seepage to all WPs in a percolation subregion; seepage fractions are determined for each WP type. Percolation subregions are described in Section 6.3.2.2.1 of the parent document. The abstractions of drift seepage and seepage fraction are explained in Section 6.3.3 of the parent document; the abstraction of the TH environment is described in Section 6.3.2 of the parent document. The modeling studies and technical basis for these abstractions are documented in *Multiscale Thermohydrologic Model* (SNL 2007 [DIRS 181383]) and *Abstraction of Drift Seepage* (SNL 2007 [DIRS 181244]).

8.3.3.1.1[a] Capability of Upper Natural Barrier to Prevent or Reduce Movement of Water to the Waste

Net Infiltration as Percentage of Annual Precipitation—Net infiltration as a percentage of climate dependent annual precipitation is the metric used to provide insights to the effectiveness of the surficial soils and topography to prevent or reduce the rate of water flow into the UZ. In addition, examining the partitioning of precipitation into the various water balance components (i.e., change in water storage in soil, run-off, evapotranspiration, and sublimation) is also useful in explaining the factors controlling net infiltration. The focus here is on the three climate states in the first 10,000 years (Section 6.3.1 of the parent document), namely, the present-day climate defined as occurring for 600 years; monsoon climate defined as occurring from 600 years to 2,000 years; and the glacial-transition which is defined to occur from 2,000 years to 10,000 years.

The following estimates of mean net infiltration rate as a percentage of mean precipitation rate for each climate state are taken from Tables 6.5.7.4-1 through 6.5.7.4-3 of the recent infiltration study (SNL 2008 [DIRS 182145]), namely:

- Present-day climate: $\bar{I} \sim 8.02\%$ of $\bar{P}$
- Monsoon climate: $\bar{I} \sim 8.69\%$ of $\bar{P}$
- Glacial-transition climate: $\bar{I} \sim 10.38\%$ of $\bar{P}$

where $\bar{I}$ is the mean net infiltration rate as a percentage of $\bar{P}$, the mean precipitation rate. Ranges of net infiltration for the four infiltration scenarios (defined by the 10th, 30th, 50th, and 90th percentiles of spatially averaged infiltration, see Section 6.3.1 of the parent document) can be summarized as follows. Estimated average present-day net infiltration ranges from less than 3 percent of precipitation for the drier 10th percentile infiltration scenario to about 13 percent of precipitation for the 90th percentile infiltration scenario (SNL 2008 [DIRS 182145], Table 6.5.7.1-3). For the monsoon climate, average net infiltration rate estimates for the 10th to 90th percentile infiltration scenarios range from about 3 percent to 17 percent of precipitation (SNL 2008 [DIRS 182145], Table 6.5.7.2-3). For the glacial-transition climate, the average net infiltration rate estimates for the 10th to 90th percentile infiltration scenarios range from about 5 percent to 16 percent of precipitation (SNL 2008 [DIRS 182145], Table 6.5.7.3-3). Note that the ratios of net infiltration to precipitation presented above are averaged over the entire infiltration model domain, not over the repository footprint area.

Water balance components tabulated in *Simulation of Net Infiltration for Present-Day and Potential Future Climates* (SNL 2008 [DIRS 182145]) show that the process of evapotranspiration (i.e., transfer of moisture from soil to the atmosphere by evaporation and transpiration from plants) alone accounts for most of the reduction in infiltration into the surficial soils; this reduction ranges from 85 to 88 percent of the mean precipitation rate (SNL 2008 [DIRS 182145], Tables 6.5.7.4-1 through 6.5.7.4-3). The remainder of the reduction is accounted for by the change in storage of moisture in the soil and surface runoff. The infiltration study contains comparisons with published estimates for other Nevada hydrographic areas/subareas (SNL 2008 [DIRS 182145], Section 7.2.1.2[a] and Figure 7.2.1.2-2[a]).

Seepage Rate as Percentage of Local Percolation Rate—Water entering the UZ as net infiltration from precipitation at the land surface affects the overall hydrological and thermal-hydrological (TH) conditions within the Yucca Mountain UZ. Net infiltration is the ultimate source of percolation through the UZ. Water percolating downward through the UZ is the source for seepage into the drifts. Multi-dimensional modeling of water flow in the UZ rock layers suggests that average percolation flux flowing to the repository footprint is within a few percent of the net infiltration rate (SNL 2007 [DIRS 184614], Section 6.1.4). This means that lateral flow in the Paint Brush non-welded (PTn) tuff, flow focusing in faults in the northern part of the repository, and perched water zones collectively have a small effect on reducing the local percolation rate at the top of the repository horizon. Of the water flow (percolation) arriving at the repository horizon, however, only a small portion results in drift seepage. The reduction from percolation to seepage is the result of two natural processes that divert flow around and away from the emplacement drift; these processes (SNL 2007 [DIRS 181244], Section 6.1.4) are referred to as: (1) the vaporization barrier effect during the thermal period, and (2) the capillary

barrier effect after the thermal period. While the vaporization barrier effect persists for a short time relative to the compliance periods, the capillary barrier effect persists through the period of geologic stability.

The surface soil and topography, the surficial bedrock, and the TSw unit will combine to substantially reduce movement of water from the surface of Yucca Mountain into the emplacement drifts. The combination of reduced infiltration into Yucca Mountain, effects of heat during the thermal period, and capillary barrier effects in the TSw unit, results in a seepage flux that will be substantially reduced from the precipitation flux at the surface. The magnitude of this reduction is shown on Figure 8.3-3[a]. The top figure (a) illustrates the effectiveness of surficial soils and topography in preventing or reducing the rate of water flow into the UZ. The bottom figure (b) illustrates the effectiveness of decay heat and capillary diversion in limiting water movement into the drifts. On Figure 8.3-3a[a], mean spatially-averaged annual precipitation and net infiltration rates are plotted for each of the three climate states in the 10,000-year compliance period. Net infiltration rates are shown to range from approximately 5 percent of precipitation during the present-day climate to over 7 percent of precipitation during the glacial-transition climate. For the post-10,000-year period, the effects of infiltration are implicitly included in the TSPA-LA Model by using the distribution for deep percolation rate as specified in NRC Proposed Rule 10 CFR 63.342(c)(2) (70 FR 53313 [DIRS 178394]), namely, a log-uniform distribution with a range of 13 to 64 mm/yr. The mean value of deep percolation from this distribution, 32 mm/yr, is shown on Figure 8.3-3a[a].

Three mean spatially-averaged drift seepage flux curves are shown on Figure 8.3-3b[a]. The top curve denoted by the dashed line represents a zero-diversion seepage flux that would result if capillary and thermal effects at the drift wall were neglected. This volumetric seepage flux is obtained by applying the average net infiltration flux to the projected area of an intact emplacement drift segment that is 5.1 m long by 5.5 m wide. This zero-diversion seepage flux is compared to the TSPA-calculated seepage fluxes for the two demonstration modeling cases (i.e., the combined Nominal/Early Failure Modeling Case and the Seismic GM Modeling Case) to illustrate the effectiveness of the UZ barrier in limiting the movement of water into the drifts. Note that the average net infiltration flux and, thus, zero-diversion seepage flux used here, is based on a spatial averaging over the entire infiltration model domain. Therefore, the zero-diversion seepage flux is only a representative approximation of the average flux that would occur within the repository footprint.

In contrast, the TSPA-calculated seepage fluxes are based on the percolation flux within the repository footprint. The nominal seepage flux curve shows that seepage varies in the early part of the thermal period when temperatures above 100°C are achieved; as temperatures gradually decrease to lower values, seepage fluxes into the drift increase. The estimate shows that for the 10,000-year compliance period, on average, 2 to 11 percent of the zero-diversion seepage flux occurs as seepage into the drifts. The mean seepage flux for the post-10,000-year period is about 0.095 m^3/yr or about 11 percent of the zero-diversion seepage flux.

The seepage curve for the Seismic GM Modeling Case is discussed next. For the first 10,000 years, the mean seepage flux curve is almost identical to the mean curve for the combined Nominal/Early Failure Modeling Case. This similarity occurs because seismic events of sufficient magnitude that cause drift degradation are unlikely to occur in this time period. The

likelihood of seismic events is described by the mean seismic hazard curve (Figure 6.6-6 of the parent document), which shows that exceedance frequencies on the order of 10^{-4} yr^{-1} correspond to relatively small amplitude vibratory ground motions that are unlikely to result in rockfall (Section 6.6.1.2.1 of the parent document). The drift degradation aspect is based on the simulations of rockfall resulting from seismic ground motion events, which are shown on Figure 7.3.2-19 of the parent document. This figure indicates that for most realizations, drift degradation, quantified in terms of mean rubble volume per meter of drift length (i.e., seismic induced rockfall), is less than 5 m^3/m and 0.5 m^3/m for both the lithophysal and nonlithophysal rock zones, respectively, for the first 10,000 years. The lithophysal rock zones encompass approximately 80 to 85 percent of the emplacement drifts in the repository (Section 6.6.1.2.2). As described in Section 6.3.3.1.3, a mean rubble volume of less than or equal to the 5 m^3/m of drift length for lithophysal rock zone or 0.5 m^3/m for nonlithophysal rock zone indicates that the emplacement drifts are essentially intact and, thus, the seepage rates are determined by nominal flow processes in the repository horizon. Consequently, the values of the seepage rate metric are about the same as those for the combined Nominal/Early Failure Modeling Case.

For the post-10,000-year time period, the Seismic GM Modeling Case seepage rates on Figure 8.3-3b[a] are significantly different from the seepage rates for the combined Nominal/Early Failure Modeling Case. These differences are due to a greater degree of drift degradation and, at late times, to drift collapse in lithophysal rock (i.e., lithophysal rubble volume 60 m^3/m or greater). In nonlithophysal rock, once rockfall has accumulated to an amount of 0.5 m^3/m, capillary diversion is no longer considered, and the seepage rate is set to the percolation rate in the TSPA-LA Model. The spatially averaged mean seepage rates for the Seismic GM Modeling Case increase with time and are larger than those for the combined Nominal/Early Failure Modeling Case. The mean drift seepage rates for the Seismic GM Modeling Case range from 0.109 m^3/yr just after 10,000 years to about 0.434 m^3/yr at 1,000,000 years. For these same two times, the seepage rates, as a percentage of the mean zero diversion seepage rate calculated using the NRC prescribed local percolation rate, are about 12 percent and 48 percent, respectively. Although the effectiveness of capillary diversion is reduced from that of the combined Nominal/Early Failure Modeling Case, it is still substantial in the Seismic GM Modeling Case.

Seepage Fractions for Percolation Subregions—Drift seepage rates are expected to vary spatially over the length of the emplacement drifts. This means that emplacement drifts can exhibit both seeping and non-seeping environments (Section 6.3.3.1.1). In the TSPA-LA Model, this spatial variability is quantified by the seepage fraction. The seepage fraction is the ratio of the number of WPs experiencing seepage to the total WPs in a percolation subregion; separate values are computed for CDSP and CSNF WPs. Distributions of seepage fraction have been computed for each climate and for the five percolation subregions that represent the repository footprint. The calculations were performed using a three-dimensional flow model (BSC 2004 [DIRS 167652]) and a probabilistic approach (SNL 2007 [DIRS 181244], Section 6.5); implementation of the abstraction in the TSPA-LA Model is described in Section 6.3.3.2.2. Seepage fractions for all five percolation regions are provided in Tables 8.3-2[a] through Table 8.3-4[a]. Unlike seepage rates, which vary with time, seepage fractions are constant values that are based on the percolation flux at the end of the simulation period (either 10,000 years or one million years).

For the combined Nominal/Early Failure Modeling Case, statistics for the distributions of the seepage fraction are tabulated in Table 8.3-2[a] for glacial-transition climate (2,000 to 10,000 years) and in Table 8.3-3[a] for post-10,000-year deep percolation rates. The statistics consist of mean and 5th and 95th percentiles for each WP type (i.e., CDSP and CSNF). As can be noted from Table 8.3-3[a], for the post-10,000 year period the mean seepage fraction in percolation subregion 3 is ~ 0.44 for the CDSP and CSNF WP locations. Percolation subregion 5, which represents about 5 percent of the repository footprint, has the highest mean seepage fraction of ~ 0.49 for both CDSP and CSNF WPs. Averaging over the entire repository footprint, the mean seepage fractions for both CDSP and CSNF WPs are ~ 0.4; this indicates that, on average, in the post-10,000-year period, about 60 percent of the emplacement locations in the repository have non-seeping environments for the combined Nominal/Early Failure Modeling Case.

For the Seismic GM Modeling Case, the seepage fraction statistics are tabulated in Table 8.3-4[a] for glacial-transition climate (2,000 to 10,000 years) and Table 8.3-5[a] for post-10,000 year deep percolation rates. As can be noted from Table 8.3-5[a], for the post-10,000 year period the mean seepage fraction in percolation subregion 3 is about 0.72 for both CDSP and CSNF WPs. Percolation subregion 5, which represents about 5 percent of the repository footprint, has the highest mean seepage fractions of ~ 0.75 for both the CDSP and CSNF WP locations. The mean seepage fraction for the overall repository footprint is ~ 0.7 for both CDSP and CSNF WP locations. This indicates that for the post-10,000-year period, about 30 percent of the emplacement locations in the repository are in non-seeping environments for the Seismic GM Modeling Case. It is important to note that the calculations of mean seepage fractions for the Seismic GM Modeling Case account for effects of drift degradation and collapse, which reduce the flow diversion by the capillary barrier (BSC 2004 [DIRS 167652], Section 6.6.3). This is the reason that the seepage fractions are higher than those for the combined Nominal/Early Failure Modeling Case.

8.3.3.2[a] Engineered Barrier System

The basic role of the EBS is to provide long-term containment and to prevent and delay the release of radionuclides into the lower natural barrier. The EBS achieves this design intent by ensuring two important barrier functions: (1) preventing or substantially reducing the amount of seepage water and drift wall condensation that contacts the waste, and (2) preventing or substantially reducing the rate of release of radionuclides from the EBS to the lower natural barrier. The first barrier function is provided by the emplacement drift, DS, and WP OCB (Figure 6.3.6-4), whereas the second function is provided by the various waste forms, the WP OCB, corrosion products from WP internals, and the crushed tuff in the invert. The TSPA-LA Model was used to demonstrate EBS barrier capability; as described in Section 6.1.1, excluded features, events and processes are not considered in this demonstration.

Drip Shield and Waste Package Performance Metrics—To provide a basis for assessing the capability of the EBS to achieve the first barrier function, projections for three barrier capability metrics were developed for the DSs and WPs. The first metric is the DS failure time profile, which is quantified in terms of a cumulative probability distribution function (CDF) for failure time of the DS plates (Titanium Grade 7). DS failure is defined as a hole or opening through the 15-mm thick DS plate; breach of the plate by SCC cracks is not considered as a DS failure

because a crack-damaged DS will still prevent seepage water from contacting the underlying WP. The second capability metric is the WP breach time profile, which is defined as a penetration of the OCB (Alloy 22 [UNS N06022]) by either cracks or patch openings. In the combined Nominal/Early Failure Modeling Case, WP breaches include crack breaches due to SCC of the closure lid welds and patch breaches of the WP OCB due to general corrosion penetrations. In the Seismic GM Modeling Case, crack breaches include seismically-induced SCC of the WP OCB as well as SCC of the closure lid welds; patch breaches include seismically-induced rupture and puncture, in addition to general corrosion penetrations. In addition, a third metric, the capability of the EBS system to retain radionuclides, addresses the performance of the EBS as a whole.

Insights to potential WP breach modes were developed by examining the breach characteristics underlying these metrics for each of the two demonstration modeling cases. For the combined Nominal/Early Failure Modeling Case, the following two WP breach characteristics (Section 6.3.5) were calculated and are presented:

1. Fraction of WPs breached by general corrosion (i.e., patch penetration) as a function of time

2. Fraction of WPs breached by cracks (i.e., nominal process SCC in closure welds) as a function of time.

The following three WP breach characteristics (Section 6.6 of the parent document) for the Seismic GM Modeling Case are presented and discussed:

1. Fraction of WPs breached by nominal and seismic ground motion processes as a function of time

2. Fraction of WP surface area breached by nominal and seismic ground-motion induced SCC cracks per breached WP as a function of time

3. Fraction of WP surface area breached by patches resulting from general corrosion and seismic induced puncture and rupture failure mechanisms per breached WP as a function of time.

In the following discussion, WP performance is generally presented in terms of mean barrier capability metrics and breach characteristics. To illustrate uncertainty in these metrics and characteristics, quantiles (median, 5th, and 95th percentiles) are also shown. It is important to note that the TSPA-LA Model computes WP degradation metrics and breach characteristics for each of five percolation subregions that represent the repository footprint. The graphical results presented in the following sections for the WPs were computed as a weighted average combining all of the five percolation regions to arrive at a representation for the entire repository.

An assessment of the EBS capability as a whole to achieve the second barrier function was developed based on probabilistic projections of mean radionuclide activity (in curies) released from the EBS as a function of time. This barrier capability metric is calculated using the inventory balance equation:

$$\overline{R}_{EBS,k}(\tau \mid \mathbf{e}) = \overline{A}_{T,k}(\tau \mid \mathbf{e}) - \left(\overline{A}_{WP,k}(\tau \mid \mathbf{e}) + \overline{A}_{I,k}(\tau \mid \mathbf{e})\right) \qquad \text{(Eq. 8.3.3-1[a])}$$

where $\overline{R}_{EBS,k}(\tau \mid \mathbf{e})$ is the expected (average over aleatory uncertainty) activity (Ci) of radionuclide *k* released from the EBS; $\overline{A}_{T,k}(\tau \mid \mathbf{e})$ is the expected activity (Ci) of radionuclide *k* in the inventory disposed in the geologic repository (initial inventory decayed through time); $\overline{A}_{WP,k}(\tau \mid \mathbf{e})$ is the expected activity (Ci) of radionuclide *k* retained in the WPs (including the activity still in undegraded waste forms); and $\overline{A}_{I,k}(\tau \mid \mathbf{e})$ is the expected activity (Ci) of radionuclide *k* retained in the invert. The term τ is time, and $\mathbf{e}$ is the set of epistemically uncertain parameters, which are sampled in the Monte Carlo simulation (output DTN: MO0701PLOTSFIG.000 [DIRS 185207], file: *Calculation of expected activity Seismic GMD 10K.doc*). The activity quantities, $\overline{A}_{T,k}(\tau \mid \mathbf{e})$, $\overline{A}_{WP,k}(\tau \mid \mathbf{e})$, and $\overline{A}_{I,k}(\tau \mid \mathbf{e})$, are obtained from the Monte Carlo simulation performed with the TSPA-LA Model.

Basis for Engineered Barrier System Barrier Capability Projections—The conceptual models and mathematical basis for DS and WP degradation can be found in Section 6.3.5. An important aspect to note is that the DS degradation abstraction does not implement spatial variability for general corrosion rates. This means that all DSs in the repository fail in unison at the failure time determined by the general corrosion model and the DS fragility abstraction (Section 6.6.1.2.2.1 of the parent document). The uncertain parameters for DS general corrosion are derived from laboratory data for general corrosion of the Titanium Grade 7 samples and are documented in *General Corrosion and Localized Corrosion of the Drip Shield* (SNL 2007 [DIRS 180778]). Similarly, the experimental basis for the WP degradation models and parameters can be found in *General Corrosion and Localized Corrosion of Waste Package Outer Barrier* (SNL 2007 [DIRS 178519]) and *Stress Corrosion Cracking of Waste Package Outer Barrier and Drip Shield Materials* (SNL 2007 [DIRS 181953]).

Probabilistic projections for DS failure and WP breach time profiles were developed to provide insight into barrier capability (output DTN: MO0801TSPAWPDS.000 [DIRS 185077]). These projections used an optimized version of the TSPA-LA Model v5.005 that excludes all transport calculations to efficiently calculate DS and WP failure under nominal and seismic conditions for the purpose of presenting projections of DS and WP performance. The optimized version of the TSPA-LA Model uses the same Monte Carlo simulation approach as the full TSPA-LA Model, which incorporates aleatory and epistemic uncertainties by means of two separate computational loops:

1. An outer calculation loop that samples values from probability distributions for parameters with epistemic uncertainty using the Latin hypercube sampling technique (Helton and Davis 2002 [DIRS 163475])

2. An inner loop that samples, for each epistemic set, values from probability distributions of parameters describing aleatory uncertainty (i.e., randomness) in the occurrence of events.

The optimized version of the TSPA-LA Model uses the same samples for aleatory and epistemic uncertainty as are used to produce the TSPA-LA Model results shown in Section 8.1[a] and Section 8.2[a].

For the combined Nominal/Early Failure Modeling Case, the probabilistic analysis of DS capability (output DTN: MO0801TSPAWPDS.000 [DIRS 185077], file: v5.005_NC_ 000300.gsm) included general corrosion of the DS plates; other DS corrosion mechanisms such as localized corrosion have been screened out (Section 6.3.5.1 and Table 6.3.5-1). As described in Section 6.3.5, the degradation of the topside of the DS plate is based on a corrosion rate model for an aggressive water chemistry environment (i.e., elevated fluoride concentration), whereas the underside surface degradation is based on a corrosion rate model for water chemistry representative of a benign environment. For the WPs, WAPDEG was applied to analyze WP degradation, taking into account the following processes: general corrosion, microbially influenced corrosion, and SCC in the closure-lid weld region. Localized corrosion of the WPs was analyzed with a standalone model using GoldSim (external to WAPDEG) and was shown not to impact the combined Nominal/Early Failure Modeling Case or the Seismic GM Modeling Case (Section 6.3.5.2.3).

As described in Section 6.4 of the parent document, a DS or WP early failure is characterized as a through wall penetration of a WP or DS caused by manufacturing or handling-induced defects that occurs prior to or at the time of repository closure. In the case of the early DS failure, the penetration of the DS plate is assumed to represent complete failure of the DS. In addition, if an early-failed DS is located in a seeping environment, it is assumed that the underlying WP is completely degraded by localized corrosion processes. In the case of early WP failure, it is assumed that the entire surface of the WP is completely degraded. The probabilities of early failure of a randomly selected DS or WP are sampled from lognormal distributions (Sections 6.4.1.3 and 6.4.2.3).

For the Seismic GM Modeling Case (Section 6.6), analysis of the seismic impacts to the DS and WP degradation was performed by first applying WAPDEG to simulate the nominal corrosion processes, then transferring the calculation results to GoldSim to evaluate damage and breaches caused by vibratory ground motion. Details of the associated model implementation are discussed in Sections 6.6.1.3 and 6.6.2.3 of the parent document.

8.3.3.2.1[a] Engineered Barrier System Capability to Prevent or Reduce Movement of Water to the Waste

The DSs serve as the first engineered feature that prevents seepage and drift wall condensation water from contacting the WPs and thereby the waste forms. The DSs would maintain this barrier function until the 15-mm thick DS plates are fully penetrated by general corrosion or ruptured as a result of seismic events. As explained in Section 6.3.5.1.1, Table 6.3.5-1, localized corrosion of DS plates has been screened out (DTN: MO0706SPAFEPLA.001_R1 [DIRS 185200], FEP 2.1.03.03.0B). The DS capability to achieve the first barrier function is demonstrated considering both nominal general corrosion of the plate (topside and underside surfaces) and seismic induced loading (dynamic and static) causing plate failure (rupture).

The WPs serve as the second feature that prevents water from contacting the waste forms. The WP barrier capability is demonstrated by considering breaches attributed to:

- Nominal corrosion degradation conditions: SCC of the closure-lid weld region (Figure 6.3.5-7) and general corrosion of the WP OCB.

- Seismic ground motion conditions: seismic-induced SCC, rupture, and puncture of the WP OCB, combined with breaches due to nominal corrosion processes. The seismic-induced SCC of the WP OCB is attributed to a local residual stress exceeding a residual tensile stress threshold for SCC initiation and is conceptualized as a tightly spaced network of stress corrosion cracks (Section 6.6.1.1.2). Note that the DS and WP capability analysis results for these conditions also include degradation by the nominal corrosion mechanisms.

It is important to note that the process of liquid water flow through the stress corrosion cracks in the WP OCB has been screened out (Section 6.3.6.1 and DTN: MO0706SPAFEPLA.001_R1 [DIRS 185200], FEP 2.1.03.10.0A). Consequently, liquid seepage water would not contact the waste form until a patch penetration develops in the WP OCB. The significance of SCC to EBS capability to achieve the second barrier function is addressed in Section 8.3.3.2.2[a].

The following sections present results for each performance metric for the EBS capability to prevent or reduce movement of water to the waste, as well as characteristics for breaches of WPs, namely:

- DS failure time for nominal conditions
- WP breach time for nominal conditions
- WP breach characteristics for nominal conditions
- DS failure time for seismic ground motion conditions
- WP breach time for seismic ground motion conditions
- WP breach characteristics for seismic ground motion conditions.

Drip Shield Failure Time Profile for Nominal Conditions—A failure time profile for the DSs was developed via a probabilistic projection of the general corrosion degradation of the DS plates as a function of time. For this performance metric, DS failure under nominal conditions is defined as complete penetration of the DS plate by general corrosion (Section 6.3.5). Degradation of the DS framework is also considered and used in the seismic damage abstraction. However, analyses indicate that DS framework failure does not alter the capability of the DS plates to deflect seepage away from the WPs (Section 6.6.1.2.2.1).

Because spatial variability in DS general corrosion rates is not represented in the TSPA-LA Model (Section 6.3.5.1.2), the distribution of the DS failure times simplifies to a single CDF, representing the uncertainty in the failure time for all the DSs in the repository. To calculate the CDF for DS plate failure times, the WAPDEG software was run with a total of 300 epistemic realizations. Each realization is based on one sampled general corrosion rate for each of the topside and underside plate surfaces from their respective distribution (Table 6.3.5-3).

The epistemic uncertainty in the general corrosion rates for the topside and underside surfaces are represented by CDFs (SNL 2007 [DIRS 180778], Section 8.1[a]) developed from laboratory data. The corrosion rate CDF for the topside is for aggressive corrosion conditions, while the CDF for the underside is for benign corrosion conditions. The distribution of DS plate failure times is shown on Figure 8.3-4[a]. Uncertainty in failure time is dominated by the uncertainty in the general corrosion rate for the topside (Appendix K, Section K4.2, of the parent document); this is because the corrosion rate on the topside of the DS is much greater than that on the underside. The CDF for DS plate failure times has a median value of approximately 290,000 years. A histogram of this failure time profile is presented in Section 8.1[a] (Figure 8.1-4[a]), which shows the majority of the Monte Carlo realizations with DS plate failure times ranging from 270,000 to 340,000 years.

Waste Package Breach Time Profiles for Nominal Conditions—Breach time profiles for the WPs for the Nominal Modeling Case were developed via a probabilistic projection of the breaches consisting of cracks in the closure lid-weld region of the WP OCB (Section 6.3.5.1.1) and corrosion patch penetrations of the WP OCB (Section 6.3.5.1.1). Projections were made for both the CDSP and CSNF WPs over the entire repository. To calculate the breach time profile as a function of time, a total of 300 epistemic realizations were run. Spatial variability in the degradation processes is modeled by the WAPDEG software. Temporal variability in the degradation processes is represented by the temperature-dependent general corrosion rate of the WP OCB (Section 6.3.5.1.2). The breach time profiles for both types of WPs are summarized by the fraction of WPs breached as a function of time, shown on Figure 8.3-5[a]; these plots show curves corresponding to the mean, median, and 5th and 95th percentiles.

Comparing the plots on Figures 8.3-5a[a] and 8.3-5b[a], it is evident that the CDSP and CSNF WP breach time profiles for nominal conditions are very similar. This similarity is explained by the fact that the two WP types have common design characteristics (e.g., OCB material [Alloy 22], OCB thickness [25 mm], and closure-lid weld stress mitigation method [i.e., low plasticity burnishing] for the closure weld surface (Section 6.3.5.1)). A small difference in breach-time profiles is expected because the two WP types have different temperature histories (i.e., CSNF WPs have higher thermal output and therefore a hotter outer surface than the CDSP WPs (SNL 2007 [DIRS 181383], Figure 6.3-82[a])), which affects general corrosion rates. In addition, because the CSNF and CDSP WPs have different nominal diameters and therefore different closure-lid weld volumes, different values for the associated SCC-model parameters for the closure-lid weld region are expected to introduce small differences in the SCC crack breach time profiles for the WPs. Based on the 95th percentile curves, CDSP and CSNF WPs breaches are likely to begin occurring after approximately 170,000 years. The mean curves for both WP types show that approximately 54 percent of the WPs could be breached at one million years as a result of SCC crack penetration and general corrosion patch penetration.

Waste Package Breach Characteristics for Nominal Conditions—To better understand the degree of degradation of the WPs under nominal corrosion conditions in the repository, the model results were analyzed to quantify the fraction of CDSP and CSNF WPs: (1) breached by SCC as a function of time, and (2) breached by general corrosion patches as a function of time. Under nominal conditions, SCC occurs in the closure-lid weld region of the WP OCB and general corrosion occurs over the entire WP OCB surface, including the closure weld region. Additional breach characteristics were calculated to estimate the expected fraction of WP surface

area breached by crack and patch penetrations as a function of time, per breached WP. Because the breach profiles for CDSP and CSNF WPs are very similar, only the nominal corrosion breach characteristics for the CSNF WP are discussed herein. Figure 8.3-6[a] shows the projected fraction of CSNF WPs breached as a function of time, which illustrates the initiation and timing of the two breach modes.

From the 95th percentile curve on Figure 8.3-6a[a], breach of CSNF WPs by SCC becomes more likely to occur after approximately 170,000 years. At the end of the one-million-year period, the mean fraction of the WPs with at least one SCC crack breach is 0.54, or 54 percent of the CSNF WPs in the repository. This result also means that almost half of the CSNF WPs would not be breached by SCC cracks within one million years. Comparing these results with those for the first breach-time profile of CSNF WPs (Figure 8.3-5[a]) confirms that the initial breach of the WPs would be by SCC. It is important to reiterate that the cracks induced by SCC are highly tortuous, tight hairline cracks (SNL 2007 [DIRS 181953], Section 6.7.1). Because of these typical tight hairline crack properties, plus sealing the cracks by corrosion products and mineral precipitates, no water in a liquid phase would flow into the WPs and contact the waste forms; however, diffusion of water vapor through cracks and into the WPs is accounted for in the TSPA-LA Model.

Based on the 95th percentile curve on Figure 8.3-6b[a], the CSNF WP is unlikely to be breached by a general corrosion patch penetration before about 560,000 years. By one million years, the mean fraction of the CSNF WPs with at least one patch breach is approximately 0.09 or 9 percent. This suggests that about 90 percent of the CSNF WPs in the repository would not exhibit general corrosion patch penetrations before one million years. It is important to note that the curves for the 5th percentile and median are absent from Figure 8.3-6b[a] due to the large number of realizations with no patch penetration by general corrosion (i.e., zero occurrences) within one million years.

Drip Shield Failure Time Profile for Seismic Ground Motion Conditions—The mechanical strength properties of the DS plates (i.e., Titanium Grade 7) and framework (i.e., Titanium Grade 29) were specifically selected to perform their barrier function in the seismic environment of the Yucca Mountain site. However, over the very long time periods specified in the NRC regulation, the combination of dynamic loads induced by vibratory ground motion, static loads associated with drift degradation and rubble accumulation, and plate thinning due to general corrosion would ultimately cause failures of the DSs. As outlined in Section 6.6.1.1.2 of the parent document, vibratory ground motion can cause DS plates to:

1. Rupture when the local strain exceeds the ultimate tensile strain
2. Degrade by induced high residual tensile stress resulting in SCC breach.

DS plate failure by large rock block impact in the nonlithophysal zones has been screened out based on low consequence (Section 6.6.1.2.2.1 and DTN: MO0706SPAFEPLA.001_R1 [DIRS 185200], FEP 1.2.03.02.0B). In the lithophysal units, the accumulation of rubble from multiple seismic events and the dynamic motion during a seismic event can generate SCC damaged areas on DSs. Because advective flow through stress corrosion cracks in DSs sealed by corrosion products and mineral precipitates has been screened out (DTN: MO0706SPAFEPLA.001_R1 [DIRS 185200], FEP 2.1.03.10.0B), the DS damage due to SCC is

not included in the TSPA-LA Model. In addition to being affected by dynamic and static loads, the DS plates are subjected to degradation by general corrosion. Failure of the DS framework occurs as a result of buckling that would be caused by the combined processes of general corrosion of the framework and seismic-induced loads. Buckling of the framework does not alter the capability of the DS plates to divert seepage away from the WPs (Section 6.6.1.2.2.1); however, the framework failure does affect the susceptibility of the underlying WPs to seismic damage from subsequent ground motion events because it inhibits the free motion of the underlying WPs and then of the emplacement pallets.

The DS plate failure time profile for seismic ground motion conditions was computed by the TSPA-LA Model using a total of 300 epistemic realizations, with 30 aleatory realizations to represent random sequences of future seismic events for each epistemic realization. The epistemic and aleatory sampled elements are the same as those used to generate results for the Seismic GM Modeling Case for post-10,000 years (Section 8.2.4.1[a]). The failure (rupture) time profile for the DS plates is described by the CDFs presented on Figure 8.3-7[a]. The plot on Figure 8.3-7a[a] shows three types of curves: (1) the set of 300 CDFs constructed from the 30 aleatory realizations for each of the 300 epistemic realizations, (2) the best estimate CDF for DS failure time, and (3) the expected (averaged over epistemic uncertainty) CDF of DS plate failure times. Figure 8.3-7b[a] shows the CDF of expected (averaged over aleatory uncertainty) DS plate failure times, along with the 95 percent confidence interval.

As used here, the best estimate CDF is defined as an unbiased estimate of the CDF based on all the simulation outcomes for the DS plate failure times. Based on this definition, the CDF is constructed directly from all 9,000 realizations (300 epistemic and 30 aleatory) simulated by the TSPA-LA Model; this CDF includes both aleatory uncertainty (randomness) and epistemic uncertainty (uncertainty in knowledge). The best estimate CDF on Figure 8.3-7a[a] has the following statistics: (1) median of ~255,000 years, (2) 5th percentile of 191,000 years, and (3) 95th percentile of ~280,000 years. The long leading tail of the CDF indicates that very few DS plate failures occur before 100,000 years. In fact, only about 50 out of the 9,000 realizations exhibit DS plate failures before 100,000 years; this means that there is approximately a 0.55 percent chance of DS plate failure occurring at or before 100,000 years by seismic events. DS plate failures before 100,000 years are the result of low probability high magnitude seismic events. The probability of DS plate failures increases gradually after 100,000 years as thinning of the DS plate progresses by general corrosion. At about 200,000 years, the DS plate is projected to have thinned to about one-third of its original thickness or ~5 mm (assuming a mean corrosion rate of ~51 nm/yr; DTN: SN0704PADSGCMT.001_R2 [DIRS 182122]), making it much more susceptible to failure. From the best estimate CDF, the average probability of DS plate failure on or before 200,000 years is approximately 6×10^{-2}; after about 300,000 years, the probability of the DS plate failures is effectively one.

The set of 300 CDFs on Figure 8.3-7a[a] is presented to illustrate the range of uncertainty about the best estimate CDF. Each CDF represents the uncertainty introduced by parameters with aleatory uncertainty (e.g., timing of seismic event) and is conditional on the set of parameter values (e.g., general corrosion rates for topside and underside DS plate surfaces) sampled for the given epistemic realization. The spread among the CDFs gives an estimate of uncertainty in DS plate failures associated with epistemically uncertain parameters. The expected CDF highlights the influence of aleatory uncertainties. The expected CDF, which is computed by averaging over

the epistemic uncertainty, represents what should be on average the randomness in the time of DS plate failure. As can be noted from the plot, it is very close to the best estimate CDF except in the tails of the distribution.

The influence of epistemic uncertainty on DS plate failure times is highlighted by the CDF of expected DS plate failure times, which is shown on Figure 8.3-7b[a]. In this case, the CDF was constructed by averaging over the aleatory uncertainty to obtain an expected DS plate failure time for each epistemic realization, then ranking the 300 expected DS plate failure times as a CDF. Recognizing that the accuracy of this CDF is based on only 30 aleatory realizations, the 0.95 confidence interval was computed and plotted on Figure 8.3-7b[a]; this confidence interval provides an estimate of the accuracy of each estimate of expected DS plate failure time.

Waste Package Breach Time Profile for Seismic Ground Motion Conditions—The mechanical design of the CDSP and CSNF WPs, as well as the corrosion properties of the WP OCB material (i.e., Alloy 22), were specifically selected so the WP would perform its barrier function for a wide range of seismic events and corrosion conditions at the Yucca Mountain site. However, over very long time periods, the combination of dynamic impacts and stress and corrosion processes would ultimately cause breaches in the WP OCB. As outlined in Section 6.6.1.1.2, vibratory ground motion can potentially cause WP damage and breaches of the following types:

1. Breaches of the WP OCB caused by SCC (crack penetration)

2. Rupture of the WP OCB as a result of local strain exceeding the ultimate tensile strain (note that rupture can only occur after the WP internals have degraded following an earlier breach in the OCB)

3. Puncture of the WP OCB as a result of rockfall and sharp corners or edges from degraded WP internals.

With regard to the latter two breach modes, rupture can occur while the DSs are intact; puncture can occur after DS failure. In the Seismic Ground Motion Damage Submodel (Section 6.6.1), it is assumed that the WP internals degrade as structural elements when the WP OCB is breached (typically by SCC); this degradation of internals has the effect of making the WPs more susceptible to seismic damage by subsequent events. The cumulative effects from multiple seismic events are analyzed for the time period of one million years.

The statistics on the expected fraction of breached CSNF WPs as a function of time are shown on Figure 8.3-8a[a] for the nominal and seismic processes combined and for the seismic processes only on Figure 8.3-8b[a]. The same statistics for CDSP WPs breached are shown on Figure 8.3-8c[a] and Figure 8.3-8d[a] for the nominal and seismic processes combined, and the seismic processes only, respectively. The mean of the expected fraction of WPs breached under seismic conditions at 200,000 years is projected to be approximately 0.007 for the CSNF WPs (Figure 8.3-8a[a]) and 0.37 for the CDSP WPs (Figure 8.3-8c[a]). In each realization (i.e., combination of epistemic and aleatory sample elements), the fraction of breached WPs, $F_{b,WP}\left(\tau \mid \mathbf{a},\mathbf{e}\right)$, is recorded for each WP type (WP) within each percolation subregion (b) as a function of time (τ). This fraction is determined by:

$$F_{b,WP}(\tau \mid \mathbf{a}, \mathbf{e}) = \min\left[1, fN_{b,WP}(\tau \mid \mathbf{e}) + fS_{b,WP}(\tau \mid \mathbf{a}, \mathbf{e})\right] \qquad \text{(Eq. 8.3.3-2[a])}$$

where $fN_{b,WP}(\tau \mid \mathbf{e})$ is the fraction of WPs of type *WP* within percolation subregion *b* failed by nominal corrosion processes, and $fS_{b,WP}(\tau \mid \mathbf{a}, \mathbf{e})$ is the fraction failed due to seismic events. Because a seismic event affects all WPs within a percolation subregion, $fS_{b,WP}(\tau \mid \mathbf{a}, \mathbf{e})$ can only have the values 0 or 1. The expected fraction of breached WPs, $\bar{F}_{b,WP}(\tau \mid \mathbf{e})$, is estimated for each epistemic sample element as the average of $F_{b,WP}(\tau \mid \mathbf{a}, \mathbf{e})$ over the aleatory sample elements. Thus, before any seismic damage occurs, the expected fraction of breached WPs is equal to the fraction of WPs with nominal corrosion damage. However, in the absence of nominal corrosion damage, $\bar{F}_{b,WP}(\tau \mid \mathbf{e})$ can be viewed as an estimate of the probability that seismic damage has occurred.

At early times before about 200,000 years, breaches of the WPs are primarily due to seismic processes only. Therefore, the expected fraction can be interpreted as a probability that a damaging seismic event has occurred. As shown on Figure 8.3-8b[a], the 95th percentile curve transitions from an expected fraction of 0 to 3.3×10^{-2} (which is 1/30) at approximately 61,000 years for CSNF WPs. That is, for 5 percent of the 300 epistemic realizations, the probability of failure due to seismic processes only before 61,000 years is at least 1/30. For 95 percent of the realizations, this probability is lower than 1/30 (note that the probability of 1/30 is linked to the fact that 30 futures are generated to represent aleatory uncertainty). This same level of confidence is reached for CDSP WPs as early as 500 years indicating that CDSP WPs are much less resistant to seismic damage and that damage is likely to occur much earlier.

As can be noted by comparing Figures 8.3-8b[a] and 8.3-8d[a], the CSNF WPs are far less likely to be breached by seismic events than the CDSP WPs. The higher resistance to seismic damage of the CSNF WPs versus the CDSP WPs is explained by the enhanced structural response capability (i.e., damping) contributed by the massive TAD canister in the CSNF WPs (Section 6.6). For both CDSP and CSNF WPs, however, the initial breaches consist of SCC or rupture induced by seismic damage while breaches at very late times are dominated by nominal general corrosion processes. For purposes of comparison, note that for nominal conditions the initial breaches of the CSNF and CDSP WPs are likely to begin occurring, as shown by the 95th percentile curves after approximately 170,000 years (Figure 8.3-5a[a] and Figure 8.3-5b[a]); these breaches are due to the nominal process SCC in the closure-lid weld region.

Waste Package Breach Characteristics for Seismic Ground Motion Conditions—To develop a quantitative description of the extent of seismic damage to the CDSP and CSNF WPs, probabilistic projections for two breach characteristics were developed: (1) fraction of the WP OCB surface area breached by cracks, and (2) fraction of WP OCB surface area breached by patches. To provide a comparative basis, the two breach characteristics (fraction of WP OCB surface area breached by cracks and by patches) were also computed for the nominal conditions (i.e., in the absence of disruptive events).

The fraction of surface area breached by SCC cracks (i.e., crack area fraction) per breached (crack or patch) CSNF package is shown on Figure 8.3-9[a]. The probabilistic projection for the

Seismic GM Modeling Case is shown on Figure 8.3-9a[a] and for the Nominal Modeling Case on Figure 8.3-9b[a]. Focusing on the plot for the Seismic GM Modeling Case (Figure 8.3-9a[a]), the initial slope of the mean curve indicates that the seismic induced SCC would predominately occur within the first 250,000 years. After about 250,000 years, the slope of the mean curve is much smaller, due to a significant reduction in the probability of further seismic damage. This decrease in the probability of further seismic damage is attributed to the failure of DS plates from seismic induced drift degradation, which progressively fills the emplacement drift with rubble. The accumulation of rubble around the WPs after DS failure, in turn, reduces the probability of damage by dynamic impacts (e.g., WP to pallet impacts).

In terms of the mean crack-breach characteristic for seismic conditions, the peak mean crack-area fraction for the CSNF WP occurs at one million years and is approximately 4.3×10^{-5}. In contrast, the peak mean crack-area fraction for nominal conditions at one million years from Figure 8.3-9b[a] is 6.5×10^{-6}. The slope of the mean curve on Figure 8.3-9b[a] indicates a steady but gradual progression of additional crack breaches in the closure-lid weld region of the WP OCB. In the closure-weld region, additional SCC cracks can initiate over time as general corrosion removes the stress-mitigated layer of the OCB (SNL 2007 [DIRS 181953], Section 8.4.2.1).

The average crack-breach area fraction per breached WP for the CDSP WPs is presented on Figure 8.3-10[a]. The probabilistic projection for the Seismic GM Modeling Case is shown on Figure 8.3-10a[a] and for the Nominal Modeling Case on Figure 8.3-10b[a]. The mean curve for the Seismic GM Modeling Case shows a very rapid rise in the crack-breach area fraction in the first 50,000 years, then gradually transitions to a near horizontal line after about 250,000 years. The near horizontal line again reflects a sharp decrease in the probability of further seismic damage. The timing of this decrease corresponds to the time frame when the DS plates fail (Figure 8.3-7a[a]) and the emplacement drifts are being filled by rubble. The peak mean crack-breach area fraction estimated from Figure 8.3-10a[a] occurs at one million years and is approximately 2.1×10^{-4}. This estimate of a CDSP WP crack-breach open area is almost five times greater than that for a CSNF WP. The greater crack-breach open area for CDSP WPs reflects a greater accumulation of seismic damage, due to the lower resistance to seismic damage for the CDSP WPs (Section 6.6.1.1.2). Focusing on the peak mean crack-breach area fraction for nominal conditions (Figure 8.3-10b[a]), the largest mean value is 7.1×10^{-6}.

The average fraction of surface area breached by patches (i.e., patch area fraction) per breached (crack or patch) CSNF WP is shown on Figure 8.3-11[a] for the Seismic GM Modeling Case and the Nominal Modeling Case. It is important to clarify that patch breaches in the Seismic GM Modeling Case (Figure 8.3-11a[a]) include general corrosion penetrations, ruptures, and punctures of the WP OCB, whereas the patch breaches in the Nominal Modeling Case (Figure 8.3-11b[a]) include only general corrosion penetrations. Comparison of the mean curves for breaches by cracks (Figure 8.3-9[a]) and by patches (Figure 8.3-11[a]), shows that breaches by cracks are more likely to occur than patch breaches. The 5th percentile and median are absent from Figure 8.3-11[a] because of the large number of realizations with no patch breaches.

As can be noted on Figure 8.3-11a[a], the mean curve for the CSNF WP OCB average patch-breach area fraction begins abruptly at approximately 240,000 years. This abrupt increase results from the first occurrence of rupture or puncture in the Seismic GM Modeling Case. Due

to the low probability of seismic events that cause crack damage to CSNF WPs (Section 7.3.2.6.1.3.7 of the parent document), which is a prerequisite for rupture of CSNF WP, as well as the low probability of seismic events that induce ruptures or punctures in the WP OCB (Sections 7.3.2.6.1.3.5 and 7.3.2.6.1.3.6 of the parent document), ruptures and punctures occur in only a few realizations. Accordingly, until about 480,000 years, the mean curve remains relatively flat, because it is determined by the few realizations in which ruptures or punctures occur. After 480,000 years, the mean curve ascends gradually, corresponding to an increasing likelihood that general corrosion penetrations have occurred. The timing of the initiation of the general corrosion patch penetrations is consistent with the mean curve for the nominal conditions shown on Figure 8.3-11b[a]. At the end of one million years, the patch-breach area fraction attributed to seismic conditions is about 2.6×10^{-3}, whereas for nominal conditions, shown on Figure 8.3-11b[a], it is about 2.4×10^{-3}. The similarity between the expected average seismic and nominal patch-breach area fractions indicates that the majority of patch penetrations of the CSNF WP OCB are caused by general corrosion.

Summary statistics for the expected average fraction of CDSP WP surface area breached by patches (i.e., patch area fraction) per breached (crack or patch) CDSP WP are shown on Figure 8.3-12a[a] for the Seismic GM Modeling Case and Figure 8.3-12b[a] for the Nominal Modeling Case. The mean curve for the average patch-breach area fraction for the Seismic GM Modeling Case shows a sharp increase beginning at about 14,000 years and then gradually increases until about 480,000 years. Similar to the results for CSNF WPs, this part of the mean curve is determined by a few realizations in which ruptures and/or punctures occur. Because CDSP WPs are more likely to be damaged by seismic events (Figure 8.3-8c[a]), it is also more likely that CDSP WPs could be ruptured, as evident in the earlier occurrence of patch breaches for CDSP WPs (Figure 8.3-12a[a]) as compared to CSNF WPs (Figure 8.3-11a[a]). At about 480,000 years, general corrosion begins to penetrate the CDSP WP OCB (Figure 8.3-12b[a]). At the end of one million years, the patch-breach area fraction attributed to seismic conditions is about 4.5×10^{-3}, whereas for nominal conditions, shown on Figure 8.3-12b[a], it is about 2.4×10^{-3}. The larger patch-breach area fraction for CDSP WPs for seismic conditions (as compared to nominal conditions) results because damage to CDSP WPs is relatively likely to occur (Figure 8.3-8d[a]). When SCC occurs, the WP OCB begins to corrode from the inside out, effectively doubling the rate of thinning of the WP OCB (Figure 7.7.1-61[a]), and thus increasing the likelihood of general corrosion patch penetrations before one million years. In addition, the WP internals degrade after seismic damage, and thus the early occurrence of SCC increases the probability that ruptures may occur.

Summary of the Capability of the Engineered Barrier System to Prevent or Substantially Reduce Water Contacting the Waste—The capability of the EBS to prevent or limit the movement of water and prevent contact between water and waste depends on the integrity of the DSs and WPs. The performance demonstration for the EBS indicates the DSs remain intact for hundreds of thousands of years and protect the WPs from seepage. Moreover, the majority of WPs remain intact for tens of thousands to hundreds of thousands of years, thus only a fraction of the emplaced waste will be exposed to water during this period.

For the combined Nominal/Early Failure Modeling Case, with early-failed DSs notwithstanding, the performance demonstration projects a distribution of DS plate failure times (Figure 8.3-4[a]) with a median of approximately 290,000 years, with DS plate failure times generally ranging

from 270,000 to 340,000 years (Figure 8.3-4[a]). For the Seismic GM Modeling Case, the best estimate distribution of DS failure times (Figure 8.3-7a[a]) has a median of about 255,000 years, with the average probability of DS failure at or before 200,000 years being approximately 0.06.

With regards to WP performance capability, the projected distributions for the mean fraction of WPs (CDSP and CSNF) breached (Figure 8.3-5[a]) for the Nominal Modeling Case show that at 500,000 years, about 15 percent of WPs would have breaches and at one million years about 54 percent of WPs would be breached. For the Seismic GM Modeling Case, the mean of the expected fraction of WPs breached at 200,000 years is projected to be approximately 0.007 for the CSNF WPs (Figure 8.3-8a[a]) and 0.37 for the CDSP WPs (Figure 8.3-8c[a]). After 200,000 years, nominal corrosion processes start to dominate the expected fraction of breached WPs for the Seismic GM Modeling Case. These performance metrics show that the DSs and WPs together substantially reduce the contact of water with the emplaced waste for hundreds of thousands of years.

8.3.3.2.2[a] Engineered Barrier System Capability to Prevent or Reduce the Rate of Radionuclide Releases

The EBS prevents or substantially reduces the release rate of radionuclides from the waste and prevents or substantially reduces the rate of movement of radionuclides from the repository to the accessible environment. The EBS performs these functions by (1) preventing or substantially reducing the contact of water with the waste, (2) reducing the rate of release due to the slow alteration of the waste and by limited water flux into the WPs, and (3) reducing the rate of radionuclide transport from the waste form to the lower natural barrier. This section summarizes how the different processes contribute to the EBS functions, then presents results demonstrating the EBS capability to prevent or reduce radionuclide releases for undisturbed (combined Nominal/Early Failure Modeling Case) and disturbed (Seismic GM Modeling Case) conditions.

WPs can be breached through general corrosion, through seismic damage, or by early failure. In the latter case, the WPs are assumed to provide no protection from the drift environment starting at the time of repository closure. After WPs are breached, spent nuclear fuel assemblies and HLW canisters will be exposed to the drift environment including air, water vapor, and possibly dripping water. The WP exterior will be subjected to advective seepage flow only if seepage is dripping at the WP location and the DS fails—possibly due to early failure, seismic ground motion, or general corrosion of the DS. Seismic-induced rupture or puncture of the WP as well as general corrosion of the WP can provide pathways for advective flux of water into a breached WP. Stress corrosion cracks will not permit advective flux of water into the WPs; stress corrosion cracks will, however, permit the transfer of oxygen and water vapor by diffusion into the WPs.

Radionuclide transport out of the EBS and into the UZ is dependent on several processes. The processes discussed below are described in detail in Section 6.3.7 and Section 6.3.8 of the parent document. After a WP is breached, radionuclides are not available for release and transport until the following processes have occurred:

- Oxygen and water (liquid water or water vapor) enter a WP enabling degradation of the waste form and formation of a liquid pathway for radionuclide transport. At and above

the boiling point of water in the repository, a liquid pathway is assumed not to exist, and no transport of radionuclides takes place. When only water vapor enters a WP, no transport takes place until a continuous water film is formed on the internal components. This condition occurs when the WP temperature falls below 100ºC and the relative humidity in these WPs reaches 95 percent.

- The fuel cladding or HLW canister degrade and fail. (Note: The barrier capability provided by the intact cladding and canisters is not accounted for in the TSPA-LA Model.)

- The solid waste form degrades. This process provides the rate at which the radionuclides are made available for mobilization and release.

- Radionuclides are mobilized into aqueous solution, aqueous colloidal suspension, or gaseous phase. (Note: Gaseous transport is not included in the TSPA-LA Model because it is not a significant release mode (DTN: MO0706SPAFEPLA.001_R1 [DIRS 185200], FEP 2.1.12.06.0A).)

Once water and oxygen are available within a breached WP, corrosion products from degradation of steel internal components would form. In CSNF WPs, these steel components include the fuel basket guides, the TAD canister, and the inner vessel. In CDSP WPs, these steel components include the central support tube and divider assembly and the inner vessel. The TAD canister shield plug (15 in. thick) in CSNF WPs and the inner lid (9 in. thick) in CDSP WPs are not included as contributing to corrosion products available for sorption because the large mass of these components is localized at one end of the WP and therefore should not appreciably affect transport throughout the rest of the WP (SNL 2007 [DIRS 177407], Section 6.5.2.1.1.2 and Section 6.5.2.1.2).

Mobile radionuclides are transported out of the breached WPs and through the EBS to the UZ. Transport out of the breached WPs can occur by advection, when there is a liquid flux through the WPs, and by diffusion through continuous liquid pathways in the WPs, including thin films of adsorbed water. As noted above, a continuous thin film cannot form until the WP temperature falls below 100ºC and the relative humidity interior to the WPs reaches 95 percent. Diffusive transport through WP corrosion products depends on the water saturation, porosity, temperature, and relative humidity in the WPs. In the TSPA-LA Model, it is assumed that temperature and relative humidity in the WPs are equal to the temperature and relative humidity on the WP outer surfaces. The two transport processes (diffusion and advection) are each a function of the type of penetration through the DSs and WPs and the local seepage conditions. Diffusion can occur through stress corrosion cracks or through general corrosion patches in the WP both with and without liquid flux through the WPs. Advection is not considered through stress corrosion cracks or through corrosion patches in the absence of seepage flux.

The corrosion products from the WP internal components have the potential to strongly sorb actinides. The process of radionuclide sorption onto the WP corrosion products and invert ballast material (crushed tuff) is beneficial to performance because this process can retain radionuclides in the EBS and delay release to the UZ. Because the WP corrosion products are in intimate contact or directly in the flow or diffusion path of the radionuclide source inside the

WPs, retardation by corrosion products inside the WPs will occur. However, note that because corrosion products from the structural steel members of the invert are more localized and not necessarily in any flow path from the WPs, sorption onto corrosion products in the invert is not represented in the TSPA-LA Model.

The volume of liquid water that could contact a WP is the sum of the dripping seepage and any condensation that may occur on the drift wall. The volume of dripping seepage is quantified by the abstraction for drift seepage (Section 6.3.3.1 of the parent document); results from this abstraction are discussed in Section 8.3.3.1.1[a]. The occurrence and volume of condensation are quantified by the Drift Wall Condensation Submodel (Section 6.3.3.2 of the parent report), and results are summarized here.

Within the emplacement drifts, water evaporated from the emplacement drift walls and invert is transported primarily by natural convection from warmer to cooler areas, where it condenses on cooler surfaces such as the drift wall. The rates of evaporation and condensation, as well as the rate of water vapor transport in the emplacement drift, determine the extent of condensation. In-drift condensation is evaluated with the in-drift condensation model (Section 6.3.3.2). This model provides the TSPA-LA Model with both the probability and magnitude of condensation on the drift wall during cool-down. The TSPA-LA Model treats the flow of drift-wall condensation as a source of liquid water to be added to the liquid water entering the drift as seepage. The TSPA-LA Model uses this combined liquid-water source term in the EBS flow and chemical environment calculations.

The in-drift condensation model defines three stages for the occurrence of condensation. Stage 1 is when the drift wall temperature is above the boiling temperature of water at all locations in the drifts. No condensation occurs during Stage 1. Stage 2 is for times between when the first location in a drift drops below the boiling temperature and the last location drops below the boiling temperature. Stage 3 occurs after all WPs (and thus the drift wall) drop below the boiling temperature. Drift-wall condensation results are presented in Tables 8.3-6[a] and 8.3-7[a]. Results in Table 8.3-6[a] show that drift-wall condensation does not occur on CSNF WPs during Stage 2 and that there is a small probability a negligible condensation rate will occur during Stage 3 on a very small fraction of CSNF WPs. Results in Table 8.3-7[a] show that a significant drift-wall condensation rate (approximately 0.5 m^3/yr) will occur on all CDSP WPs (probability of one and mean WP fraction of one) during Stage 2 for approximately 1,000 years. For comparison, mean seepage rates at 1,500 years are presented in Table 8.3-8[a]. During Stage 3, which lasts until about 2,000 years after closure, the probability of condensation decreases dramatically and the condensation rates are negligible. Drift-wall condensation ceases after 2,000 years for both CSNF and CDSP WPs.

The impact of condensation water on the barrier capability of CDSP WPs is not significant because DSs do not fail to perform their water diversion function during the time condensation will occur. Thus, in the TSPA-LA Model condensation water is diverted around the CDSP WPs except possibly in the case of a very small number of early DS failures or in the unlikely event of DS failure by fault displacement.

Activity Releases from the Engineered Barrier System for Combined Early Drip Shield Failure, Early Waste Package Failure, and Nominal Processes

The aspects of EBS performance that determine the release of radionuclides as modeled in the TSPA-LA Model for the combined Nominal/Early Failure Modeling Case can be summarized as follows:

- Nominal processes cause only a single WP breach (output DTN: MO0710ADTSPAWO.000 [DIRS 183752], LA_v5.005_NC_000300_000.gsm) within the 0- to 10,000-year time interval over all the epistemic samples (Section 8.2.1[a]); WP breach is due to SCC of the closure-lid weld.

- Prior to 170,000 years, radionuclide releases from the EBS are determined by processes related to early DS failure and early WP failure.

- After 170,000 years, radionuclide releases from the EBS are determined primarily by processes related to the failure of WPs from nominal processes.

- DS failure for nominal conditions is defined as a complete breach of the DS plate by general corrosion (Section 6.3.5.1). DS failure times are distributed between 270,000 and 340,000 years (Figure 8.1-4[a]).

- The probability of one or more WP early failures is 0.442 (Section 8.2.2). The expected number of WP early failures is 1.09 (Section 8.2.2).

- The probability of one or more DS early failures is 0.0166 (Section 8.2.2). The expected number of DS early failures is 0.018 (Section 8.2.2).

- Early DS failure is assumed to result in WP failure only if the failed DS is located in a seeping environment; otherwise, there is no WP failure and, hence, no radionuclide release. Water flows into the failed WPs as soon as the WP temperature falls below 100ºC and advective transport occurs immediately (Section 6.4.1.3).

- Early WP failure results in releases of radionuclides only by diffusion prior to DS failure by general corrosion. After DS failure, advective transport can occur if the WP is experiencing dripping conditions.

- By about 340,000 years, all DSs have failed and the number of WPs breached by nominal corrosion processes steadily increases (Section 8.3.3.2[a]). As a result, radionuclide releases due to nominal corrosion processes also tend to increase with time (Figure 8.2-1[a]).

- The TSPA-LA Model represents 11,629 WPs (8,213 CSNF WPs and 3,416 CDSP WPs) (Table 6.3.7-1). In CDSP WPs, HLW contains most of the ^{99}Tc with an average initial inventory of 1.01×10^3 g (17.2 Ci) per CDSP WP. In contrast, the DSNF component of waste in a CDSP WP contains 1.58×10^2 g (2.69 Ci) of ^{99}Tc. The amount of ^{99}Tc

contained in the CSNF waste is substantially greater at 7.55×10^3 g (130 Ci) per CSNF WP (Section 6.3.7.1, Table 6.3.7-3, and Table 6.3.7-5).

- At 10,000 years, there is a sharp increase in radionuclide releases (Figure 8.2-6a[a]) resulting from the early failure of CSNF WPs. Diffusive transport from early failed CSNF WPs begins between 9,000 years and 14,000 years, whereas diffusive transport from early failed CDSP WPs begins between 500 years and 3,000 years (Section 7.7.1.1[a]). CSNF WPs are hotter than CDSP WPs (SNL 2007 [DIRS 181383], Section 6.3.5, Figure 6.3-53), with the result that releases from CSNF WPs are delayed until both the WP temperature falls below 100ºC and the relative humidity interior to these packages reaches 95 percent, at which time a continuous thin film of adsorbed water required for diffusive radionuclide transport is assumed to be present (Section 6.3.8.1). Because infiltration rates and temperatures vary across the repository footprint, the time at which a continuous thin film of adsorbed water required for diffusive radionuclide transport begins also varies (Section 6.3.8.1).

- Because ^{99}Tc is assumed to have no solubility limit and to be non-sorbing (Section 6.3.7.5), released technetium moves very rapidly from the EBS to the UZ. The EBS release characteristics of ^{99}Tc are representative of other highly soluble and non-sorbing radionuclides such as ^{129}I.

- Because the Waste Package Early Failure Modeling Case is the most dominant case in the first few thousand years for the combined Nominal/Early Failure Modeling Case, ^{239}Pu is not an important contributor to expected dose over this time period (Figure 8.2-4a[a] and Figure 8.2-6a[a]). Much of the mobilized plutonium sorbs onto stationary corrosion products and its subsequent release depends on the rates of desorption (Section 6.3.8), which results in the slow but steady release of ^{239}Pu from the WP. (Appendix K of the parent document, Figure K5.3.3-4 and Figure K5.3.5-4 illustrate release of dissolved ^{239}Pu from the EBS for early failure of one CDSP WP and one CSNF WP, respectively).

- The initial release of ^{239}Pu from the EBS is primarily from DSNF waste forms, which are conservatively assumed to immediately degrade when a CDSP WP is breached (Section 6.3.7.4.2). The releases of ^{239}Pu later in the first 10,000 years are primarily from HLW, which degrades relatively slowly over time. Releases of ^{239}Pu from CSNF WPs are delayed until diffusive transport begins after about 9,000 years (Section 7.7.1.1[a]).

Figure 8.3-13[a] compares the mean total activity of all radionuclides remaining after decay of the initial inventory to the mean total activity of all radionuclides released from the EBS for the combined Nominal/Early Failure Modeling Case for both compliance periods. The plots indicate that under nominal conditions, including early failure of DSs and WPs, only a small fraction (less than 3.9×10^{-7}) of the activity in the total radionuclide inventory would be released from the EBS in 10,000 years. After one million years, the mean total release would be about 7 percent of the inventory.

Figure 8.3-13[a] indicates that for both the first 10,000 year time period and the post-10,000-year time period, of the 12 radionuclides selected for analysis, ^{99}Tc is the most significant contributor to mean activity release from the EBS, comprising most of the mean total activity released, even though ^{99}Tc provides less than one percent of the total activity 1,000 years after closure (Figure 8.3-1a[a]). The contribution for the other radionuclides selected is much less. In the case of plutonium species, the plots on Figure 8.3-13[a] show the activity of radionuclides transported irreversibly sorbed to colloids (designated by the superscript I) and the total activity of the mass in dissolved phase, and reversibly and irreversibly associated with colloids (designated by the superscript T). For americium, only the total activity is plotted because the colloidal phase is small compared to the dissolved phase.

The release of ^{99}Tc during the first 10,000 years (Figure 8.3-13a[a]) is primarily due to diffusive releases from early failure of WPs and, to a lesser extent, advective releases from early DS failure and concomitant WP failure. Nominal WP degradation processes are not likely to cause WP failures prior to about 170,000 years after closure (Figure 8.3-5[a], as shown by the 95th percentile curve). As a result, average releases from the EBS prior to 170,000 years are determined by processes related to early DS failure and early WP failure. The expected number of early failed WPs is about sixty times greater than the expected number of early failed DSs. In addition, early DS failure is assumed to result in WP failure only if the early failed DS is experiencing seeping conditions. Otherwise, there is no WP failure and, hence, no radionuclide release. Under nominal conditions, approximately 69 percent of the WP locations in the repository have non-seeping conditions (Table 8.3-2[a]); therefore, only about 31 percent of early failed DSs result in failure of the underlying WP. Thus, on average, the number of early failed WPs is about one hundred times greater than the number of failed WPs associated with early-failed DSs. Hence, releases due to early WP failure tend to be substantially greater than releases due to early DS failure.

Furthermore, of those WPs that become breached, radionuclide releases during the first 10,000 years are primarily from the cooler CDSP WPs. As noted above, CSNF WPs are hotter than the CDSP WPs (SNL 2007 [DIRS 181383], Section 6.3.5) with the result that releases from early failed CSNF WPs are delayed until after 9,000 years; whereas releases from early failed CDSP WPs are delayed until after 500 years to allow formation of a continuous thin film of adsorbed water, which is required to initiate diffusive radionuclide transport (Section 6.3.8.1). The initiation of transport from CSNF WPs is illustrated on Figure 8.3-13b[a] by the sharp increases in radionuclide releases at around 10,000 years.

Figure 8.3-1[a] indicates that radionuclides such as ^{90}Sr, ^{137}Cs, and ^{241}Am dominate the total inventory activity at the earliest times. Figure 8.3-13a[a] shows that these radionuclides are released in small amounts from the EBS from early failure of CDSP WPs and/or DSs, and experience only moderate sorption and negligible delay during transport out of the EBS (Section 6.3.7 and Section 6.3.8). Due to the short half-lives of ^{90}Sr and ^{137}Cs, these radionuclides are secondary contributors to the mean total activity releases from the EBS for only a few hundred years. Because of the longer half-life of ^{241}Am, this radionuclide is a secondary contributor to the mean total activity releases until about 2,000 years. A second peak in activity releases of ^{241}Am occurs just after 10,000 years, caused by releases from early failed CSNF WPs (Figure 8.3-13b[a]).

From about 2,000 to 10,000 years, ^{239}Pu and ^{240}Pu are important contributors to mean total activity released. These two radionuclides dominate the total inventory at 10,000 years with ^{239}Pu and ^{240}Pu contributing 52 percent and 40 percent of the mean total activity, respectively (Figure 8.3-1[a]). ^{239}Pu and ^{242}Pu are less mobile solutes that reversibly sorb to stationary corrosion products in the WPs, which reduces releases from the WPs. On Figure 8.3-13[a], the activity releases of ^{239}Pu and ^{242}Pu are shown as totals (denoted by $^{239}Pu^{T}$ and $^{242}Pu^{T}$) of the mass in dissolved phase and the mass sorbed on colloids (reversibly and irreversibly); the activity releases of ^{239}Pu and ^{242}Pu irreversibly sorbed on colloids (only) are denoted by $^{239}Pu^{I}$ and $^{242}Pu^{I}$. The comparison shows that the irreversible colloids contribute only about 1 percent of the mean activity releases of these radionuclides.

The relatively small value of mean total activity release from the EBS after 10,000 years and prior to about 170,000 years (Figure 8.3-13b[a]) is explained by the absence of DS failure (except for early failures) and the limited number of WP failures prior to 170,000 years. As noted above and described in Section 8.3.3.2.1[a], DS failure times range from 270,000 to 340,000 years. In addition, SCC penetrations of the WP closure-lid welds are unlikely to occur before approximately 170,000 years (as shown by the 95th percentile curves on Figure 8.3-9b[a] and Figure 8.3-10b[a]). As SCC penetrations occur, releases from the WPs and EBS increase, as illustrated by the increase in releases of ^{99}Tc at around 170,000 years (Figure 8.3-13b[a]). The amount of activity released from the EBS by moderately soluble and weakly to moderately sorbing radionuclides in the lower natural barrier system (Categories 3 and 4, Section 8.3.1[a]), such as ^{237}Np, ^{242}Pu, and ^{234}U, increases after 200,000 years as well, but substantial increases are not observed until general corrosion failures of WPs begin to occur at about 600,000 years (as shown by the 95th percentile curves; Figures 8.3-11b[a] and 8.3-12b[a]) and subsequent advective releases become significant. However, these releases remain small compared to ^{99}Tc throughout the one-million-year period.

As discussed above, the performance of the EBS in preventing or substantially reducing the rate of radionuclide release to the lower natural barrier is a function of several features and uncertain processes in the EBS. The degree of degradation of the WP is uncertain, spatially variable, and controls the amount and rate of water that may enter the WP and potentially allow degradation of the waste forms. The thermal and chemical environment is also uncertain and spatially variable and affects the degradation rate and characteristics of the waste forms and, more importantly, affects the solubility of the radionuclides in the aqueous phase, as well as the stability of colloids to which radionuclides may be attached. The rate of release is affected by the advective and diffusive transport pathways out of the WPs and through the invert. The transport pathways through the EBS are generally diffusive and their properties are treated as uncertain. Solubility limits significantly control the rate of radionuclide diffusion as they define the concentration gradient through which radionuclides may diffuse. Solubility limits are treated as uncertain except for those radionuclides that are not solubility limited, such as ^{99}Tc (Section 6.3.7.5). Finally, the sorption of radionuclides onto stationary corrosion products from the degraded WPs and internal structural supports is treated as uncertain and affects the release of those radionuclides that are highly sorbed on iron substrates.

To illustrate the resulting uncertainty associated with the release of radionuclide activity (in curies) from the EBS, radionuclide-specific release plots for ^{99}Tc and ^{239}Pu are presented on Figures 8.3-14[a] and 8.3-15[a] for the combined Nominal/Early Failure Modeling Case and both

the first 10,000 year time period and the post-10,000 year time period. Shown on each plot are the mean total inventory for that radionuclide along with the mean release curve and 5th and 95th percentile release curves. These plots illustrate that the mean release is affected by the range of the values of the uncertain parameters used in the analysis as summarized above. As illustrated, the mean release is typically close to the 95th percentile of the uncertain results indicating that the mean release is determined by a relatively few realizations with comparatively large releases. The uncertainty in ^{99}Tc and ^{239}Pu releases prior to 200,000 years is dominated by uncertain parameters that determine the number of early failure WPs and DSs, the degradation rates of HLW glass and CSNF, and the diffusive transport of ^{99}Tc and ^{239}Pu from the waste form to the WP outer barrier (Appendix K, Section K5.3 of the parent document). In addition, uncertainty in the release of ^{239}Pu is also influenced by uncertain parameters that determine the solubility of plutonium and sorption of ^{239}Pu onto stationary corrosion products.

Activity Releases from Engineered Barrier System Due to Seismic Ground Motion Damage of Engineered Barrier System Components

Many of the aspects of EBS performance under nominal and early failure conditions summarized in the preceding discussion are relevant to the Seismic GM Modeling Case. The following factors indicate EBS performance for the Seismic GM Modeling Case:

- Prior to about 170,000 years, radionuclide releases from the EBS are determined by processes related to vibratory ground motion-induced WP failures. The mean release from these processes is significantly greater than the mean release from the combined Nominal/Early Failure Modeling Case (Figure 8.3-13[a] and Figure 8.3-16[a]).

- Between 170,000 to 600,000 years, radionuclide releases from the EBS are determined by contributions from both nominal and vibratory ground motion-induced DS and WP failures (Figure 8.3-8[a]).

- After about 600,000 years, radionuclide releases from the EBS are determined primarily by processes related to the failure of WPs from nominal general corrosion processes (Figure 8.3-6[a]).

- Seismically-induced SCC of the CSNF WPs is not likely to occur before approximately 61,000 years (Figure 8.3-9a[a]), whereas breaches of CDSP WPs may occur much earlier (Figure 8.3-10a[a]). For purposes of comparison, based on the 95th percentile, nominal corrosion breaches of the CSNF and CDSP WPs are not likely to occur before about 170,000 years (Figure 8.3-6a[a]); these breaches, however, are due to nominal process SCC in the closure-lid weld region.

- DS failures by combined seismically-induced rupture and general corrosion are largely distributed between about 40,000 and 300,000 years (Figure 8.3-7[a]) as compared to DS failures by general corrosion alone (under nominal conditions), which are distributed from about 270,000 to 340,000 years (Figure 8.3-4[a]).

- Vibratory ground motion-induced drift collapse during the post-10,000-year period causes the mean seepage fraction to increase to 70 percent as compared to the mean value of 40 percent in the Nominal Modeling Case (Table 8.3-5[a] and Table 8.3-3[a]).

- Much of the mobilized plutonium sorbs onto stationary corrosion products, and its subsequent release depends on the rates of desorption from the corrosion products (Section 6.3.8 of the parent document and Figures 7.7.1-6[a] and 7.7.1-8[a]). ^{242}Pu is a key contributor to expected dose late in the post-10,000-year period (Section 8.1.1.5[a] and Figure 8.2-12[a]).

The EBS capability to prevent or reduce the release of radionuclides in the presence of seismic damage is shown on Figure 8.3-16[a] for both compliance periods.

In the Seismic GM Modeling Case, the CDSP WPs are much more likely to be damaged during 10,000 years after closure (Figure 8.3-8[a]) because the CSNF WPs are much stronger and more failure resistant (Section 7.3.2.6.1). The CSNF WPs include two inner stainless-steel vessels instead of one: namely, an inner vessel and its lid that is similar to the CDSP WPs and an additional stainless-steel TAD canister (SNL 2007 [DIRS 179394], Table 4-3). During the first 10,000 years after closure, the predominant mechanism that causes damage to CDSP WPs is SCC by vibratory ground motion-induced residual stresses in the WP OCB (Figure 8.3-10[a]). The DSs remain intact for seismic events occurring in the first 10,000 years (Figure 8.3-7[a]). As a result, dripping seepage cannot contact the WPs. Therefore, water enters the WP only by vapor diffusion through the cracks in the WP OCB. As CDSP WPs cool and the DSNF and HLW degrade, water films form on WP internals, permitting the diffusive transport of radionuclides through the small cracks and into the invert (Section 6.3.8). Comparing estimates of EBS release of ^{99}Tc shown on Figure 8.3-13[a] with Figure 8.3-16[a] indicates a reduction in EBS capability to retain ^{99}Tc by a factor of about 70 as compared to the combined Nominal/Early Failure Modeling Case. However, the comparison still indicates substantial and similar EBS capability during 10,000 years after closure for the less mobile radionuclides.

Estimates of the EBS release shown on Figure 8.3-16b[a] indicate a reduction in the EBS capability to retain ^{99}Tc by a factor of about 140 at 100,000 years as compared to the combined Nominal/Early Failure Modeling Case. There is also a reduction in EBS capability by a factor of between 4 and 10 for less mobile radionuclides at 100,000 years and one million years, including ^{226}Ra, ^{242}Pu, and ^{237}Np, which are key contributors to dose during the post-10,000-year period. Note that the activity of these radionuclides increases substantially after about 600,000 years when failure of the WPs by general corrosion processes begin to occur. By one million years, the total activity released in both the Seismic GM Modeling Case and the combined Nominal/Early Failure Modeling Case is approximately the same (Figures 8.3-13b[a] and 8.3-16b[a]), indicating that the overall reduction in barrier capability in each case, in terms of total activity released (Figure 8.3-1[a]), is about a factor of 10 after one million years.

The performance of the EBS in preventing or substantially reducing the rate of radionuclide release to the lower natural barrier as a result of combined seismic ground motion-induced degradation and nominal degradation processes is a function of several features and uncertain processes in the EBS. Similar to the combined Nominal/Early Failure Modeling Case, the degree of degradation of the WP controls the amount and rate of water that may enter the WP

and potentially allow degradation of the waste form. The degree of WP degradation is highly uncertain and spatially variable and is significantly influenced by the magnitude and timing of seismic ground motions that are also uncertain. After about 600,000 years (Figure 8.3-11[a]), radionuclide releases from the EBS begin to be determined primarily by processes related to the failure of WPs from nominal processes. Again thermal, chemical, waste-form degradation, and transport processes determine the radionuclide releases from the EBS once WPs are breached. The uncertainty in these processes contributes uncertainty to the projected radionuclide releases from the EBS.

To illustrate the uncertainty associated with the release of radionuclide activity from the EBS, radionuclide-specific release plots for selected radionuclides are presented on Figures 8.3-17[a] to 8.3-22[a] for Seismic GM Modeling Case (which includes degradation processes by nominal general corrosion processes):

- Figure 8.3-17[a]: ^{99}Tc
- Figure 8.3-18[a]: ^{237}Np
- Figure 8.3-19[a]: ^{234}U
- Figure 8.3-20[a]: ^{226}Ra
- Figure 8.3-21[a]: ^{239}Pu
- Figure 8.3-22[a]: ^{242}Pu.

The results in these figures are expected releases (averaged over the aleatory uncertainties) and thus largely reflect the influence of epistemic uncertainties. This series of plots is presented to illustrate the impact of uncertainties on the projections of the EBS radionuclide releases. As can be noted from these plots, the EBS releases for all six radionuclides corresponding to the 95th percentile are consistently close to the corresponding mean release curves but are distant from the 5th percentile curves. This demonstrates that the mean releases are determined by expected releases for a relatively small number of epistemic sample elements for which the expected releases are comparatively large.

8.3.3.3[a] Lower Natural Barrier

As noted earlier, the lower natural barrier component (Section 8.3.2.3) of the repository system includes: (1) the UZ below the repository horizon, and (2) the SZ below the repository that extends downgradient from the repository footprint to the accessible environment. The role of the lower natural barrier is to prevent or substantially reduce the rate of movement of radionuclides from the repository to the accessible environment. The lower natural barrier performs this role through the intrinsic site characteristics that are directly reflected by such factors and processes as:

- Slow advective water transport
- Matrix diffusion and sorption of dissolved phase radionuclides
- Dispersion/dilution of dissolved and colloidal phase radionuclides
- Reversible filtration of colloids that have irreversibly sorbed radionuclides.

These intrinsic site characteristics along with radioactive decay properties of individual radionuclides determine the projected capability of the lower natural barrier. Insights to the

overall effectiveness of the lower natural barrier were developed via probabilistic projections. The projections were generated using the TSPA-LA Model to simulate the evolution of releases from the repository and ensuant radionuclide transport through the UZ and SZ and radionuclide activity at the accessible environment boundary.

To ensure that the capability of the lower natural barrier was examined for a range of release conditions, two demonstration modeling cases were selected:

1. Combined Nominal/Early Failures
2. Seismic GM, including nominal corrosion processes.

The combined Nominal/Early Failure Modeling Case provides insight to barrier capability to reduce radionuclide movement for conditions of early releases from a few early-failed WPs and late releases (e.g., from general corrosion patch penetrations after ~ 400,000 years) from a large number of WPs. The Seismic GM Modeling Case examines the lower natural barrier's capability to reduce radionuclide movement for conditions of releases distributed over both the 10,000-year and post-10,000-year time periods. As described in Section 8.3.3.2[a], the radionuclide releases computed for the Seismic GM Modeling Case occur from a variety of breach modes (e.g., seismic induced SCC cracking, rupture/puncture, and general corrosion patches).

To provide a metric of barrier effectiveness, the activity (in curies) of each radionuclide released from the UZ and SZ was computed using the TSPA-LA Model and the balance equations:

$$\overline{R}_{UZ,k}\left(t\,|\,\mathbf{e}\right)=\overline{A}_{T,k}\left(t\,|\,\mathbf{e}\right)-\left(\overline{A}_{WP,k}\left(t\,|\,\mathbf{e}\right)+\overline{A}_{I,k}\left(t\,|\,\mathbf{e}\right)+\overline{A}_{UZ,k}\left(t\,|\,\mathbf{e}\right)\right) \quad \text{(Eq. 8.3.3-3[a])}$$

$$\overline{R}_{SZ,k}\left(t\,|\,\mathbf{e}\right)=\overline{A}_{T,k}\left(t\,|\,\mathbf{e}\right)-\left(\overline{A}_{WP,k}\left(t\,|\,\mathbf{e}\right)+\overline{A}_{I,k}\left(t\,|\,\mathbf{e}\right)+\overline{A}_{UZ,k}\left(t\,|\,\mathbf{e}\right)+\overline{A}_{SZ,k}\left(t\,|\,\mathbf{e}\right)\right) \quad \text{(Eq. 8.3.3-4[a])}$$

where $\overline{R}_{UZ,k}\left(t\,|\,\mathbf{e}\right)$ and $\overline{R}_{SZ,k}\left(t\,|\,\mathbf{e}\right)$ are the expected activities (in curies) of releases of radionuclide k from the UZ and SZ, respectively. The term $\overline{A}_{T,k}\left(t\,|\,\mathbf{e}\right)$ is the expected total activity of radionuclide k in the inventory (initial inventory decayed through time); $\overline{A}_{WP,k}\left(t\,|\,\mathbf{e}\right)$ is the expected activity of radionuclide k in a WP (including the activity in undegraded waste forms); $\overline{A}_{I,k}\left(t\,|\,\mathbf{e}\right)$ is the expected activity of radionuclide k in the invert; $\overline{A}_{UZ,k}\left(t\,|\,\mathbf{e}\right)$ is the expected activity of radionuclide k in the UZ; and $\overline{A}_{SZ,k}\left(t\,|\,\mathbf{e}\right)$ is the expected activity of radionuclide k in the SZ.

The means of the quantities $\overline{R}_{UZ,k}\left(t\,|\,\mathbf{e}\right)$ and $\overline{R}_{SZ,k}\left(t\,|\,\mathbf{e}\right)$ are denoted by $\overline{\overline{R}}_{UZ,k}\left(t\right)$ and $\overline{\overline{R}}_{SZ,k}\left(t\right)$, respectively, and are compared with the mean EBS releases, $\overline{\overline{R}}_{EBS,k}\left(t\right)$, to provide an indication of barrier capability. The mean percent reduction ($\overline{\overline{PR}}$) in activity achieved by the UZ alone and by the lower natural barrier as a whole is estimated from the equations:

$$\overline{\overline{PR}}_{UZ,k}=\left(1-\left[\overline{\overline{R}}_{UZ,k}\Big/\overline{\overline{R}}_{EBS,k}\right]\right)\times 100 \quad \text{(Eq. 8.3.3-5[a])}$$

$$\overline{\overline{PR}}_{LNB,k} = \left(1 - \left[\overline{\overline{R}}_{SZ,k} \Big/ \overline{\overline{R}}_{EBS,k}\right]\right) \times 100 \qquad \text{(Eq. 8.3.3-6[a])}$$

where $\overline{\overline{R}}_{EBS,k}$, $\overline{\overline{R}}_{UZ,k}$, and $\overline{\overline{R}}_{SZ,k}$ are the peak values (at any time) of the mean activity release of radionuclide *k* within the time period under consideration (i.e., time 0 to 10,000 years and 10,000 years to 1,000,000 years). The calculations of $\overline{\overline{PR}}_{UZ,k}$ and $\overline{\overline{PR}}_{LNB,k}$, which are presented below, can be found in output DTN: MO0701PLOTSFIG.000 ([DIRS 185207], *Releases from UZ & SZ updated.xls*).

In the special case of decay chain radionuclides, the quantities $\overline{R}_{UZ,k}(t \mid \mathbf{e})$ and $\overline{R}_{SZ,k}(t \mid \mathbf{e})$ are typically dominated by ingrowth rather than transport of the individual species. This is the case for ^{230}Th and ^{226}Ra; their activities in the lower natural barrier are generally in secular equilibrium with their respective precursors according to the simple decay chain:

^{234}U (half-life 240,000 yrs) → ^{230}Th (half-life 77,000 yrs) → ^{226}Ra (half-life 1,600 years).

Both ^{230}Th and ^{226}Ra move through the lower natural barrier at significantly slower rates than their precursor ^{234}U (SNL 2008 [DIRS 183750], Table 6.10[a]). As a result, their activities are primarily determined by the chain decay process as opposed to by groundwater transport of their individual species. As documented in Section 6.3.7 of the parent document and Sections 6.3.9[a] and 6.3.10[a], the radionuclide half-life values used in the EBS, UZ, and SZ submodels are from DTN: MO0702PASTREAM.001_R0 [DIRS 179925]. The following discussion uses these half-life values (Table 6.3.9-1[a]).

Basis for Lower Natural Barrier Capability Projections—The conceptual models and mathematical basis for the UZ and SZ transport can be found in Sections 6.3.9 and 6.3.10; those sections also describe the implementation of the UZ and SZ abstractions in the overall TSPA-LA Model. The simulation methodology and abstractions of dissolved and colloidal phase transport are documented in: (1) *Particle Tracking Model and Abstraction of Transport Processes* (SNL 2008 [DIRS 184748]), which describes the UZ transport simulation model; (2) *Site-Scale Saturated Zone Transport* (SNL 2008 [DIRS 184806]); and (3) *Saturated Zone Flow and Transport Model Abstraction* (SNL 2008 [DIRS 183750]), which collectively describe the SZ transport simulation model. The experimental data used to characterize UZ and SZ transport model parameters are documented in *Radionuclide Transport Models Under Ambient Conditions* (SNL 2007 [DIRS 177396]).

The TSPA-LA Model uses a Monte Carlo simulation methodology that incorporates aleatory and epistemic uncertainties into the projections. For the combined Nominal/Early Failure Modeling Case, the epistemic loop performs 300 realizations. For the Seismic GM Modeling Case, the probabilistic projections are based on 9,000 realizations consisting of 300 epistemic and 30 aleatory realizations. The aleatory and epistemic sample elements are the same as those used in the analyses presented in Section 8.3.3.2[a].

8.3.3.3.1[a] Capability of Lower Natural Barrier to Prevent or Substantially Reduce the Rate of Radionuclide Movement

A demonstration of lower natural barrier capability was developed using the TSPA-LA Model to simulate radionuclide movement from the EBS through the combined UZ and SZ groundwater path. The UZ portion includes the Topopah Springs welded (TSw) and Calico Hills nonwelded (CHn) tuffs of the Crater Flat Group. Within the repository footprint, the present-day water table varies from around 730 m to 850 m above mean sea level (BSC 2004 [DIRS 169855], Figure 6.2). For wetter climates such as the monsoon and glacial-transition climates, a water table rise up to 120 m for the wetter climate reduces the length of the UZ transport path (Section 6.3.9). The SZ flow path, which extends 18 km from below the repository footprint to the accessible environment boundary, is composed of volcanic units and alluvium (Section 6.3.10). The projected groundwater transport pathway is southeast from the repository site, transitioning to a southerly direction towards the designated accessible environment boundary in the Amargosa Desert. The first 12 to 14 km of the SZ flow path is in fractured volcanic rocks; the remainder of the 18-km flow path is composed of alluvium. The model components of the TSPA-LA Model account for transport in fractured-porous media and are based on: (1) a dual-continuum approach for the UZ (Section 6.3.9.2), and (2) a dual-porosity approach for the fractured volcanic units and an equivalent-continuum approach for the alluvium in the SZ (SNL 2008 [DIRS 183750], Section 6.3.1).

Probabilistic projections of radionuclide releases for the 12 representative radionuclides selected in Section 8.3.1[a] are used to compute the radionuclide releases (in Ci) (from Equation 8.3.3-3[a] and Equation 8.3.3-4[a]) and mean activity reductions (from Equation 8.3.3-5[a] and Equation 8.3.3-6[a]). The radionuclides considered are: ^{137}Cs, ^{90}Sr, ^{241}Am, ^{240}Pu, ^{99}Tc, ^{239}Pu, ^{242}Pu, ^{237}Np, ^{234}U, ^{243}Am, ^{230}Th, and ^{226}Ra. Of these 12 radionuclides, five are transported in the dissolved phase and reversibly and irreversibly sorbed to colloids, namely: ^{241}Am, ^{240}Pu, ^{239}Pu, ^{242}Pu, and ^{243}Am. The calculations of radionuclide release reductions are based on the total activity of these radionuclides, designated with superscript T; it is noteworthy to mention that the activity releases for these five radionuclides are dominated by the dissolved phase activities.

Barrier Capability for Combined Nominal/Early Failure Modeling Case—The aim of this performance demonstration is to estimate the natural barrier capability for a broad range of undisturbed conditions (i.e., in the absence of disruptive events). As will be shown, the early failures of DSs and WPs produce relatively low mean releases starting immediately at repository closure and persisting for the simulated time period of 1,000,000 years. Added to these releases are radionuclides released due to DS and WP failure by nominal processes that mainly occur in the post-10,000-year period (Section 8.3.3.2.1[a]); these failures ultimately lead to relatively large advective radionuclide releases from a large number of WPs.

Projections of Barrier Capability for 10,000 Years after Closure—The projected mean activity releases from the lower natural barrier, specifically $\overline{\overline{R}}_{SZ,k}(t)$, are shown on Figure 8.3-23[a] for the combined Nominal/Early Failure Modeling Case; this figure also shows the corresponding plot for the projected releases from the EBS for 10,000 years after closure (Figure 8.3-23b[a]). At 10,000 years, the mean of total activity released from the SZ (summed

over all radionuclides) is approximately 6 Ci, compared to the mean total activity released from the EBS of about 15 Ci and the mean total activity in the inventory of about 4×10^7 Ci. ^{99}Tc comprises most of the mean total release from the EBS. Figure 8.3-23[a] indicates an overall reduction in activity release due to the lower natural barrier of about 60 percent, although the reduction varies widely for individual radionuclides, as discussed next.

As shown on Figure 8.3-23b[a], the shapes of the curves for various radionuclides released from the EBS vary as a function of time. The variation in shape provides insights into the capability of the EBS to prevent or reduce the rate of movement of radionuclides from the repository to the lower natural barrier and how this capability changes with time. The slope of the activity release curve for a given radionuclide changes with time and typically starts with a positive slope that gradually decreases to zero prior to becoming negative. This shape is attributed to the interplay of the release rate of a radionuclide from the EBS (or mass retention rate in the EBS) compared to its radioactive decay rate. As shown in Equation 8.3.3-1[a], the activity release of a given radionuclide from the EBS is computed by taking the difference between the activity of the emplaced inventory and that retained in the EBS. The positive slope in the activity release curve indicates that the rate of mass release from the EBS is greater than the effective rate of decay of the emplaced mass, where the effective rate of decay accounts for any ingrowth from decay of a parent radionuclide. A positive slope typically occurs when the release rate out of the EBS is large. When the slope is zero, the release rate from the EBS is the same as the effective decay rate; a negative slope occurs when mass is released from the EBS slower than the effective rate of decay. This is typically the case when the EBS release rate becomes negligible and the slope of the activity release curve approaches the rate of change corresponding to the effective decay rate.

In comparing the peak mean activity radionuclide releases for the large initial inventory group (Section 8.3.1[a]): ^{137}Cs (transported as a solute and reversibly sorbed on colloids); ^{90}Sr (transported as a solute); ^{241}Am (transported as a solute and reversibly and irreversibly sorbed on colloids); and ^{240}Pu (transported as a solute and reversibly and irreversibly sorbed on colloids); the calculations of $\overline{\overline{PR}}_{LNB,k}$ indicate that the lower natural barrier effectively accounts for the following reductions in the activity released from the EBS:

- ^{137}Cs (half-life 30.1 yrs): ~100 percent reduction (from ~40 μCi to ~0 μCi)
- ^{90}Sr (half-life 28.8 yrs): ~100 percent reduction (from ~7 μCi to ~0 μCi)
- ^{241}Am (half-life 433 yrs): ~99.9 percent reduction (from ~3 mCi to ~4 μCi)
- ^{240}Pu (half-life 6,560 yrs): ~99.5 percent reduction (from ~17 mCi to ~80 μCi).

The barrier effectiveness of the UZ is supported by detailed particle tracking calculations (SNL 2008 [DIRS 184748], Sections 6.6.2.1[a], [b], and 6.6.2.2[a], [b]) that indicate mean water transport times (to the water table) from the southern part of the repository on the order of 400 years or longer, which means that any mass of ^{137}Cs and ^{90}Sr released in the southern part of the repository would experience more than 10 half-lives of decay before reaching the water table. Mean transport times from northern repository locations, however, are shorter because of the predominance of flow through fractures. In addition, calculations for the SZ (SNL 2008 [DIRS 183750], Table 6-10[a]) indicate median radionuclide transport times ranging from 42,000 years to greater than 1,000,000 years for cesium species and from 9,000 years to greater

than 1,000,000 years for strontium species (SNL 2008 [DIRS 183750], Table 6-10[a]). In the case of ^{241}Am and ^{240}Pu, reductions in radionuclide activity released are primarily the result of retardation effects arising from a combination of (1) mean seepage fractions that are less than 0.5 (Table 8.3-2[a]), indicating that (on average) more than half of the mass released from the EBS diffuses into the matrix of the UZ; (2) sorption of dissolved phase radionuclides, reversible exchanges from dissolved to colloidal phases, and reversible colloidal filtration; and (3) radionuclide decay occurring during transport through the lower natural barrier.

For ^{99}Tc (half-life 2.13 × 10^5 yrs), $\overline{\overline{PR}}_{LNB,k}$ indicates a reduction of about 62 percent within 10,000 years (~14 Ci to ~5.3 Ci), with the UZ accounting for about three quarters of this reduction. The level of activity reduction of this non-sorbing radionuclide indicates a significant degree of transport through the rock matrix occurring during the first 10,000 years. This effectiveness of the lower natural barrier is due to the interplay of radionuclide transport through the invert and rock matrix, matrix diffusion between fractures and matrix of the UZ, and matrix diffusion in the volcanic units of the SZ in combination with transport time in the SZ. Median transport time for technetium through the SZ is estimated to range from 10 years to about 22,000 years, which means that the capability of the SZ to reduce the rate of movement would be limited for the 10,000-year compliance period. These release characteristics for other highly soluble and non-sorbing radionuclides with long half-lives, such as ^{129}I, are expected to be similar to those of ^{99}Tc.

Regarding projections of $\overline{\overline{PR}}_{LNB,k}$ for radionuclides in the category of low to moderate solubility, low sorption, and long half-life, such as ^{239}Pu, ^{242}Pu, ^{237}Np, and ^{234}U, the reductions in peak mean activities released are estimated to be:

- ^{239}Pu (half-life 2.41 × 10^4 yrs): ~99.6 percent reduction (from ~60 mCi to ~0.3 mCi)
- ^{242}Pu (half-life 3.75 × 10^5 yrs): ~99.1 percent reduction (from ~62 µCi to ~0.5 µCi)
- ^{237}Np (half-life 2.14 × 10^6 yrs): ~78 percent reduction (from ~0.3 mCi to ~77 µCi)
- ^{234}U (half-life 2.46 × 10^5 yrs): ~89 percent reduction (from ~0.1 mCi to ~16 µCi).

With the half-lives of these radionuclides being much greater than 10,000 years, the projected reductions in the activity are primarily attributed to delay in the subsurface transport produced by: (1) the combined processes of matrix diffusion and sorption in the UZ, and (2) matrix diffusion and sorption in volcanic units and sorption in the alluvium of the SZ. With regard to ^{239}Pu and ^{242}Pu, the percent reductions are nearly the same because they have the same sorption properties.

For ^{243}Am, ^{230}Th, and ^{226}Ra, the projected reductions in peak mean activity achieved by the lower natural barrier within 10,000 years after closure are estimated to be:

- ^{243}Am (half-life 7,370 yrs): ~99.8 percent reduction (from ~2 mCi to ~4 µCi)
- ^{230}Th (half-life 7.54 × 10^4 yrs): ~99.4 percent reduction (from ~76 µCi to ~0.5 µCi)
- ^{226}Ra (half-life 1,600 yrs): ~99.9 percent reduction (from ~0.6 mCi to ~0.3 µCi).

More than half of the projected activity reductions in the lower natural barrier are achieved by the UZ. These large reductions occur due to very strong sorption in both the zeolitic and

devitrified tuff layers (Table 6.3.9-2) of the UZ, as well as in the volcanic units and alluvium (Table 6.3.10-2) of the SZ.

Projections of Barrier Capability for Post-10,000 Years after Closure—The plot for the projected mean activity released from the lower natural barrier for the combined Nominal/Early Failure Modeling Case is shown on Figure 8.3-24[a]. Also shown on this figure, is the corresponding projection for mean activity released from the EBS. The peak mean total activity released from the SZ (summed over all radionuclides) is approximately 2.8×10^4 Ci at 800,000 years, compared to the peak mean total activity released from the EBS of about 4×10^4 Ci at 900,000 years. ^{99}Tc comprises most of the mean total release from the EBS. Figure 8.3-24[a] indicates an overall reduction (peak to peak) in activity releases due to the lower natural barrier of about 30 percent.

Of the four radionuclides in the large inventory group (i.e., ^{137}Cs, ^{90}Sr, ^{241}Am, and ^{240}Pu), the inventories for ^{137}Cs and ^{90}Sr are essentially depleted by radioactive decay by 1,000 years (e.g., more than 30 half-lives of decay) after closure (Figure 8.3-1[a]). As a result, there would be no releases of these radionuclides from the EBS or SZ in the post-10,000-year period. In the case of ^{241}Am and ^{240}Pu, however, their total repository inventories are still substantial at 10,000 years (i.e., approximately 1.4×10^4 Ci for ^{241}Am and 1.6×10^7 Ci for ^{240}Pu) (Figure 8.3-1[a]) . Consequently, releases of these radionuclides occur until about 150,000 years.

The calculations of $\overline{\overline{PR}}_{LNB,k}$ for the post-10,000-year period show the following reductions in the peak mean activity of ^{241}Am and ^{240}Pu:

- ^{241}Am (half-life 433 yrs): ~100 percent reduction (from ~0.2 mCi to ~0 mCi)
- ^{240}Pu (half-life 6,560 yrs): ~98 percent reduction (from ~60 mCi to ~1 mCi).

These activity reductions are similar to those projected for the 10,000-year period. Moreover, most of the ^{241}Am activity reduction is accounted for by the UZ portion of the lower natural barrier. In the case of ^{240}Pu, the UZ accounts for about 50 percent of the reduction.

For ^{99}Tc (half-life 2.13×10^5 yrs), the lower natural barrier achieves a reduction of about 5 percent (from $\sim 2.8 \times 10^4$ Ci to $\sim 2.6 \times 10^4$ Ci) at 1,000,000 years. This reduction is predominantly the result of matrix diffusion in the rock layers of the UZ and the volcanic units of the SZ. This activity reduction is considerably smaller than the reductions projected for the 10,000-year period; however, this is due to the fact that the technetium released from the EBS in the first 10,000-year period may not have been released from the SZ within 10,000 years. Note that for ^{99}Tc, the travel time ranges between 10 and 22,190 years within the SZ with a median travel time of 230 years (SNL 2008 [DIRS 183750], Table 6-10[a]). Regarding projections of $\overline{\overline{PR}}_{LNB,k}$ for radionuclides in the category of low to moderate solubility, low sorption, and long half-life, such as ^{239}Pu, ^{242}Pu, ^{237}Np, and ^{234}U, the reductions in peak mean activities released are lower than those for the 10,000-year period. The projected percent reductions are:

- ^{239}Pu (half-life 2.41×10^4 yrs): ~90 percent reduction (from ~0.8 Ci to ~0.08 Ci)
- ^{242}Pu (half-life 3.75×10^5 yrs): ~66 percent reduction (from ~44 Ci to ~15 Ci)

- ^{237}Np (half-life 2.14×10^6 yrs): ~23 percent reduction (from ~16 Ci to ~13 Ci)
- ^{234}U (half-life 2.46×10^5 yrs): ~32 percent reduction (from ~1.5 Ci to ~1 Ci).

With regard to ^{239}Pu and ^{242}Pu, the percent reductions are distinct because of the effects of radioactive decay and ^{239}Pu having a small half-life compared to the 1,000,000-year time period. The UZ accounts for almost half of the reduction in ^{239}Pu and ^{242}Pu activities. In contrast, the UZ accounts for only about one-third of the reduction in ^{237}Np and ^{234}U activities.

In the case of ^{243}Am, ^{230}Th, and ^{226}Ra, the projected reductions achieved by the lower natural barrier are comparable to those for the 10,000-year period. They are estimated to be:

- ^{243}Am (half-life 7,370 yrs): ~99.6 percent reduction (from ~0.2 Ci to ~0.7 mCi)
- ^{230}Th (half-life 7.54×10^4 yrs): ~85 percent reduction (from ~4.5 Ci to ~0.7 Ci)
- ^{226}Ra (half-life 1,600 yrs): ~97.6 percent reduction (from ~28 Ci to ~0.7 Ci).

The UZ portion of the lower natural barrier accounts for about 40 percent of the ^{230}Th activity reduction and about 80 percent of the activity reduction for $^{243}Am^T$ and ^{226}Ra.

Barrier Capability for Seismic Ground Motion Modeling Case—The intent of this demonstration modeling case is to examine the capability of the lower natural barrier under conditions of EBS releases attributed to vibratory ground motion events (i.e., disruptive events). The Seismic GM Modeling Case is particularly relevant because it was shown to be important to projections for the Individual Protection Standard (Section 8.1.1.2[a]). In this demonstration modeling case, damage and failure of the DSs and WPs occur as a result of vibratory ground motion and nominal corrosion processes. Moreover, the WP breach modes are quite varied, including seismic-induced SCC, rupture and puncture, as well as general corrosion penetration of the WP OCB and SCC of the closure-lid welds. These breach modes ultimately lead to a broad range of slow diffusive and fast advective releases to the lower natural barrier.

Projections of Barrier Capability for 10,000 Years after Closure—The projected mean activity released from the lower natural barrier is shown on Figure 8.3-25[a]; also shown on this figure is the corresponding plot for the projected releases from the EBS for 10,000 years after closure. At 10,000 years, the mean of total activity released from the SZ (summed over all radionuclides) is approximately 540 Ci, compared to the mean total activity released from the EBS of about 1,200 Ci and the mean total activity in the inventory of about 4×10^7 Ci. ^{99}Tc comprises most of the mean total release from the EBS. Figure 8.3-25[a] indicates an overall reduction in activity releases due to the lower natural barrier of about 55 percent, although the reduction varies widely for individual radionuclides, as discussed next.

In comparing the peak mean activity radionuclide releases for the large initial inventory group (Section 8.3.1[a]): ^{137}Cs (transported as a solute and reversibly sorbed on colloids); ^{90}Sr (transported solute); $^{241}Am^T$ (transported as a solute and reversibly and irreversibly sorbed on colloids); and $^{240}Pu^T$ (transported as a solute and reversibly and irreversibly sorbed on colloids); the calculations of $\overline{\overline{PR}}_{LNB,k}$ indicate that the lower natural barrier effectively accounts for the following reductions in the peak mean activity:

- ^{137}Cs (half-life 30.1 yrs): ~100 percent reduction (from ~0.6 μCi to ~0 μCi)

- ^{90}Sr (half-life 28.8 yrs): ~100 percent reduction (from ~0.03 μCi to ~0 μCi)
- ^{241}Am (half-life 433 yrs): ~100 percent reduction (from ~73 μCi to ~0 μCi)
- ^{240}Pu (half-life 6,560 yrs): ~99.6 percent reduction (from ~15 mCi to ~55 μCi).

These percent reductions are almost identical to those estimated for the combined Nominal/Early Failure Modeling Case. Also similar is the fact that the UZ accounts for very significant reductions (e.g., 80 to 88 percent) of ^{137}Cs, ^{90}Sr, and ^{241}Am activities. It is worth noting that although the percent reductions are similar, the EBS releases for the Seismic Ground Motion are much higher than those for the combined Nominal/Early Failure Modeling Case (Figure 8.3-23[a]).

The mean activity reduction projected for ^{99}Tc (half-life 2.13×10^5 yrs) for the first 10,000 years is approximately 55 percent (from 941 Ci to 427 Ci), with more than half of the reduction provided by the UZ (output DTN: MO0710PLOTSFIG.000 [DIRS 185207], *Releases from UZ & SZ Updated.xls*). This level of activity reduction for ^{99}Tc is similar to that for the combined Nominal/Early Failure Modeling Case, but the curies released in the Seismic Modeling Case are much higher.

The percent reductions projected for ^{239}Pu, ^{242}Pu, ^{237}Np, and ^{234}U for the lower natural barrier are as follows:

- ^{239}Pu (half-life 2.41×10^4 yrs): ~99.6 percent reduction (from ~48 mCi to ~0.2 mCi)
- ^{242}Pu (half-life 3.75×10^5 yrs): ~99.6 percent reduction (from ~49 μCi to ~0.2 μCi)
- ^{237}Np (half-life 2.14×10^6 yrs): ~81 percent reduction (from ~0.1 mCi to ~20 μCi)
- ^{234}U (half-life 2.46×10^5 yrs): ~93 percent reduction (from ~0.3 mCi to ~22 μCi).

These percent reductions are very similar to those projected for the combined Nominal/Early Failure Modeling Case.

Finally, for ^{243}Am, ^{230}Th, and ^{226}Ra, the projected reductions are estimated to be:

- ^{243}Am (half-life 7,370 yrs): ~100 percent reduction (from ~10 μCi to ~0 μCi)
- ^{230}Th (half-life 7.54×10^4 yrs): ~96.2 percent reduction (from ~11 μCi to ~0.4 μCi)
- ^{226}Ra (half-life 1,600 yrs): ~100 percent reduction (from ~30 mCi to ~0.6 μCi).

These percent reductions are also very similar to those projected for the combined Nominal/Early Failure Modeling Case.

Projections of Barrier Capability for Post-10,000 Years after Closure—The plot for the projected mean activity released from the lower natural barrier is shown on Figure 8.3-26[a]; this figure also shows the corresponding projection for mean activity released from the EBS. The peak mean total activity released from the SZ (summed over all radionuclides) is approximately 3×10^4 Ci at 800,000 years; compared to the peak mean total activity released from the EBS of about 5×10^4 Ci at 800,000 years. ^{99}Tc comprises most of the mean total release from the EBS. Figure 8.3-26[a] indicates an overall reduction (peak to peak) in activity releases due to the lower natural barrier of about 40 percent.

Of the four radionuclides in the large inventory group (i.e., ^{137}Cs, ^{90}Sr, ^{241}Am, and ^{240}Pu), the inventories for ^{137}Cs and ^{90}Sr are essentially depleted by radioactive decay by 1,000 years (e.g., more than 30 half-lives of decay) after closure (Figure 8.3-1[a]). As a result, there would be no releases of these radionuclides from the EBS or SZ in the post-10,000-year period. In the case of ^{241}Am and ^{240}Pu, however, their total repository inventories are still substantial and estimated to be approximately 1.4×10^4 Ci for ^{241}Am and 1.6×10^7 Ci for ^{240}Pu remaining in the repository at 10,000 years after closure.

For the post-10,000-year period, the calculations of $\overline{\overline{PR}}_{LNB,k}$ show the following reductions in the peak mean activity of ^{241}Am and ^{240}Pu:

- ^{241}Am (half-life 433 yrs): ~100 percent reduction (from ~3 μCi to ~0 μCi)
- ^{240}Pu (half-life 6,560 yrs): ~97 percent reduction (from ~0.1 Ci to ~4 mCi).

The UZ accounts for about half of the ^{241}Am activity reductions and nearly all of the ^{240}Pu activity reductions. These reductions are very similar to those estimated for the combined Nominal/Early Failure Modeling Case for the post-10,000-year period.

For ^{99}Tc (half-life 2.13×10^5 yrs), the lower natural barrier is projected to achieve a reduction of about 5 percent (from ~3.3×10^4 Ci to ~3.1×10^4 Ci) at 1,000,000 years. This level of barrier effectiveness is similar to the reduction estimated for the combined Nominal/Early Failure Modeling Case for the post-10,000-year period.

Regarding projections for radionuclides in the category of low-to-moderate solubility; low sorption in the UZ and SZ; and long half-life, such as ^{239}Pu, ^{242}Pu, ^{237}Np, and ^{234}U; the reductions in peak mean activities released are less than those for the 10,000-year period. The projected percent reductions are:

- ^{239}Pu (half-life 2.41×10^4 yrs): ~88 percent reduction (from ~11 Ci to ~1.4 Ci)
- ^{242}Pu (half-life 3.75×10^5 yrs): ~70 percent reduction (from ~200 Ci to ~62 Ci)
- ^{237}Np (half-life 2.14×10^6 yrs): ~20 percent reduction (from ~100 Ci to ~81 Ci)
- ^{234}U (half-life 2.46×10^5 yrs): ~25 percent reduction (from ~14 Ci to ~10 Ci).

The UZ accounts for roughly half of the reductions in ^{239}Pu and ^{242}Pu activity; whereas for ^{237}Np and ^{234}U, it only accounts for about one-quarter of the reductions (output DTN: MO0710PLOTSFIG.000 [DIRS 185207], *Releases from UZ & SZ Updated.xls*). These reductions are very similiar and consistent with those projected for the combined Nominal/Early Failure Modeling Case for the post-10,000-year time period.

In the case of the radionuclides ^{243}Am, ^{230}Th, and ^{226}Ra, the projected reductions are comparable to those shown earlier for the combined Nominal/Early Failure Modeling Case for the post-10,000-year period. The reductions are estimated to be:

- ^{243}Am (half-life 7,370 yrs): ~99.8 percent reduction (from ~3 mCi to ~8 μCi)
- ^{230}Th (half-life 7.54×10^4 yrs): ~89 percent reduction (from ~71 Ci to ~8 Ci)
- ^{226}Ra (half-life 1,600 yrs): ~97 percent reduction (from ~260 Ci to ~8 Ci).

For these three radionuclides, the UZ accounts for one-half or more of the activity reductions (output DTN: MO0710PLOTSFIG.000 [DIRS 185207], *Releases from UZ & SZ Updated.xls*). Again, these reductions are consistent with those projected for the combined Nominal/Early Failure Modeling Case and post-10,000-year time period.

Uncertainty in Projections of Lower Natural Barrier Capability—Uncertainty in the projections of lower natural barrier capability is influenced by uncertainties in of the models for flow and transport processes. The TSPA-LA Model accounts for these epistemic uncertainties by using probabilistic representations of the input parameters in the component models for UZ flow, UZ transport, SZ flow, and SZ transport. In the case of UZ flow and transport (Section 6.3.9), the parameters of primary importance include (1) sorption coefficients for various radionuclides, (2) matrix diffusion coefficient, and (3) infiltration scenario. Important parameters related to groundwater flow (or advection) in the SZ (Section 6.3.10) are: (1) groundwater specific discharge, (2) flowing interval porosity, (3) alluvium effective porosity, and (4) horizontal anisotropy. The process of matrix diffusion is dependent on flowing interval spacing, effective diffusion coefficient, and matrix porosity. The process of radionuclide sorption on the fractured and porous media is a function of the sorption coefficients, bulk density and porosity for various radionuclides, and geologic media. Tables presented in Sections 6.3.9 and 6.3.10 summarize the values and uncertainty distributions for all parameters used in the UZ and SZ transport simulations.

To illustrate the uncertainty associated with the release of radionuclide activity from the lower natural barrier, radionuclide-specific release plots for selected radionuclides are presented on Figures 8.3-27[a] to 8.3-32[a] for combined nominal and seismic ground motion-induced degradation processes:

- Figure 8.3-27[a]: ^{99}Tc
- Figure 8.3-28[a]: ^{237}Np
- Figure 8.3-29[a]: ^{234}U
- Figure 8.3-30[a]: ^{226}Ra
- Figure 8.3-31[a]: ^{239}Pu
- Figure 8.3-32[a]: ^{242}Pu.

The results in these figures are expected releases (averaged over the aleatory uncertainties) and thus largely reflect the impact of epistemic uncertainties. These plots are presented to illustrate the impact of uncertainties on the projections of the lower natural barrier radionuclide releases. As can be noted from these plots, the lower natural barrier releases for all six radionuclides corresponding to the 95th percentile are consistently close to the corresponding mean release curves but are distant from the 5th percentile curves. The aleatory and epistemic sample elements are the same as those used in the analyses presented in Section 8.3.3.2[a].

8.3.3.4[a] Summary of Barrier Capability Demonstration

As illustrated on Figure 8-1 of the parent document, the multiple barriers of the Yucca Mountain repository system consist of three primary barriers: (1) upper natural barrier, (2) EBS, and (3) lower natural barrier. The upper natural barrier consists of the topography and surficial soils of the mountain, the unsaturated tuff units above the repository, and rock strata in which the

repository is constructed. The EBS includes the emplacement drifts, WPs, DSs, waste forms, cladding (associated with the CSNF, DSNF, and naval SNF), pallets, and the drift invert; no credit is taken, however, for cladding performance. The lower natural barrier below the repository includes the unsaturated rock layers beneath the repository as well as the volcanic rock units and the alluvium in the SZ, which extends from the repository site to the designated accessible environment boundary. Collectively, these three barriers function to:

1. Prevent or substantially reduce the rate of movement of water or radionuclides from the repository to the accessible environment, and

2. Prevent or substantially reduce the release of radionuclides from the repository.

Probabilistic projections for two demonstration modeling cases were developed to quantify the capability for the three primary barriers. These two demonstration modeling cases are: (1) combined Nominal/Early Failure Modeling Case (representative of the absence of disruptive events), and (2) Seismic GM Modeling Case (representative of the presence of disruptive events).

Upper Natural Barrier—Barrier capability analyses demonstrate that topography and surficial soils substantially reduce the net infiltration into the underlying UZ rock layers above the repository. For climate states projected for the first 10,000 years after closure, the topography and surficial soils prevent on average about 90 percent or more of the precipitation from entering the underlying UZ rock layers. More specifically, the mean net infiltration rate ($\overline{I}$) as a percentage of precipitation rate ($\overline{P}$) for each climate state is estimated to be: (1) present-day climate: $\overline{I} \sim 8.0$ percent of $\overline{P}$; (2) monsoon climate: $\overline{I} \sim$ 8.7 percent of $\overline{P}$; and (3) glacial-transition climate: $\overline{I} \sim 10.4$ percent of $\overline{P}$.

Of the water ultimately reaching the repository horizon (i.e., Topopah Springs welded [TSw]), only a fraction of the local percolation would enter the emplacement drifts as a result of the capillary barrier effect. This capillary barrier effect diverts ambient water flow around the emplacement drifts (Section 6.3.1.1). Taking this effect into account, the mean drift seepage ($\overline{S}$) is less than 11 percent of mean annual percolation rate for intact drifts, and is less than 12 to 48 percent for degraded drifts, varying with the extent of drift degradation.

These seepage rate reductions indicate that very small fractions of the precipitation and ensuant net infiltration would enter the emplacement drifts.

Engineered Barrier System—The EBS prevents or substantially reduces the release rate of radionuclides from the waste forms and prevents or substantially reduces the rate of movement of radionuclides from the repository to the accessible environment. It performs these functions by virtue of the materials and design of the emplacement drifts, DSs, WPs and waste forms, and WP internals. In addition, the EBS provides for chemical and TH environments that lead to low solubilities for the radionuclides that make up the greatest fraction of the inventory activity. Finally, the EBS environments are such that radionuclide transport from the waste to the UZ is limited to a small fraction of the available inventory (less than 3×10^{-3} percent in 10,000 years and 5 percent in 1 million years), even in the case of seismic-induced mechanical degradation.

Lower Natural Barrier—Projections of barrier capability demonstrate that for large initial inventory, soluble, and short half-life radionuclides, such as ^{137}Cs and ^{90}Sr, the mean activity released from the EBS would be reduced by 100 percent (i.e., they are highly unlikely to reach the accessible environment). For radionuclides with longer half-lives such as ^{241}Am and ^{240}Pu, the mean activity released would be reduced by 97 to 100 percent by the natural barrier. For radionuclides of low to moderate solubility, weak to strong sorption, and long half life, such as ^{237}Np, ^{242}Pu, and ^{239}Pu, mean activity released from the EBS would be reduced by 80 percent to 100 percent before reaching the accessible environment during the 10,000-year period and by 20 percent to 88 percent during the post-10,000-year period. In terms of total mean activity, the lower natural barrier reduces the total mean activity released (primarily due to highly soluble, long half-life, non-sorbing ^{99}Tc) from the EBS by 55 percent for the 10,000-year period, and 5 percent for post-10,000-year period, respectively. These reductions of EBS releases would be achieved by the combination of lower natural barrier processes, including slow advective water transport, matrix diffusion and sorption of dissolved phase radionuclides, dispersion/dilution of dissolved and colloidal phase radionuclides, and reversible filtration of colloidal phase radionuclides, as well as radioactive decay.

The demonstration of barrier capability for the EBS and lower natural barrier was developed using the TSPA-LA Model. The values of the parameters used in the TSPA-LA Model are the same as those used in the demonstration of compliance with the individual and groundwater protection standards presented in Section 8.1[a]. Although uncertainty exists in the parameters and models of the relevant processes that affect the assessment of barrier capability, this uncertainty has been appropriately addressed in the assessments. In summary, these barrier capability projections demonstrate that the multiple barriers increase the confidence that the postclosure performance objectives specified in NRC Proposed Rule 10 CFR 63.113(b) and (c) [DIRS 180319] would be achieved.

INTENTIONALLY LEFT BLANK

Table 8.3-2[a]. Seepage Fractions for CDSP and CSNF Waste Packages for Combined Nominal/Early Failure Modeling Case for Glacial-Transition Climate, 2,000 to 10,000 Years

Percolation Subregion		Seepage Fraction for CDSP Waste Packages			Seepage Fraction for CSNF Waste Packages		
Subregion Index	Quantile Range	5th Percentile	Mean	95th Percentile	5th Percentile	Mean	95th Percentile
1	$p < 0.05$	0.0031	0.0881	0.2764	0.0020	0.0887	0.2823
2	$0.05 \le p < 0.30$	0.0261	0.2292	0.5782	0.0217	0.2308	0.5780
3	$0.30 \le p < 0.70$	0.0448	0.3306	0.7395	0.0455	0.3294	0.7439
4	$0.70 \le p < 0.95$	0.0453	0.3846	0.7955	0.0431	0.3848	0.7998
5	$p \ge 0.95$	0.0880	0.4656	0.8447	0.0870	0.4666	0.8386
Repository Average		0.0441	0.3134	0.6898	0.0424	0.3134	0.6950

Source: Output DTN: MO0710PLOTSFIGS.000 [DIRS 185207], file: LA_v5.005_NC_000300_004_Seepage_Fraction.xls.

NOTE: The repository average values are based on weighted averages for each realization using the percolation subregion quantile ranges.

Table 8.3-3[a]. Seepage Fractions for CDSP and CSNF Waste Packages for Combined Nominal/Early Failure Modeling Case for Post-10,000-Year Period

Percolation Subregion		Seepage Fraction for CDSP Waste Packages			Seepage Fraction for CSNF Waste Packages		
Subregion Index	Quantile Range	5th Percentile	Mean	95th Percentile	5th Percentile	Mean	95th Percentile
1	$p < 0.05$	0.0092	0.1251	0.3166	0.0082	0.1251	0.3121
2	$0.05 \le p < 0.30$	0.0623	0.3393	0.6525	0.0617	0.3402	0.6555
3	$0.30 \le p < 0.70$	0.0933	0.4382	0.8072	0.0949	0.4369	0.7943
4	$0.70 \le p < 0.95$	0.0626	0.4365	0.8464	0.0606	0.4364	0.8439
5	$p \ge 0.95$	0.0941	0.4935	0.8872	0.0934	0.4944	0.8802
Repository Average		0.0750	0.4001	0.7483	0.0784	0.3999	0.7449

Source: Output DTN: MO0710PLOTSFIGS.000 [DIRS 185207], file: LA_v5.005_NC_000300_000_Seepage_Fraction.xls.

NOTE: The repository average values are based on weighted averages for each realization using the percolation subregion quantile ranges.

Table 8.3-4[a]. Seepage Fractions for CDSP and CSNF Waste Packages for Seismic Ground Motion Modeling Case for Glacial-Transition Climate, 2,000 to 10,000 Years

Percolation Subregion		Seepage Fraction for CDSP Waste Packages			Seepage Fraction for CSNF Waste Packages		
Subregion Index	Quantile Range	5th Percentile	Mean	95th Percentile	5th Percentile	Mean	95th Percentile
1	$p < 0.05$	0.0031	0.0881	0.2764	0.002	0.0887	0.2823
2	$0.05 \le p < 0.30$	0.0261	0.2292	0.5782	0.0217	0.2308	0.578
3	$0.30 \le p < 0.70$	0.0448	0.3306	0.7395	0.0455	0.3294	0.7439
4	$0.70 \le p < 0.95$	0.0453	0.3846	0.7955	0.0431	0.3848	0.7998
5	$p \ge 0.95$	0.088	0.4656	0.8447	0.087	0.4666	0.8386
Repository Average		0.0441	0.3134	0.6898	0.0424	0.3134	0.6950

Source: Output DTN: MO0710PLOTSFIGS.000 [DIRS 185207], file: LA_v5.005_SM_009000_001_Seepage_Fraction.xls.

NOTE: The repository average values are based on weighted averages for each realization using the percolation subregion quantile ranges.

Table 8.3-5[a]. Seepage Fractions for CDSP and CSNF Waste Packages for Seismic Ground Motion Modeling Case for Post-10,000-Year Period

Percolation Subregion		Seepage Fraction for CDSP Waste Packages			Seepage Fraction for CSNF Waste Packages		
Subregion Index	Quantile Range	5th Percentile	Mean	95th Percentile	5th Percentile	Mean	95th Percentile
1	$p < 0.05$	0.3252	0.4666	0.6965	0.3231	0.4673	0.6923
2	$0.05 \le p < 0.30$	0.3077	0.6484	0.9164	0.3089	0.6491	0.9173
3	$0.30 \le p < 0.70$	0.309	0.7196	0.9725	0.3114	0.7193	0.975
4	$0.70 \le p < 0.95$	0.231	0.7051	0.9793	0.226	0.7041	0.9803
5	$p \ge 0.95$	0.3076	0.7525	0.9878	0.3107	0.7518	0.9869
Repository Average		0.2909	0.6871	0.9450	0.2912	0.6870	0.9465

Source: Output DTN: MO0710PLOTSFIGS.000 [DIRS 185207], file: LA_v5.005_SM_009000_003_Seepage_Fraction.xls.

NOTE: The repository average values are based on weighted averages for each realization using the percolation subregion quantile ranges.

Table 8.3-6[a]. Drift Wall Condensation for CSNF Waste Packages for Stage 2 and Stage 3 Condensation

Percolation Subregion	CSNF Waste Packages							
	Stage 2				Stage 3			
	Probability	Mean WP Fraction	Mean Flux (m^3/yr)	Mean Duration	Probability at 1,500 Years	Mean WP Fraction	Mean Flux (m^3/yr) at 1,500 Years	Mean Duration
1	0	0	0	NA	0.020	0.020	7.50E-05	750 to 2,000 years
2	0	0	0	NA	0.023	0.023	6.74E-05	750 to 2,000 years
3	0	0	0	NA	0.020	0.020	7.94E-05	750 to 2,000 years
4	0	0	0	NA	0.0067	0.0067	6.95E-06	750 to 2,000 years
5	0	0	0	NA	0.010	0.010	4.78E-05	750 to 2,000 years

Source: Output DTN: MO0801TSPAMVAC.000 [DIRS 185080], file: *condensation_rates_and_fractions.xls.*

NOTE: Drift-wall condensation fraction and flux are the same for both the combined Nominal/Early Failure and Seismic Ground Motion Modeling Cases.

Table 8.3-7[a]. Drift Wall Condensation for CDSP Waste Packages for Stage 2 and Stage 3 Condensation

Percolation Subregion	CDSP Waste Packages							
	Stage 2				Stage 3			
	Probability	Mean WP Fraction	Mean Flux (m^3/yr)	Mean Duration	Probability at 1,500 Years	Mean WP Fraction	Mean Flux (m^3/yr) at 1,500 Years	Mean Duration
1	1	1	0.54	0 to 1,000 years	0.020	0.020	6.78E-05	750 to 2,000 years
2	1	1	0.54	0 to 1,000 years	0.017	0.017	5.97E-05	750 to 2,000 years
3	1	1	0.54	0 to 1,000 years	0.017	0.017	7.16E-05	750 to 2,000 years
4	1	1	0.54	0 to 1,000 years	0.0033	0.0033	6.00E-06	750 to 2,000 years
5	1	1	0.54	0 to 1,000 years	0.010	0.010	4.32E-05	750 to 2,000 years

Source: Output DTN: MO0801TSPAMVAC.000 [DIRS 185080], file: *condensation_rates_and_fractions.xls.*

NOTE: Drift-wall condensation fraction and flux are the same for both the combined Nominal/Early Failure and Seismic Ground Motion Modeling Cases.

Table 8.3-8[a]. Mean Seepage Rates for Waste Packages during Stage 2 and Stage 3 Condensation

Percolation Subregion		Mean Seepage Rates (m^3/yr) 0 to 2,000 years (Seepage at 1,500 years)	
Subregion Index	Quantile Range	CNSF Waste Packages	CDSP Waste Packages
1	$p < 0.05$	0.011176	0.011055
2	$0.05 \le p < 0.30$	0.051718	0.051666
3	$0.30 \le p < 0.70$	0.073576	0.073266
4	$0.70 \le p < 0.95$	0.080291	0.079843
5	$p \ge 0.95$	0.11245	0.11025
Repository Average		0.068614	0.068249

Source: Output DTN: MO0801TSPAMVAC.000 [DIRS 185080], file: *condensation_rates_and_fractions.xls*.

NOTES: Mean seepage flux is the same for both the Nominal/Early Failure and Seismic Ground Motion Modeling Cases over the first 2,000 years.

The repository average values are weighted averages using the percolation subregion quantile ranges.

8.4[a] VALIDITY AND DEFENSIBILITY OF PERFORMANCE DEMONSTRATION

The validation activities are presented in Section 7 of the parent document and an additional set of analyses are presented in Section 7[a] of this addendum. Any additions to the description of the TSPA-LA Model presented in Section 6 of the parent document are presented in Section 6[a]. The technical basis for the component models and TSPA input database is documented in supporting model reports. The parent document and supporting documentation were prepared in a manner that would ensure the technical basis is auditable and traceable so as to facilitate the licensing review.

The issuance of this addendum reflects the TSPA methodology defined in the parent document, which specifies:

- Continued scrutiny of the conceptual and mathematical models through internal and external peer reviews
- Further development and testing of TSPA component models and submodels
- Statistical analysis of data and development of improved characterizations of uncertainty.

In this addendum, the issues identified in Appendix P of the parent document have been addressed, the rationale for their use explained, and their impact on postclosure performance metrics evaluated.

This section provides a summary of the specific YMP technical and programmatic activities conducted to ensure that the DOE postclosure performance demonstration is suitable to support the LA for the nuclear waste repository at Yucca Mountain. This section has not changed and applies to the work presented in this addendum.

8.4.1[a] Validation of TSPA Model and Component Models

No change.

8.4.2[a] Verification and Validation of TSPA Software and Input Data

No change.

8.4.3[a] Uncertainty Characterization Reviews

No change.

8.4.4[a] Corroboration of TSPA-LA Results

No change.

8.4.5[a] Peer Reviews of YMP TSPA Methodology

No change.

INTENTIONALLY LEFT BLANK

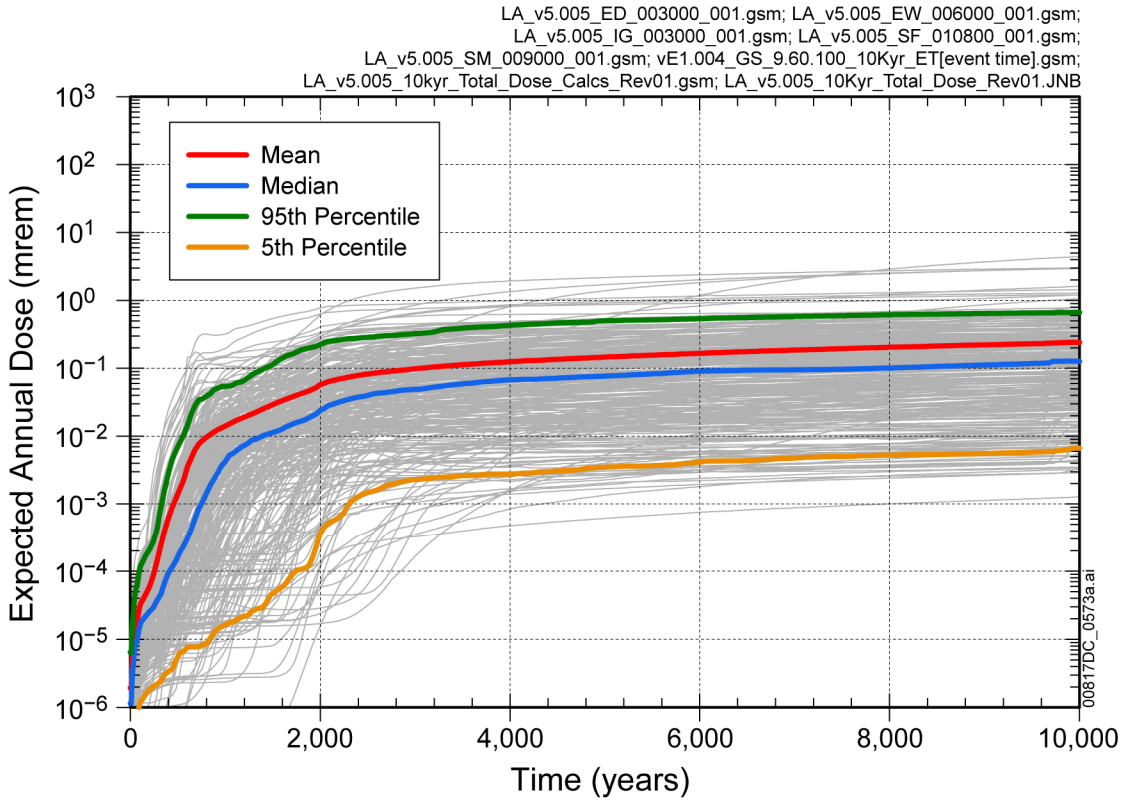

Source: Output DTNs: MO0710ADTSPAWO.000 [DIRS 183752]; MO0710PLOTSFIG.000 [DIRS 185207]; and MO0709TSPAREGS.000 [DIRS 182976].

Figure 8.1-1[a]. Distribution of Total Expected Annual Dose for 10,000 Years after Repository Closure

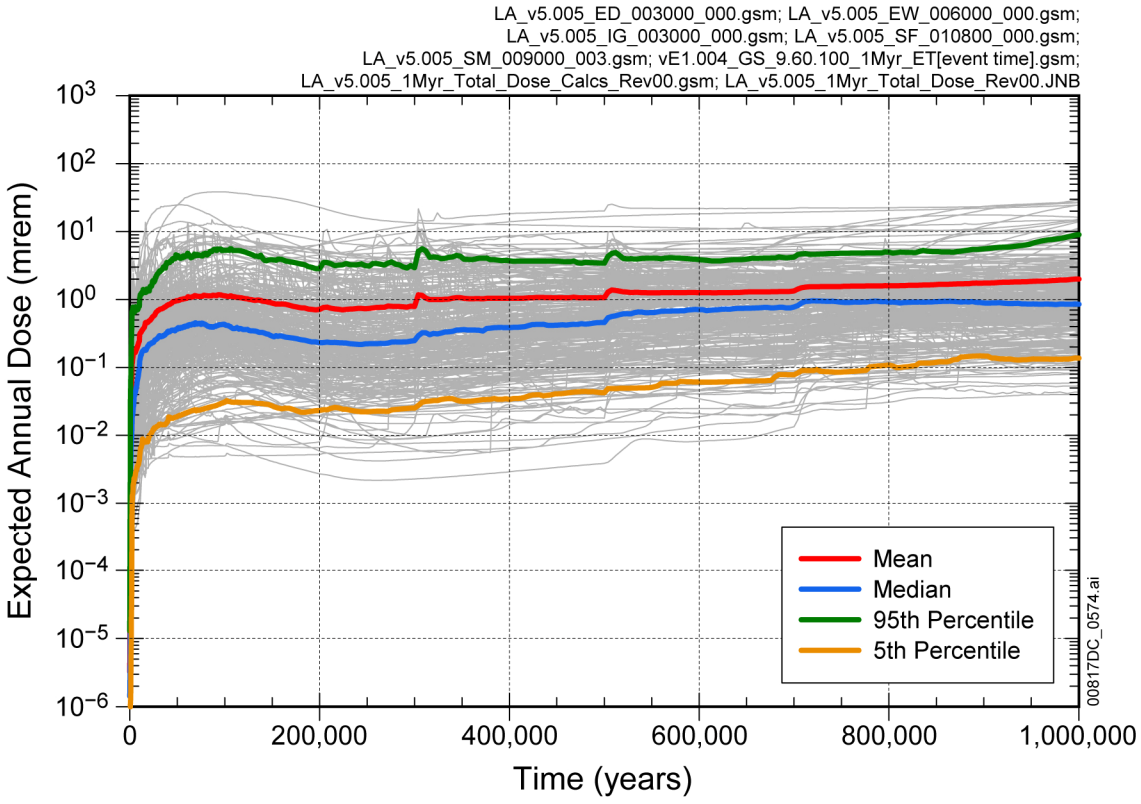

Source: Output DTNs: MO0710ADTSPAWO.000 [DIRS 183752]; MO0710PLOTSFIG.000 [DIRS 185207]; and MO0709TSPAREGS.000 [DIRS 182976].

Figure 8.1-2[a]. Distribution of Total Expected Annual Dose for 1,000,000 Years after Closure

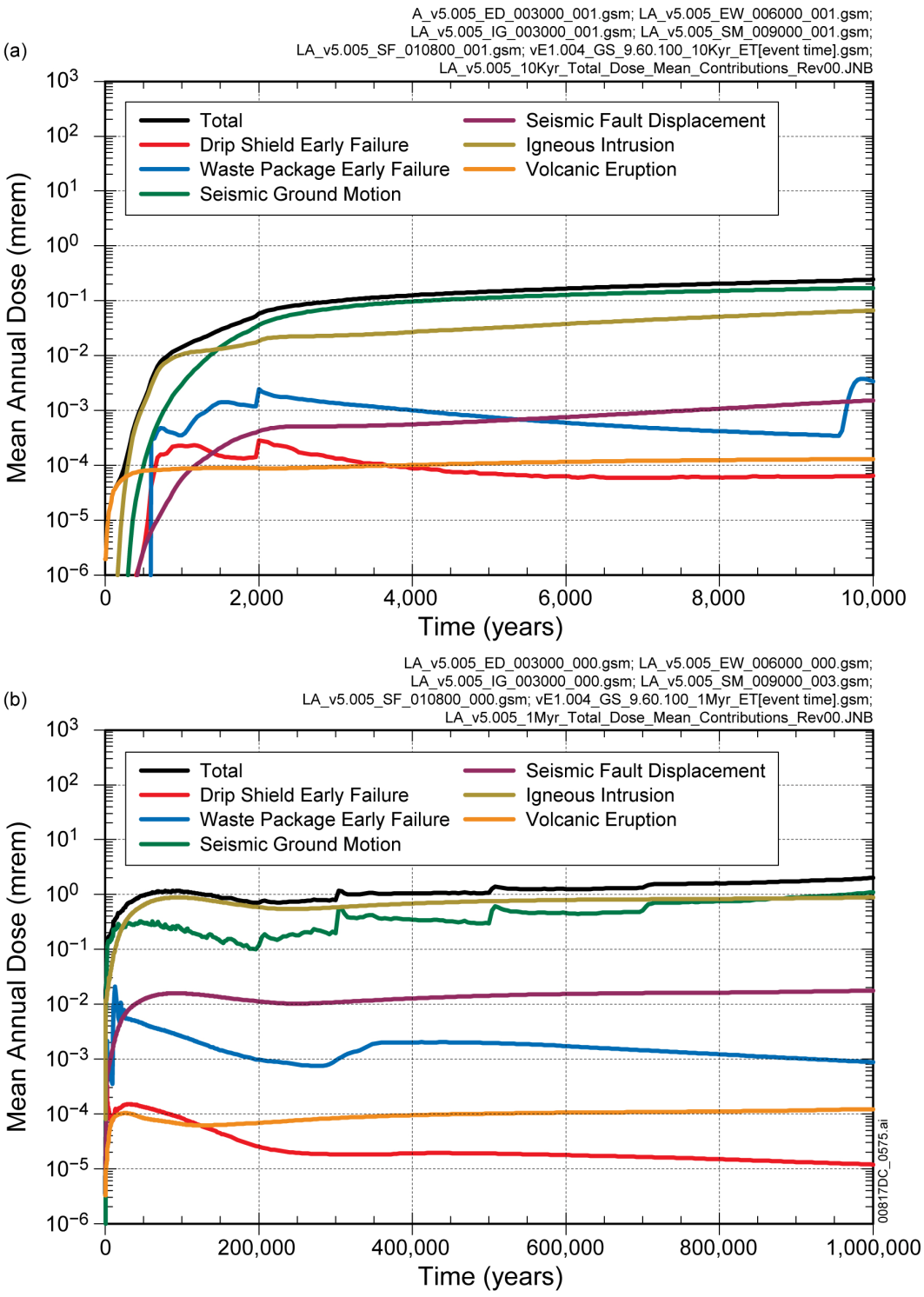

Source: Output DTNs: MO0710ADTSPAWO.000 [DIRS 183752]; and MO0709TSPAREGS.000 [DIRS 182976].

Figure 8.1-3[a]. Relative Contributions of Modeling Cases to Total Mean Annual Dose for (a) 10,000 Years and (b) 1,000,000 Years after Repository Closure

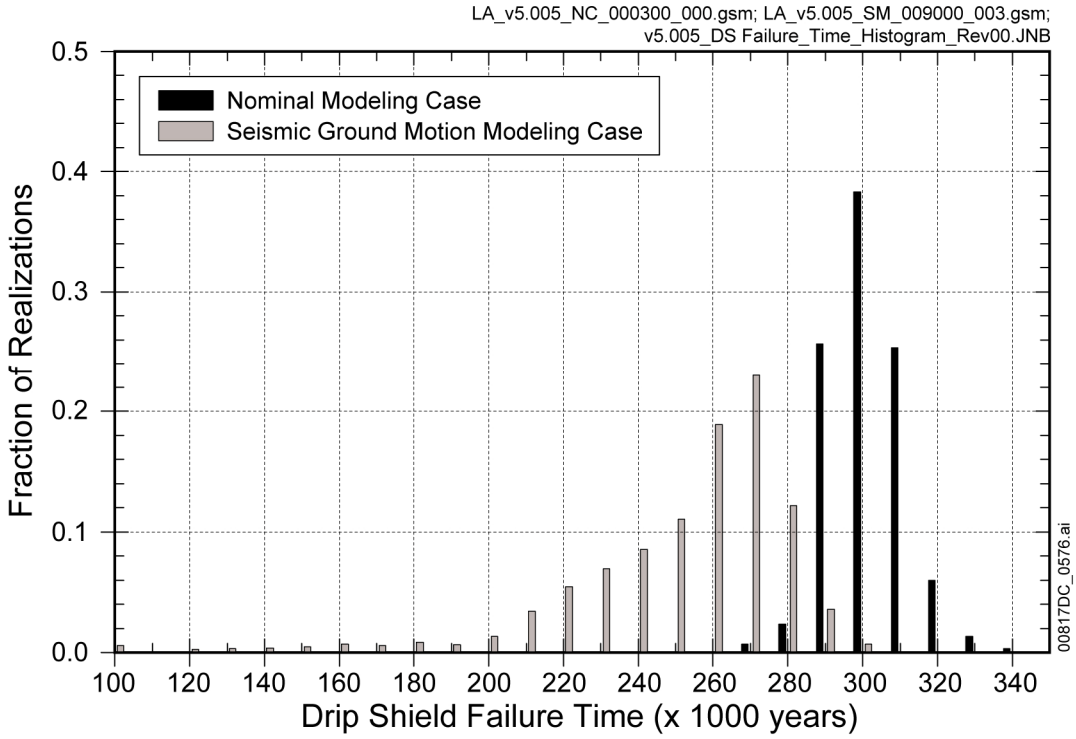

Source: Output DTN: MO0710ADTSPAWO.000 [DIRS 183752].

NOTE: Nominal failures are due to general corrosion. Seismic ground motion failures are caused by the combined effects of general corrosion, vibratory ground motion, and rockfall.

Figure 8.1-4[a]. Histogram of the Time of Drip Shield Failure for the Nominal and Seismic Ground Motion Modeling Cases

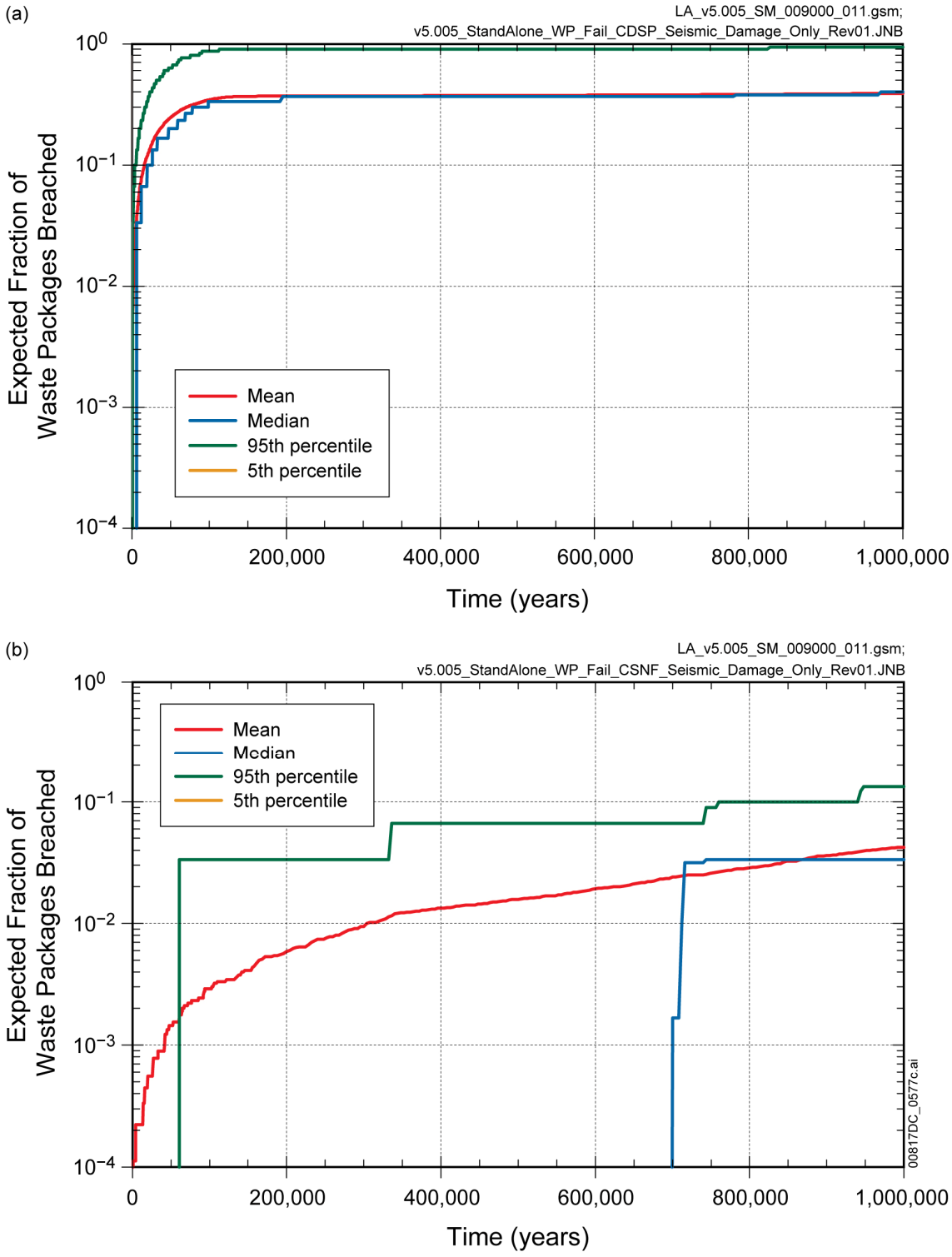

Source: Output DTN: MO0801TSPAWPDS.000 [DIRS 185077].

Figure 8.1-5[a]. Fraction of (a) CDSP Waste Packages and (b) CSNF Waste Packages Failed by Seismic Damage as a Function of Time

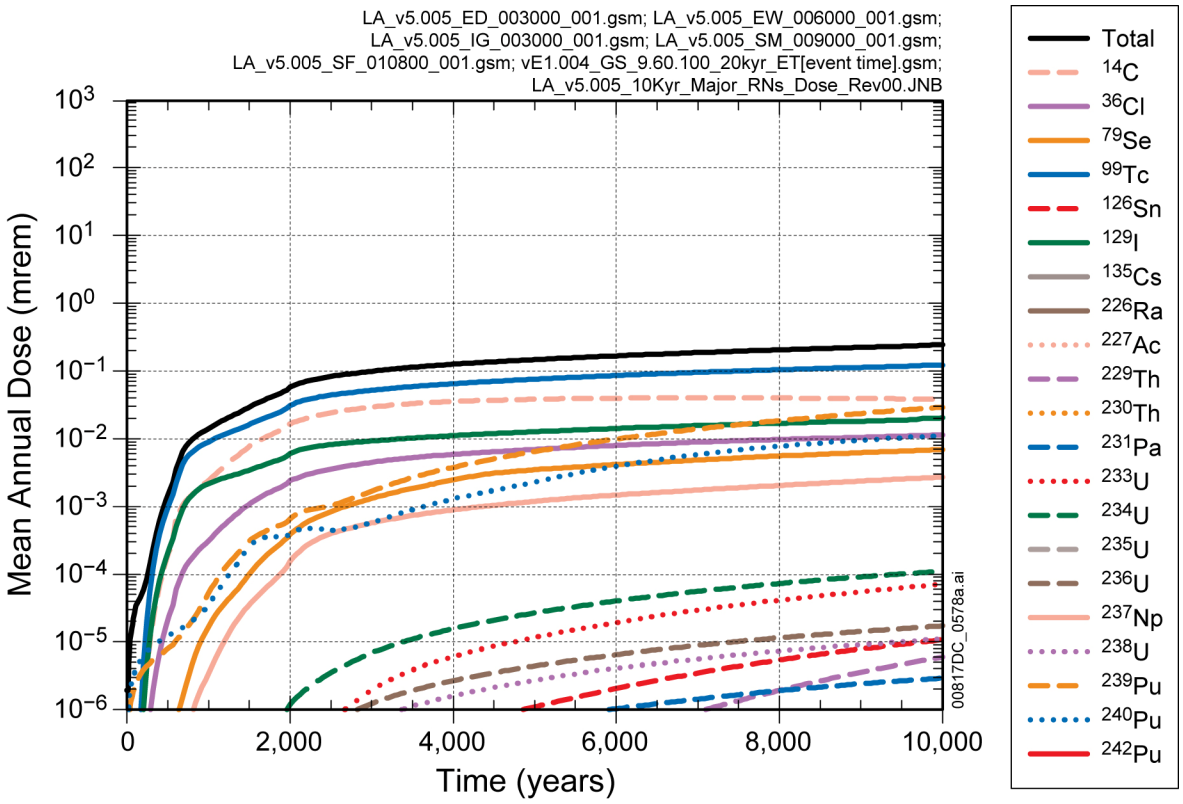

Source: Output DTNs: MO0710ADTSPAWO.000 [DIRS 183752]; MO0710PLOTSFIG.000 [DIRS 185207]; and MO0709TSPAREGS.000 [DIRS 182976].

Figure 8.1-6[a]. Contribution of Individual Radionuclides to Total Mean Annual Dose for 10,000 Years after Repository Closure

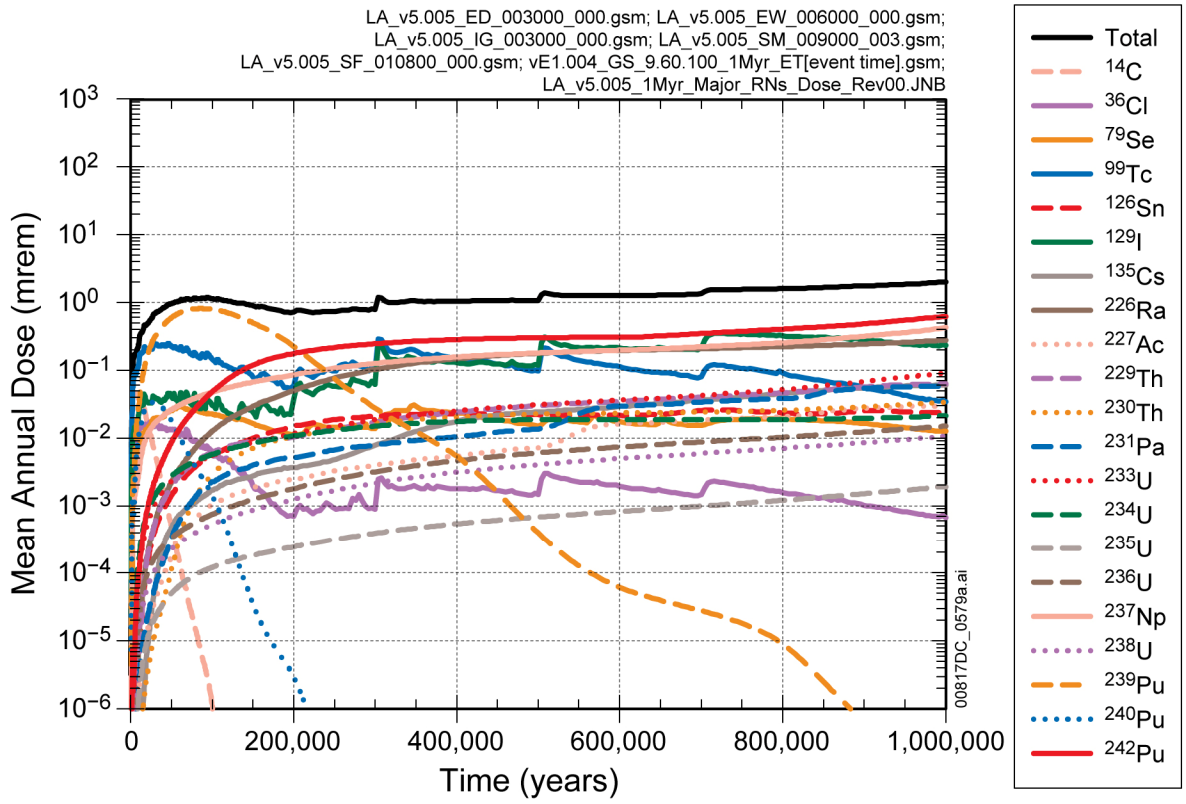

Source: Output DTNs: MO0710ADTSPAWO.000 [DIRS 183752]; MO0710PLOTSFIG.000 [DIRS 185207]; and MO0709TSPAREGS.000 [DIRS 182976].

Figure 8.1-7[a]. Contribution of Individual Radionuclides to Total Mean Annual Dose for 1,000,000 Years after Repository Closure

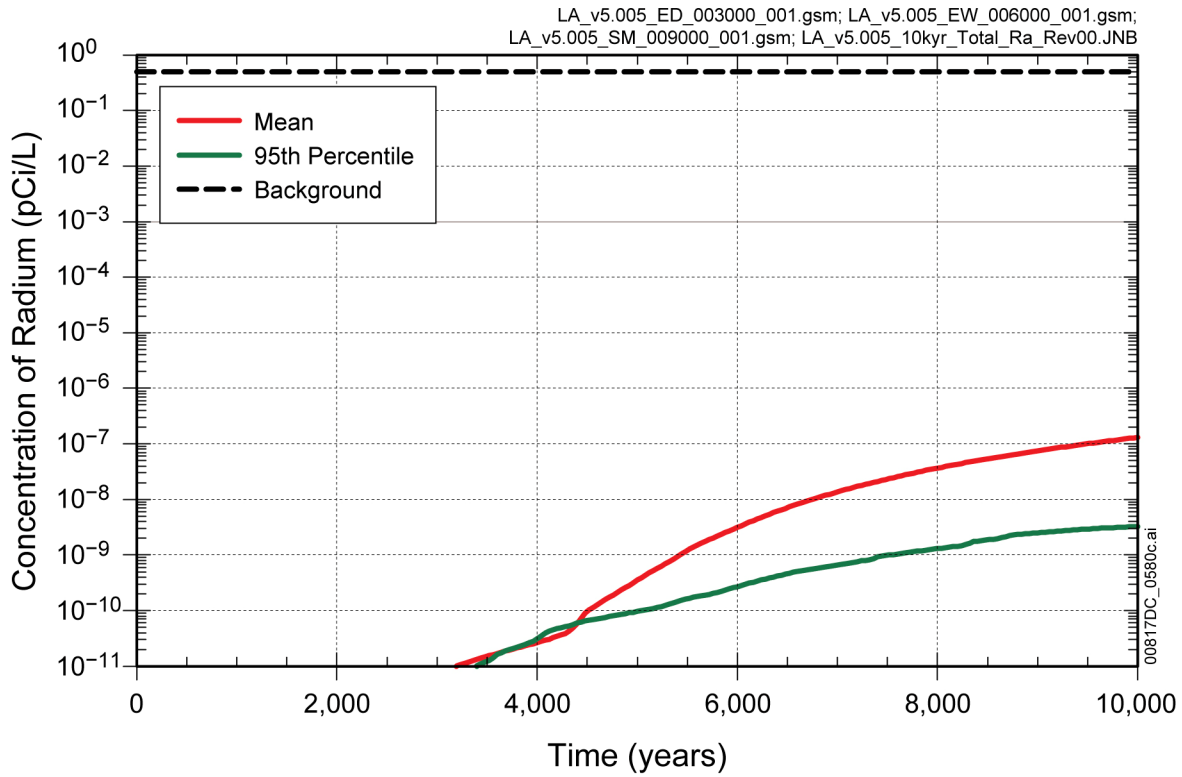

Source: Output DTNs: MO0710ADTSPAWO.000 [DIRS 183752]; and MO0710PLOTSFIG.000 [DIRS 185207].

Figure 8.1-9[a]. Summary Statistics for Activity Concentrations of Total Radium (^{226}Ra and ^{228}Ra) in Groundwater, Excluding Natural Background, for 10,000 Years after Repository Closure

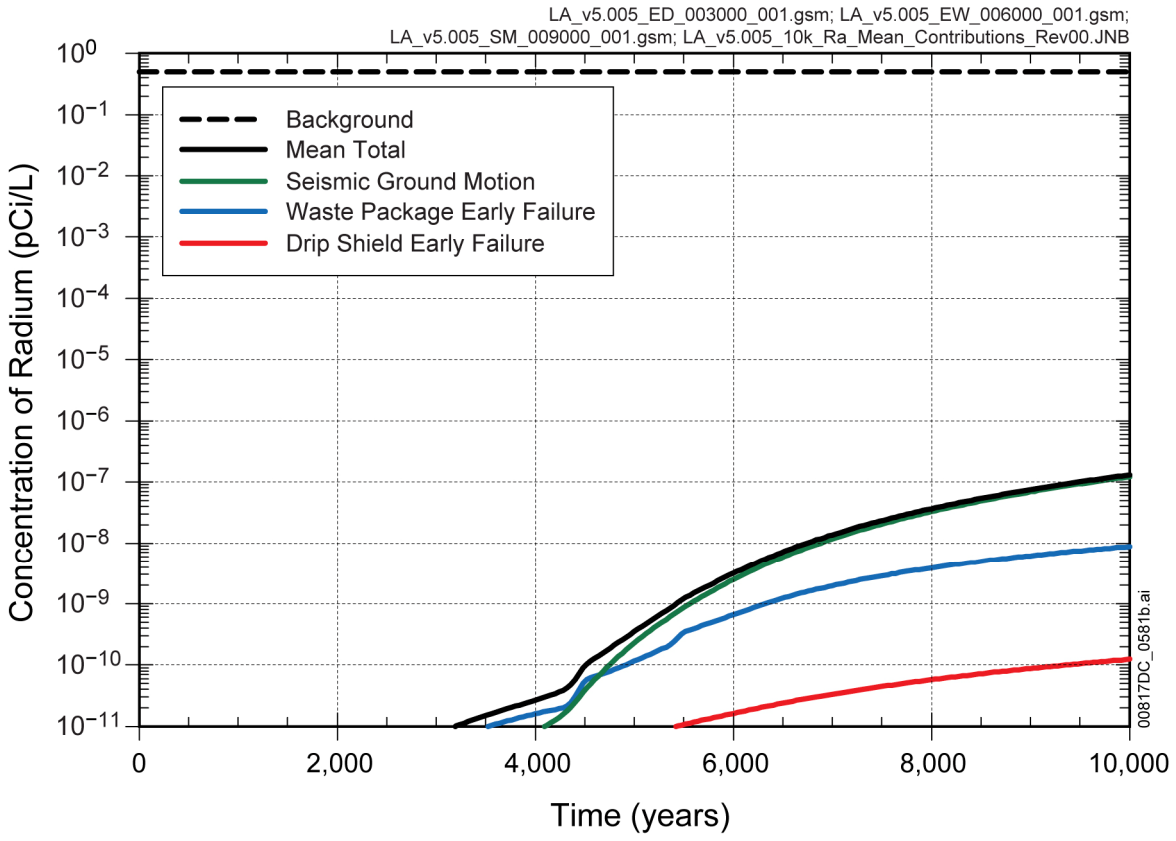

Source: Output DTNs: MO0710ADTSPAWO.000 [DIRS 183752]; and MO0710PLOTSFIG.000 [DIRS 185207].

Figure 8.1-10[a]. Contributions of the Modeling Cases to the Mean Combined ^{226}Ra and ^{228}Ra Activity Concentration in Groundwater, Excluding Natural Background, for 10,000 Years after Repository Closure

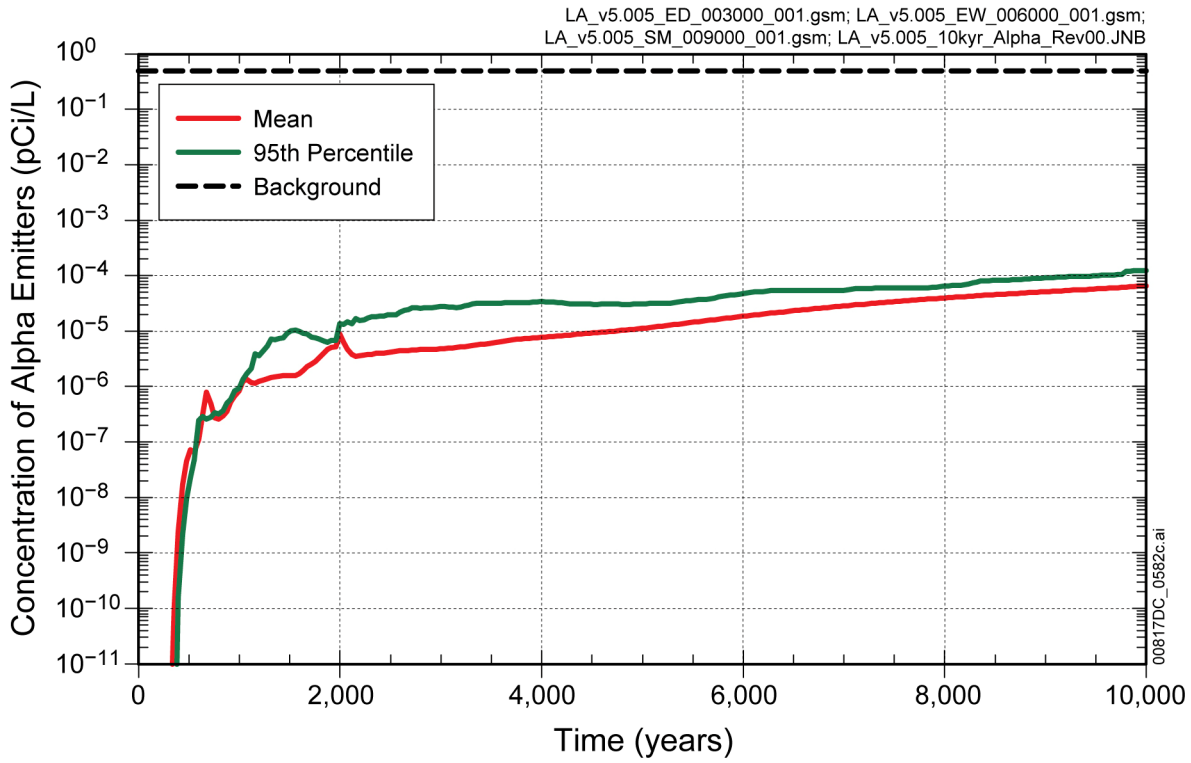

Source: Output DTNs: MO0710ADTSPAWO.000 [DIRS 183752]; and MO0710PLOTSFIG.000 [DIRS 185207].

Figure 8.1-11[a]. Summary Statistics for Activity Concentration of Gross Alpha and ^{226}Ra (Excluding Radon and Uranium) in Groundwater for 10,000 Years after Repository Closure

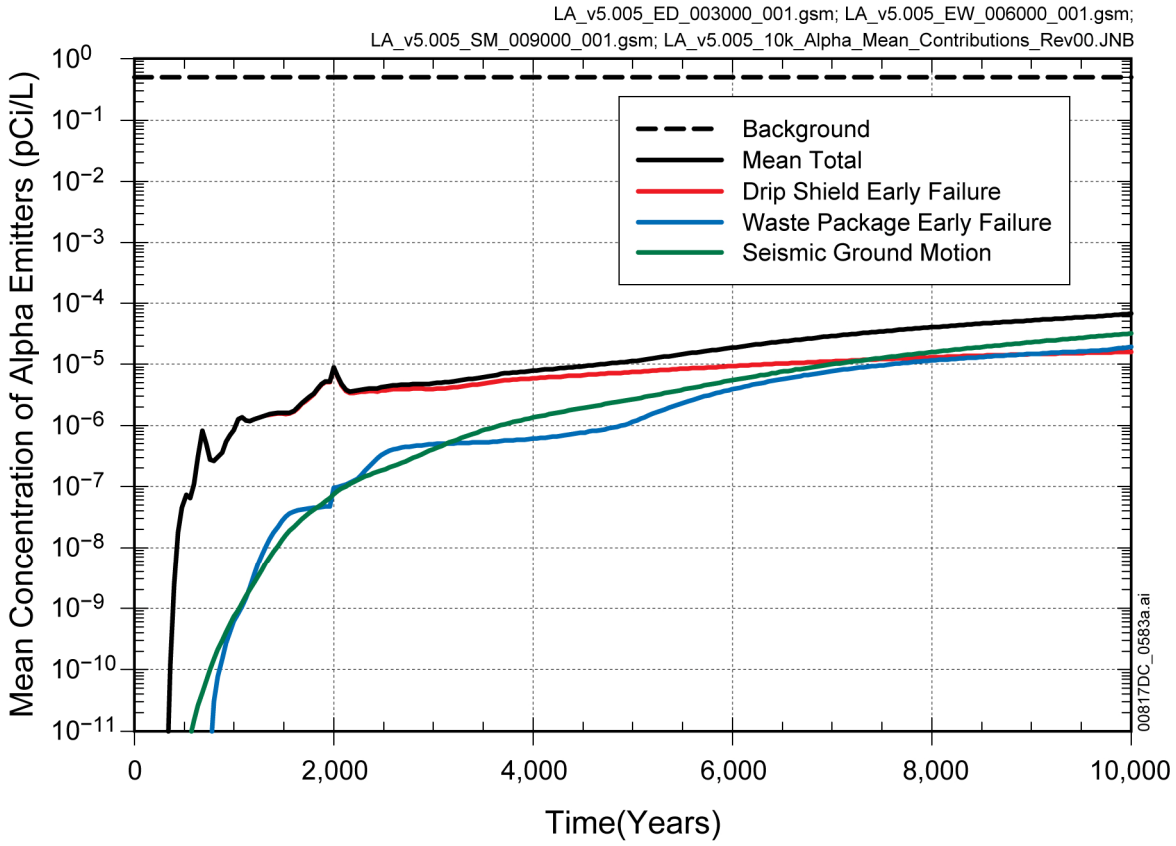

Source: Output DTNs: MO0710ADTSPAWO.000 [DIRS 183752]; and MO0710PLOTSFIG.000 [DIRS 185207].

Figure 8.1-12[a]. Contributions of the Modeling Cases to the Mean Gross Alpha Activity Concentrations (Including ^{226}Ra but Excluding Radon and Uranium) in Groundwater for 10,000 Years after Repository Closure

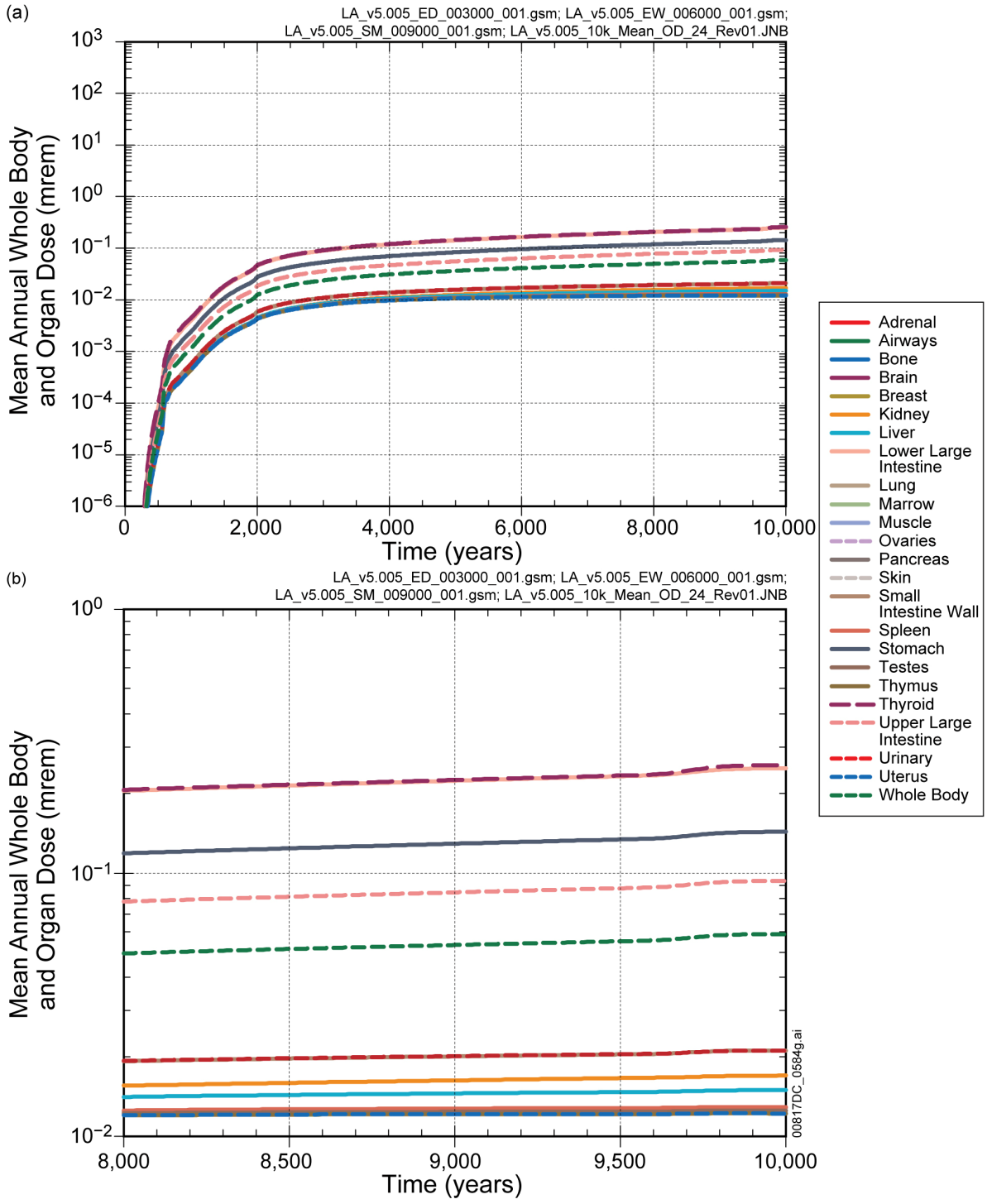

Source: Output DTNs: MO0710ADTSPAWO.000 [DIRS 183752]; and MO0710PLOTSFIG.000 [DIRS 185207].

NOTE: There are 24 dose histories in the plot: 23 organs and one for the whole body.

Figure 8.1-13[a]. Mean Annual Dose from Beta-Photon Dose for All Organs, Including the Whole Body for (a) 10,000 Years after Repository Closure and (b) Detail for 8,000 to 10,000 Years after Repository Closure

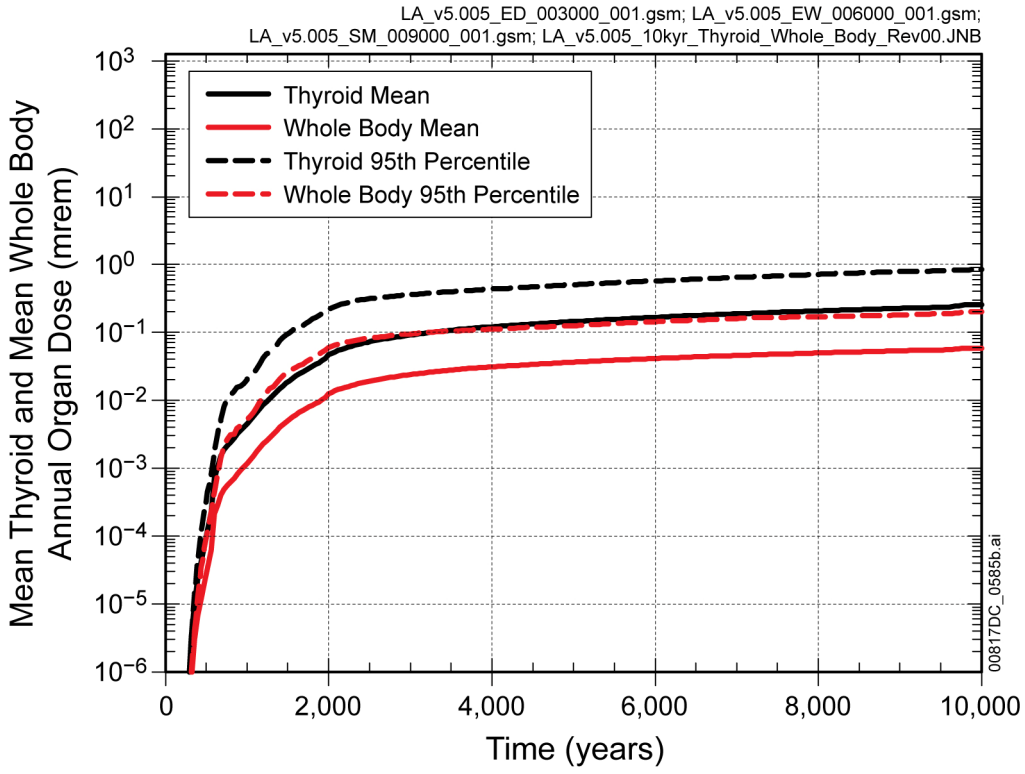

Source: Output DTNs: MO0710ADTSPAWO.000 [DIRS 183752]; and MO0710PLOTSFIG.000 [DIRS 185207].

Figure 8.1-14[a]. Summary Statistics for Annual Drinking Water Doses for Combined Beta and Photon Emitting Radionuclides for 10,000 Years after Repository Closure

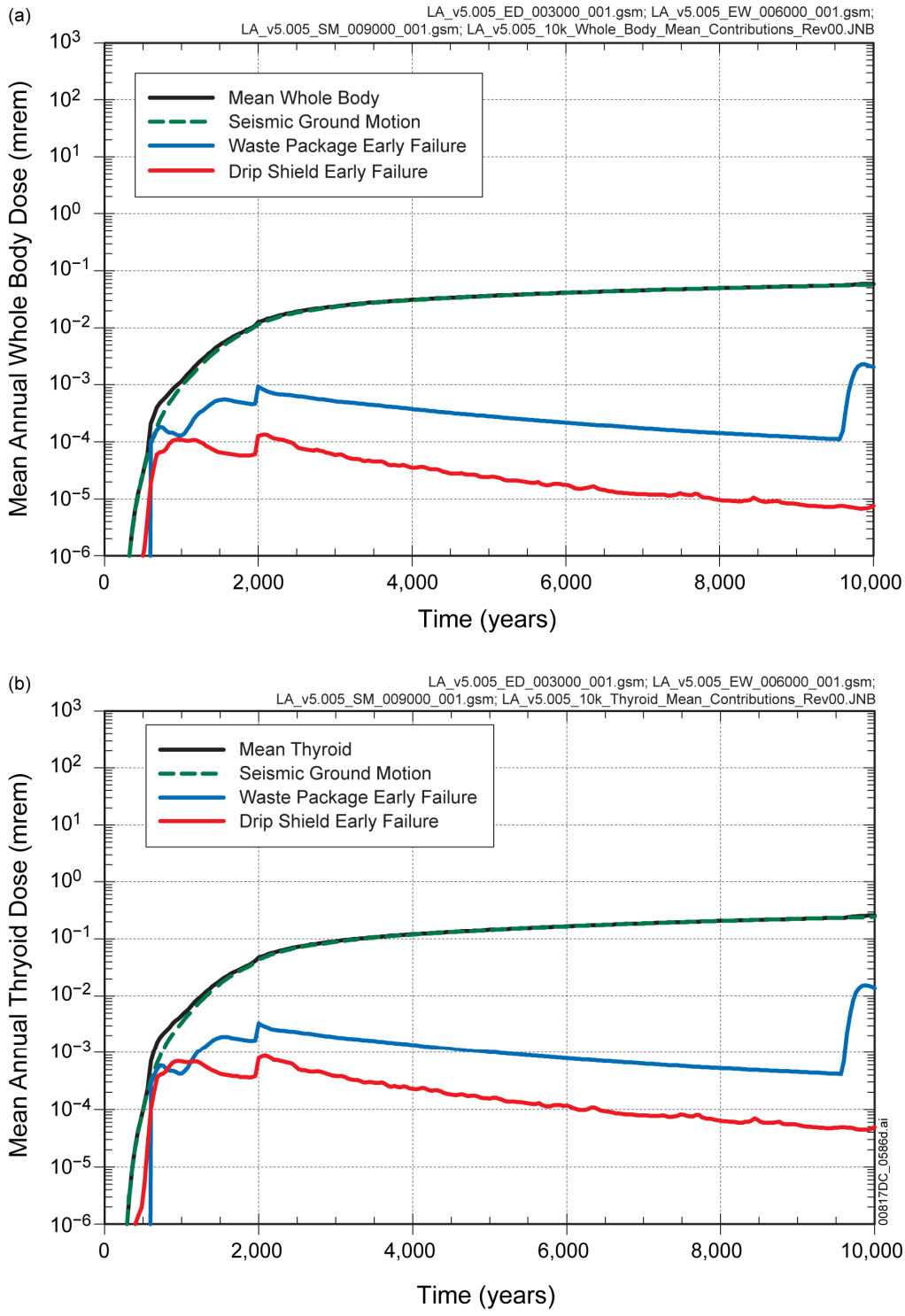

Source: Output DTNs: MO0710ADTSPAWO.000 [DIRS 183752]; and MO0710PLOTSFIG.000 [DIRS 185207].

Figure 8.1-15[a]. Contributions of Modeling Cases to the (a) Whole Body Dose and (b) Thyroid for 10,000 Years after Repository Closure

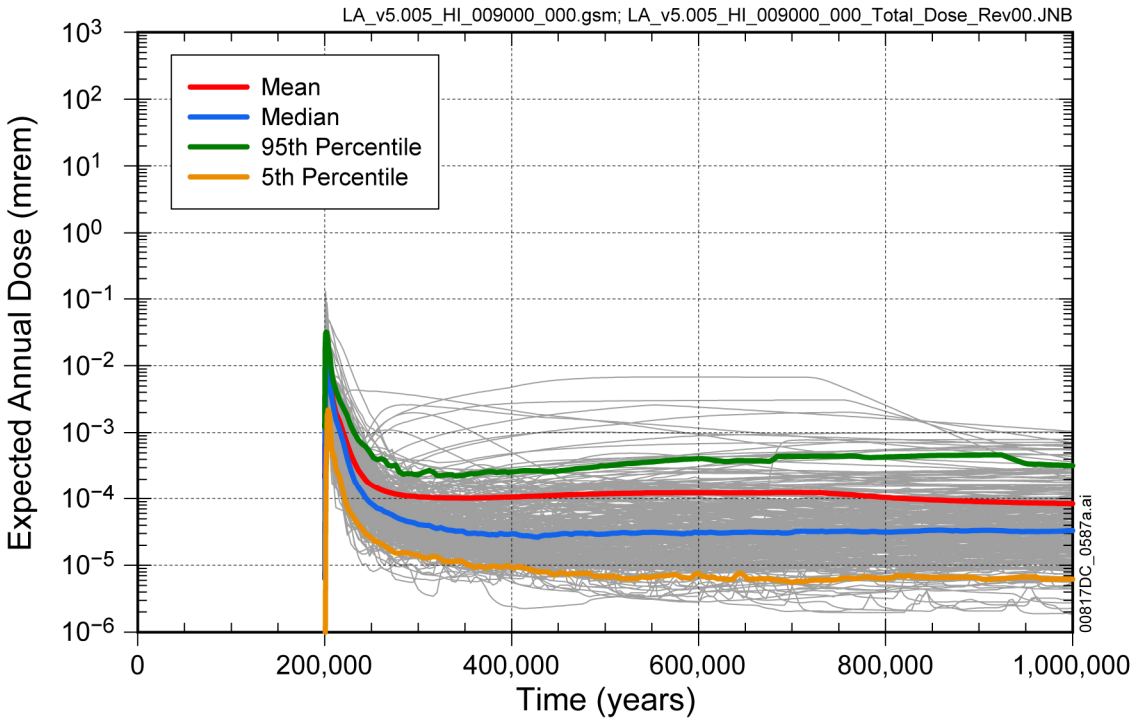

Source: Output DTNs: MO0710ADTSPAWO.000 [DIRS 183752]; and MO0710PLOTSFIG.000 [DIRS 185207].

Figure 8.1-16[a]. Distribution of Expected Annual Doses for the Human Intrusion Scenario for 1,000,000 Years after Repository Closure with Drilling Event at 200,000 Years

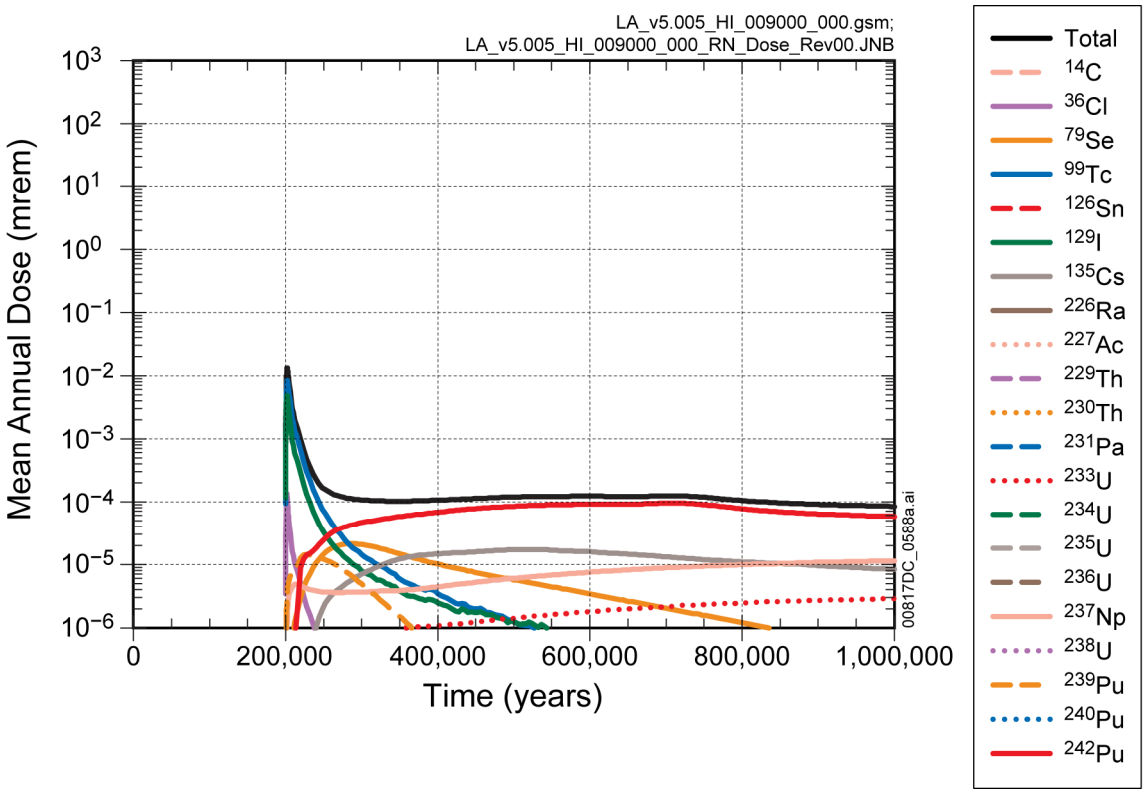

Source: Output DTN: MO0710ADTSPAWO.000 [DIRS 183752].

Figure 8.1-17[a]. Contribution of Individual Radionuclides to Mean Annual Dose for the Human Intrusion Scenario for 1,000,000 Years after Repository Closure

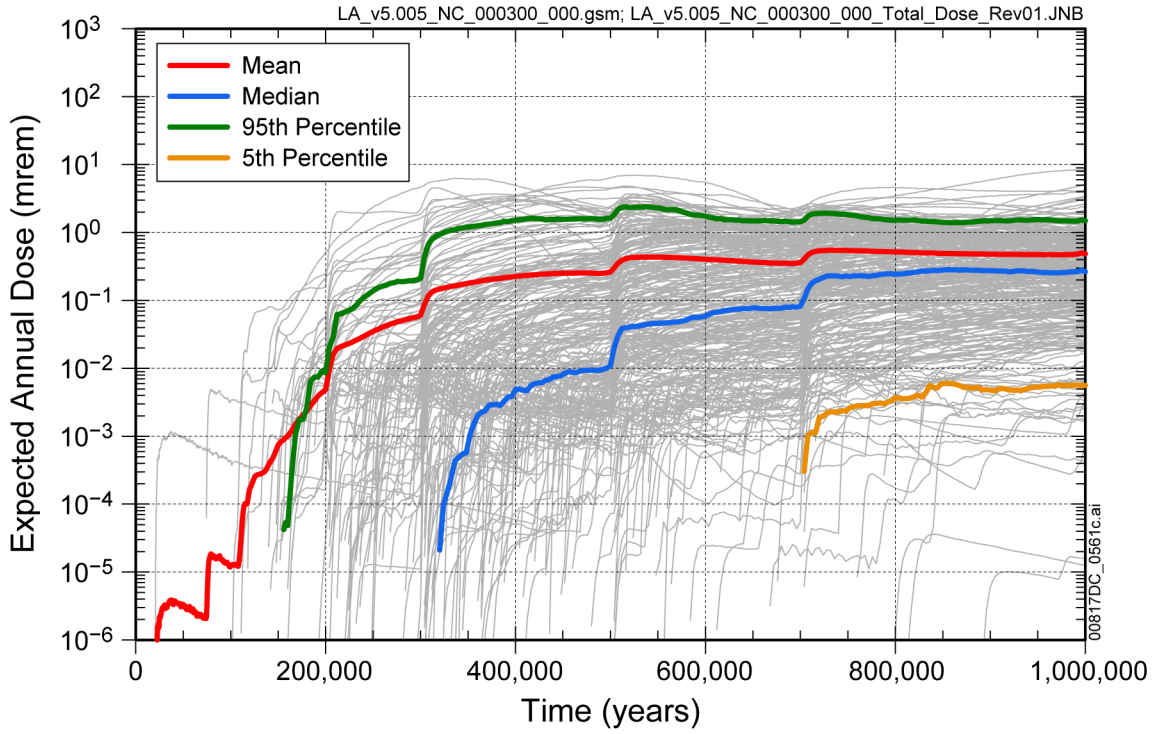

Source: Output DTNs: MO0710ADTSPAWO.000 [DIRS 183752]; and MO0710PLOTSFIG.000 [DIRS 185207].

Figure 8.2-1[a]. Distributions of Expected Annual Dose for the Nominal Modeling Case for 1,000,000 Years after Repository Closure

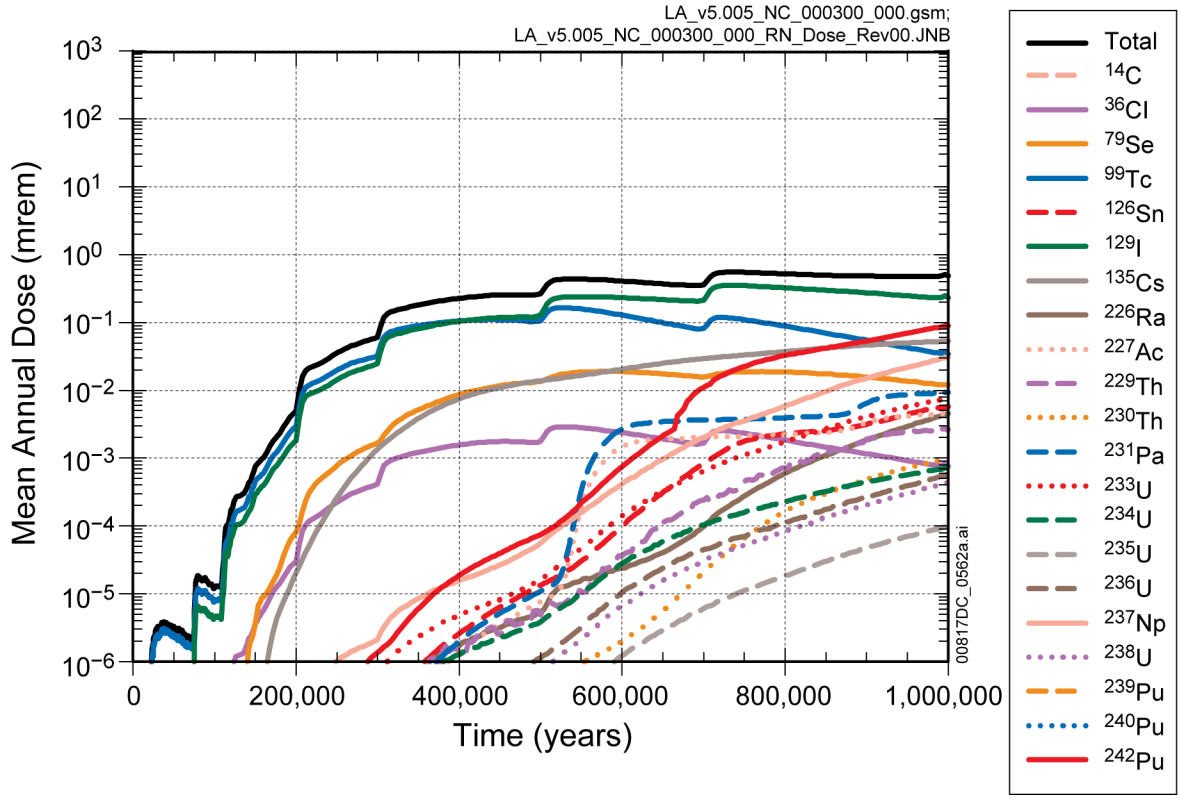

Source: Output DTNs: MO0710ADTSPAWO.000 [DIRS 183752]; and MO0710PLOTSFIG.000 [DIRS 185207].

Figure 8.2-2[a]. Contribution of Individual Radionuclides to Mean Annual Dose for the Nominal Modeling Case for 1,000,000 Years after Repository Closure

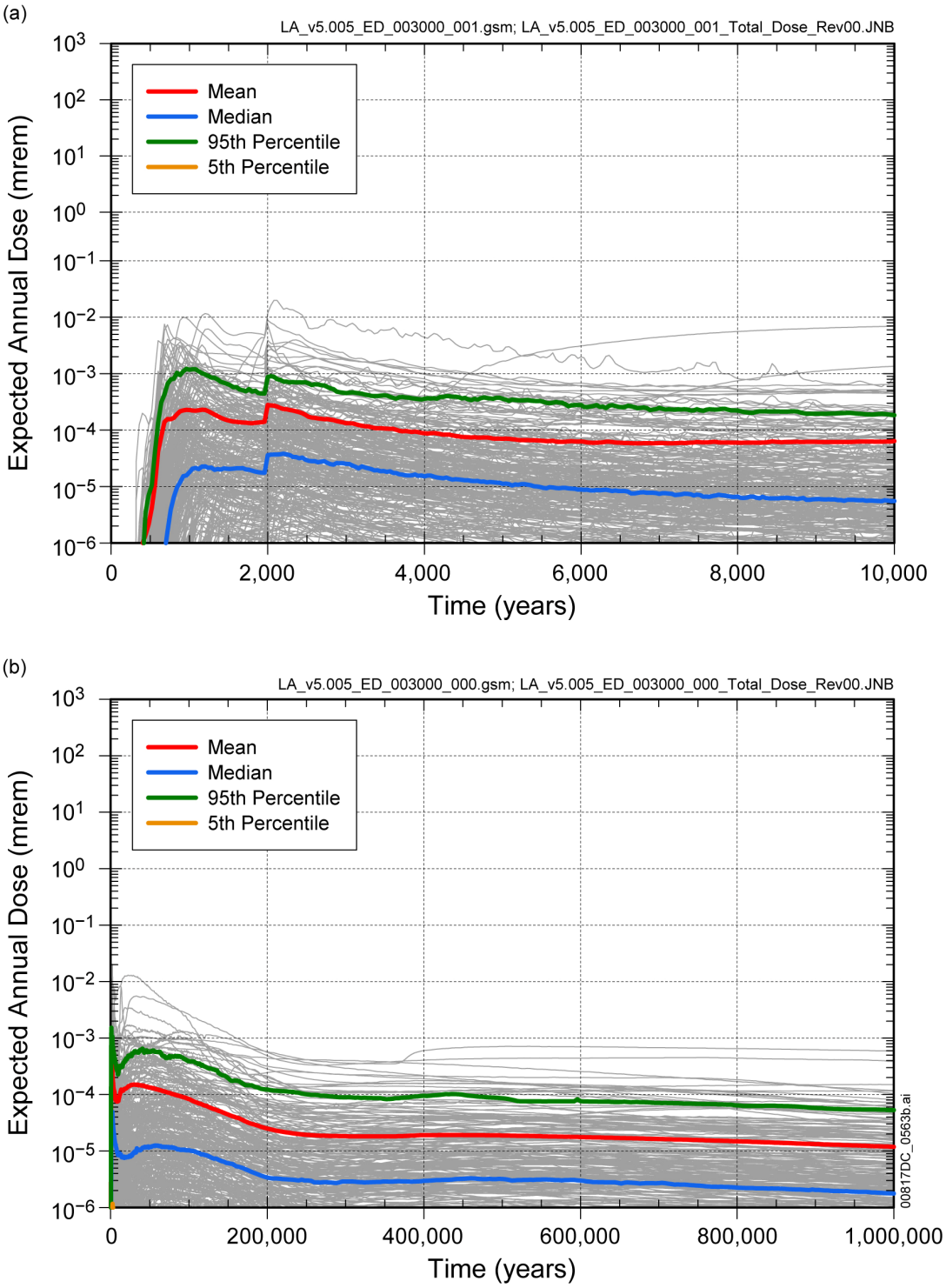

Source: Output DTNs: MO0710ADTSPAWO.000 [DIRS 183752]; and MO0710PLOTSFIG.000 [DIRS 185207].

Figure 8.2-3[a]. Distributions of Expected Annual Dose for the Drip Shield Early Failure Modeling Case for (a) 10,000 Years and (b) 1,000,000 Years after Repository Closure

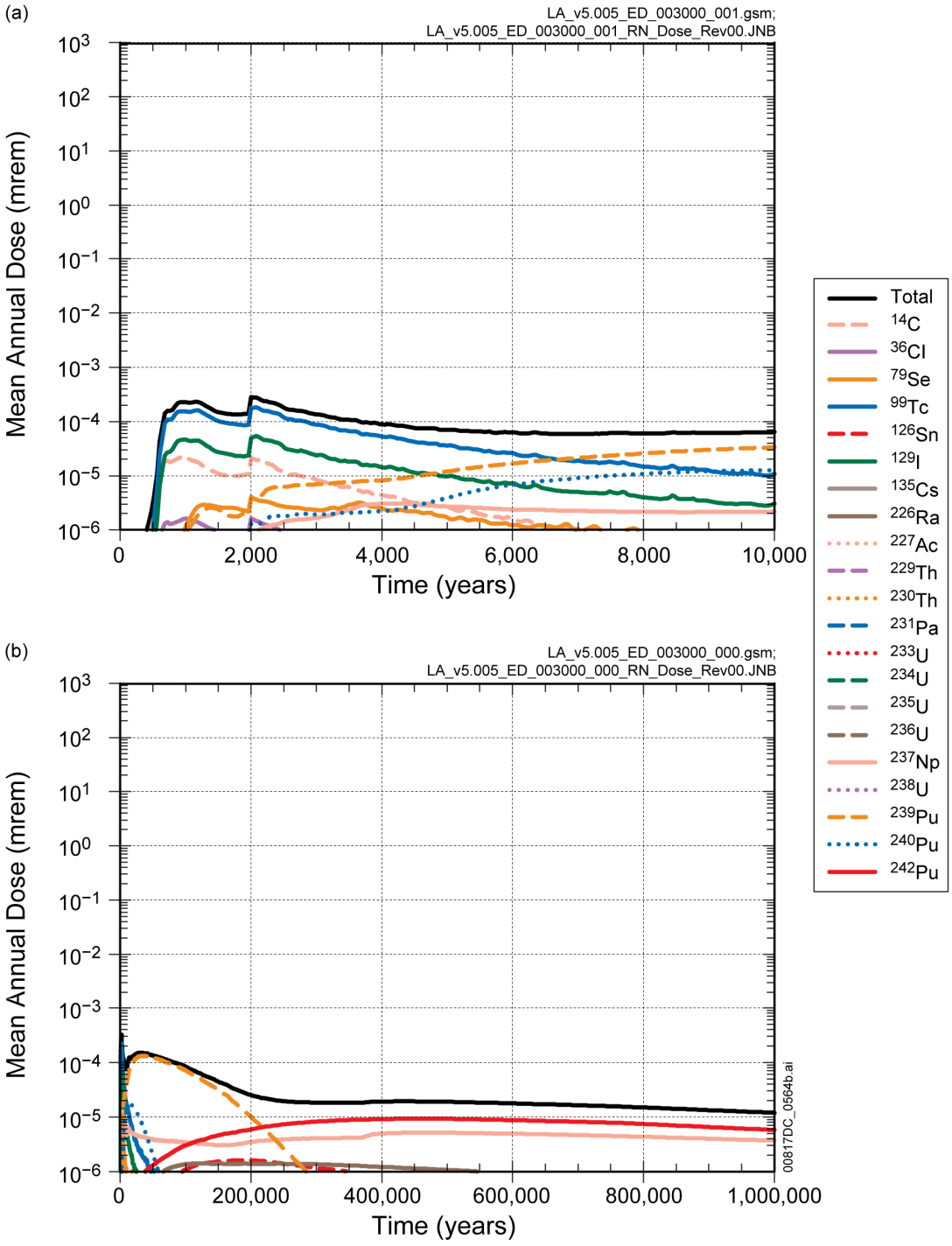

Source: Output DTNs: MO0710ADTSPAWO.000 [DIRS 183752]; and MO0710PLOTSFIG.000 [DIRS 185207].

Figure 8.2-4[a]. Contribution of Individual Radionuclides to Mean Annual Dose for Drip Shield Early Failure Modeling Case for (a) 10,000 Years and (b) 1,000,000 Years after Repository Closure

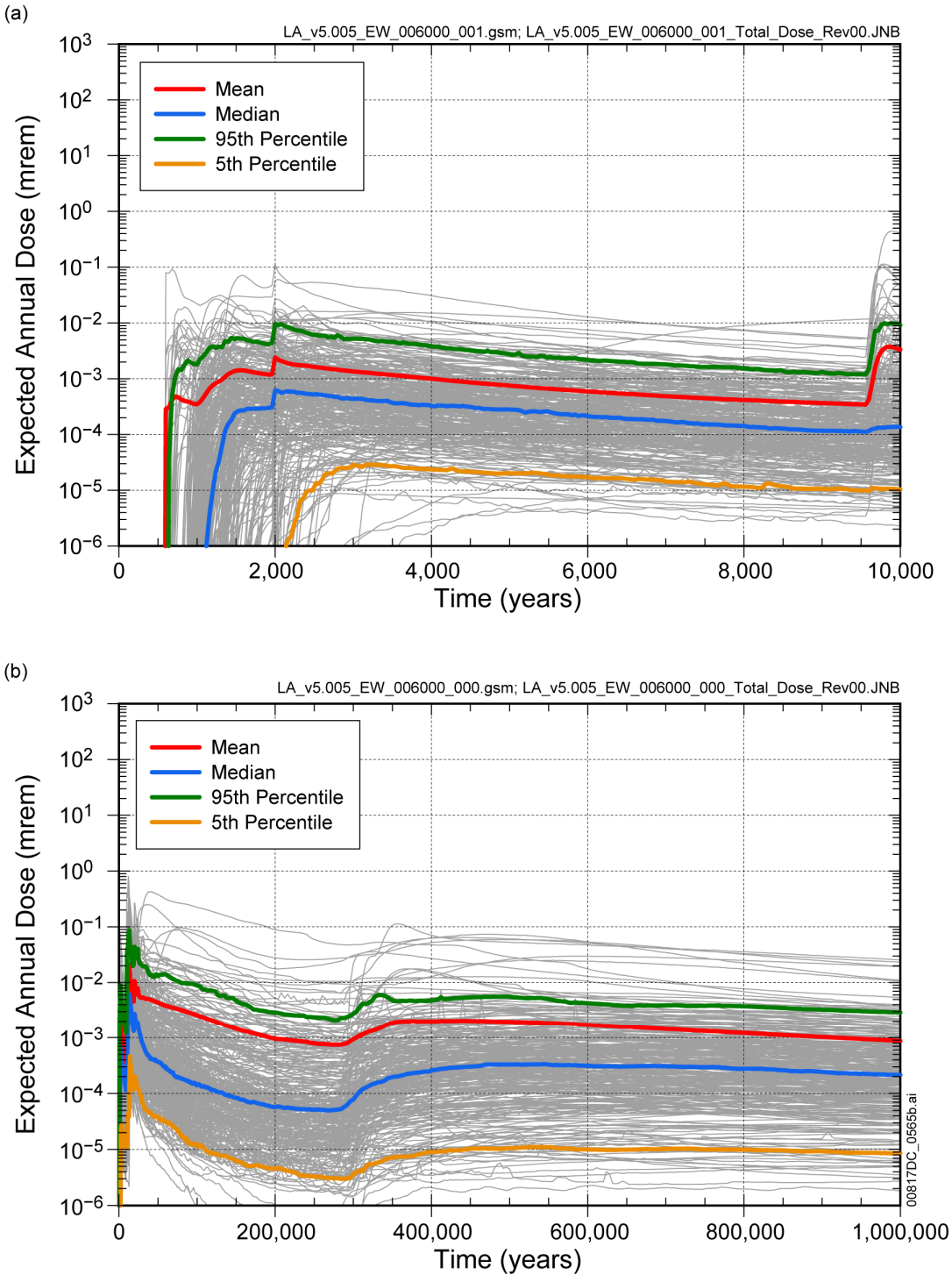

Source: Output DTNs: MO0710ADTSPAWO.000 [DIRS 183752]; and MO0710PLOTSFIG.000 [DIRS 185207].

Figure 8.2-5[a]. Distributions of Expected Annual Dose for Waste Package Early Failure Modeling Case for (a) 10,000 Years and (b) 1,000,000 Years after Repository Closure

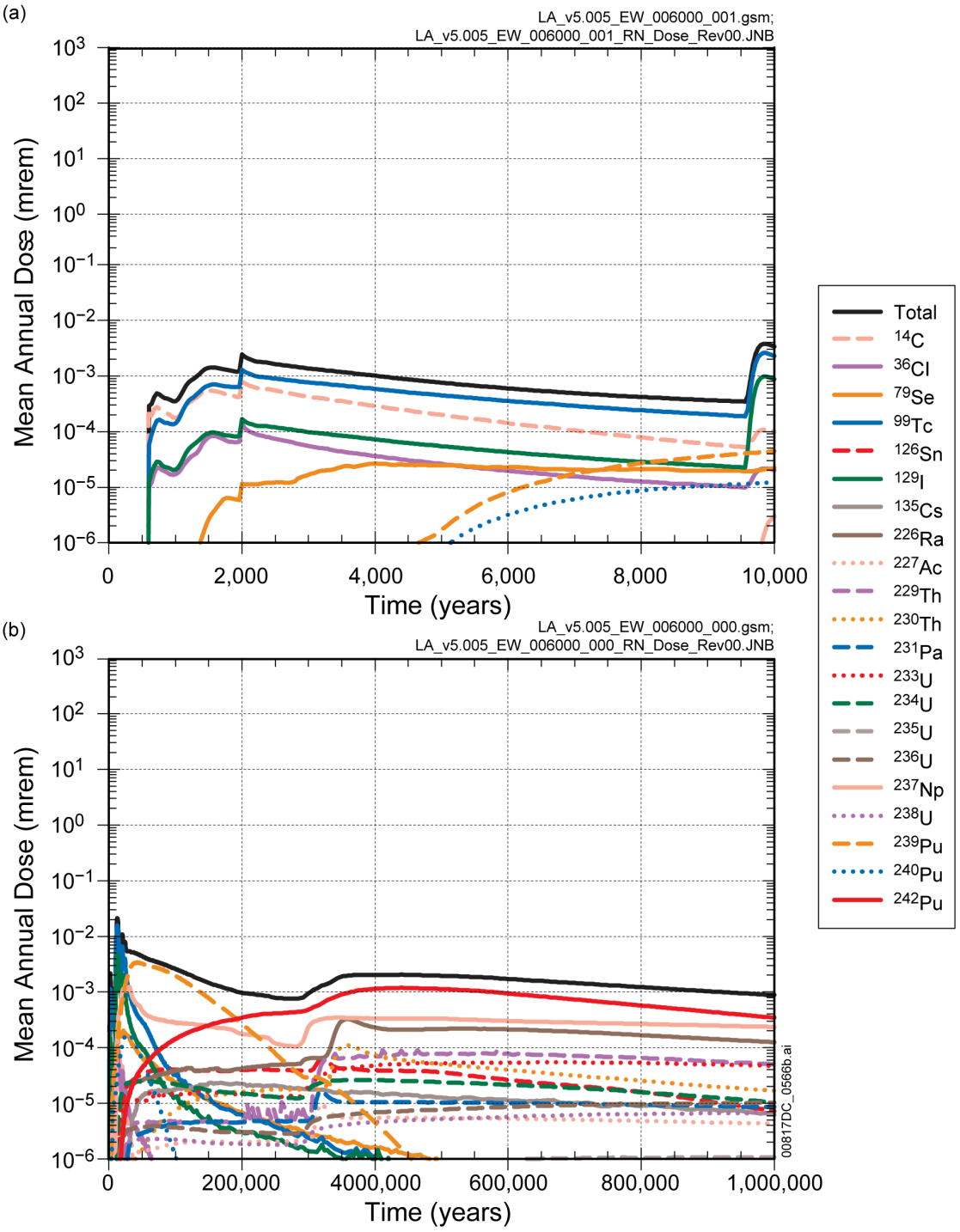

Source: Output DTNs: MO0710ADTSPAWO.000 [DIRS 183752]; and MO0710PLOTSFIG.000 [DIRS 185207].

Figure 8.2-6[a]. Contribution of Individual Radionuclides to Mean Annual Dose for Waste Package Early Failure Modeling Case for (a) 10,000 Years and (b) 1,000,000 Years after Repository Closure

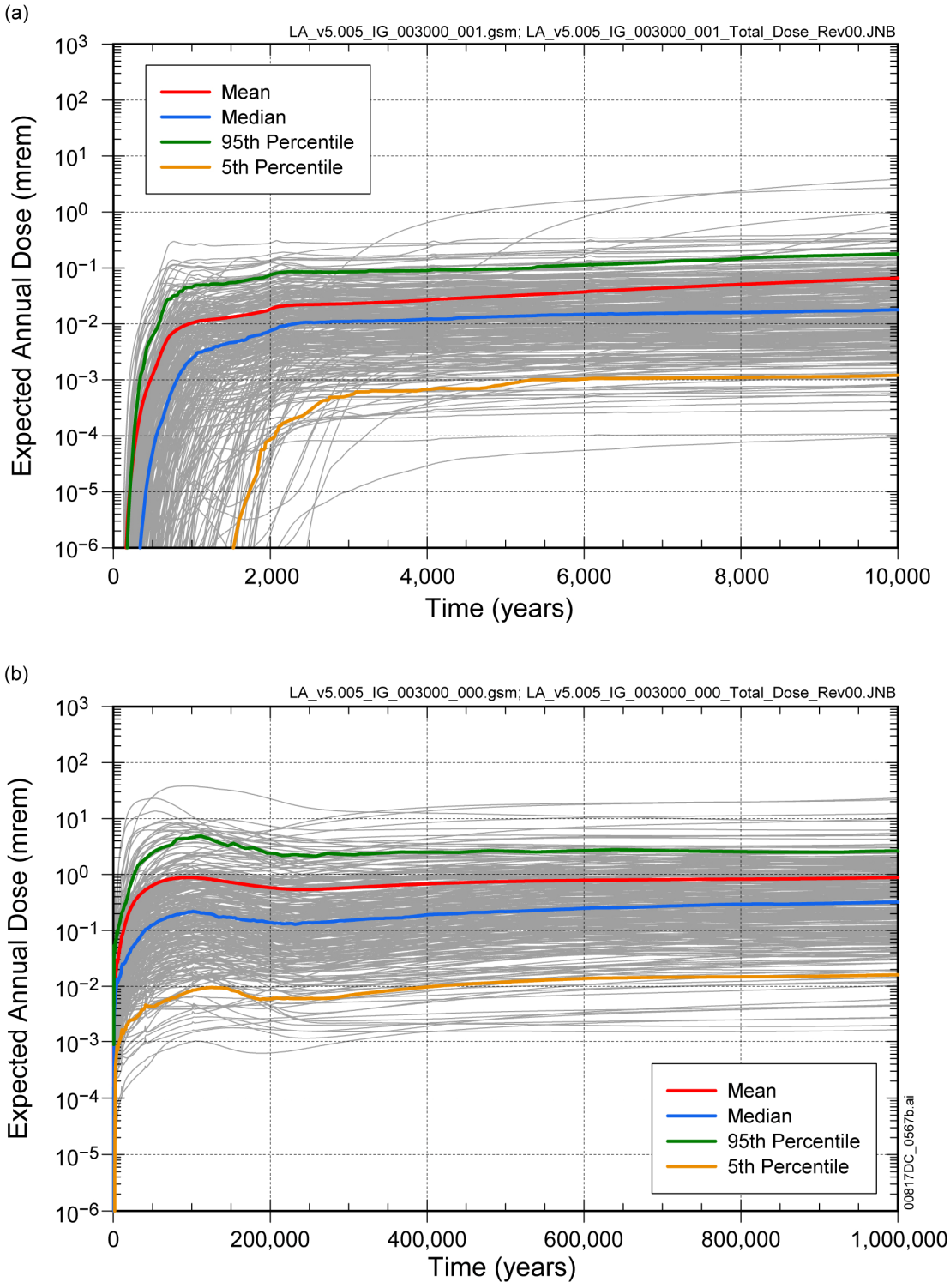

Source: Output DTNs: MO0710ADTSPAWO.000 [DIRS 183752]; and MO0710PLOTSFIG.000 [DIRS 185207].

Figure 8.2-7[a]. Distributions of Expected Annual Dose for the Igneous Intrusion Modeling Case for (a) 10,000 Years and (b) 1,000,000 Years after Repository Closure

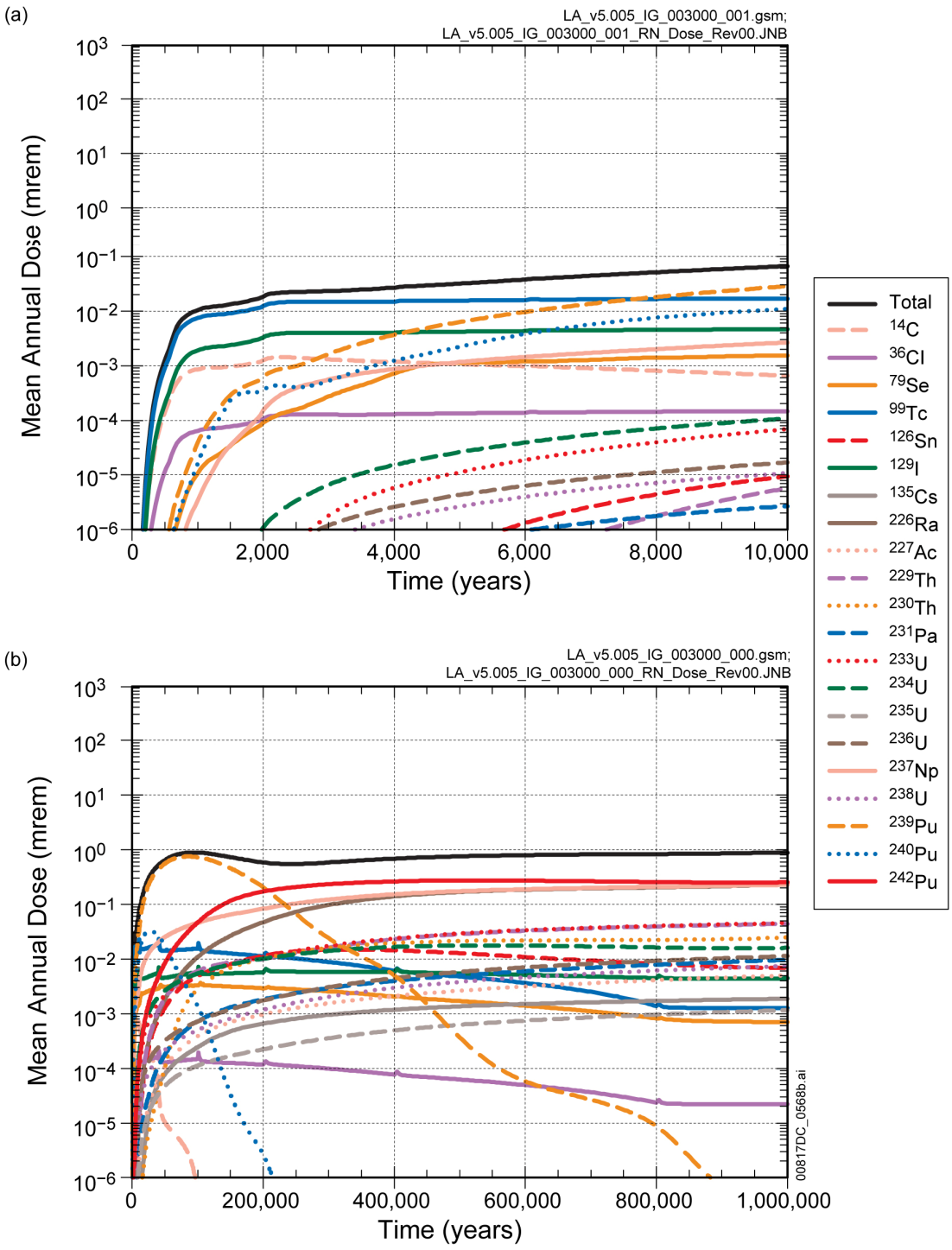

Source: Output DTNs: MO0710ADTSPAWO.000 [DIRS 183752]; and MO0710PLOTSFIG.000 [DIRS 185207].

Figure 8.2-8[a]. Contribution of Individual Radionuclides to Mean Annual Dose for the Igneous Intrusion Modeling Case for (a) 10,000 Years and (b) 1,000,000 Years after Repository Closure

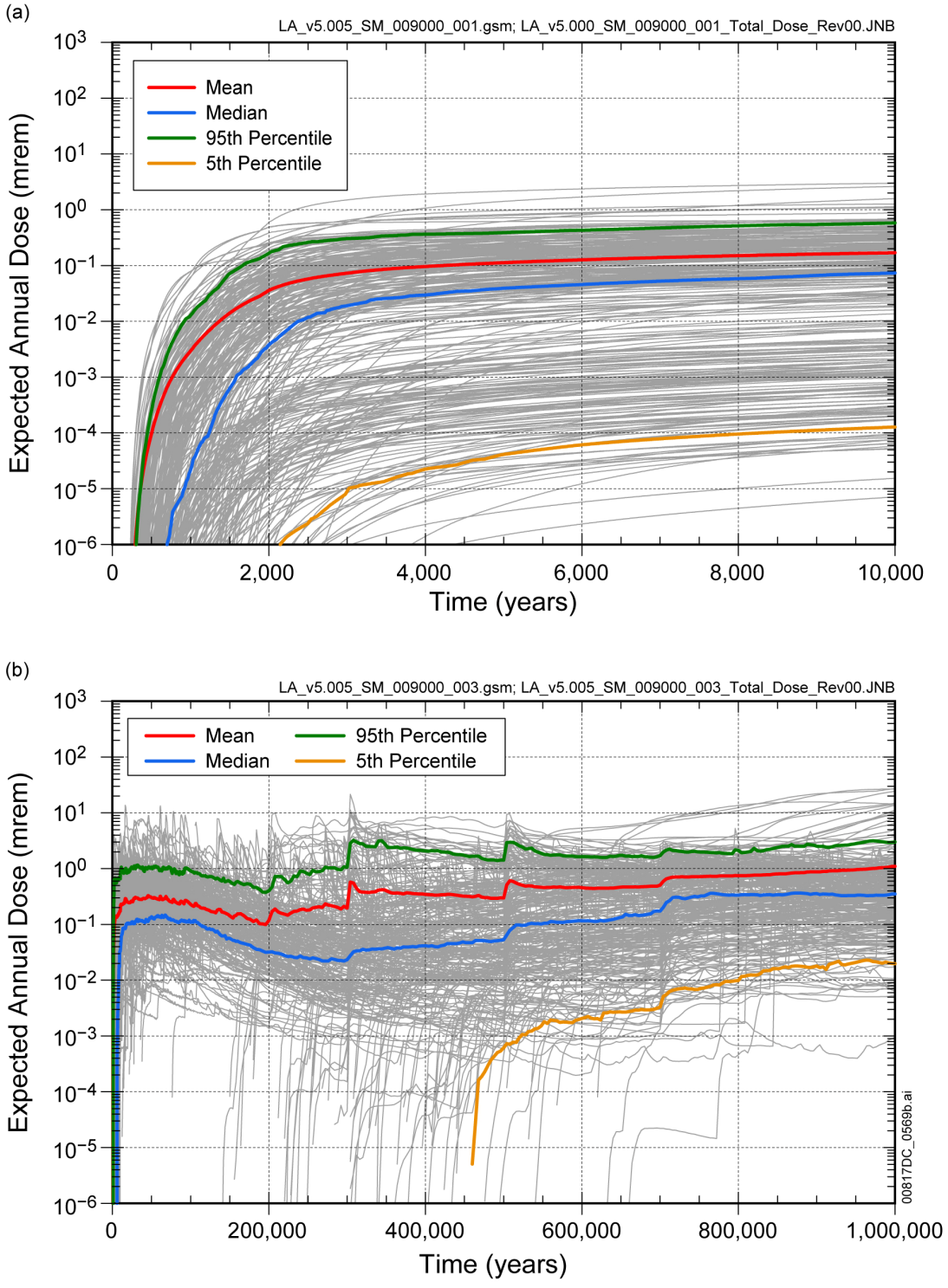

Source: Output DTNs: MO0710ADTSPAWO.000 [DIRS 183752]; and MO0710PLOTSFIG.000 [DIRS 185207].

Figure 8.2-11[a]. Distributions of Expected Annual Dose for the Seismic Ground Motion Modeling Case for (a) 10,000 Years and (b) 1,000,000 Years after Repository Closure

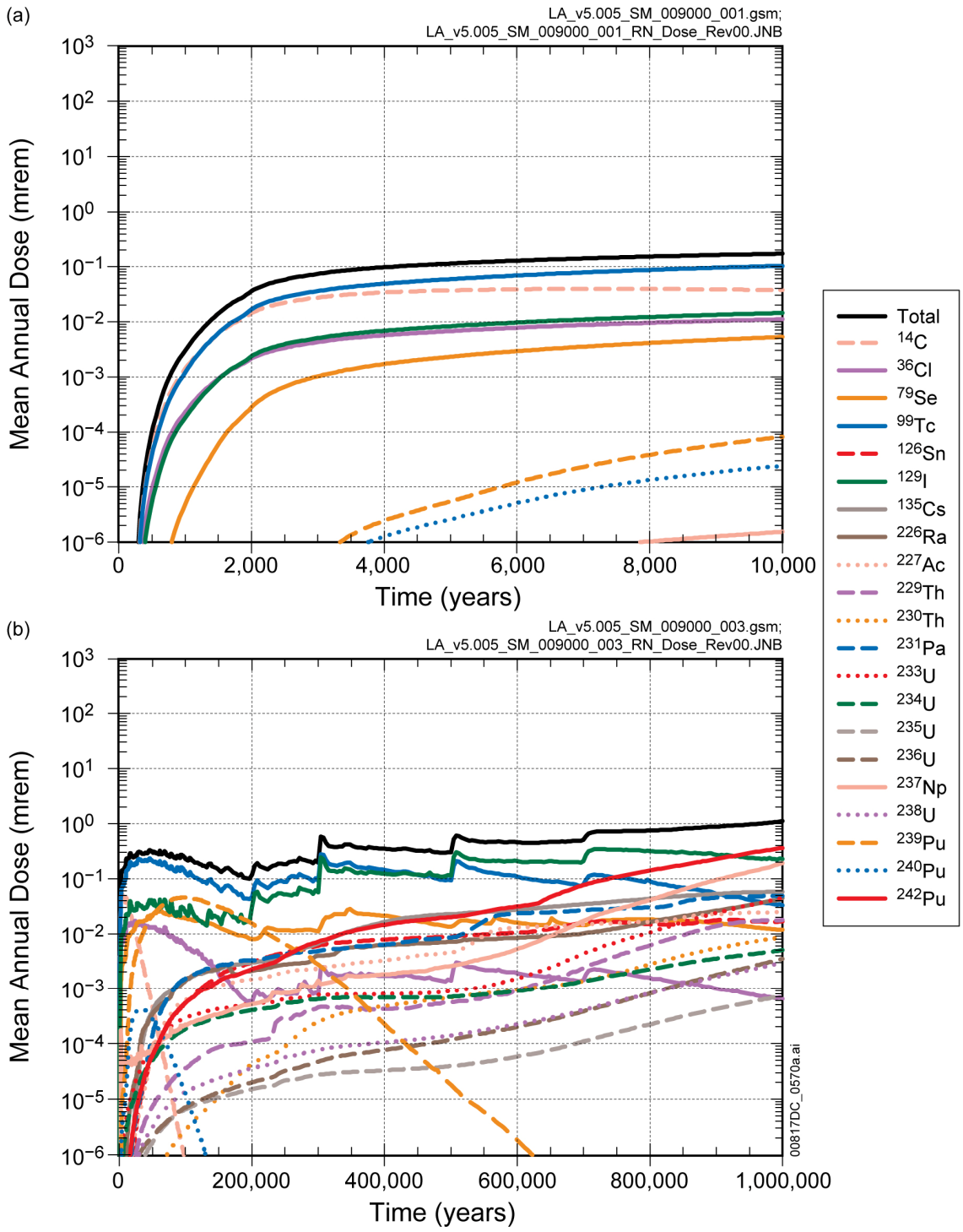

Source: Output DTNs: MO0710ADTSPAWO.000 [DIRS 183752]; and MO0710PLOTSFIG.000 [DIRS 185207].

Figure 8.2-12[a]. Contribution of Individual Radionuclides to Mean Annual Dose for the Seismic Ground Motion Modeling Case for (a) 10,000 Years and (b) 1,000,000 Years after Repository Closure

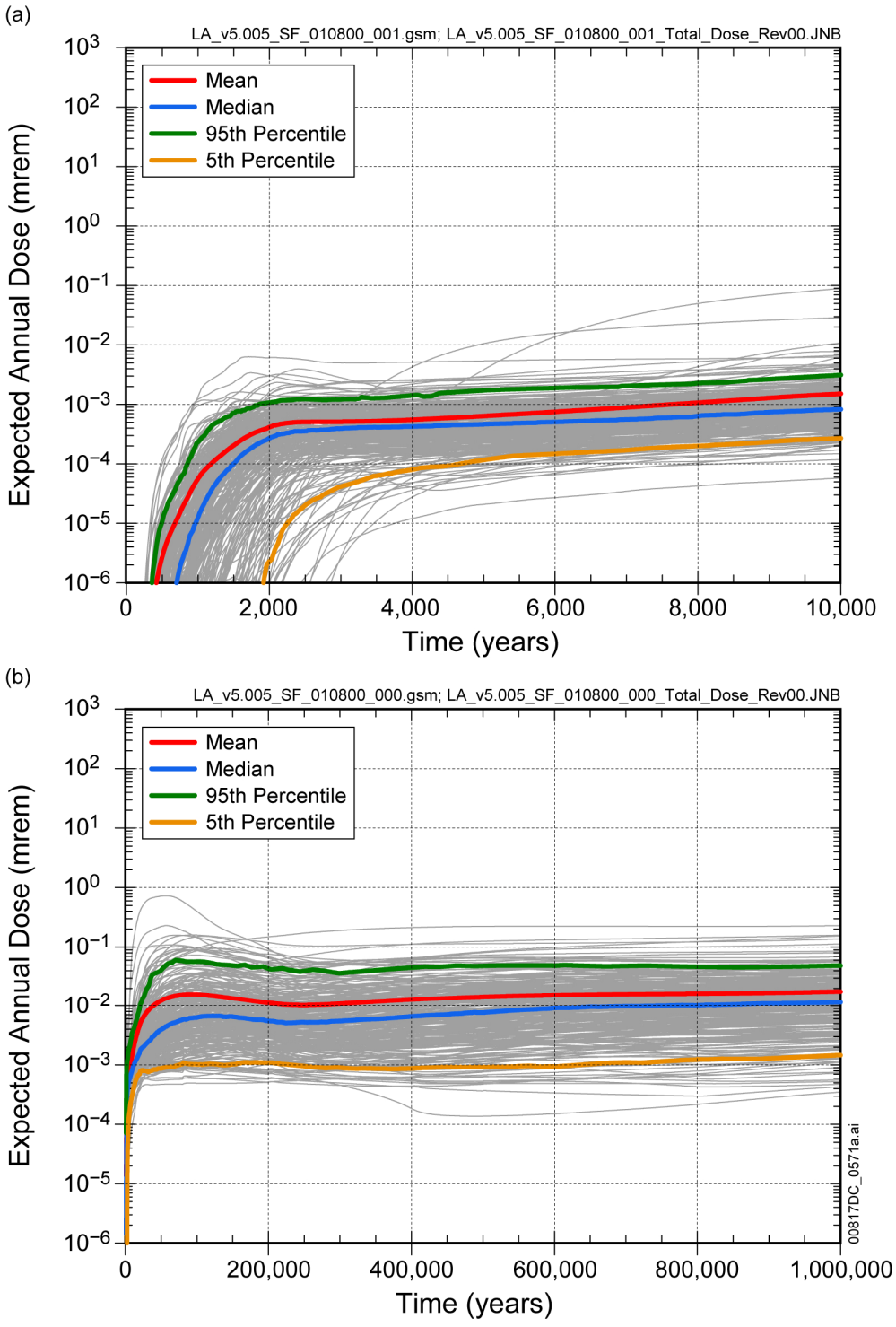

Source: Output DTNs: MO0710ADTSPAWO.000 [DIRS 183752]; and MO0710PLOTSFIG.000 [DIRS 185207].

Figure 8.2-13[a]. Distributions of Expected Annual Dose for the Seismic Fault Displacement Modeling Case for (a) 10,000 Years and (b) 1,000,000 Years after Repository Closure

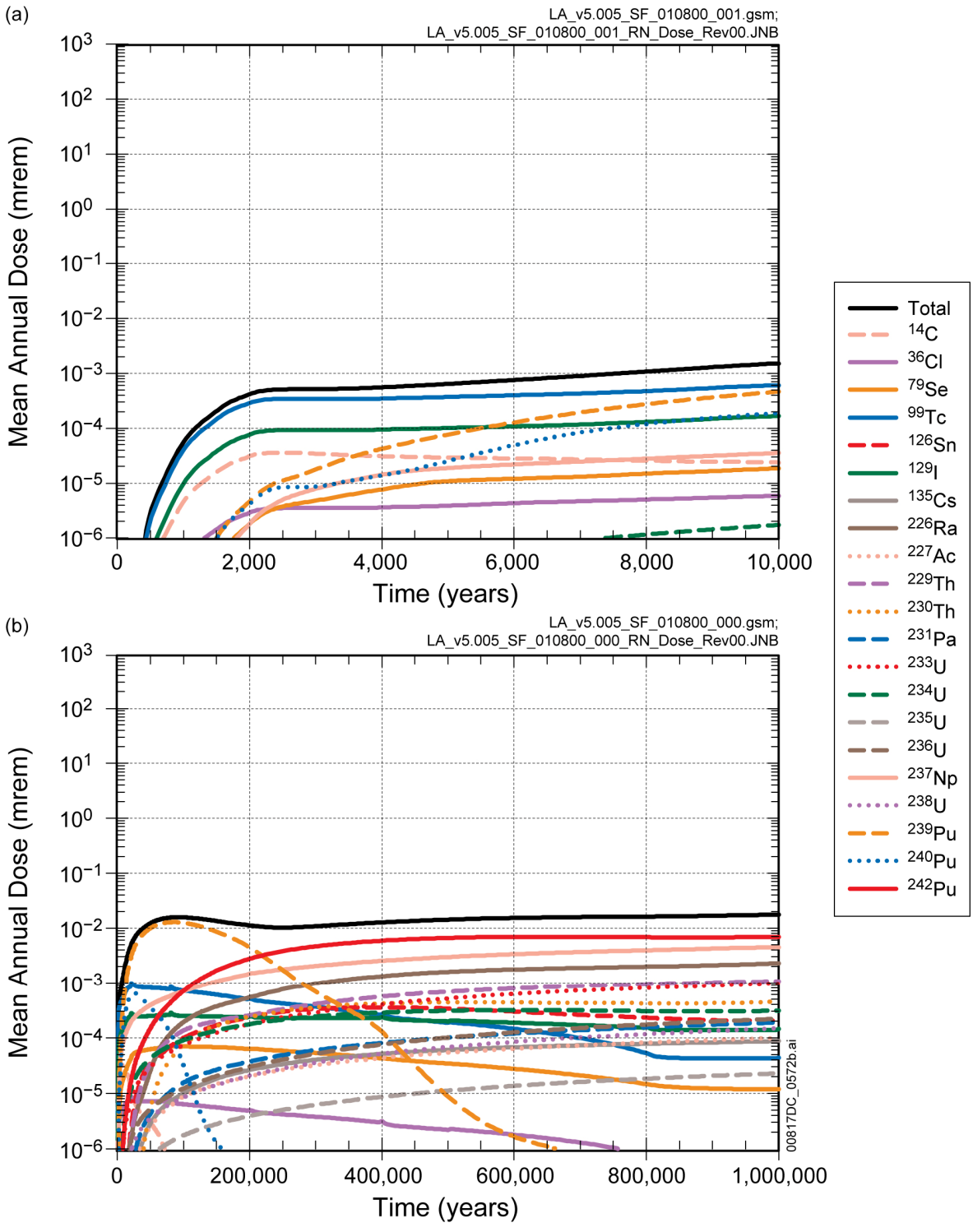

Source: Output DTNs: MO0710ADTSPAWO.000 [DIRS 183752]; and MO0710PLOTSFIG.000 [DIRS 185207].

Figure 8.2-14[a]. Contribution of Individual Radionuclides to Mean Annual Dose for the Seismic Fault Displacement Modeling Case for (a) 10,000 Years and (b) 1,000,000 Years after Repository Closure

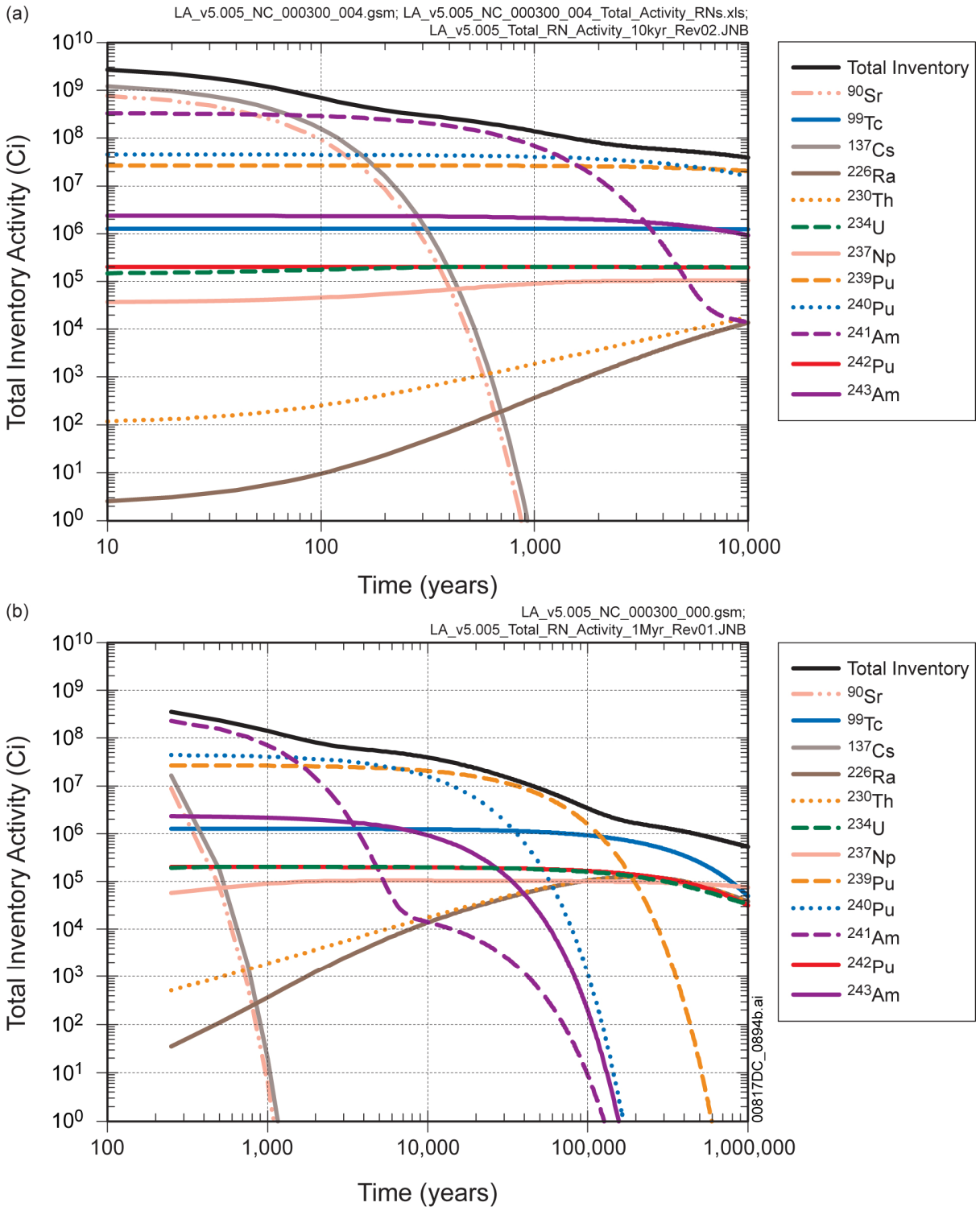

Source: Output DTNs: MO0710ADTSPAWO.000 [DIRS 183752]; and MO0710PLOTSFIG.000 [DIRS 185207].

Figure 8.3-1[a]. Mean Radionuclide Activities for Total Repository Inventory as a Function of Time for (a) 10,000 Years and (b) 1,000,000 Years after Repository Closure

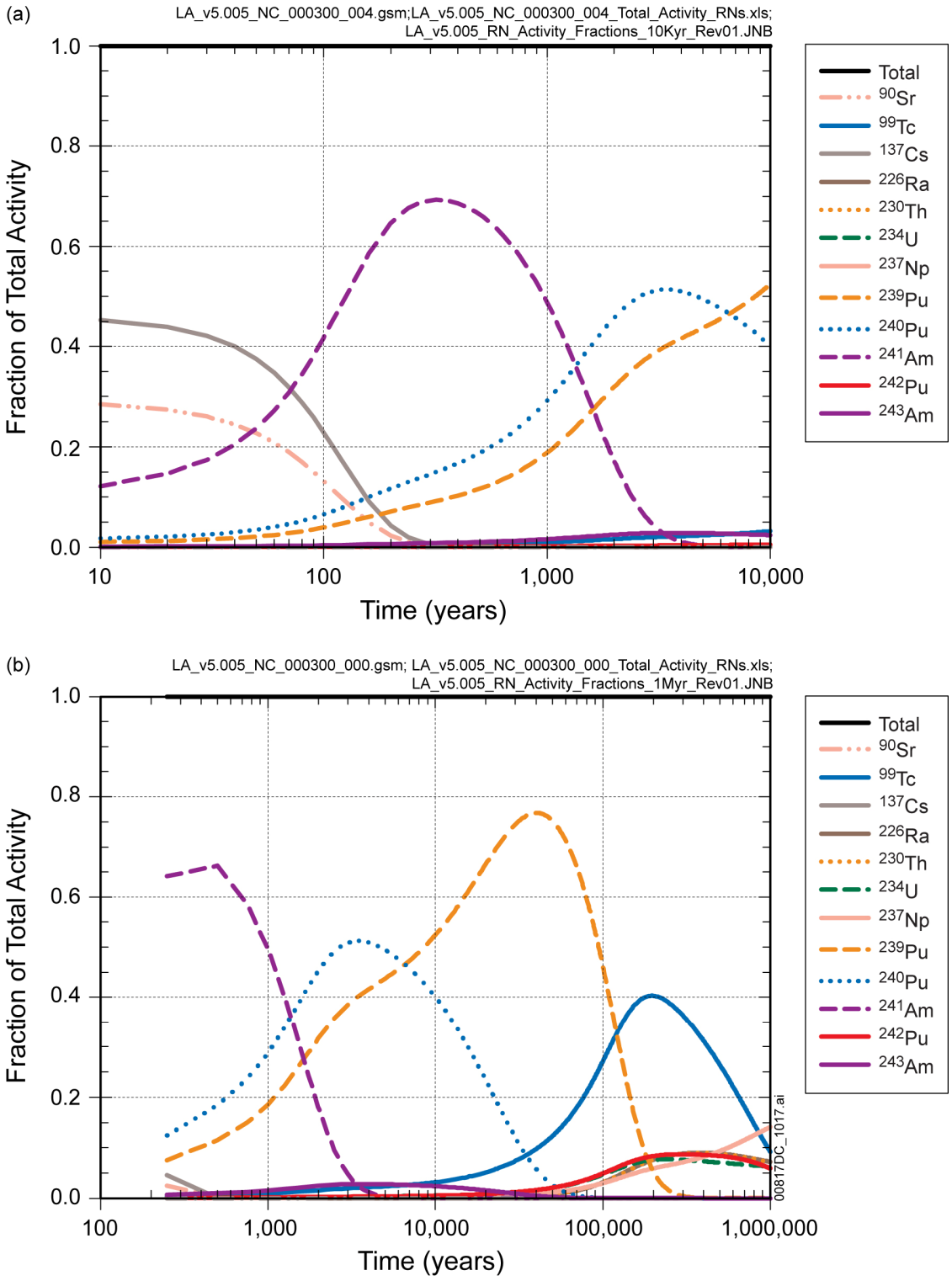

Source: Output DTNs: MO0710ADTSPAWO.000 [DIRS 183752]; and MO0710PLOTSFIG.000 [DIRS 185207].

Figure 8.3-2[a]. Mean Radionuclide Contributions to Total Inventory as a Function of Time for (a) 10,000 Years and (b) 1,000,000 Years after Repository Closure

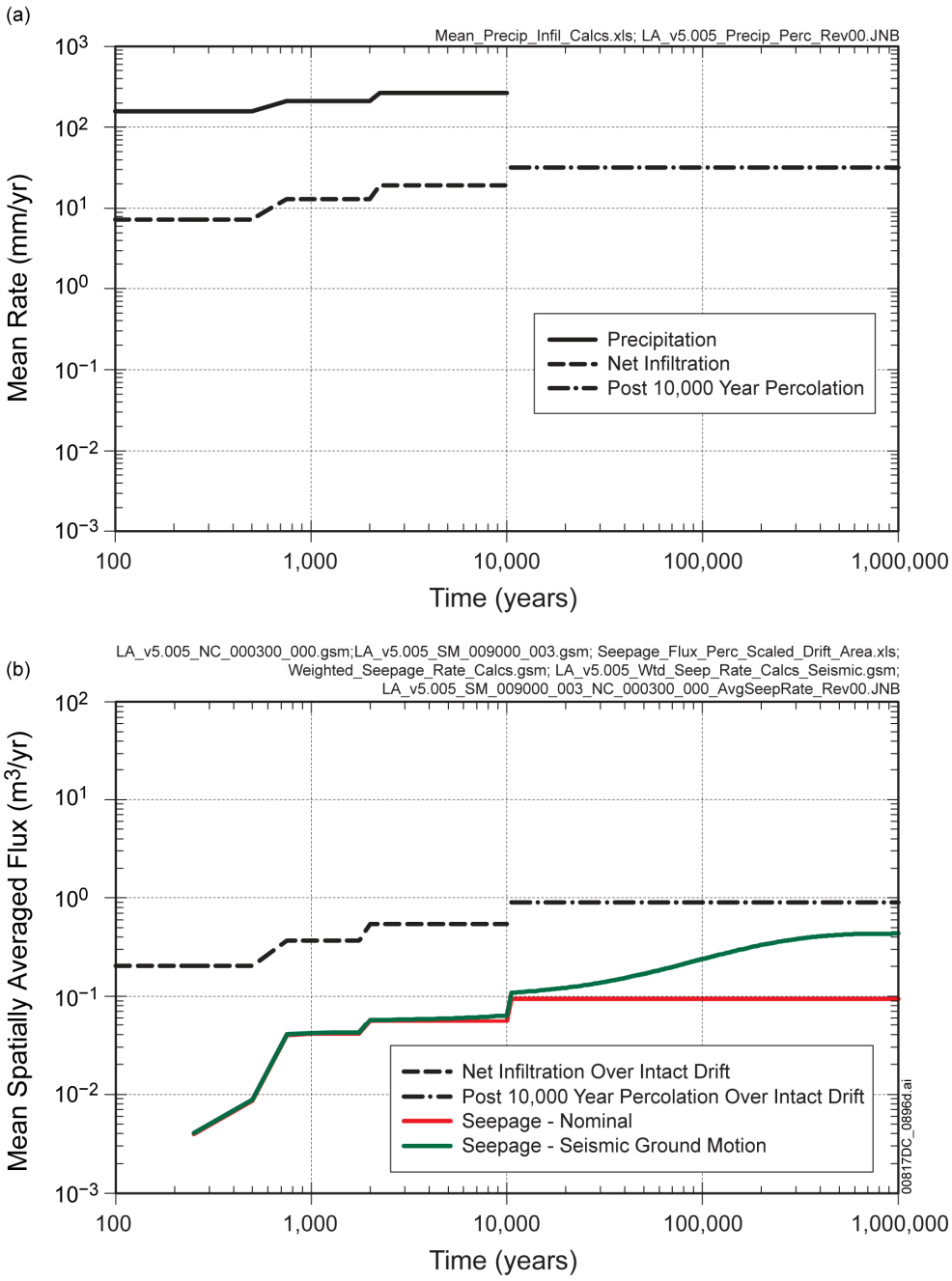

Source: SNL 2007 [DIRS 182145], Tables 6.5.7.1-3, 6.5.7.2-3, and 6.5.7.3-3; NRC Proposed Rule 10 CFR 63.342(c)(2) [DIRS 178394]; and Output DTNs: MO0710ADTSPAWO.000 [DIRS 183752]; MO0710PLOTSFIG.000 [DIRS 185207].

NOTE: For comparison to seepage, volumetric fluxes (m^3/yr) of infiltration and post-10,000 year percolation are calculated by multiplying the net infiltration and post-10,000 year percolation rates by the plan area over an intact drift (m^2).

Figure 8.3-3[a]. Upper Natural Barrier Capability to Prevent or Substantially Reduce the Rate of Water Movement to the Waste for the Mean Spatially-Averaged (a) Annual Precipitation, Net Infiltration, and Post-10,000-Year Percolation Rates and (b) Drift Seepage Fluxes for the Combined Nominal/Early Failure Modeling Case and the Seismic Ground Motion Modeling Case – 1,000,000-Year Period

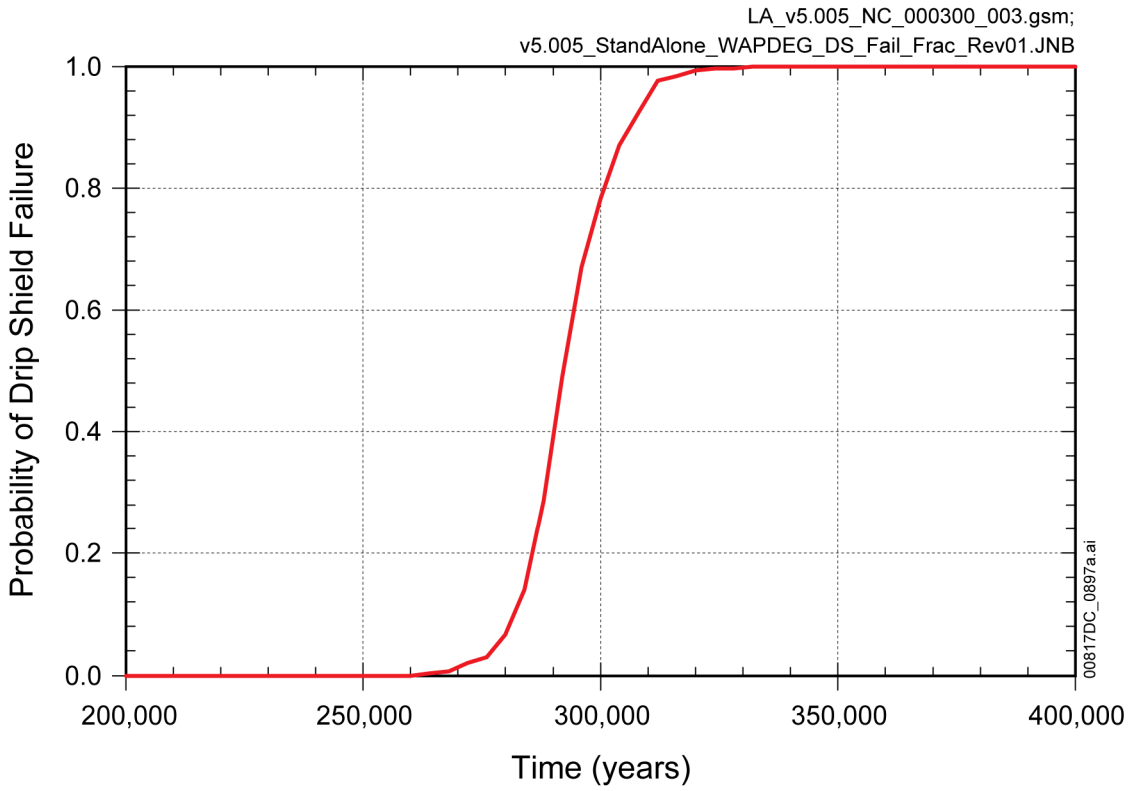

Source: Output DTNs: MO0801TSPAWPDS.000 [DIRS 185077]; and MO0710PLOTSFIG.000 [DIRS 185207].

Figure 8.3-4[a]. Probability of Drip Shield Failure by General Corrosion for the Nominal Modeling Case Based on 300 Epistemic Realizations of Drip Shield General Corrosion Rates

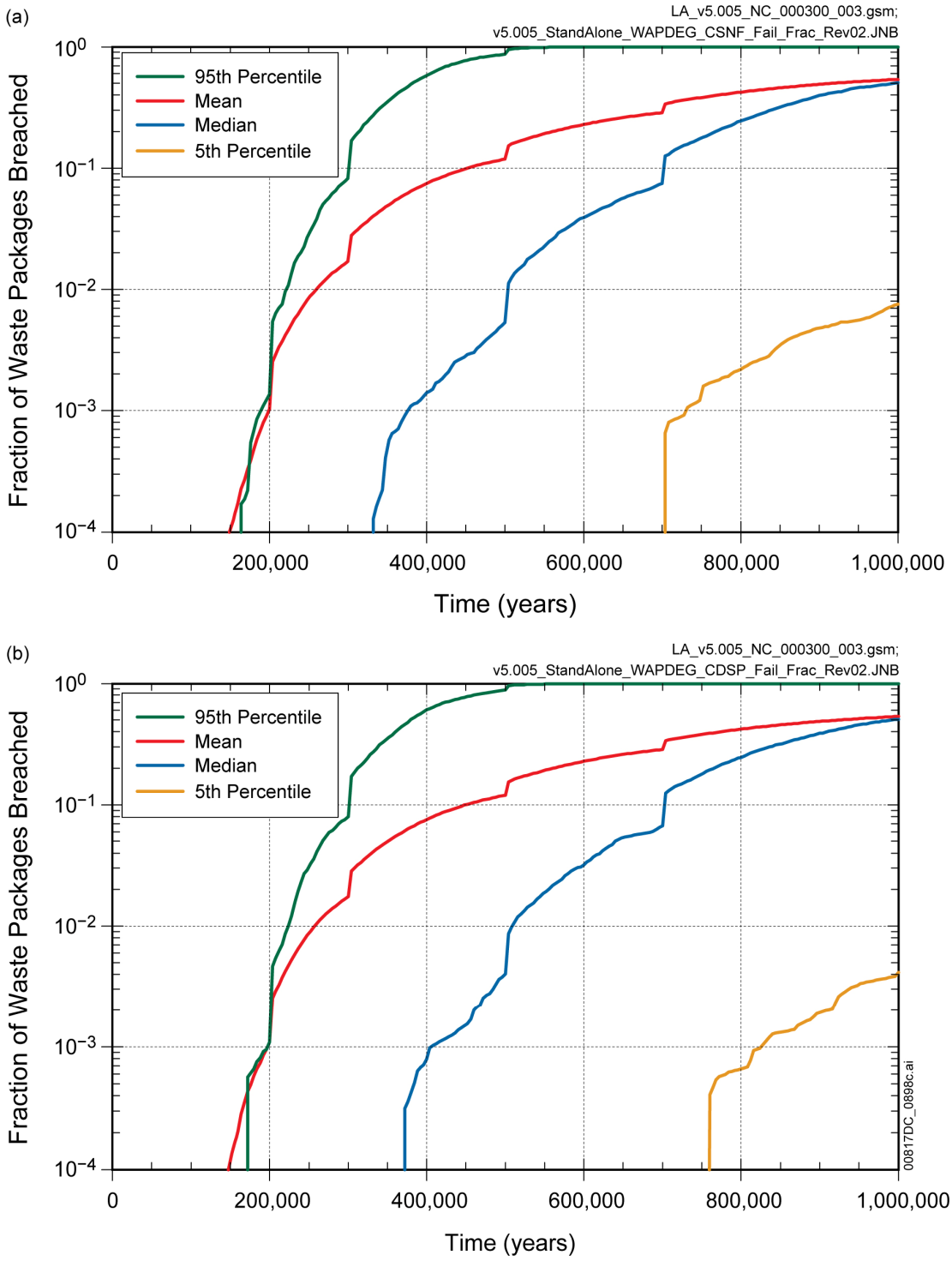

Source: Output DTN: MO0801TSPAWPDS.000 [DIRS 185077].

Figure 8.3-5[a]. Summary Statistics for Fraction of Waste Packages Breached for (a) CSNF Waste Packages and (b) CDSP Waste Packages for the Nominal Modeling Case as a Function of Time

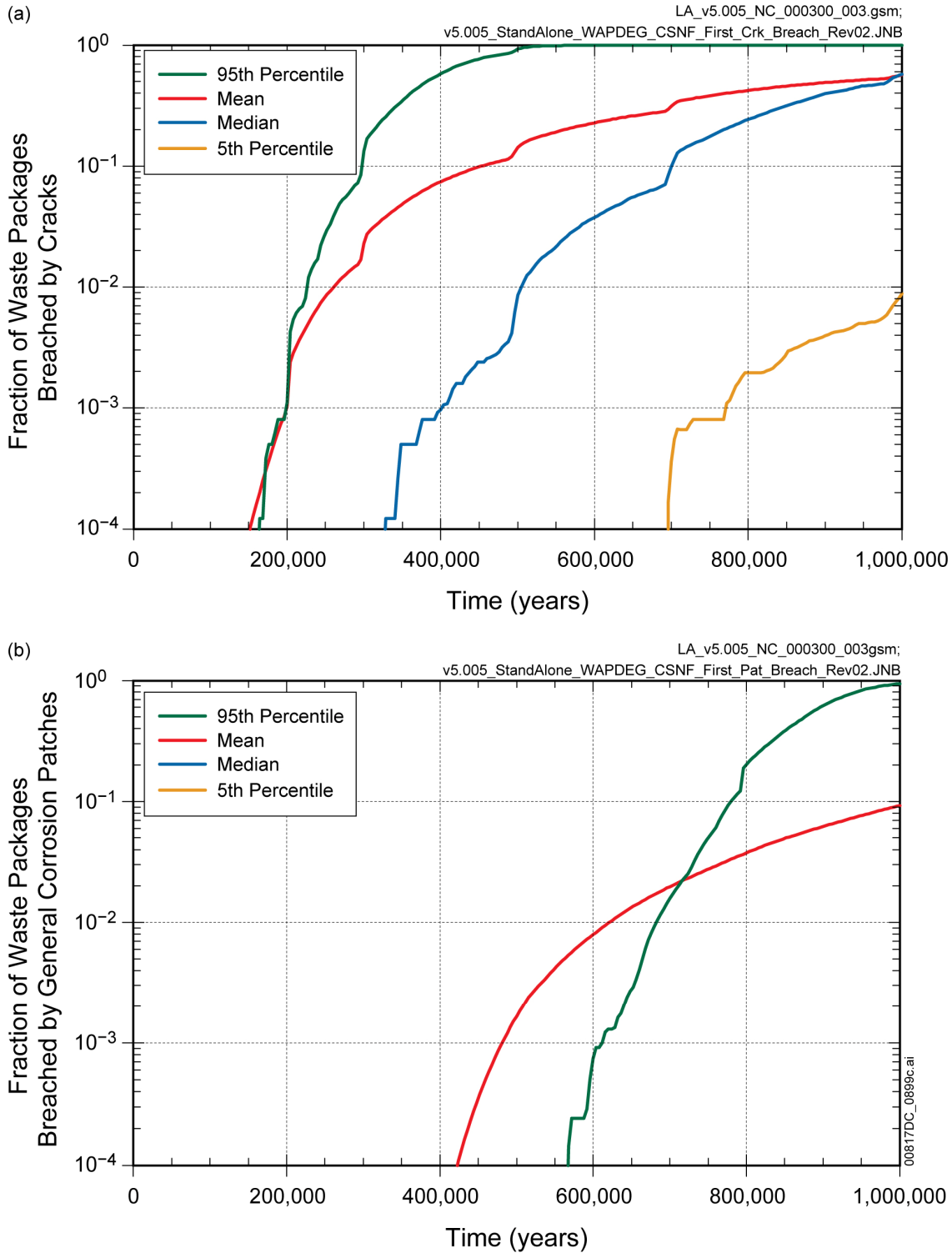

Source: Output DTN: MO0801TSPAWPDS.000 [DIRS 185077].

Figure 8.3-6[a]. Summary Statistics for Fraction of CSNF Waste Packages (a) Breached by Stress Corrosion Cracking and (b) Breached by General Corrosion Patches for the Nominal Modeling Case as a Function of Time

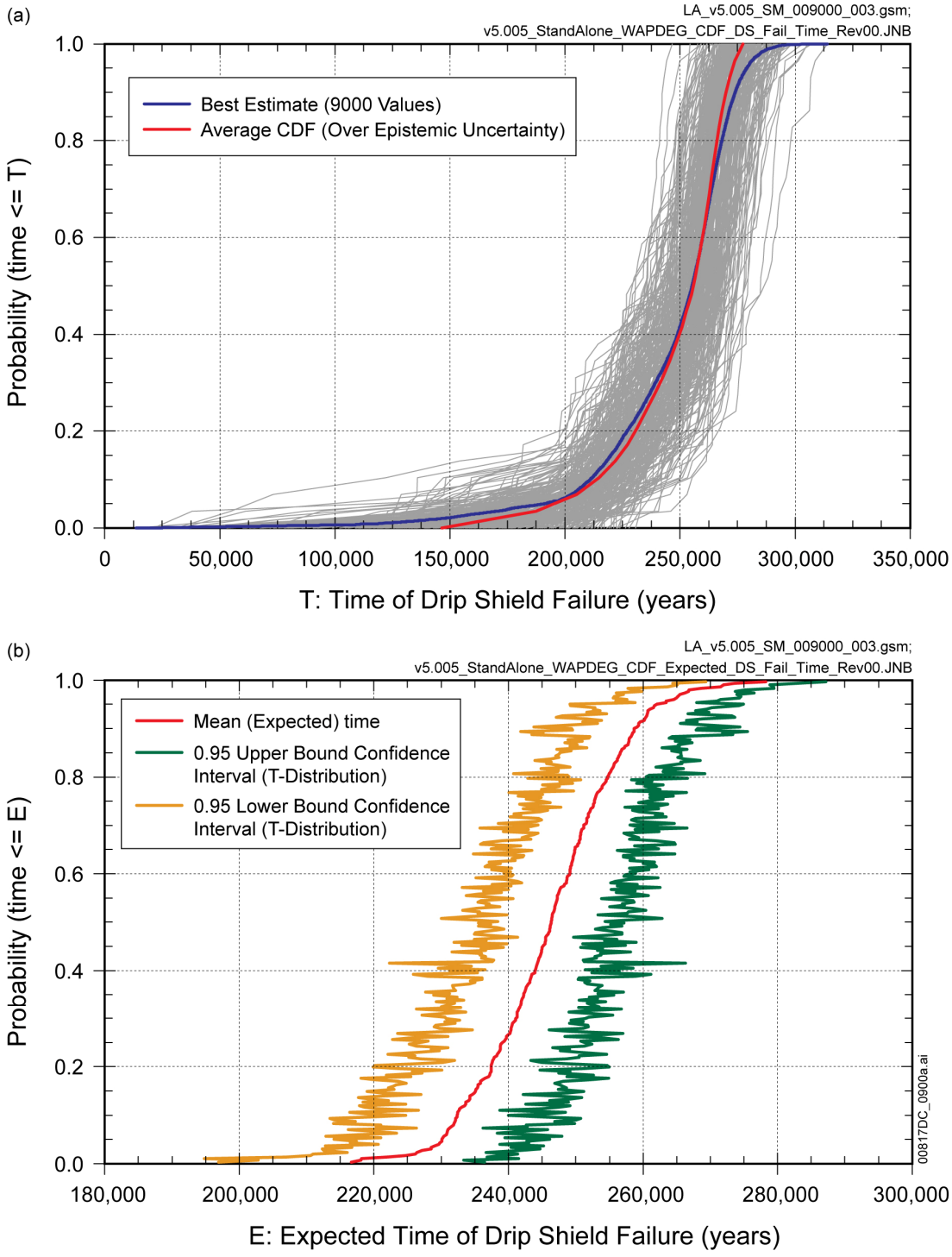

Source: Output DTN: MO0710ADTSPAWO.000 [DIRS 183752].

Figure 8.3-7[a]. Cumulative Distribution Functions of Drip Shield Failure Time for (a) Distributions of Failure Time for 300 Epistemic Sample Elements and (b) Distribution of Expected (Over Aleatory) Failure Time with Confidence Interval for the Seismic Ground Motion Modeling Case

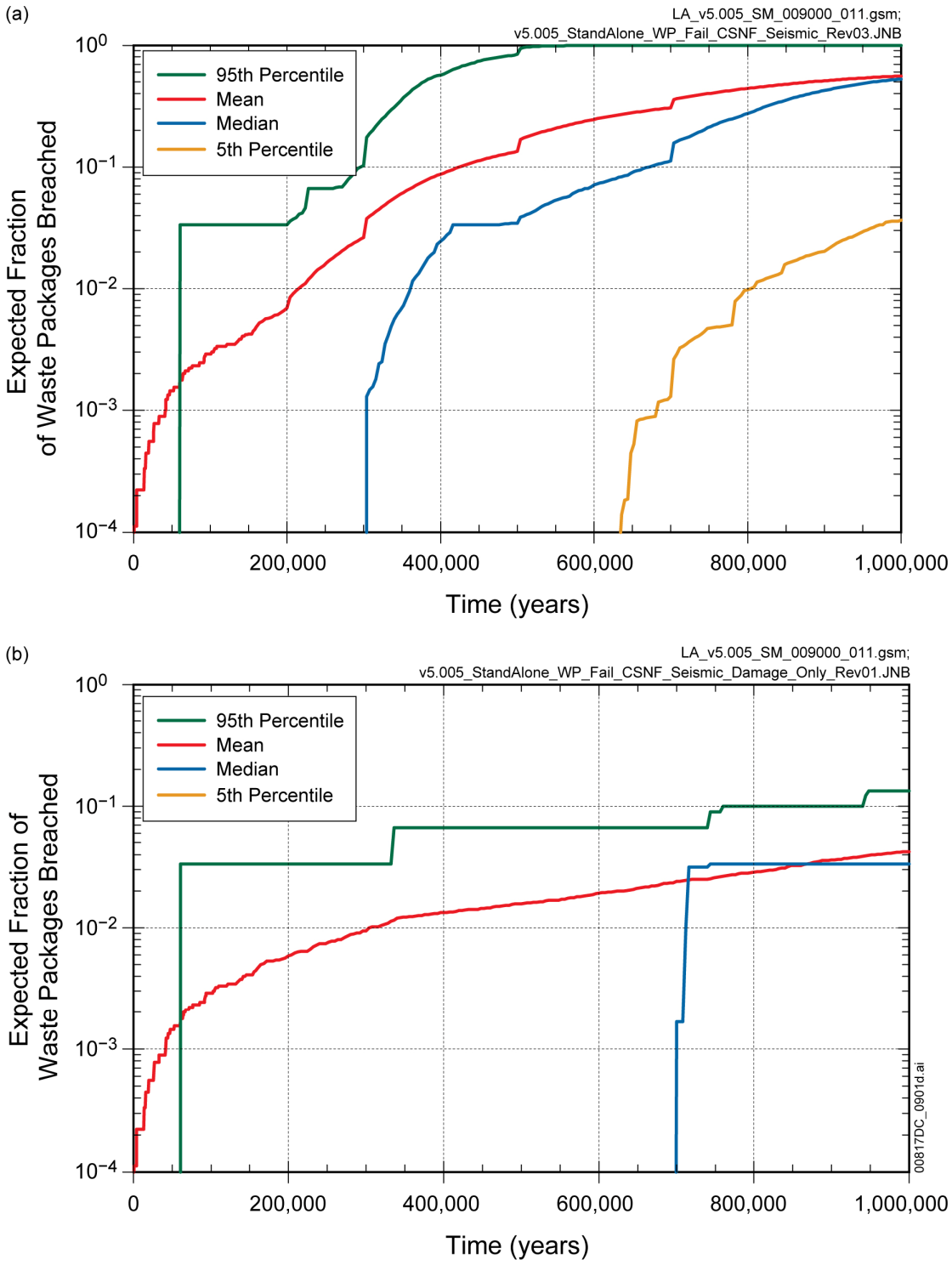

Source: Output DTN: MO0801TSPAWPDS.000 [DIRS 185077].

Figure 8.3-8[a]. Summary Statistics for Expected Fraction of CSNF WPs (a) Breached by Seismic and Nominal Processes and (b) Breached by Seismic Processes Only; and CDSP WPs (c) Breached by Seismic and Nominal Processes and (d) Breached by Seismic Processes Only for the Seismic Ground Motion Modeling Case as a Function of Time

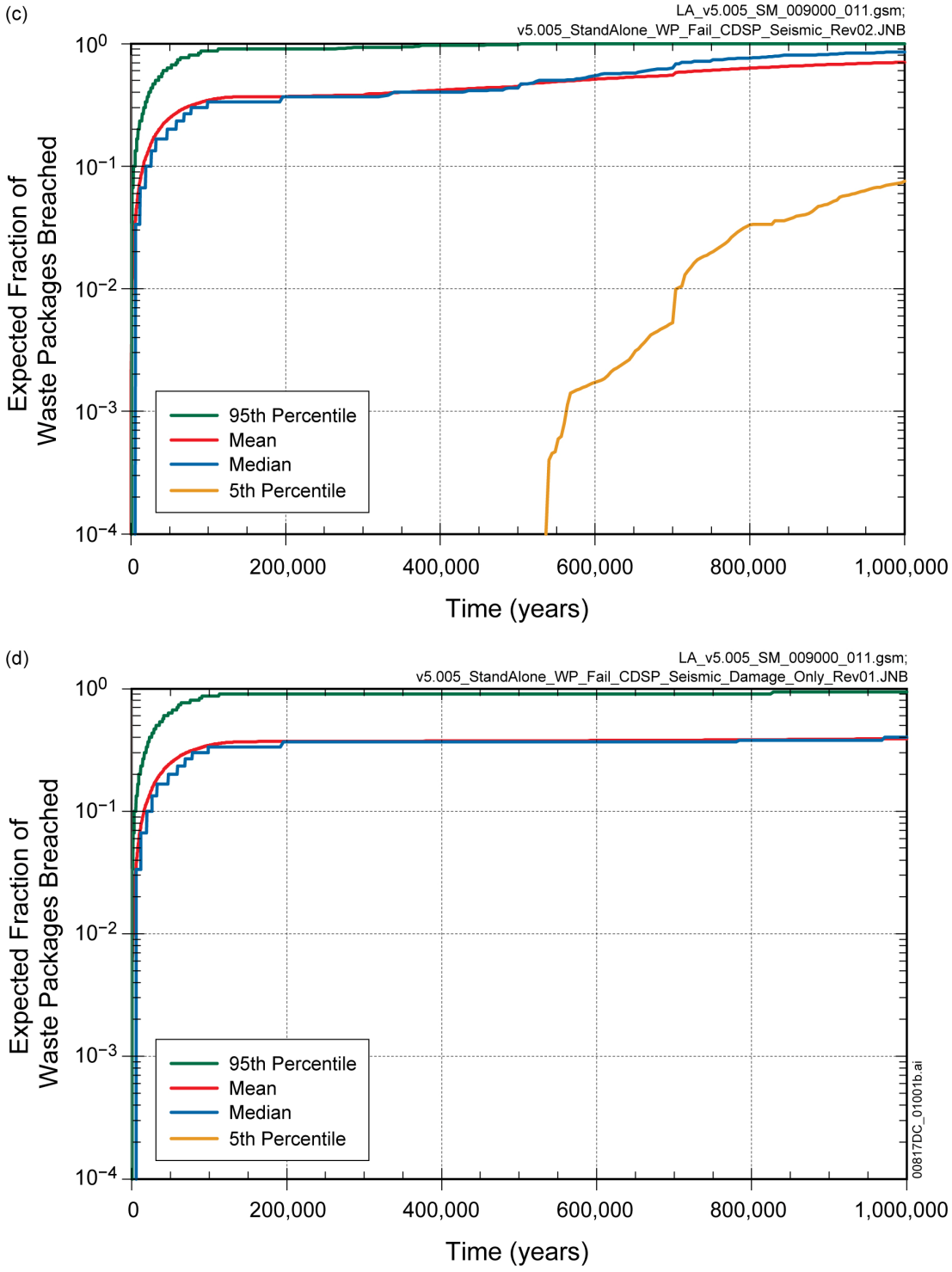

Source: Output DTN: MO0801TSPAWPDS.000 [DIRS 185077].

Figure 8.3-8[a]. Summary Statistics for Expected Fraction of CSNF WPs (a) Breached by Seismic and Nominal Processes and (b) Breached by Seismic Processes Only; and CDSP WPs (c) Breached by Seismic and Nominal Processes and (d) Breached by Seismic Processes Only for the Seismic Ground Motion Modeling Case as a Function of Time (continued)

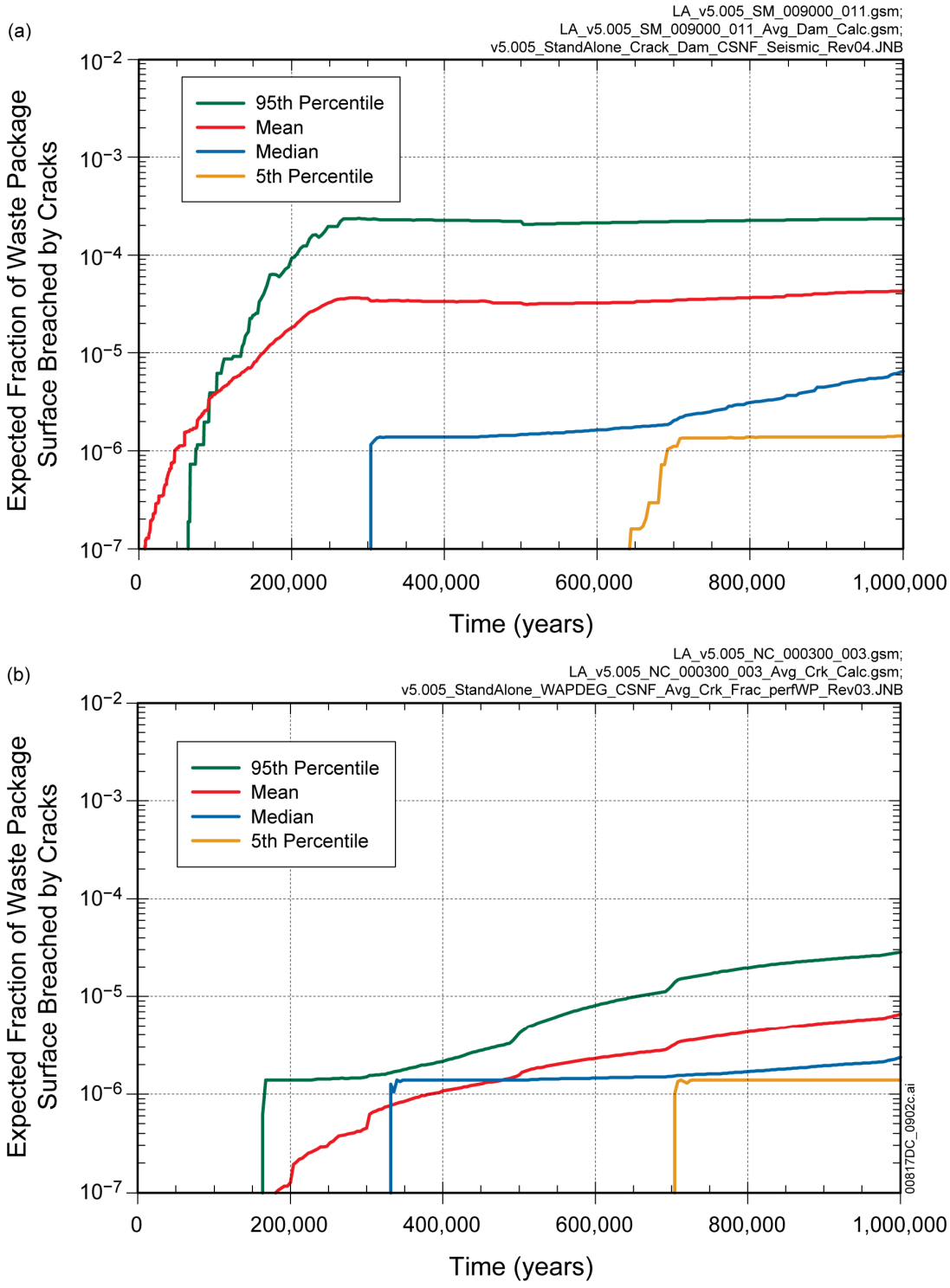

Source: Output DTN: MO0801TSPAWPDS.000 [DIRS 185077].

Figure 8.3-9[a]. Summary Statistics for Average Fraction of CSNF Waste Package Surface Breached by Cracks per Breached Waste Package for (a) the Seismic Ground Motion Modeling Case and (b) the Nominal Modeling Case as a Function of Time

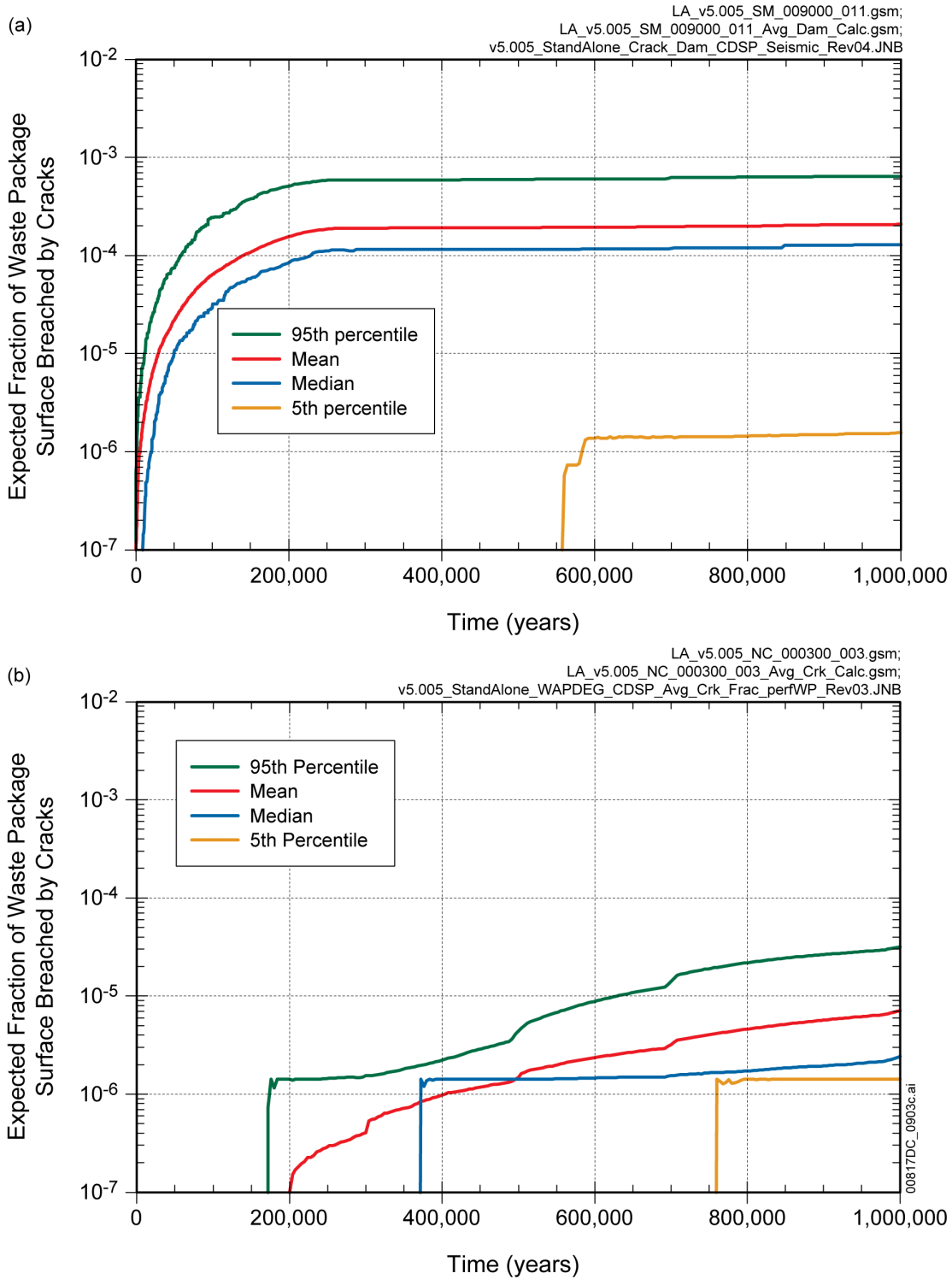

Source: Output DTN: MO0801TSPAWPDS.000 [DIRS 185077].

Figure 8.3-10[a]. Summary Statistics for Fraction of CDSP Waste Package Surface Breached by Cracks per Breached Waste Package for (a) the Seismic Ground Motion Modeling Case and (b) the Nominal Modeling Case as a Function of Time

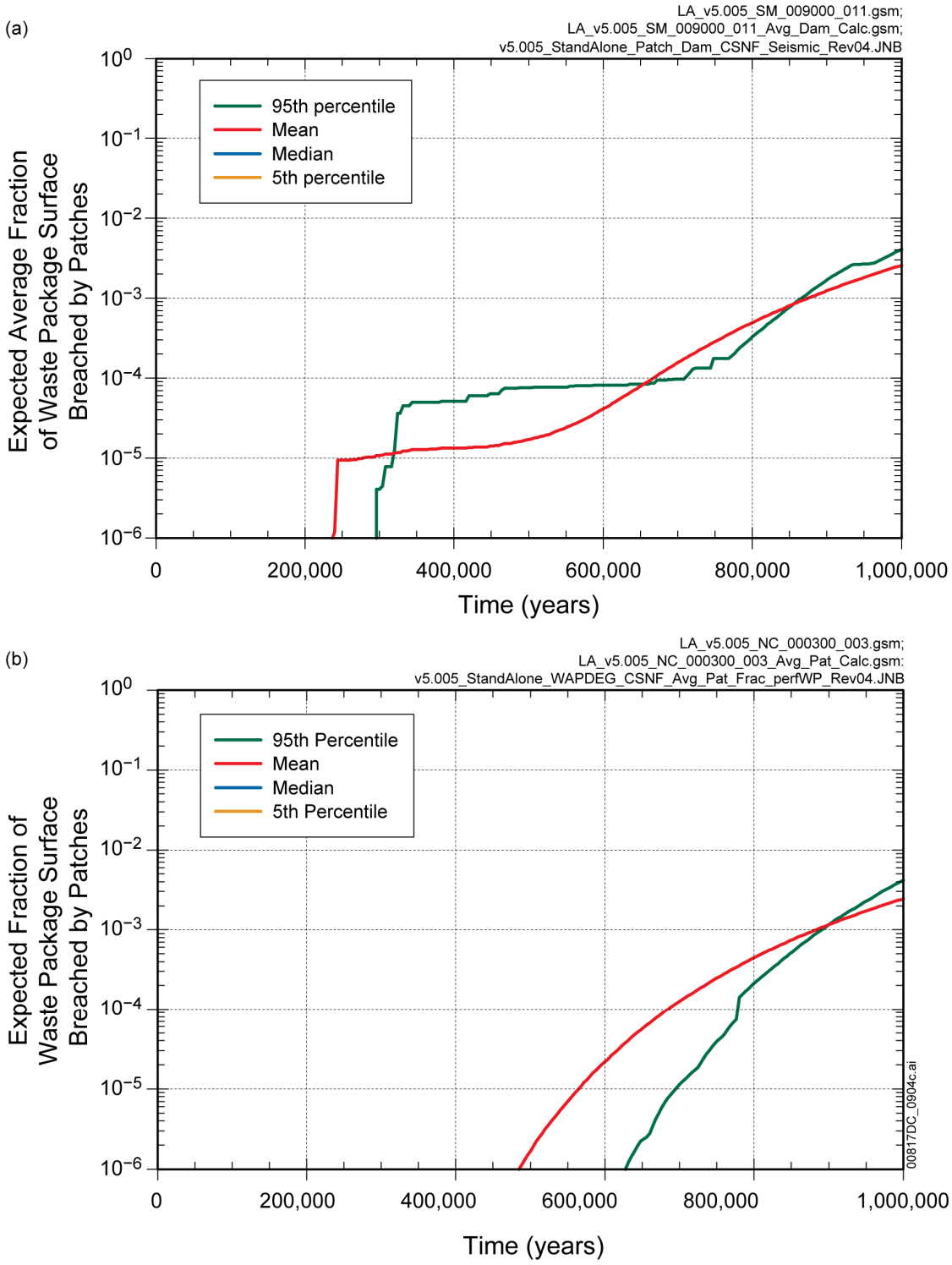

Source: Output DTN: MO0801TSPAWPDS.000 [DIRS 185077].

Figure 8.3-11[a]. Summary Statistics for Fraction of CSNF Waste Package Surface Breached by Patches per Breached Waste Package for (a) the Seismic Ground Motion Modeling Case and (b) the Nominal Modeling Case as a Function of Time

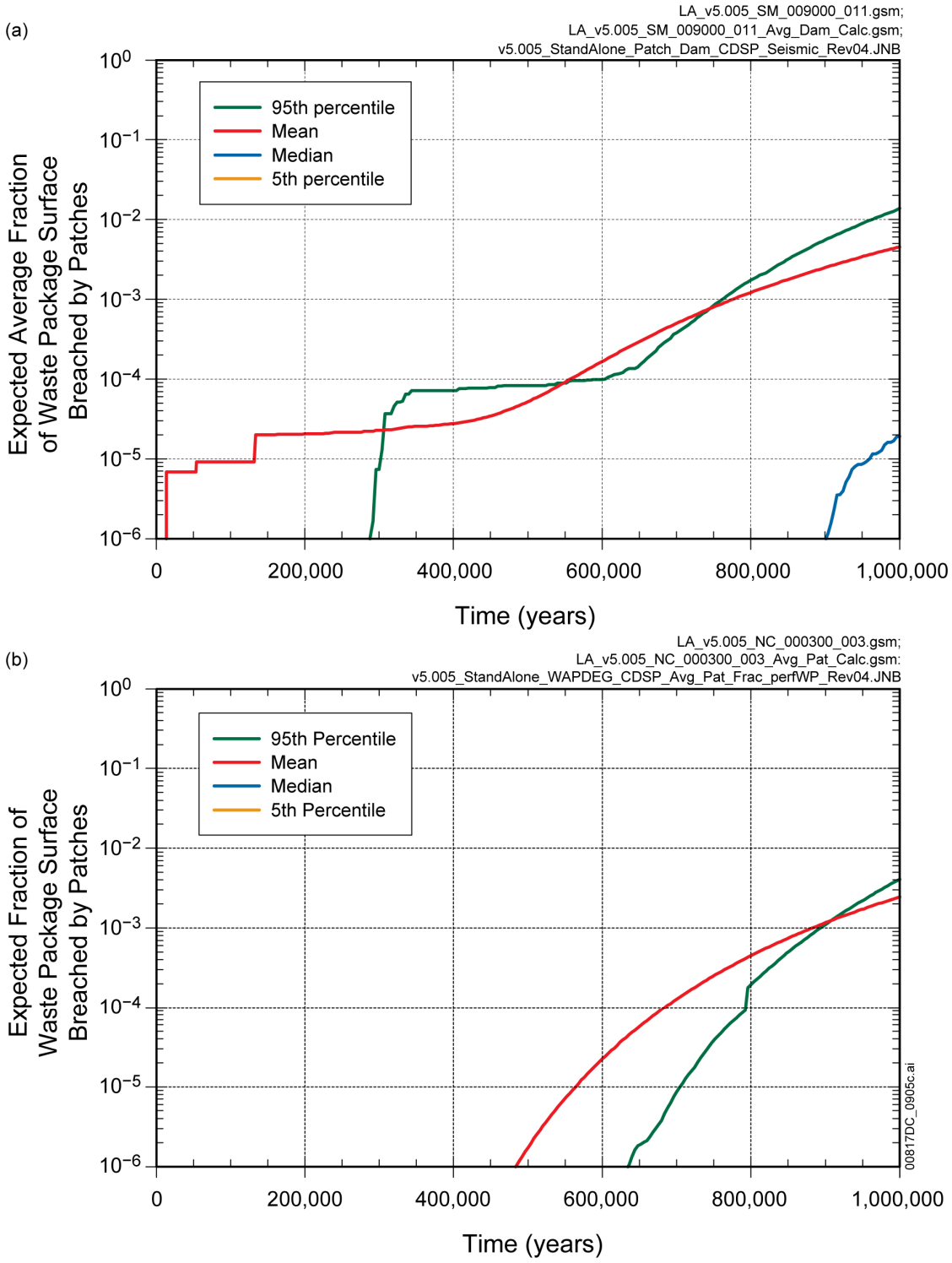

Source: Output DTN: MO0801TSPAWPDS.000 [DIRS 185077].

Figure 8.3-12[a]. Summary Statistics for Fraction of CDSP WP Surface Breached by Patches per Breached Waste Package for (a) the Seismic Ground Motion Modeling Case and (b) the Nominal Modeling Case as a Function of Time

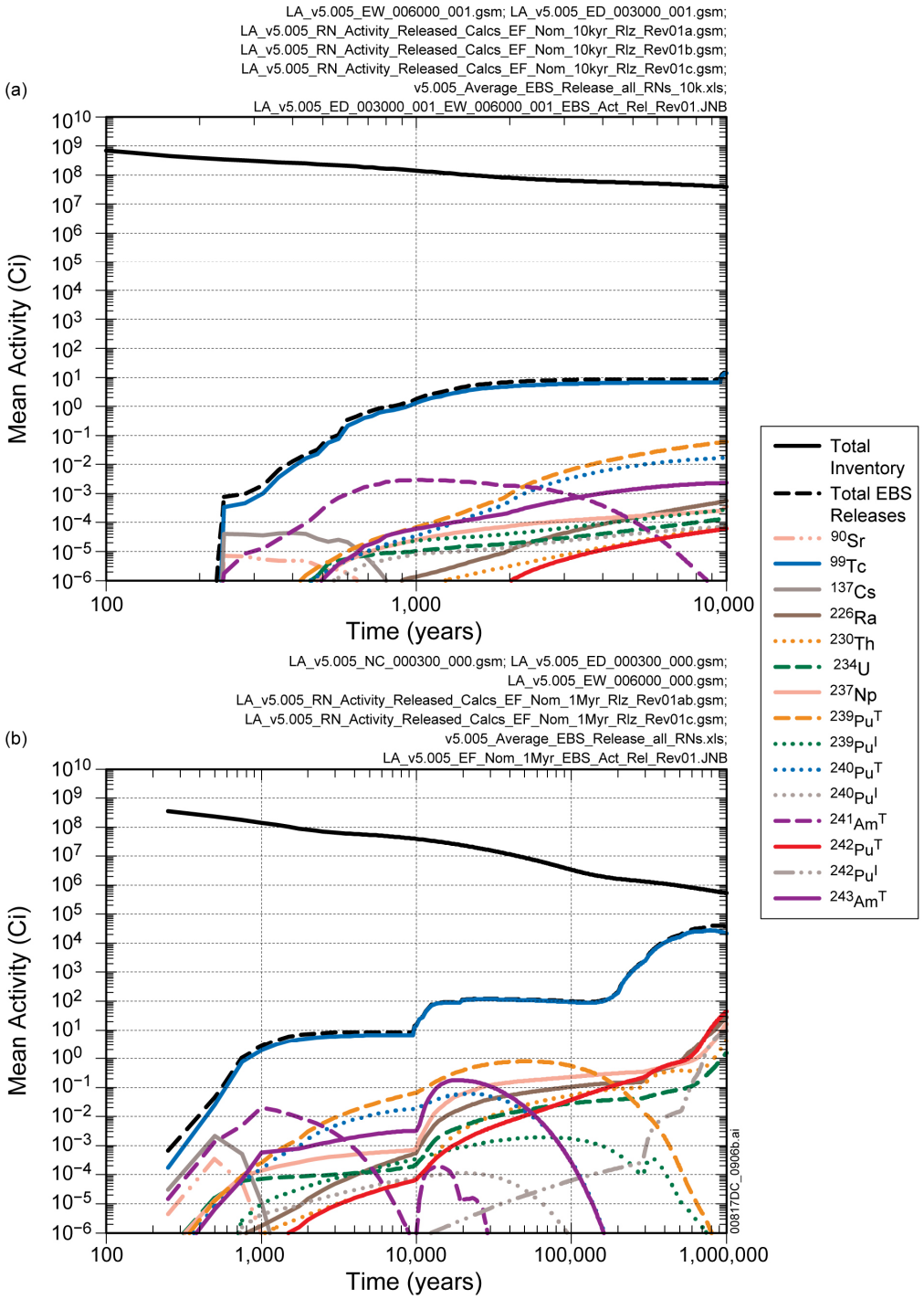

Source: Output DTNs: MO0710ADTSPAWO.000 [DIRS 183752]; and MO0710PLOTSFIG.000 [DIRS 185207].

NOTE: Total inventory indicates the repository total activity as a function of time and is included for comparison to the activity released.

Figure 8.3-13[a]. Mean Activity Released from the Engineered Barrier System for the Combined Nominal/Early Failure Modeling Case for (a) 10,000 Years after Repository Closure and (b) Post-10,000-Years after Repository Closure

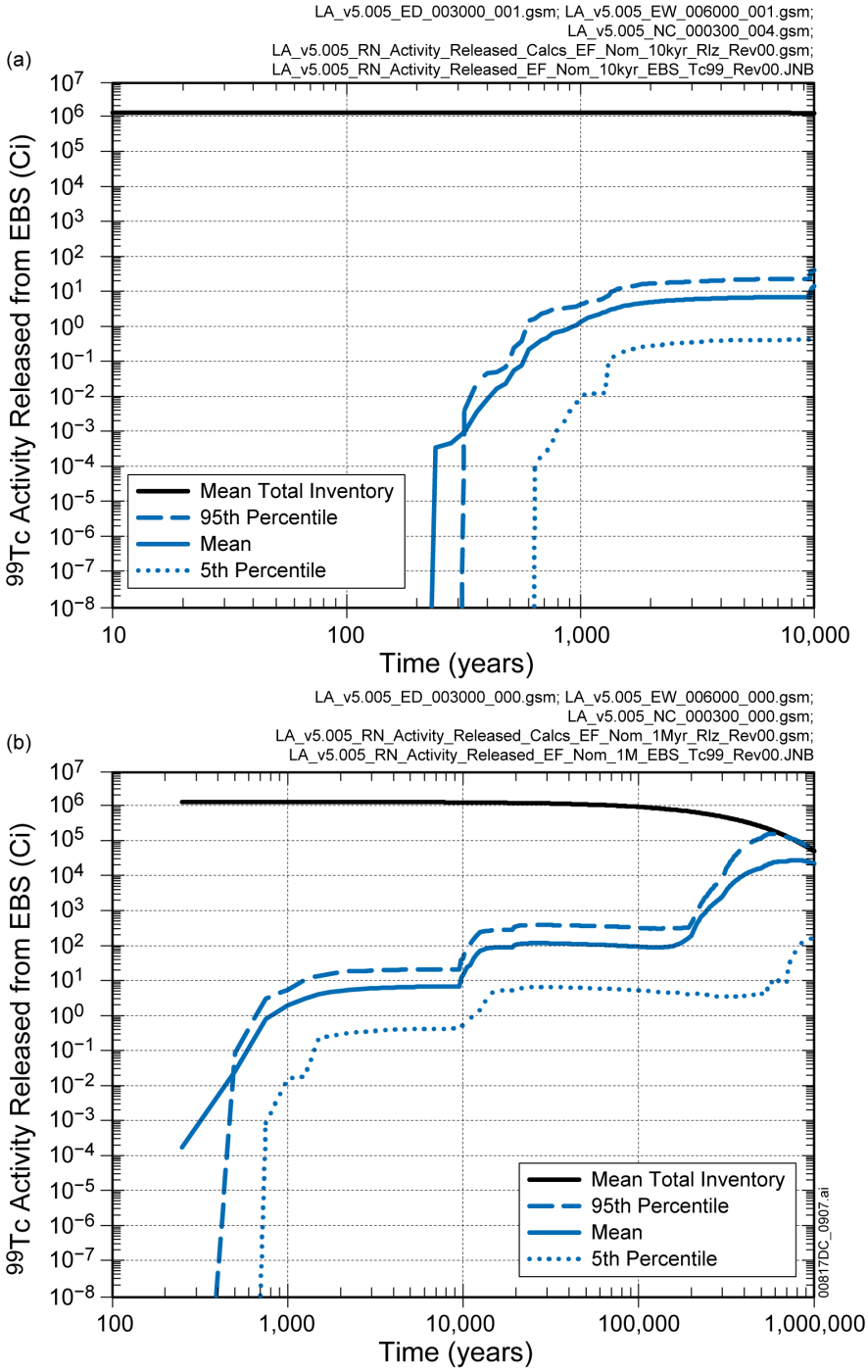

Source: Output DTNs: MO0710ADTSPAWO.000 [DIRS 183752]; and MO0710PLOTSFIG.000 [DIRS 185207].

NOTE: Mean total inventory indicates the repository total ^{99}Tc activity as a function of time and is included for comparison to the activity released.

Figure 8.3-14[a]. Uncertainty in Activity of ^{99}Tc Released from the Engineered Barrier System for the Combined Nominal/Early Failure Modeling Case for (a) 10,000 Years and (b) 1,000,000 Years after Repository Closure

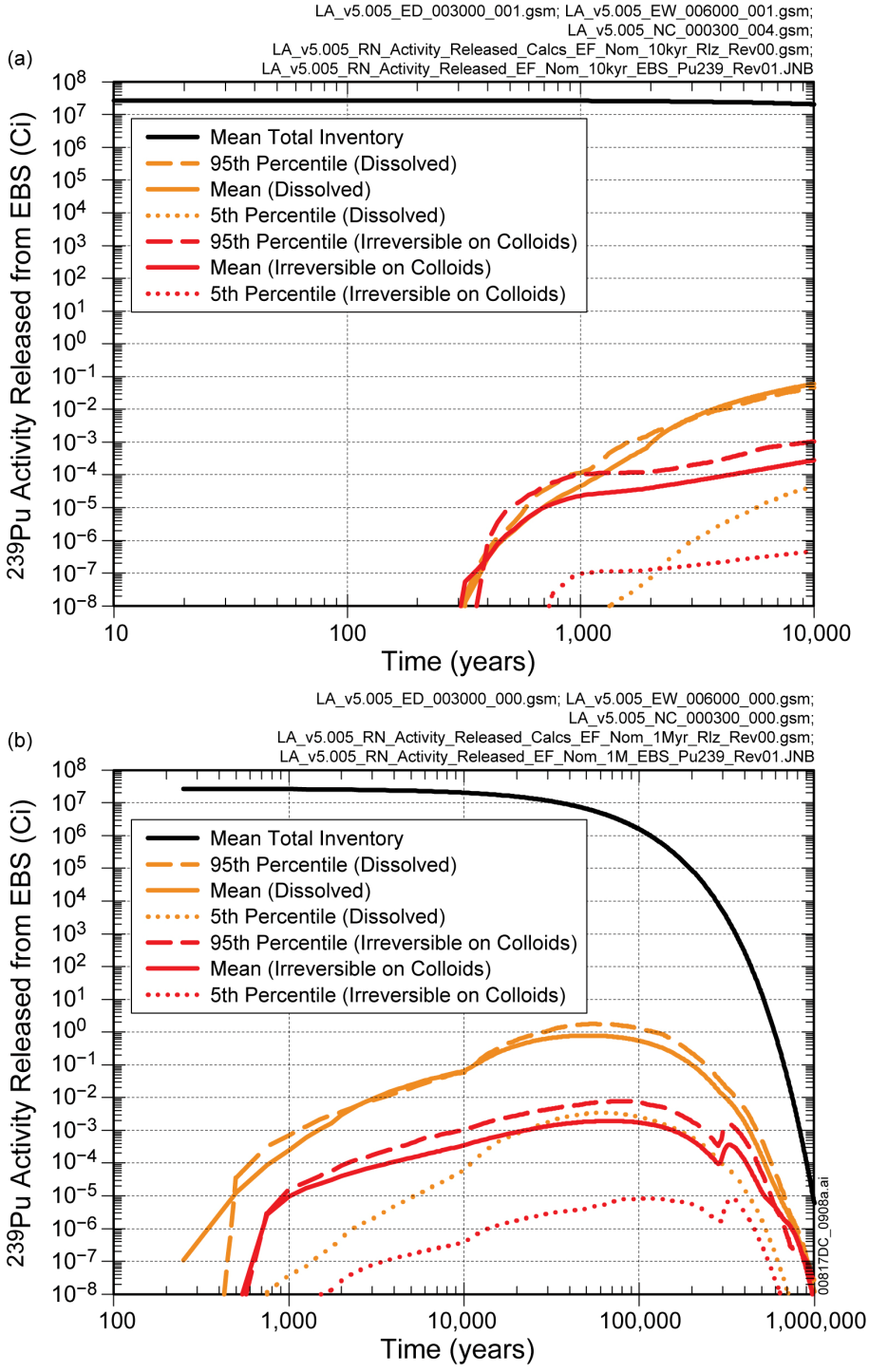

Source: Output DTNs: MO0710ADTSPAWO.000 [DIRS 183752]; and MO0710PLOTSFIG.000 [DIRS 185207].

NOTE: Mean total inventory indicates the repository total ^{239}Pu activity as a function of time and is included for comparison to the activity released.

Figure 8.3-15[a]. Uncertainty in Activity of ^{239}Pu Released from the Engineered Barrier System for the Combined Nominal/Early Failure Modeling Case for (a) 10,000 Years and (b) 1,000,000 Years after Repository Closure

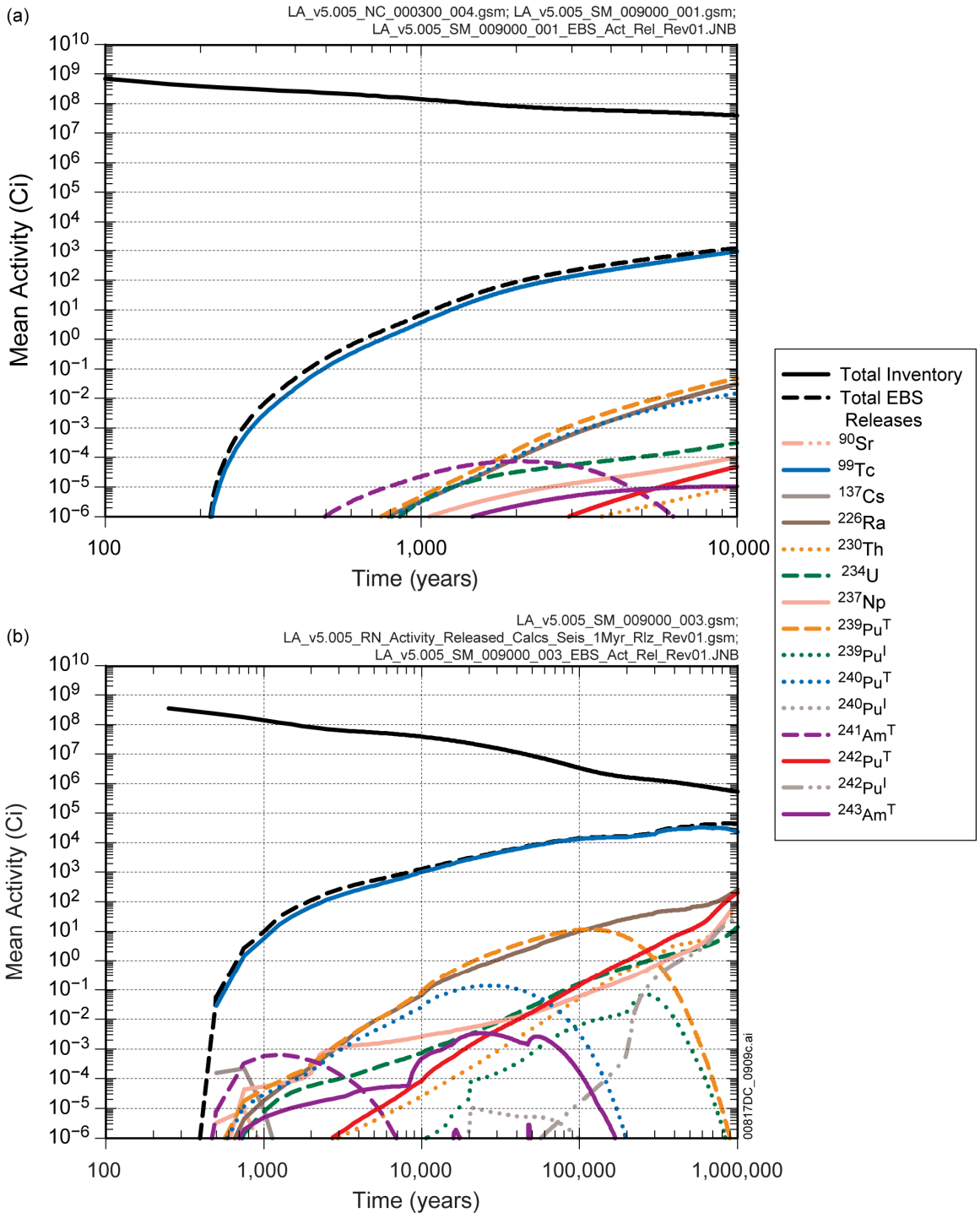

Source: Output DTNs: MO0710ADTSPAWO.000 [DIRS 183752]; and MO0710PLOTSFIG.000 [DIRS 185207].

NOTE: Total inventory indicates the repository total activity as a function of time and is included for comparison to the activity released.

Figure 8.3-16[a]. Mean Activity Released from the Engineered Barrier System for the Seismic Ground Motion Modeling Case for (a) 10,000 Years and (b) 1,000,000 Years after Repository Closure

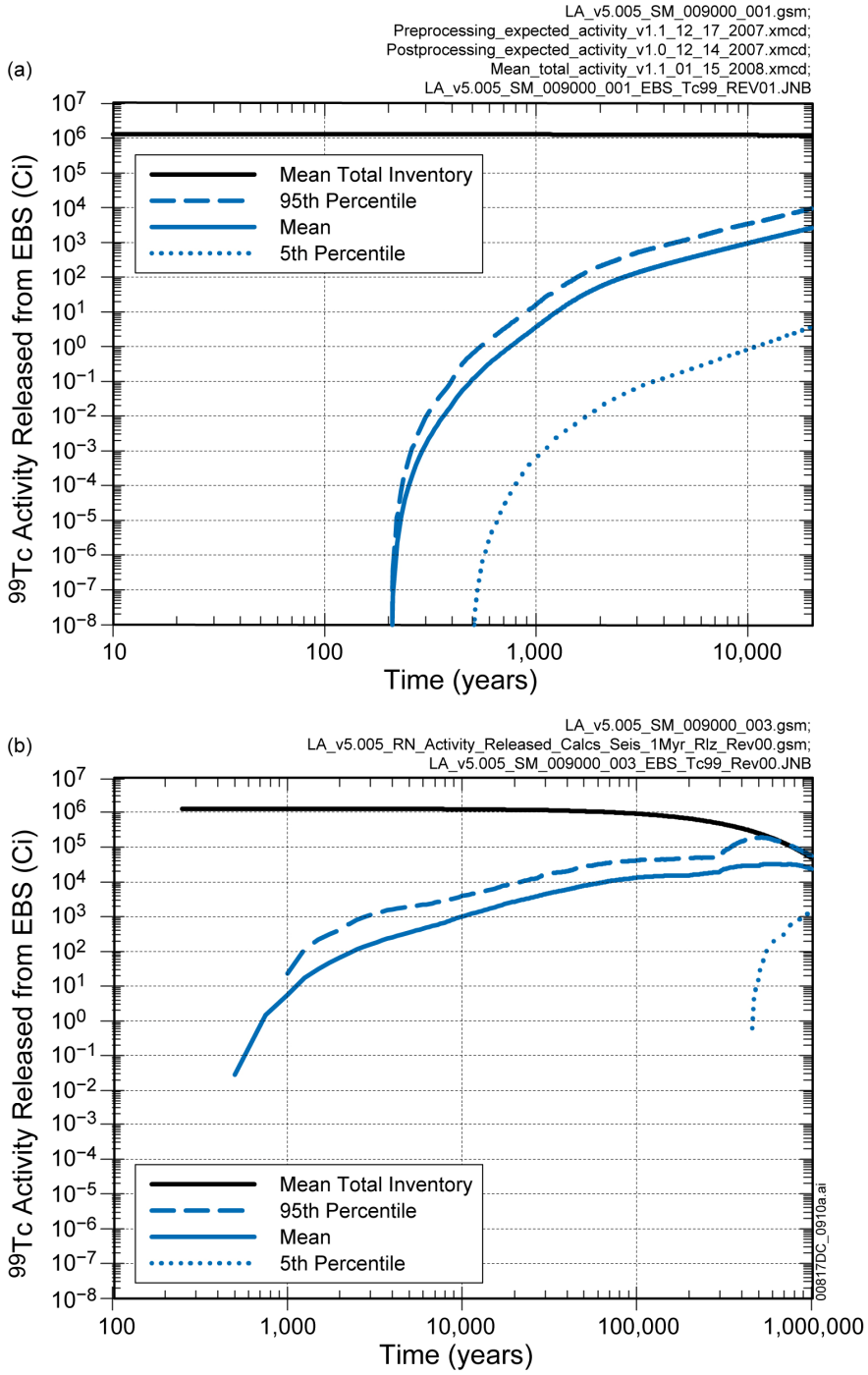

Source: Output DTNs: MO0710ADTSPAWO.000 [DIRS 183752]; and MO0710PLOTSFIG.000 [DIRS 185207].

NOTE: Mean total inventory indicates the repository total ^{99}Tc activity as a function of time and is included for comparison to the activity released.

Figure 8.3-17[a]. Uncertainty in Activity of ^{99}Tc Released from the Engineered Barrier System for the Seismic Ground Motion Modeling Case for (a) 10,000 Years and (b) 1,000,000 Years after Repository Closure

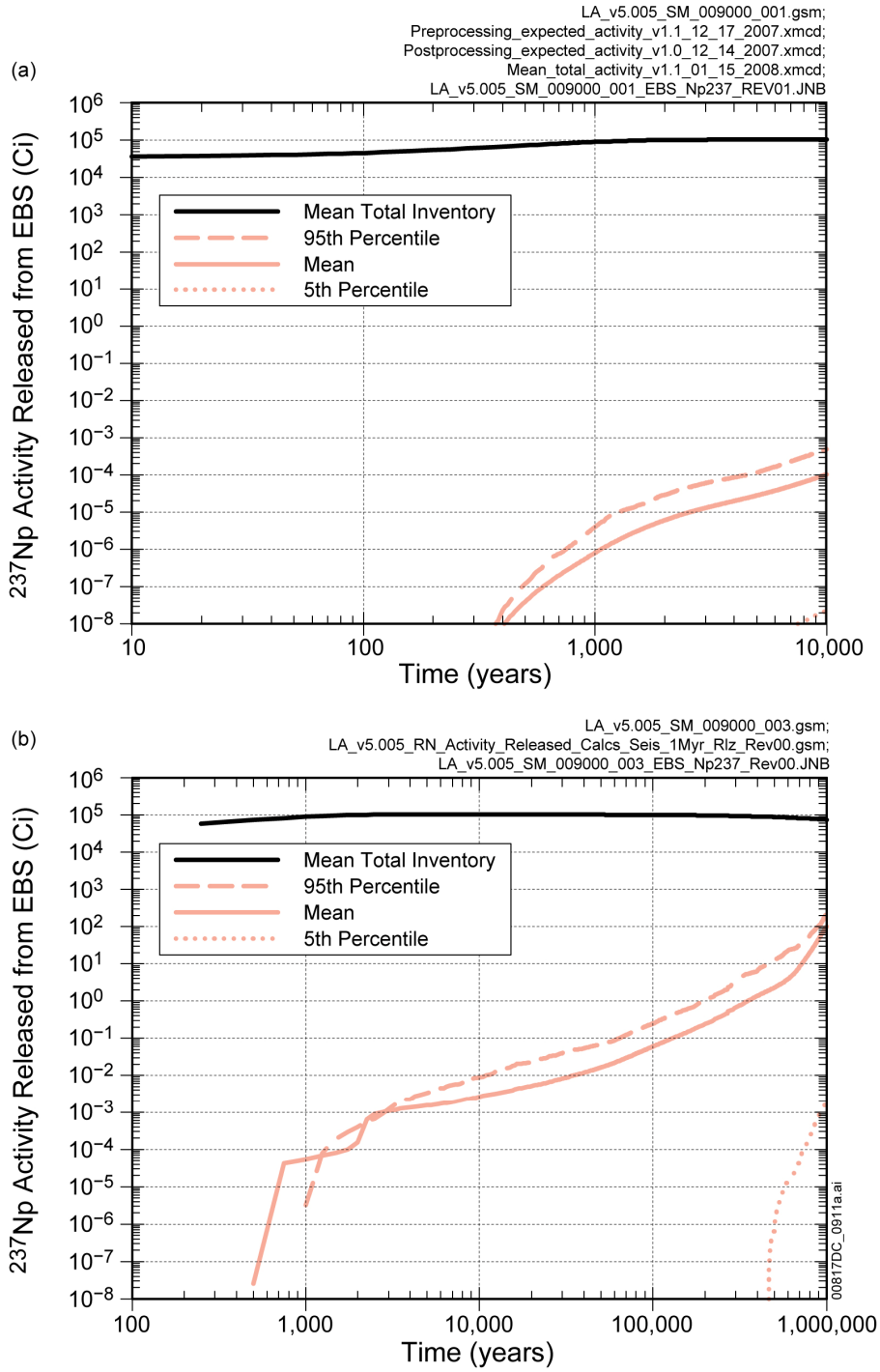

Source: Output DTNs: MO0710ADTSPAWO.000 [DIRS 183752]; and MO0710PLOTSFIG.000 [DIRS 185207].

NOTE: Mean total inventory indicates the repository total ^{237}Np activity as a function of time and is included for comparison to the activity released.

Figure 8.3-18[a]. Uncertainty in Activity of ^{237}Np Released from the Engineered Barrier System for the Seismic Ground Motion Modeling Case for (a) 10,000 Years and (b) 1,000,000 Years after Repository Closure

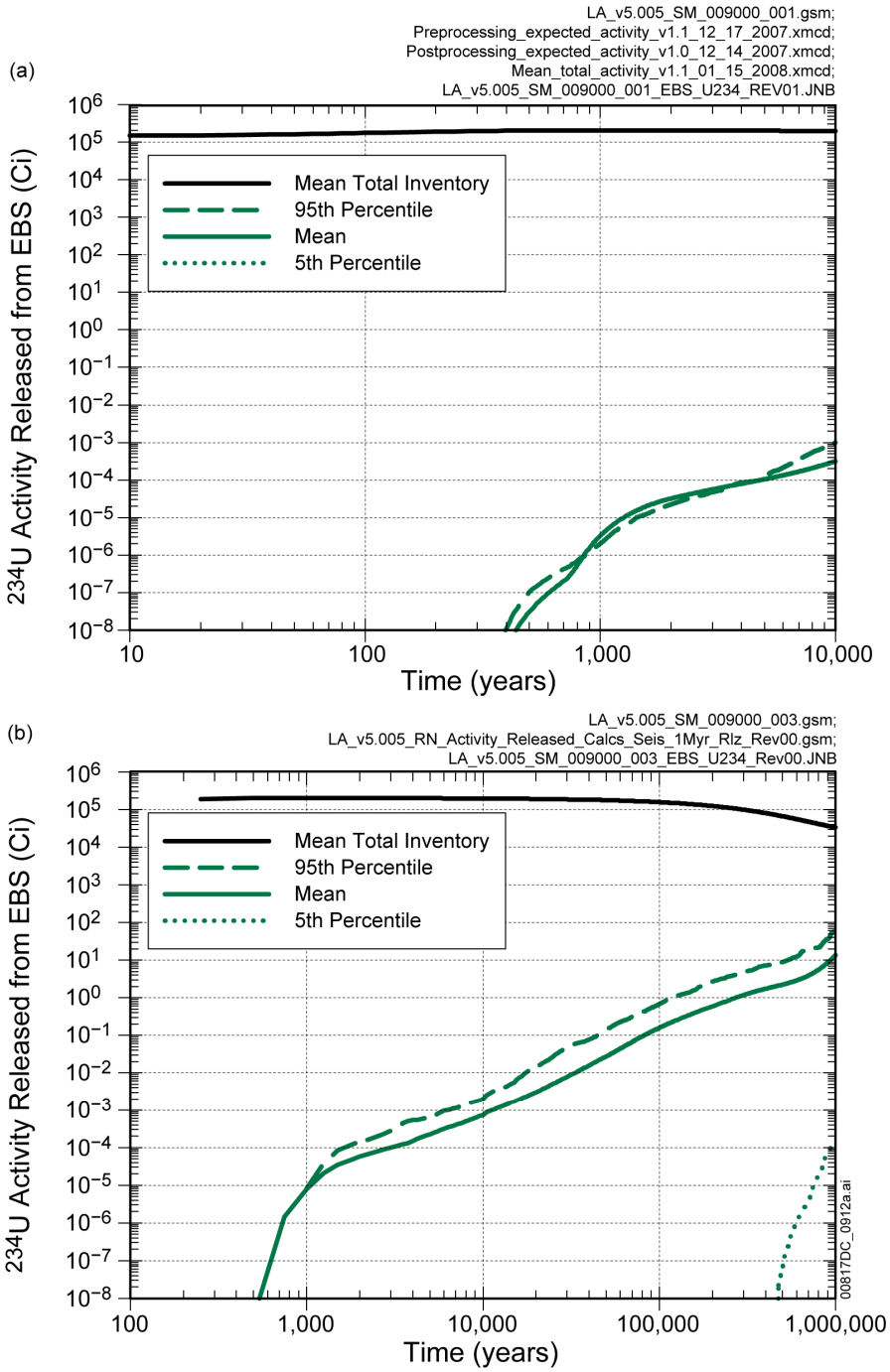

Source: Output DTNs: MO0710ADTSPAWO.000 [DIRS 183752]; and MO0710PLOTSFIG.000 [DIRS 185207].

NOTE: Mean total inventory indicates the repository total ^{234}U activity as a function of time and is included for comparison to the activity released.

Figure 8.3-19[a]. Uncertainty in Activity of ^{234}U Released from the Engineered Barrier System for the Seismic Ground Motion Modeling Case for (a) 10,000 Years and (b) 1,000,000 Years after Repository Closure

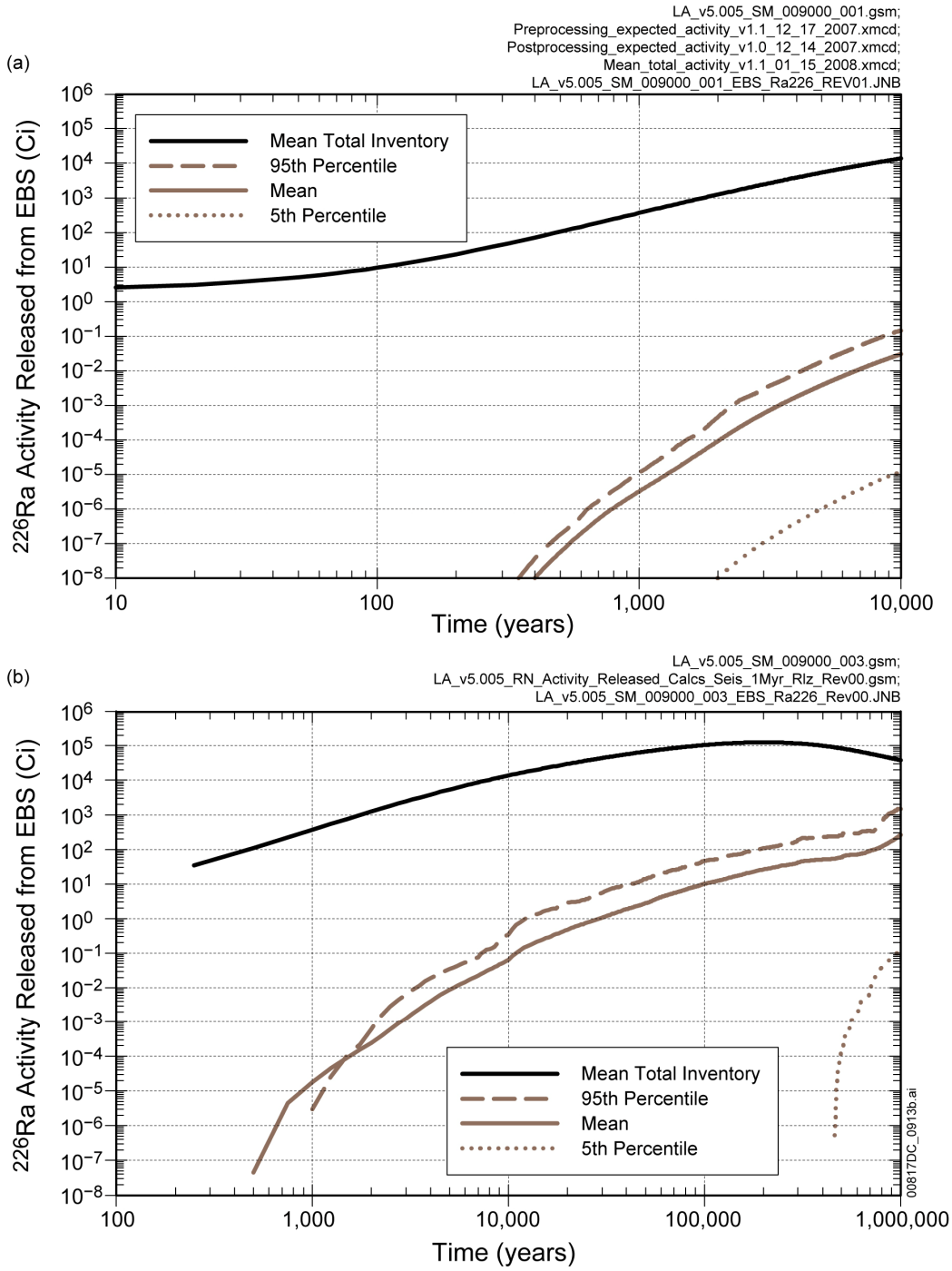

Source: Output DTNs: MO0710ADTSPAWO.000 [DIRS 183752]; and MO0710PLOTSFIG.000 [DIRS 185207].

NOTE: Mean total inventory indicates the repository total ^{226}Ra activity as a function of time and is included for comparison to the activity released.

Figure 8.3-20[a]. Uncertainty in Activity of ^{226}Ra Released from the Engineered Barrier System for the Seismic Ground Motion Modeling Case for (a) 10,000 Years and (b) 1,000,000 Years after Repository Closure

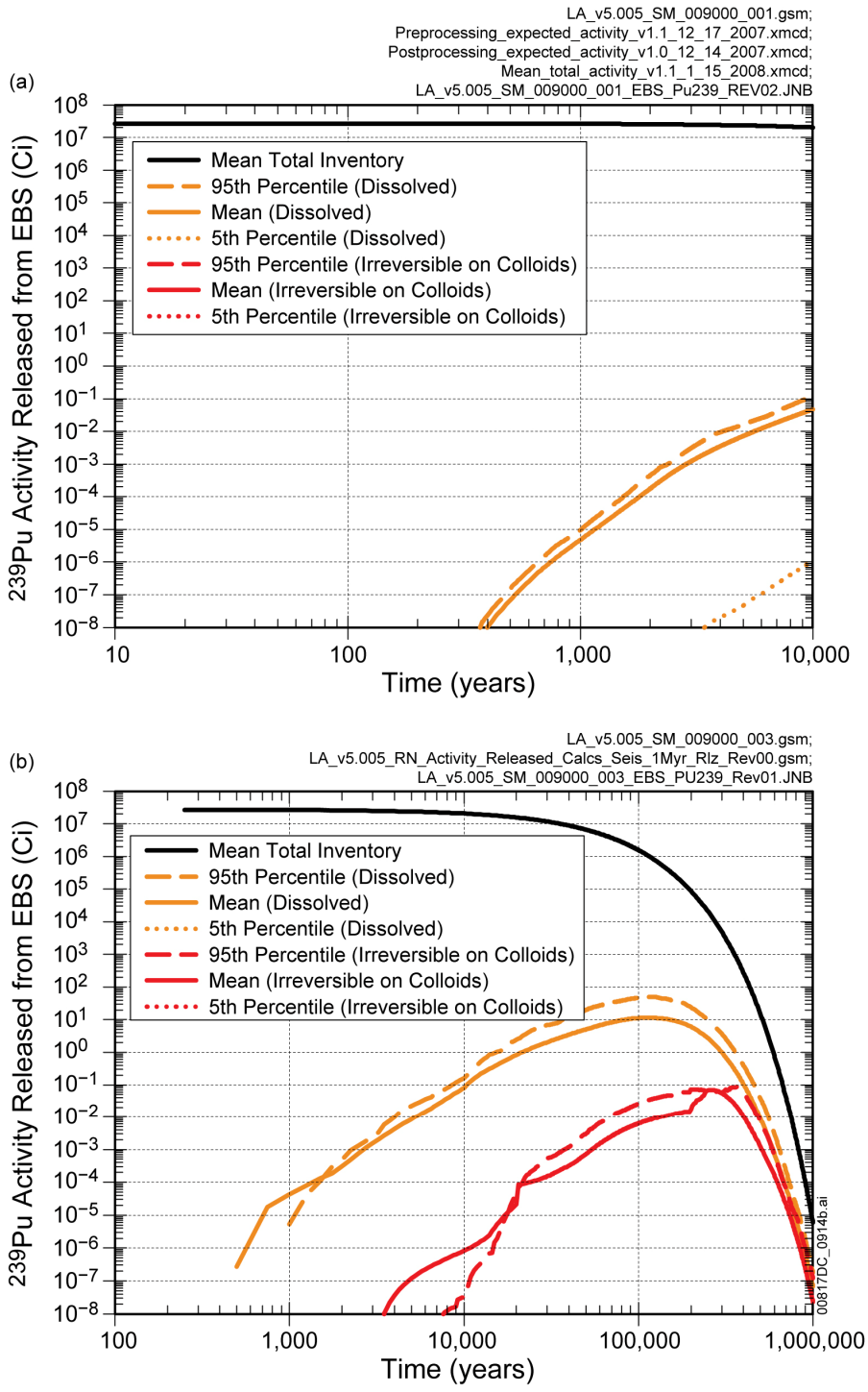

Source: Output DTNs: MO0710ADTSPAWO.000 [DIRS 183752]; and MO0710PLOTSFIG.000 [DIRS 185207].

NOTE: Mean total inventory indicates the repository total ^{239}Pu activity as a function of time and is included for comparison to the activity released.

Figure 8.3-21[a]. Uncertainty in Activity of ^{239}Pu Released from the Engineered Barrier System for the Seismic Ground Motion Modeling Case for (a) 10,000 Years and (b) 1,000,000 Years after Repository Closure

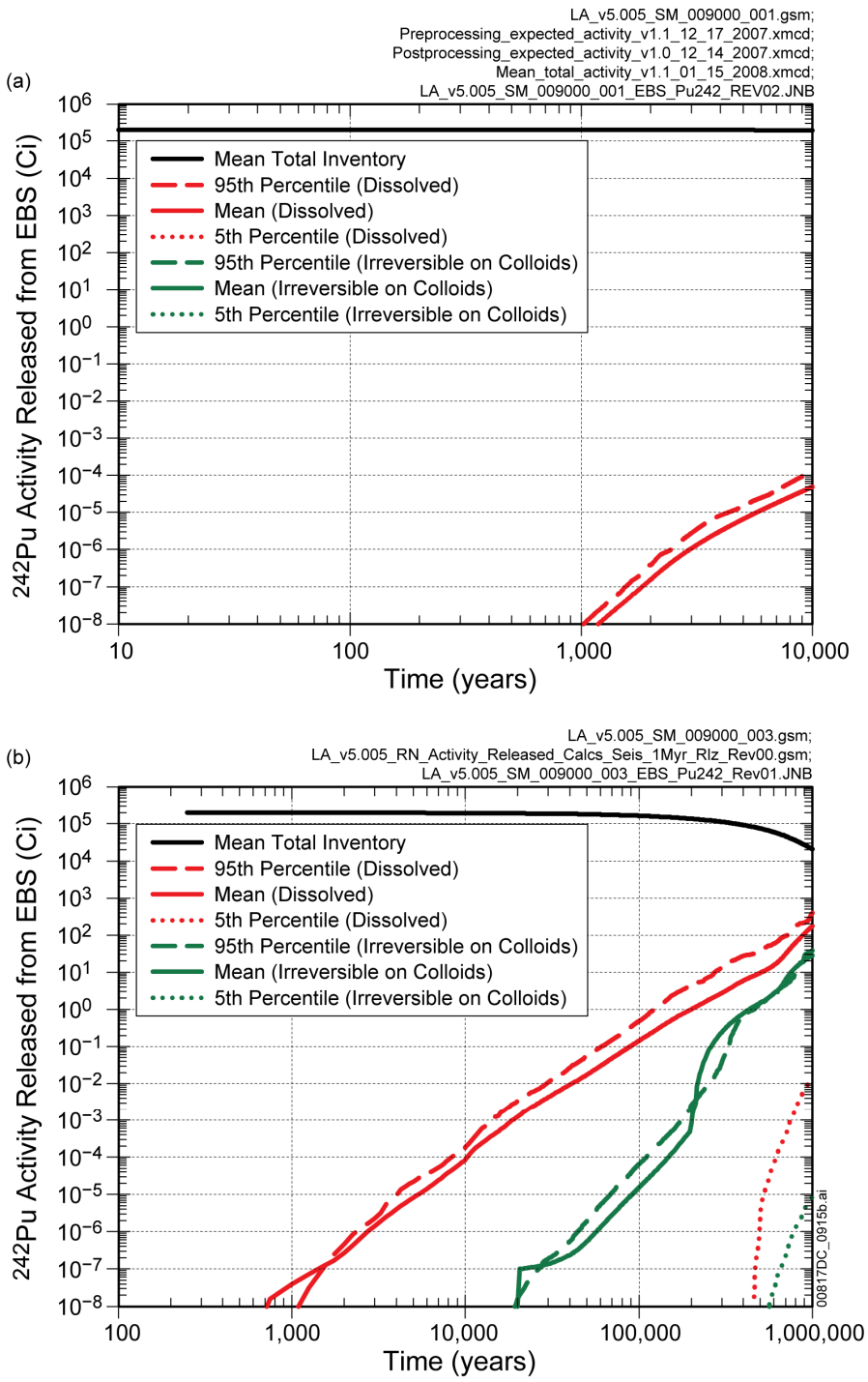

Source: Output DTNs: MO0710ADTSPAWO.000 [DIRS 183752]; and MO0710PLOTSFIG.000 [DIRS 185207].

NOTE: Mean total inventory indicates the repository total ^{242}Pu activity as a function of time and is included for comparison to the activity released.

Figure 8.3-22[a]. Uncertainty in Activity of ^{242}Pu Released from the Engineered Barrier System for the Seismic Ground Motion Modeling Case for (a) 10,000 Years and (b) 1,000,000 Years after Repository Closure

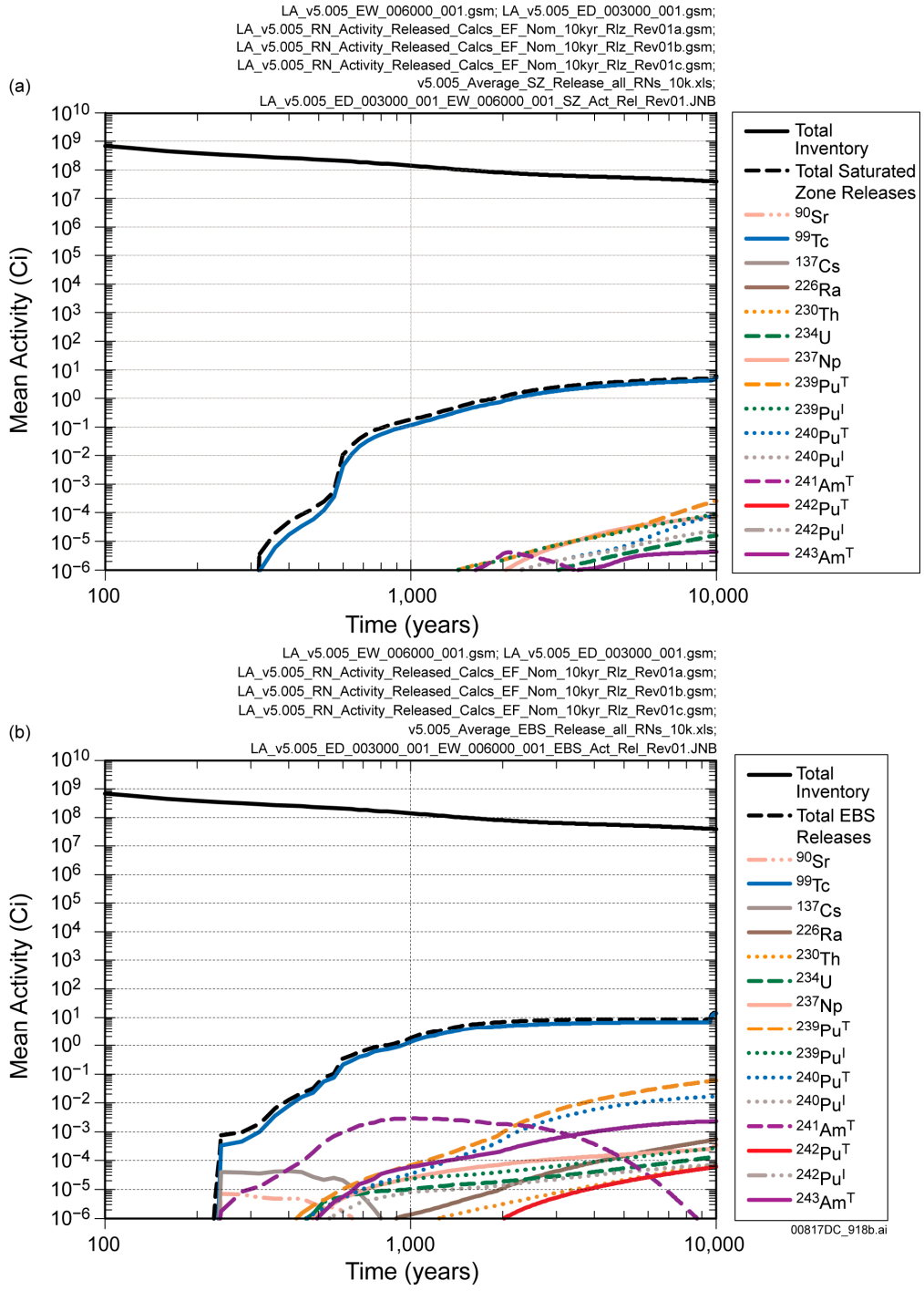

Source: Output DTNs: MO0710ADTSPAWO.000 [DIRS 183752]; and MO0710PLOTSFIG.000 [DIRS 185207].

NOTE: Total inventory indicates the repository total activity as a function of time and is included for comparison to the activity released.

Figure 8.3-23[a]. Mean Activity Released from the (a) Saturated Zone and (b) Engineered Barrier System for the Combined Nominal/Early Failure Modeling Case for 10,000 Years after Repository Closure

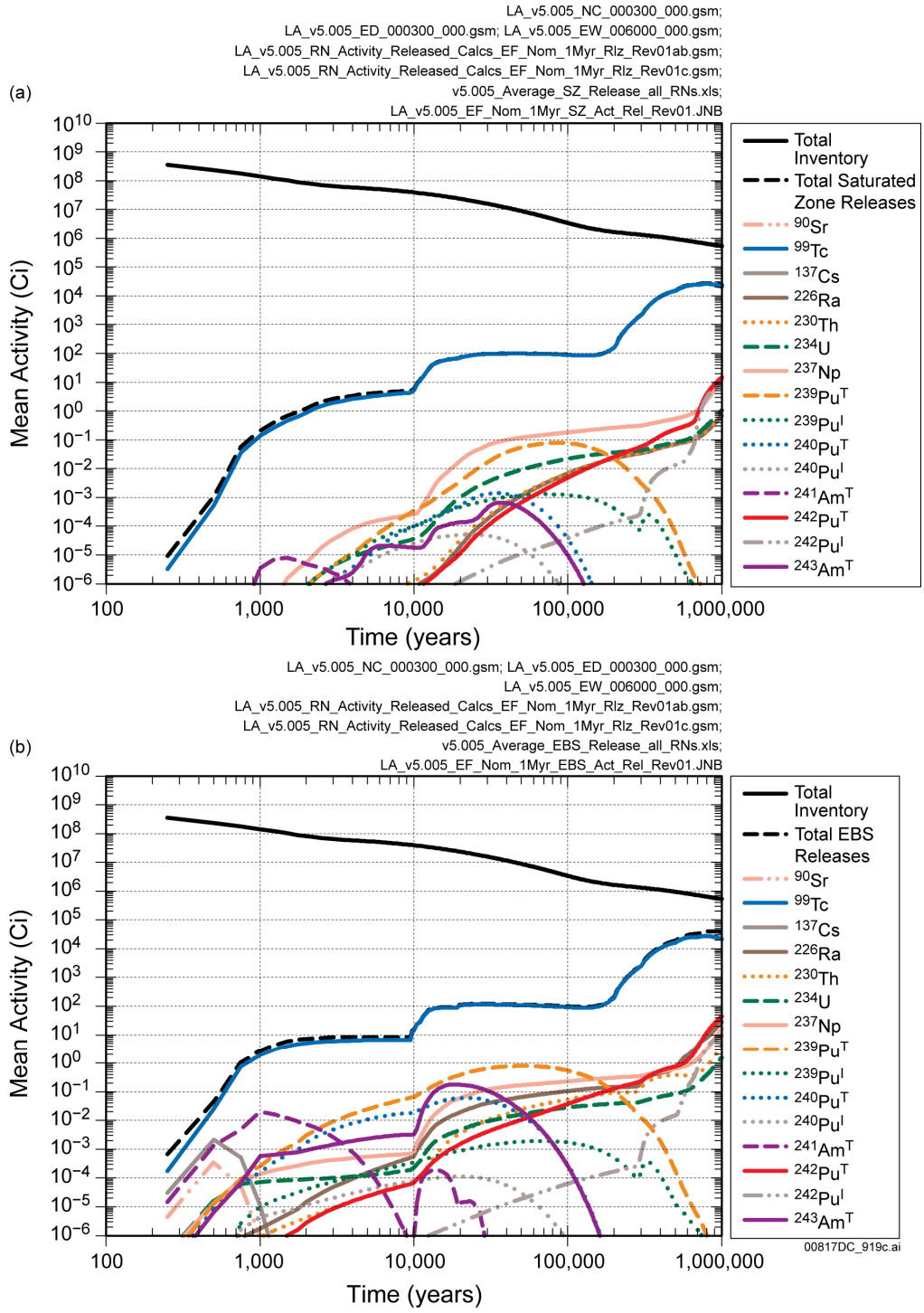

Source: Output DTNs: MO0710ADTSPAWO.000 [DIRS 183752]; and MO0710PLOTSFIG.000 [DIRS 185207].

NOTE: Total inventory indicates the repository total activity as a function of time and is included for comparison to the activity released.

Figure 8.3-24[a]. Mean Activity Released from the (a) Saturated Zone and (b) Engineered Barrier System for the Combined Nominal/Early Failure Modeling Case for 1,000,000 Years after Repository Closure

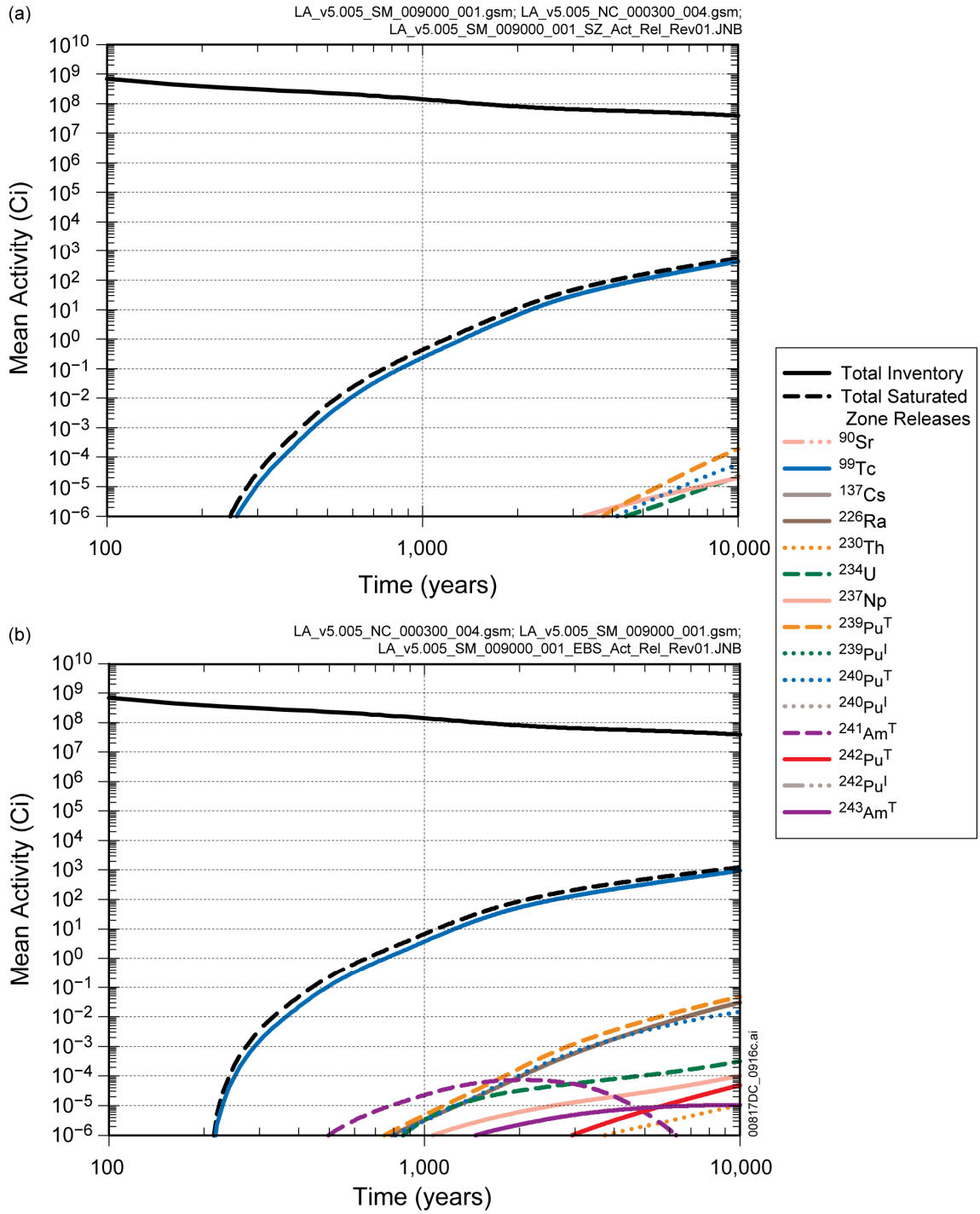

Source: Output DTNs: MO0710ADTSPAWO.000 [DIRS 183752]; and MO0710PLOTSFIG.000 [DIRS 185207].

NOTE: Total inventory indicates the repository total activity as a function of time and is included for comparison to the activity released.

Figure 8.3-25[a]. Mean Activity Released from the (a) Saturated Zone and (b) Engineered Barrier System for the Seismic Ground Motion Modeling Case for 10,000 Years after Repository Closure

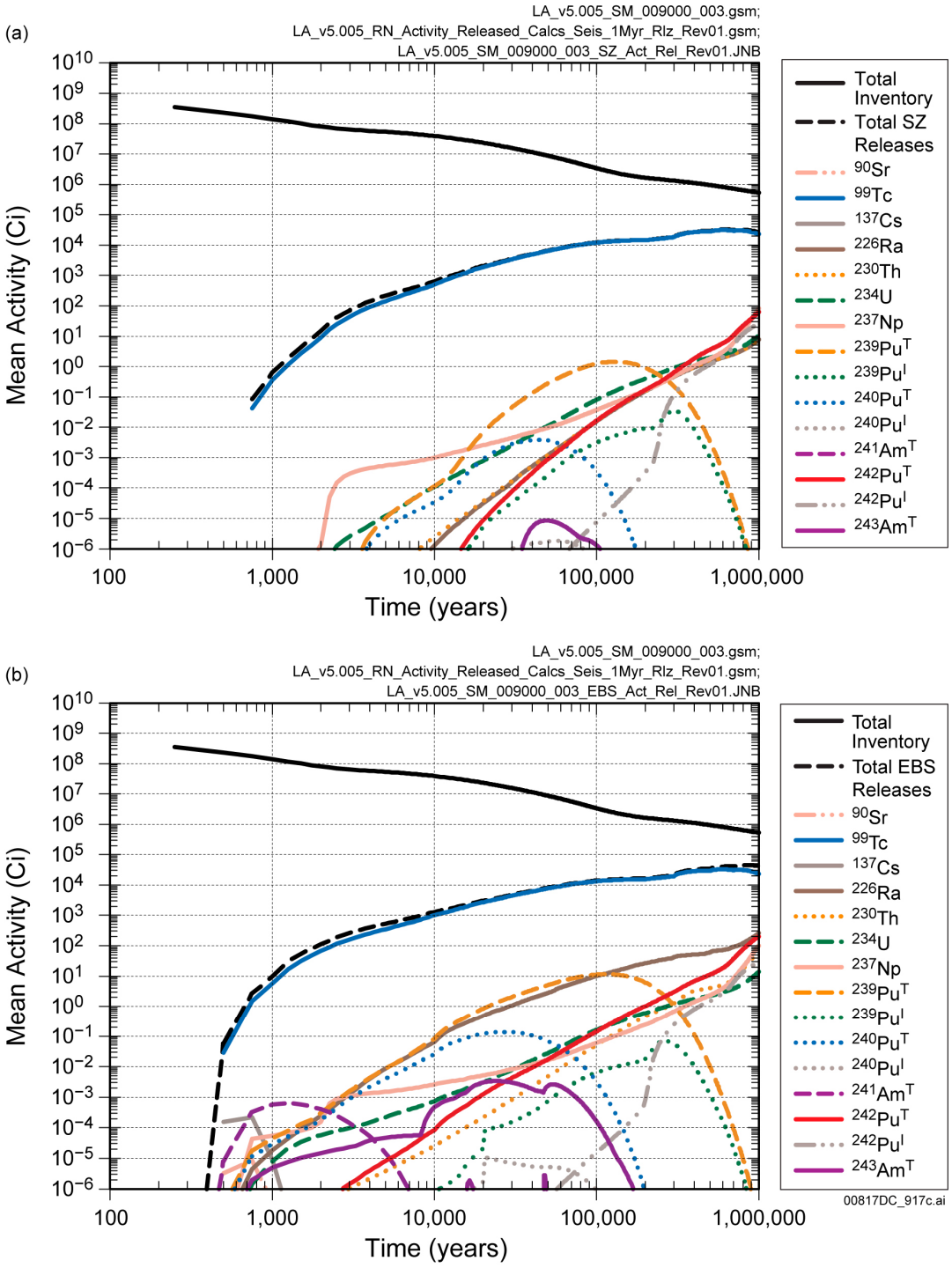

Source: Output DTNs: MO0710ADTSPAWO.000 [DIRS 183752]; and MO0710PLOTSFIG.000 [DIRS 185207].

NOTE: Total inventory indicates the repository total activity as a function of time and is included for comparison to the activity released.

Figure 8.3-26[a]. Mean Activity Released from the (a) Saturated Zone and (b) Engineered Barrier System for the Seismic Ground Motion Modeling Case for 1,000,000 Years after Repository Closure

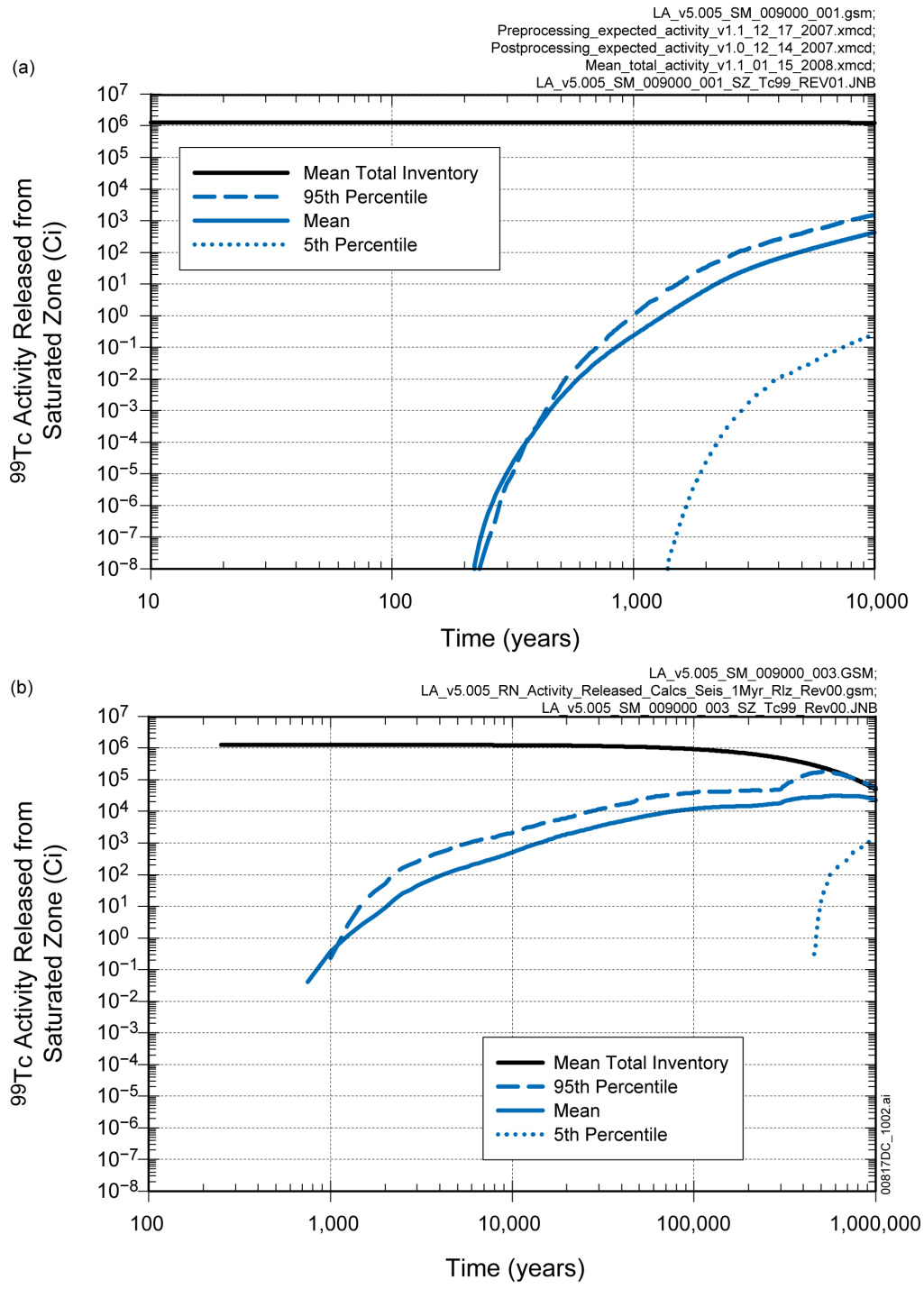

Source: Output DTN: MO0710ADTSPAWO.000 [DIRS 183752].

NOTE: Mean total inventory indicates the repository total ^{99}Tc activity as a function of time and is included for comparison to the activity released.

Figure 8.3-27[a]. Uncertainty in Activity of ^{99}Tc Released from the Saturated Zone for the Seismic Ground Motion Modeling Case for (a) 10,000 Years and (b) 1,000,000 Years after Repository Closure

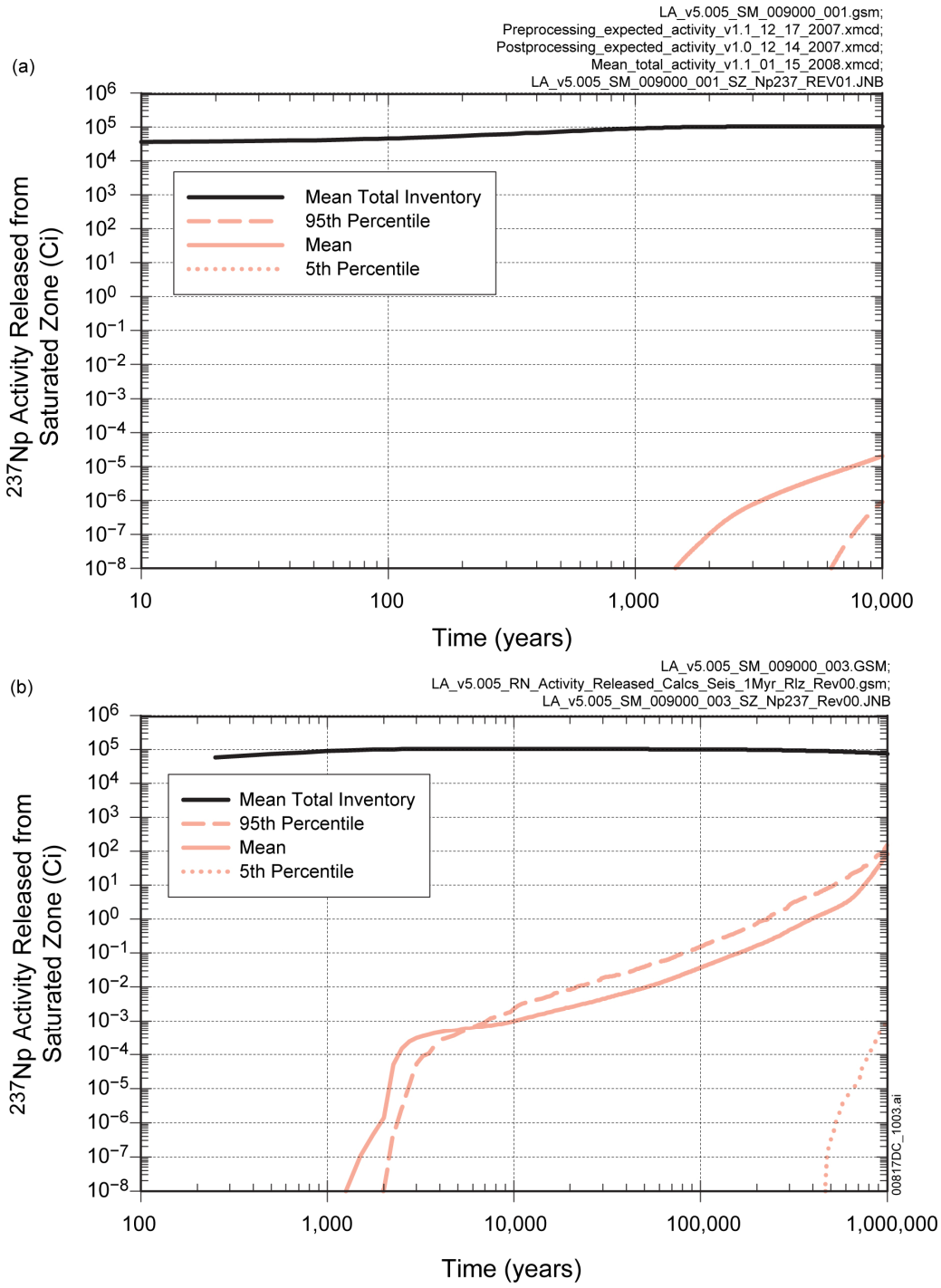

Source: Output DTN: MO0710ADTSPAWO.000 [DIRS 183752].

NOTE: Mean total inventory indicates the repository total ^{237}Np activity as a function of time and is included for comparison to the activity released.

Figure 8.3-28[a]. Uncertainty in Activity of ^{237}Np Released from the Saturated Zone for the Seismic Ground Motion Modeling Case for (a) 10,000 Years and (b) 1,000,000 Years after Repository Closure

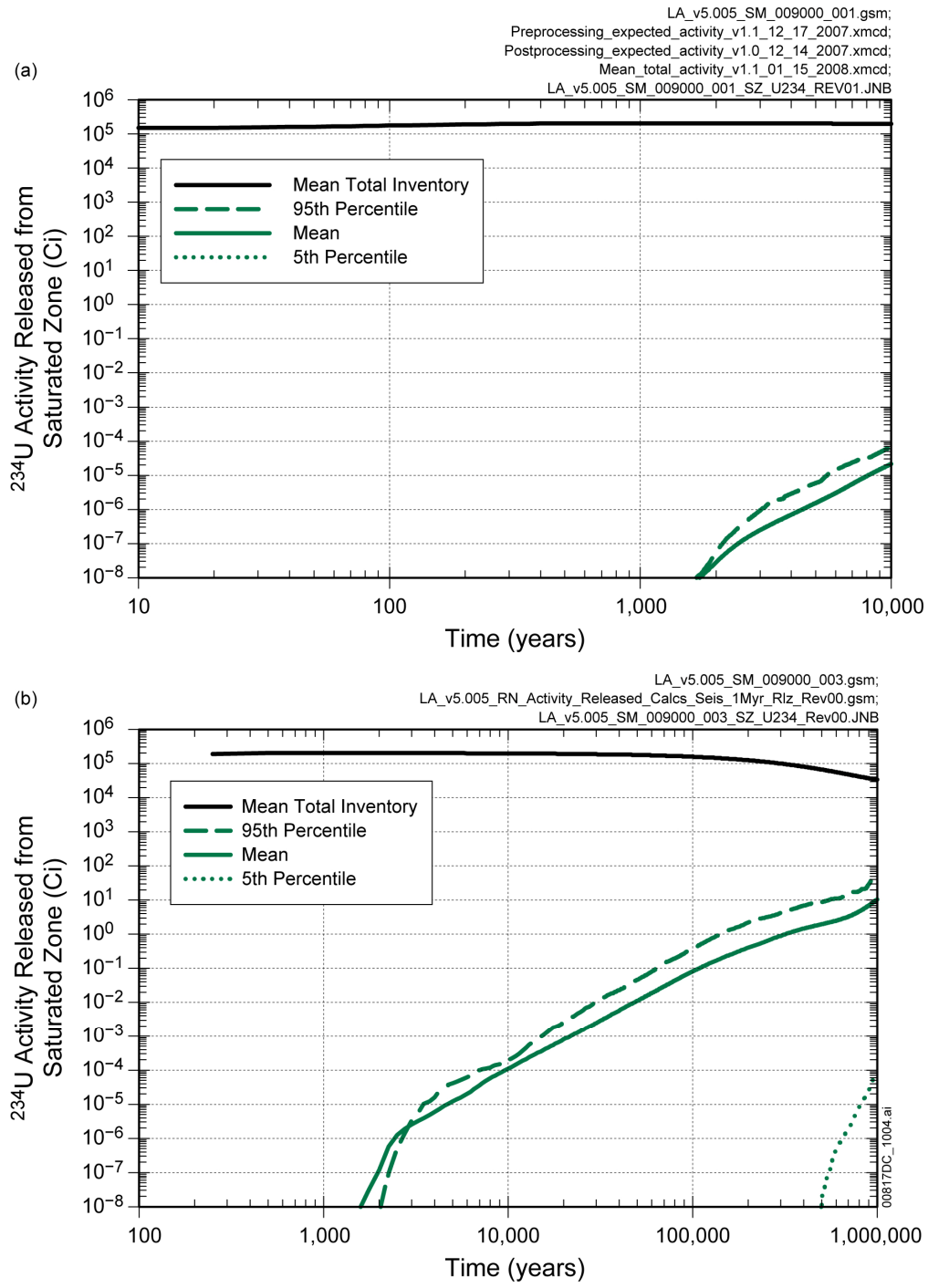

Source: Output DTN: MO0710ADTSPAWO.000 [DIRS 183752].

NOTE: Mean total inventory indicates the repository total ^{234}U activity as a function of time and is included for comparison to the activity released.

Figure 8.3-29[a]. Uncertainty in Activity of ^{234}U Released from the Saturated Zone for the Seismic Ground Motion Modeling Case for (a) 10,000 Years and (b) 1,000,000 Years after Repository Closure

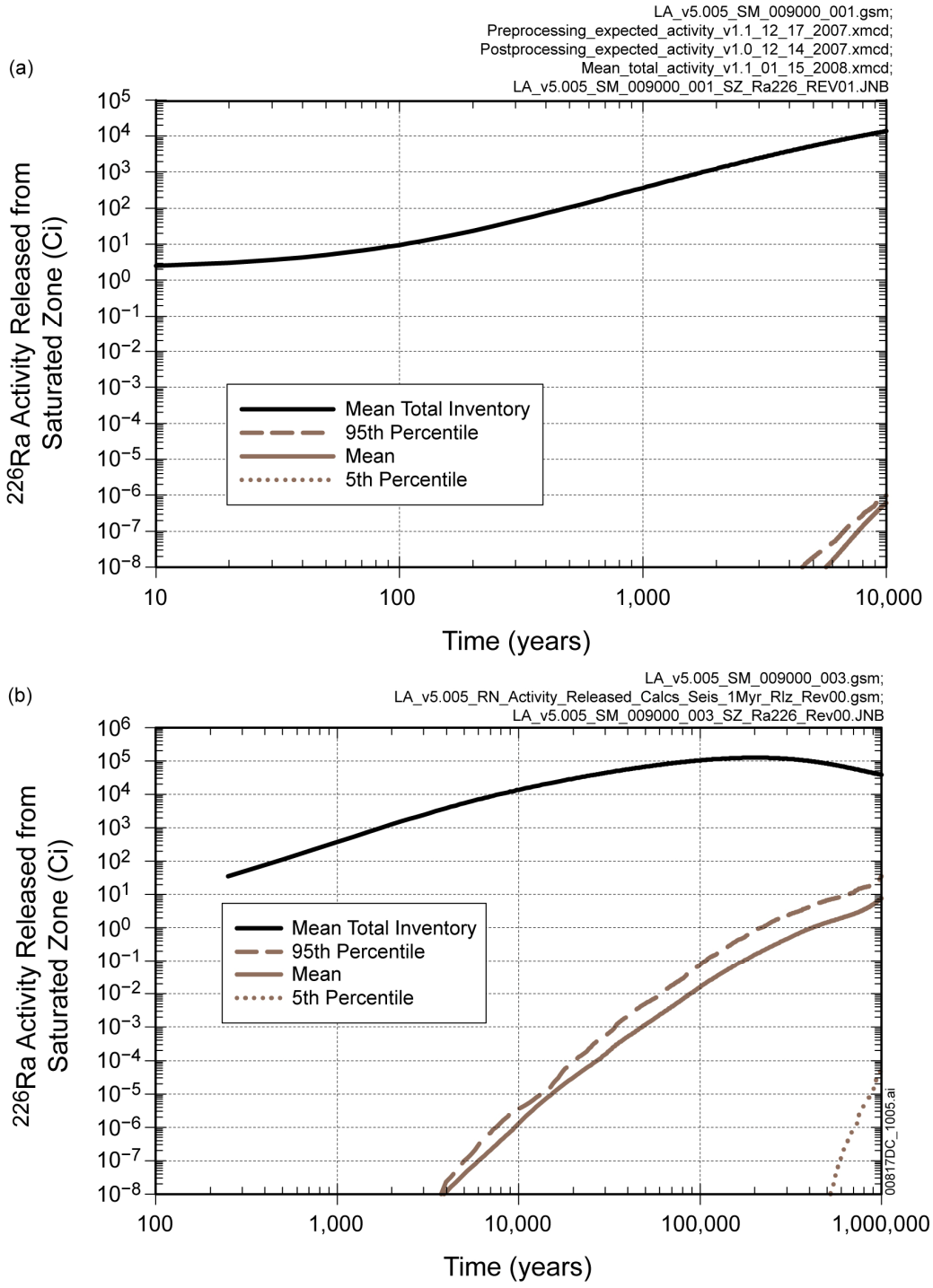

Source: Output DTN: MO0710ADTSPAWO.000 [DIRS 183752].

NOTE: Mean total inventory indicates the repository total ^{226}Ra activity as a function of time and is included for comparison to the activity released.

Figure 8.3-30[a]. Uncertainty in Activity of ^{226}Ra Released from the Saturated Zone for the Seismic Ground Motion Modeling Case for (a) 10,000 Years and (b) 1,000,000 Years after Repository Closure

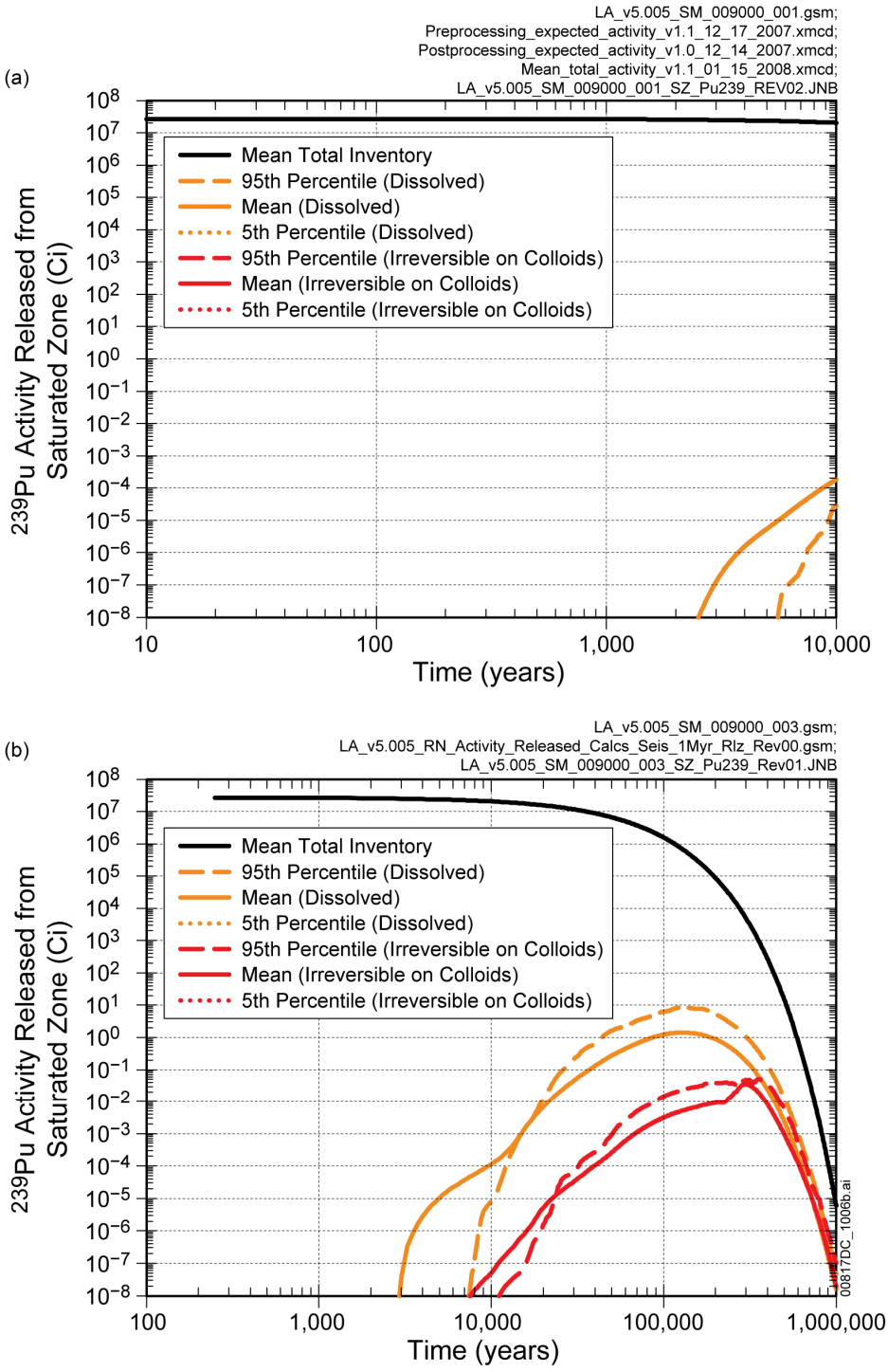

Source: Output DTN: MO0710ADTSPAWO.000 [DIRS 183752].

NOTE: Mean total inventory indicates the repository total ^{239}Pu activity as a function of time and is included for comparison to the activity released.

Figure 8.3-31[a]. Uncertainty in Activity of ^{239}Pu Released from the Saturated Zone for the Seismic Ground Motion Modeling Case for (a) 10,000 Years and (b) 1,000,000 Years after Repository Closure

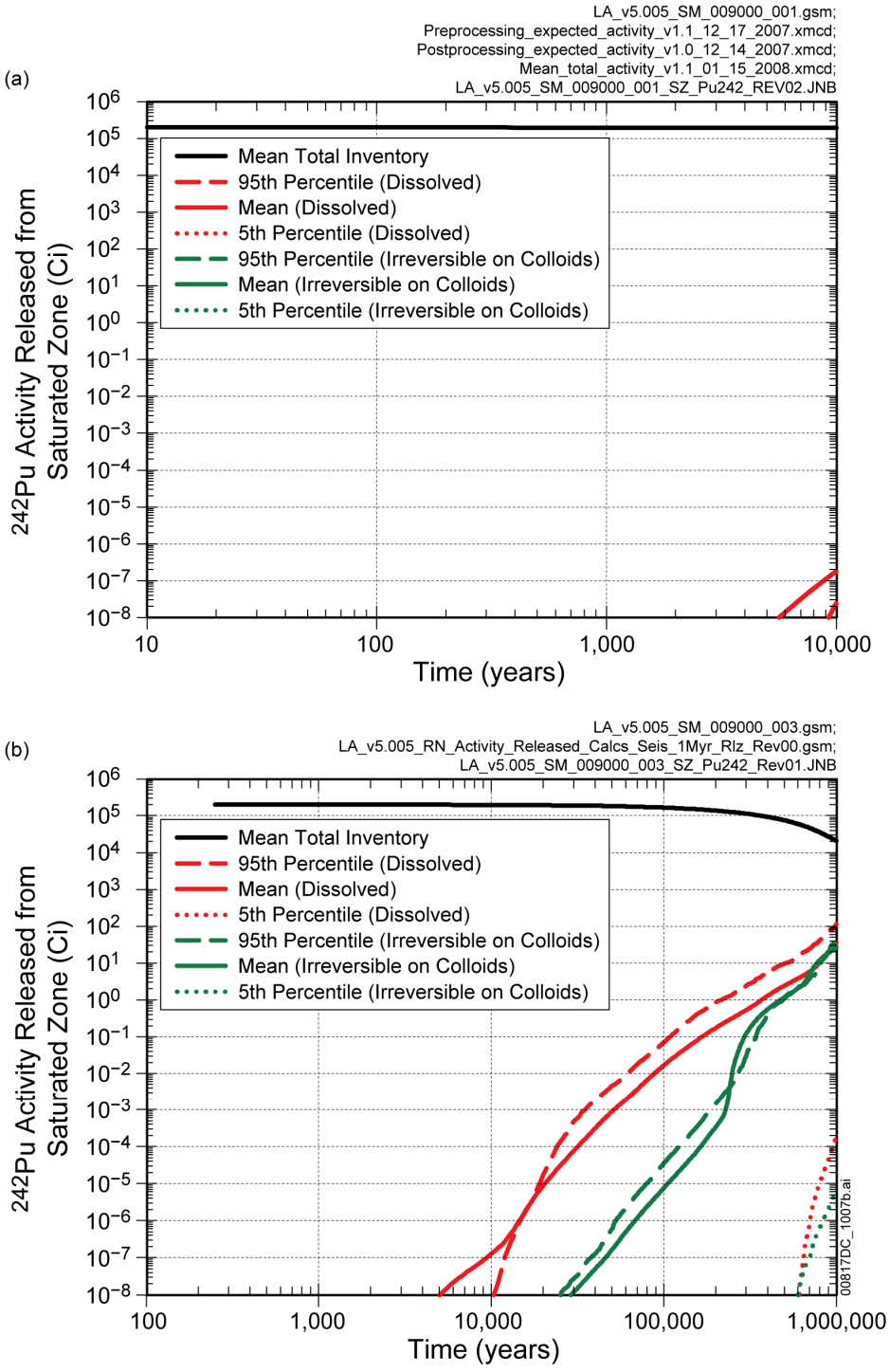

Source: Output DTN: MO0710ADTSPAWO.000 [DIRS 183752].

NOTE: Mean total inventory indicates the repository total ^{242}Pu activity as a function of time and is included for comparison to the activity released.

Figure 8.3-32[a]. Uncertainty in Activity of ^{242}Pu Released from the Saturated Zone for the Seismic Ground Motion Modeling Case for (a) 10,000 Years and (b) 1,000,000 Years after Repository Closure

INTENTIONALLY LEFT BLANK

9[a]. INPUTS AND REFERENCES

9.1[a] DOCUMENTS CITED

182229 Apted, M. and Ross, A. 2005. Program on Technology Innovation: Evaluation of a Spent Fuel Repository at Yucca Mountain, Nevada, 2005 Progress Report. EPRI TR 1010074. Palo Alto, California: Electric Power Research Institute. TIC: 259561.

185068 Breeding, R.J.; Helton, J.C.; Murfin, W.B.; Smith, L.N.; Johnson, J.D.; Jow, H.-N.; and Shiver, A.W. 1992. "The NUREG-1150 Probabilistic Risk Assessment for the Surry Nuclear Power Station." *Nuclear Engineering and Design, 135,* 29-59. [New York, New York]: North-Holland. ACC: 260059.

107727 Breeding, R.J.; Helton, J.C.; Gorham, E.D.; and Harper, F.T. 1992. "Summary Description of the Methods Used in the Probabilistic Risk Assessments for NUREG-1150." *Nuclear Engineering and Design, 135,* 1-27. New York, New York: Elsevier. TIC: 246312.

185069 Brown, T.D.; Breeding, R.J.; Helton, J.C.; Jow, H.N.; Higgins, S.J.; and Shiver, A.W. 1992. "The NUREG-1150 Probabilistic Risk Assessment for the Grand Gulf Nuclear Station." *Nuclear Engineering and Design, 135,* 117-137. [New York, New York]: North-Holland. TIC: 260060.

170038 BSC (Bechtel SAIC Company) 2004. *Analysis of Hydrologic Properties Data.* ANL-NBS-HS-000042 REV 00. Las Vegas, Nevada: Bechtel SAIC Company. ACC: DOC.20041005.0004; DOC.20050815.0003.

169987 BSC 2004. *CSNF Waste Form Degradation: Summary Abstraction.* ANL-EBS-MD-000015 REV 02. Las Vegas, Nevada: Bechtel SAIC Company. ACC: DOC.20040908.0001; DOC.20050620.0004.

169988 BSC 2004. Defense HLW Glass Degradation Model. ANL-EBS-MD-000016 REV 02. Las Vegas, Nevada: Bechtel SAIC Company. ACC: DOC.20041020.0015; DOC.20050922.0002.

170002 BSC 2004. *Future Climate Analysis.* ANL-NBS-GS-000008 REV 01. Las Vegas, Nevada: Bechtel SAIC Company. ACC: DOC.20040908.0005.

170006 BSC 2004. *Saturated Zone Colloid Transport*. ANL-NBS-HS-000031 REV 02. Las Vegas, Nevada: Bechtel SAIC Company. ACC: DOC.20041008.0007; DOC.20051215.0005.

167652 BSC 2004. *Seepage Model for PA Including Drift Collapse.* MDL-NBS-HS-000002 REV 03. Las Vegas, Nevada: Bechtel SAIC Company. ACC: DOC.20040922.0008; DOC.20051205.0001.

169861 BSC 2004. *UZ Flow Models and Submodels.* MDL-NBS-HS-000006 REV 02. Las Vegas, Nevada: Bechtel SAIC Company. ACC: DOC.20041101.0004; DOC.20050629.0003.

169855 BSC (Bechtel SAIC Company) 2004. *Development of Numerical Grids for UZ Flow and Transport Modeling.* ANL-NBS-HS-000015 REV 02. Las Vegas, Nevada: Bechtel SAIC Company. ACC: DOC.20040901.0001.

173433 BSC (Bechtel SAIC Company) 2005. *EBS Radionuclide Transport Abstraction.* ANL-WIS-PA-000001 REV 02. Las Vegas, Nevada: Bechtel SAIC Company. ACC: DOC.20050825.0008.

174116 BSC 2005. *Parameter Sensitivity Analysis for Unsaturated Zone Flow.* ANL-NBS-HS-000049 REV 00. Las Vegas, Nevada: Bechtel SAIC Company. ACC: DOC.20050808.0005; DOC.20060329.0020.

177492 BSC 2006. *Technical Work Plan for: Infiltration Model Assessment, Revision, and Analyses of Downstream Impacts.* TWP-NBS-HS-000012 REV 02. Las Vegas, Nevada: Bechtel SAIC Company. ACC: DOC.20060831.0006.

184391 BSC 2007. *Software Problem Report, GoldSim Version 9.60.100. Software Tracking Number: 10344-9.60-01.* SPR013420071203. Las Vegas, Nevada: Bechtel SAIC Company. ACC: MOL.20080122.0108.

185064 Campbell, J.E.; Dillon, R.T.; Tierney, M.S.; Davis, H.T.; McGrath, P.E.; Pearson, F.J., Jr.; Shaw, H.R.; Helton J.C.; and Donath, F.A. 1978. *Risk Methodology for Geologic Disposal of Radioactive Waste: Interim Report.* NUREG/CR-0458. Washington, D.C.: U.S. Nuclear Regulatory Commission. ACC: HQS.19880517.2632.

185066 Cranwell, R.M.; Campbell, J.E.; Helton, J.C.; Iman, R.L.; Longsine, D.E.; Ortiz, N.R.; Runkle, G.E.; and Shortencarier, M.J. 1987. *Risk Methodology for Geologic Disposal of Radioactive Waste: Final Report.* NUREG/CR-2452. Washington, D.C.: U.S. Nuclear Regulatory Commission. ACC: NNA.19910123.0035.

101234 Cranwell, R.M.; Guzowski, R.V.; Campbell, J.E.; and Ortiz, N.R. 1990. *Risk Methodology for Geologic Disposal of Radioactive Waste, Scenario Selection Procedure.* NUREG/CR-1667. Washington, D.C.: U.S. Nuclear Regulatory Commission. ACC: NNA.19900611.0073.

143665 CRWMS M&O 2000. *Total System Performance Assessment for the Site Recommendation.* TDR-WIS-PA-000001 REV 00. Las Vegas, Nevada: CRWMS M&O. ACC: MOL.20001005.0282.

184463 Davison, A.C. and Kuonen, D. 2002. "An Introduction to the Bootstrap with Applications in R." *Statistical Computing & Statistical Graphics Newsletter, 13,* (1), 6-11. Alexandria, Virginia: American Statistical Association. TIC: 259980.

181107 DOE (U.S. Department of Energy) 2007. *Design Document for: GoldSim v9.60.* Document ID: 10344-DD-9.60-01. Las Vegas, Nevada: U.S. Department of Energy, Office of Repository Development. ACC: MOL.20070416.0338.

182051 DOE 2007. *Quality Assurance Requirements and Description.* DOE/RW-0333P, Rev. 19. Washington, D. C.: U.S. Department of Energy, Office of Civilian Radioactive Waste Management. ACC: DOC.20070717.0006.

181106 DOE 2007. *Requirements Document for: GoldSim v9.60.* Document ID: 10344-RD-9.60-00. Las Vegas, Nevada: U.S. Department of Energy, Office of Repository Development. ACC: MOL.20070416.0330.

181108 DOE 2007. *User Information Document for: GoldSim Version 9.60.* Document ID: 10344-UID-9.60-00. Las Vegas, Nevada: U.S. Department of Energy, Office of Repository Development. ACC: MOL.20070416.0339.

185016 DOE 2008. *Software Validation Report for: GoldSim Version 9.60.300 on Windows 2000*. Document ID: 10344-SVR-9.60-03-WIN2000. Las Vegas, Nevada: U.S. Department of Energy, Office of Repository Development. ACC: MOL.20080125.0059.

185017 DOE 2008. *Software Validation Report for: GoldSim Version 9.60.300 on Windows Server 2003*. Document ID: 10344-SVR-9.60-03-WIN2003. Las Vegas, Nevada: U.S. Department of Energy, Office of Repository Development. ACC: MOL.20080125.0061.

185018 DOE 2008. *Software Validation Report for: GoldSim Version 9.60.300 on Windows XP*. Document ID: 10344-SVR-9.60-03-WINXP. Las Vegas, Nevada: U.S. Department of Energy, Office of Repository Development. ACC: MOL.20080125.0057.

100975 DOE 1996. *Title 40 CFR Part 191 Compliance Certification Application for the Waste Isolation Pilot Plant.* DOE/CAO-1996-2184. Twenty-one volumes. Carlsbad, New Mexico: U.S. Department of Energy, Carlsbad Area Office. TIC: 240511.

155354 Eisenberg, N.A.; Lee, M.P.; Federline, M.V.; Wingefors, S.; Andersson, J.; Norrby, S.; Sagar, B.; and Wittmeyer, G.W. 1999. *Regulatory Perspectives on Model Validation in High-Level Radioactive Waste Management Programs: A Joint NRC/SKI White Paper.* NUREG-1636. Washington, D.C.: U.S. Nuclear Regulatory Commission. TIC: 246310.

171782 Gisch, R.G. 2004. Postclosure Source Term Information for Naval Spent Fuel with Attachment Entitled "NNPP Postclosure Source Term Discussion for Seismic Disruptive Event Scenario". Letter from R.G. Gisch (DOE) to W.J. Arthur, III (DOE/ORD), September 2, 2004, 09130043151, NA:FA:KAKenney U#04-02635, with attachment. ACC: MOL.20040922.0363.

181727 GoldSim Technology Group 2007. *User's Guide, GoldSim Probabilistic Simulation Environment.* Version 9.60. Two volumes. Issaquah, Washington: GoldSim Technology Group. TIC: 259221.

185070 Gregory, J.J.; Breeding, R.J.; Helton, J.C.; Murfin, W.B.; Higgins, S.J.; and Shiver, A.W. 1992. "The NUREG-1150 Probabilistic Risk Assessment for the Sequoyah Nuclear Plant." *Nuclear Engineering and Design, 135,* 95-115. [New York, New York]: North-Holland. TIC: 260061.

170558 Helton, J.C. 2003. "Mathematical and Numerical Approaches in Performance Assessment for Radioactive Waste Disposal: Dealing with Uncertainty." Chapter 12 of *Modelling Radioactivity in the Environment.* Scott, E.M., ed. Radioactivity in the Environment. New York, New York: Elsevier. TIC: 256241.

100452 Helton, J.C. 1993. "Uncertainty and Sensitivity Analysis Techniques for Use in Performance Assessment for Radioactive Waste Disposal." *Reliability Engineering and System Safety, 42,* (2-3), 327-367. Barking, Essex, England: Elsevier. TIC: 237878.

107739 Helton, J.C. 1994. "Treatment of Uncertainty in Performance Assessments for Complex Systems." *Risk Analysis, 14,* (4), 483-511. New York, New York: Plenum Press. TIC: 245848.

107496 Helton, J.C. 1997. "Uncertainty and Sensitivity Analysis in the Presence of Stochastic and Subjective Uncertainty." *Journal of Statistical Computation and Simulation, 57,* (1-4), 3-76. New York, New York: Gordon and Breach Science Publishers. TIC: 245958.

184402 Helton, J.C. and Breeding, R.J. 1993. "Calculation of Reactor Accident Safety Goals." *Reliability Engineering and System Safety, 39,* 129-158. [New York, New York]: Elsevier. TIC: 259936.

163475 Helton, J.C. and Davis, F.J. 2002. Latin Hypercube Sampling and the Propagation of Uncertainty in Analyses of Complex Systems. SAND2001-0417. Albuquerque, New Mexico: Sandia National Laboratories. TIC: 254367.

170518 Helton, J.C. and Davis, F.J. 2003. "Latin Hypercube Sampling and the Propagation of Uncertainty in Analyses of Complex Systems." *Reliability Engineering & System Safety, 81,* ([1]), 23-69. [New York, New York]: Elsevier. TIC: 256239.

171759 Helton, J.C. and Marietta, M.G. 2000. "The 1996 Performance Assessment for the Waste Isolation Pilot Plant." *Reliability Engineering and System Safety, 69,* 1-3. [New York, New York]: Elsevier. TIC: 256585.

185072 Helton, J.C. and Sallaberry, C.J. 2007. *Illustration of Sampling-Based Approaches to the Calculation of Expected Dose in Performance Assessments for the Proposed High Level Radioactive Waste Repository at Yucca Mountain, Nevada.* SAND2007-1353. Albuquerque, New Mexico: Sandia National Laboratories. ACC: LLR.20080221.0240.

183873 Helton, J.C.; Johnson, J.D.; Sallaberry, C.J.; and Storlie, C.B. 2006. "Survey of Sampling-Based Methods for Uncertainty and Sensitivity Analysis." *Reliability Engineering and System Safety, 91,* 1175-1209. [New York, New York]: Elsevier. TIC: 259831.

146012 Iman, R.L. 1982. "Statistical Methods for Including Uncertainties Associated with the Geologic Isolation of Radioactive Waste Which Allow for a Comparison with Licensing Criteria." Proceedings of the Symposium on Uncertainties Associated with the Regulation of the Geologic Disposal of High-Level Radioactive Waste, Gatlinburg, Tennessee, March 9-13, 1981. Kocher, D.C., ed. NUREG/CP-0022. Pages145-157. Washington, D.C.: U.S. Nuclear Regulatory Commission. TIC: 213069.

165064 Iman, R.L. and Conover, W.J. 1982. *Sensitivity Analysis Techniques: Self-Teaching Curriculum.* NUREG/CR-2350. Washington, D.C.: U.S. Nuclear Regulatory Commission. ACC: HQS.19880517.2724.

185067 Iman, R.L. and Helton, J.C. 1985. *A Comparison of Uncertainty and Sensitivity Analysis Techniques for Computer Models.* NUREG/CR-3904. Washington, D.C.: U.S. Nuclear Regulatory Commission. ACC: NNA.19890907.0001.

124198 Iman, R.L.; Conover, W.J.; and Campbell, J.E. 1980. *Risk Methodology for Geologic Disposal of Radioactive Waste: Small Sample Sensitivity Analysis Techniques for Computer Models, with an Application to Risk Assessment.* NUREG/CR-1397. Washington, D.C.: U.S. Nuclear Regulatory Commission. TIC: 211289.

159559 Iman, R.L.; Helton, J.C.; and Campbell, J.E. 1978. *Risk Methodology for Geologic Disposal of Radioactive Waste: Sensitivity Analysis Techniques.* NUREG/CR-0394. Washington, D.C.: U.S. Nuclear Regulatory Commission. TIC: 208076.

100557 Kaplan, S. and Garrick, B.J. 1981. "On the Quantitative Definition of Risk." *Risk Analysis, 1,* (1), 11-27. New York, New York: Plenum Press. TIC: 241205.

107800 Lewis, H.W.; Budnitz, R.J.; Kouts, H.J.C.; Loewenstein, W.B.; Rowe, W.D.; von Hippel, F.; and Zachariasen, F. 1978. *Risk Assessment Review Group Report to the U.S. Nuclear Regulatory Commission.* NUREG/CR-0400. Washington, D.C.: U.S. Regulatory Commission. TIC: 206094.

127905 McKay, M.D.; Beckman, R.J.; and Conover, W.J. 1979. "A Comparison of Three Methods for Selecting Values of Input Variables in the Analysis of Output from a Computer Code." *Technometrics, 21,* (2), 239-245. Alexandria, Virginia: American Statistical Association. TIC: 221741.

182657 McKenzie, J.M. 2007. Postclosure Radionuclide Release Source Term for Representative Naval SNF Waste Package - Igneous Intrusive and Nominal/Early Failure Scenarios. Letter from J.M. McKenzie to E.F. Sproat, III, August 22, 2007, NR:RA:GFHOLDEN U#07-03303, with enclosure. ACC: LLR.20070823.0027.

107798 NRC (U.S. Nuclear Regulatory Commission) 1990. *Severe Accident Risks: An Assessment for Five U.S. Nuclear Power Plants.* NUREG-1150. Washington, D.C.: U.S. Nuclear Regulatory Commission. TIC: 214826.

163274 NRC 2003. *Yucca Mountain Review Plan, Final Report.* NUREG-1804, Rev. 2. Washington, D.C.: U.S. Nuclear Regulatory Commission, Office of Nuclear Material Safety and Safeguards. TIC: 254568.

107799 NRC 1975. *Reactor Safety Study: An Assessment of Accident Risks in U.S. Commercial Nuclear Power Plants.* WASH-1400. Washington, D.C.: U.S. Nuclear Regulatory Commission. TIC: 236923.

107814 Payne, A.C., Jr. 1992. *Analysis of the LaSalle Unit 2 Nuclear Power Plant: Risk Methods Integration and Evaluation Program (RMIEP).* NUREG/CR-4832. Washington, D.C.: U.S. Nuclear Regulatory Commission. TIC: 246147.

185071 Payne, A.C., Jr.; Breeding, R.J.; Helton, J.C.; Smith, L.N.; Johnson, J.D.; Jow, H.-N.; and Shiver, A.W. 1992. "The NUREG-1150 Probabilistic Risk Assessment for the Peach Bottom Atomic Power Station." *Nuclear Engineering and Design, 135,* 61-94. [New York, New York]: North-Holland. TIC: 260062.

107812 PLG (Pickard, Lowe, and Garrick) 1982. *Indian Point Probabilistic Safety Study.* Irvine, California: Pickard, Lowe, and Garrick. TIC: 247144.

185063 PLG 1983. *Seabrook Station Probabilistic Safety Assessment.* Irvine, California: Pickard, Lowe and Garrick. TIC: 255977.

145383 Rechard, R.P. 1999. "Historical Relationship Between Performance Assessment for Radioactive Waste Disposal and Other Types of Risk Assessment." *Risk Analysis, 19,* (5), 763-807. New York, New York: Kluwer Academic / Plenum Publishers. TIC: 246972.

185124 Senger, R. 2008. "Re: Appendix M, TSPA-LA Addendum [Corroborative Data]." E-mail from R. Senger to K. Brooks, February 27, 2008. ACC: LLR.20080227.0161.

177081 SNL (Sandia National Laboratories) 2006. *Data Analysis for Infiltration Modeling: Extracted Weather Station Data Used to Represent Present-Day and Potential Future Climate Conditions in the Vicinity of Yucca Mountain.* ANL-MGR-MD-000015 REV 00. Las Vegas, Nevada: Sandia National Laboratories. ACC: DOC.20070109.0002.

181244 SNL 2007. *Abstraction of Drift Seepage.* MDL-NBS-HS-000019 REV 01 ADD 01. Las Vegas, Nevada: Sandia National Laboratories. ACC: DOC.20070807.0001.

177399 SNL 2007. *Biosphere Model Report.* MDL-MGR-MD-000001 REV 02. Las Vegas, Nevada: Sandia National Laboratories. ACC: DOC.20070830.0007.

179545 SNL 2007. *Calibrated Unsaturated Zone Properties.* ANL-NBS-HS-000058 REV 00. Las Vegas, Nevada: Sandia National Laboratories. ACC: DOC.20070530.0013.

177418 SNL 2007. *Dissolved Concentration Limits of Elements with Radioactive Isotopes.* ANL-WIS-MD-000010 REV 06. Las Vegas, Nevada: Sandia National Laboratory. ACC: DOC.20070918.0010.

177407 SNL 2007. *EBS Radionuclide Transport Abstraction.* ANL-WIS-PA-000001 REV 03. Las Vegas, Nevada: Sandia National Laboratories. ACC: DOC.20071004.0001.

180778 SNL 2007. *General Corrosion and Localized Corrosion of the Drip Shield.* ANL-EBS-MD-000004 REV 02 ADD 01. Las Vegas, Nevada: Sandia National Laboratories. ACC: DOC.20060427.0002; DOC.20070807.0004; DOC.20071003.0019.

178519 SNL 2007. *General Corrosion and Localized Corrosion of Waste Package Outer Barrier.* ANL-EBS-MD-000003 REV 03. Las Vegas, Nevada: Sandia National Laboratories. ACC: DOC.20070730.0003; DOC.20070807.0007.

180506 SNL 2007. *In-Package Chemistry Abstraction*. ANL-EBS-MD-000037 REV 04 ADD 01. Las Vegas, Nevada: Sandia National Laboratories. ACC: DOC.20070816.0004.

180472 SNL 2007. *Initial Radionuclide Inventories.* ANL-WIS-MD-000020 REV 01 ADD 01. Las Vegas, Nevada: Sandia National Laboratories. ACC: DOC.20050927.0005; DOC.20070801.0001.

181383 SNL 2007. *Multiscale Thermohydrologic Model.* ANL-EBS-MD-000049 REV 03 ADD 01. Las Vegas, Nevada: Sandia National Laboratories. ACC: DOC.20070831.0003.

177424 SNL 2007. *Radionuclide Screening.* ANL-WIS-MD-000006 REV 02. Las Vegas, Nevada: Sandia National Laboratories. ACC: DOC.20070326.0003.

177396 SNL 2007. *Radionuclide Transport Models Under Ambient Conditions.* MDL-NBS-HS-000008 REV 02 ADD 01. Las Vegas, Nevada: Sandia National Laboratories. ACC: DOC.20050823.0003; DOC.20070718.0003.

177391 SNL 2007. *Saturated Zone Site-Scale Flow Model.* MDL-NBS-HS-000011 REV 03. Las Vegas, Nevada: Sandia National Laboratories. ACC: DOC.20070626.0004; DOC.20071001.0013.

176828 SNL 2007. *Seismic Consequence Abstraction.* MDL-WIS-PA-000003 REV 03. Las Vegas, Nevada: Sandia National Laboratories. ACC: DOC.20070928.0011.

181953 SNL 2007. *Stress Corrosion Cracking of Waste Package Outer Barrier and Drip Shield Materials.* ANL-EBS-MD-000005 REV 04. Las Vegas, Nevada: Sandia National Laboratories. ACC: DOC.20070913.0001.

179394 SNL 2007. *Total System Performance Assessment Data Input Package for Requirements Analysis for Transportation Aging and Disposal Canister and Related Waste Package Physical Attributes Basis for Performance Assessment.* TDR-TDIP-ES-000006 REV 00. Las Vegas, Nevada: Sandia National Laboratories. ACC: DOC.20070918.0005.

179354 SNL (Sandia National Laboratories) 2007. *Total System Performance Assessment Data Input Package for Requirements Analysis for Engineered Barrier System In-Drift Configuration.* TDR-TDIP-ES-000010 REV 00. Las Vegas, Nevada: Sandia National Laboratories. ACC: DOC.20070921.0008.

184614 SNL 2007. *UZ Flow Models and Submodels*. MDL-NBS-HS-000006 REV 03 AD 01. Las Vegas, Nevada: Sandia National Laboratories. ACC: DOC.20080108.0003; DOC.20080114.0001.

184748 SNL 2008. *Particle Tracking Model and Abstraction of Transport Processes.* MDL-NBS-HS-000020 REV 02 AD 02. Las Vegas, Nevada: Sandia National Laboratories. ACC: DOC.20080129.0008.

183750 SNL 2008. *Saturated Zone Flow and Transport Model Abstraction.* MDL-NBS-HS-000021 REV 03 AD 02. Las Vegas, Nevada: Sandia National Laboratories. ACC: DOC.20080107.0006.

182145 SNL 2007. *Simulation of Net Infiltration for Present-Day and Potential Future Climates.* MDL-NBS-HS-000023 REV 01 AD 01. Las Vegas, Nevada: Sandia National Laboratories.

184806 SNL 2008. *Site-Scale Saturated Zone Transport.* MDL-NBS-HS-000010 REV 03 AD 01. Las Vegas, Nevada: Sandia National Laboratories. ACC: DOC.20080121.0003.

184920 SNL 2008. *Technical Work Plan for: Total System Performance Assessment FY 07-08 Activities.* TWP-MGR-PA-000045 REV 01 ICN 02. Las Vegas, Nevada: Sandia National Laboratories. ACC: DOC.20080131.0048.

157307 Williams, N.H. 2001. "Contract No. DE-AC08-01RW12101 – Total System Performance Assessment – Analyses for Disposal of Commercial and DOE Waste Inventories at Yucca Mountain – Input to Final Environmental Impact Statement and Site Suitability Evaluation REV 00 ICN 02." Letter from N.H. Williams (BSC) to J.R. Summerson (DOE/YMSCO), December 11, 2001, RWA:cs-1204010670, with enclosure. ACC: MOL.20011213.0056.

9.2[a] CODES, STANDARDS, REGULATIONS, AND PROCEDURES

175755 40 CFR 197. 2005. Protection of Environment: Public Health and Environmental Radiation Protection Standards for Yucca Mountain, Nevada. ACC: MOL.20051121.0084.

156671 66 FR 55732. Disposal of High-Level Radioactive Wastes in a Proposed Geologic Repository at Yucca Mountain, NV, Final Rule. 10 CFR Parts 2, 19, 20, 21, 30, 40, 51, 60, 61, 63, 70, 72, 73, and 75. ACC: MOL.20050324.0102; MOL.20050418.0124.

177357 70 FR 49014. Public Health and Environmental Radiation Protection Standards for Yucca Mountain, NV. Internet Accessible.

178394 70 FR 53313. Implementation of a Dose Standard After 10,000 Years. Internet Accessible.

180319 CFR 63. 2007. Energy: Disposal of High-Level Radioactive Wastes in a Geologic Repository at Yucca Mountain, Nevada. Internet Accessible.

175544 EPA (U.S. Environmental Protection Agency) 2002. Federal Guidance Report 13, CD Supplement, Cancer Risk Coefficients for Environmental Exposure to Radionuclides, EPA. EPA-402-C-99-001, Rev. 1. [Washington, D.C.]: U.S. Environmental Protection Agency. ACC: MOL.20051013.0016.

100016 Nuclear Waste Policy Amendments Act of 1987. Public Law No. 100-203, 101 Stat. 1330. TIC: 223717.

9.3[a] SOFTWARE CODES

181034 ASHPLUME_DLL_LA V. 2.0. 2003. WINDOWS 2000. STN: 11117-2.0-00.

181035 ASHPLUME_DLL_LA V. 2.1. 2006. WinDOWS 2000/XP. STN: 11117-2.1-00.

180147 ASHPLUME_DLL_LA V. 2.1. 2007. WINDOWS 2003. STN: 11117-2.1-01.

162809 CWD V. 2.0. 2003. WINDOWS 2000. STN: 10363-2.0-00.

181037 CWD V. 2.0. 2007. WINDOWS 2003. STN: 10363-2.0-01.

182102 EXDOC_LA V. 2.0. 2007. WINDOWS XP, WINDOWS 2000 & WINDOWS 2003. STN: 11193-2.0-00.

180002 FAR V. 1.1. 2007. WINDOWS 2000 & 2003. STN: 11190-1.1-00.

182225 FAR V. 1.2. 2007. WINDOWS 2000 & WINDOWS 2003. STN: 11190-1.2-00.

173139 FEHM V. 2.23. 2005. WINDOWS 2000. STN: 10086-2.23-00.

179419 FEHM V. 2.24-01. 2007. WIN2003, 2000, & XP, Red Hat Linux 2.4.21, OS 5.9. STN: 10086-2.24-01-00.

181040 GetThk_LA V. 1.0. 2006. WINDOWS 2000 & WINDOWS 2003. STN: 11229-1.0-00.

180224 GoldSim V. 9.60. 2007. WINDOWS 2000, WINDOWS XP, WINDOWS 2003. STN: 10344-9.60-00.

181903 Goldsim V. 9.60.100. 2007. WIN 2000, 2003, XP. STN: 10344-9.60-01.

184387 Goldsim V. 9.60.300. 2007. WIN 2000, 2003, XP. STN: 10344-9.60-03.

167885 InterpZdll_LA V. 1.0. 2004. WINDOWS 2000. STN: 11107-1.0-00.

181043 InterpZdll_LA V. 1.0. 2007. WINDOWS 2003. STN: 11107-1.0-01.

167884 MFCP_LA V. 1.0. 2003. WINDOWS 2000. STN: 11071-1.0-00.

181045 MFCP_LA V. 1.0. 2006. WINDOWS 2003. STN: 11071-1.0-01.

174528 MkTable V. 1.00. 2003. WINDOWS 2000. STN: 10505-1.00-00.

181047 Mkable_LA V. 1.0. 2006. WINDOWS 2000. STN: 11217-1.0-00.

181048 MkTable_LA V. 1.0. 2007. WINDOWS 2003. STN: 11217-1.0-01.

181049 MView V. 4.0. 2007. WINDOWS XP. STN: 10072-4.0-01.

169130 PassTable1D_LA V. 1.0. 2004. WINDOWS 2000. STN: 11142-1.0-00.

181050 PassTable1D_LA V. 1.0. 2006. WINDOWS 2003. STN: 11142-1.0-01.

181051 PassTable1D_LA V. 2.0. 2007. WINDOWS 2000 & WINDOWS 2003. STN: 11142-2.0-00.

168980 PassTable3D_LA V. 1.0. 2004. WINDOWS 2000. STN: 11143-1.0-00.

181052 PassTable3D_LA V. 1.0. 2007. WINDOWS 2003. STN: 11143-1.0-01.

182556 PassTable3D_LA V. 2.0. 2007. WINDOWS 2000 & WINDOWS 2003. STN: 11143-2.0-00.

181157 SCCD V. 2.01. 2003. WINDOWS 2000. STN: 10343-2.01-00.

181054 SCCD V. 2.01. 2007. WINDOWS 2003. STN: 10343-2.01-01.

173435 SEEPAGEDLL_LA V. 1.2. 2005. WINDOWS 2000. STN: 11076-1.2-00.

180318 SEEPAGEDLL_LA V. 1.3. 2006. WINDOWS 2000. STN: 11076-1.3-00.

181053 PREWAP_LA V. 1.1. 2006. WINDOWS 2000. STN: 10939-1.1-00.

181058 SEEPAGEDLL_LA V. 1.3. 2007. WINDOWS 2003. STN: 11076-1.3-01.

164180 Software Code: SZ_Convolute V. 3.0. 2003. PC, Windows 2000. 10207-3.0-00.

161256 Software Code: TOUGHREACT V. 3.0. 2002. DEC ALPHA/OSF1 V5.1, DEC ALPHA/OSF1 V5.0, Sun UltraSparc/Sun OS 5.5.1, PC/Linux Redhat 7.2. STN: 10396-3.0-00.

167883 Soilexp_LA V. 1.0. 2004. WINDOWS 2000. STN: 10933-1.0-00.

181060 SZ_CONVOLUTE V. 3.10.01. 2007. WINDOWS 2000 & WINDOWS 2003. STN: 10207-3.10.01-00.

146654 T2R3D V. 1.4. 1999. UNIX, WINDOWS 95/98NT 4.0. STN: 10006-1.4-00.

161491 TOUGH2 V. 1.6. 2003. DOS Emulation (win95/98), SUN OS 5.5.1., OSF1 V4.0. STN: 10007-1.6-01.

181061 TSPA_Input_DB V. 2.2. 2006. WINDOWS 2000. STN: 10931-2.2-00.

181062 TSPA_Input_DB V. 2.2. 2006. WINDOWS 2003. STN: 10931-2.2-01.

181774 WAPDEG V. 4.07. 2003. Windows 2000. STN: 10000-4.07-00.

181064 WAPDEG V. 4.07. 2007. WINDOWS SERVER 2003. STN: 10000-4.07-01.

9.4[a] SOURCE DATA LISTED BY DATA TRACKING NUMBER

171584 LA0408AM831341.001. Unsaturated Zone Distribution Coefficients (Kds) for U, Np, Pu, Am, Pa, Cs, Sr, Ra, and Th. Submittal date: 08/24/2004.

180497 LA0701PANS02BR.003. UZ Transport Parameters. Submittal date: 04/23/2007.

180322 LA0702PANS02BR.001. Repository and Water Table Bins. Submittal date: 04/16/2007.

179299 LB0701PAKDSESN.001. Unsaturated Zone Sorption Coefficients for Selenium and Tin. Submittal date: 01/31/2007.

181635 LB0702PASEEP02.001. Seepage Abstraction for Degraded Drifts. Submittal date: 06/29/2007.

180776 LB0702PAUZMTDF.001. Unsaturated Zone Matrix Diffusion Coefficients. Submittal date: 05/10/2007.

180439 MO0701PACSNFCP.000. CSNF Colloid Parameters. Submittal date: 04/17/2007.

180440 MO0701PAIRONCO.000. Colloidal Iron Corrosion Products Parameters. Submittal date: 04/17/2007.

181219 MO0702PAFLUORI.000. Fluoride Uncertainty Associated with Dissolved Concentration Limits. Submittal date: 06/01/2007.

179328 MO0702PAGWPROS.001. Groundwater Protection Standards Conversion Factors. Submittal date: 02/06/2007.

179925 MO0702PASTREAM.001. Waste Stream Composition and Thermal Decay Histories for LA. Submittal date: 02/15/2007.

183148 MO0703PASDSTAT.001. Statistical Analyses for Seismic Damage Abstractions. Submittal date: 09/21/2007.

183156 MO0703PASEISDA.002. Seismic Damage Abstractions for TSPA Compliance Case. Submittal date: 09/21/2007.

184647 MO0704PAFEHMBR.001. FEHM Model and Input. Submittal date: 01/10/2008.

185200 MO0706SPAFEPLA.001. FY 2007 LA FEP List and Screening. Submittal date: 03/05/2008.

184664 MO0712PBANLNWP.000. Probabilistic Analysis of Navy Waste Packages. Submittal date: 12/13/2007.

168761 SN0310T0505503.004. Initial Radionuclide Inventories for TSPA-LA. Submittal date: 10/27/2003.

180523 SN0701PAEBSPCE.001. PCE TDIP Potential Seepage Water Chemistry Lookup Tables. Submittal date: 04/25/2007.

182961 SN0701PAWPHIT1.001. Number of Waste Packages Hit by Igneous Events. Submittal date: 09/13/2007.

179504 SN0702PASZFTMA.001. Saturated Zone Flow and Transport Model Abstraction. Submittal date: 02/06/2007

183471 SN0702PASZFTMA.002. Saturated Zone 1-D Transport Model. Submittal date: 10/15/2007.

183217 SN0703PAEBSRTA.001. Inputs Used in the Engineered Barrier System (EBS) Radionuclide Transport Abstraction. Submittal date: 09/28/2007.

182122 SN0704PADSGCMT.001. Drip Shield General Corrosion Models Based on 2.5-Year Titanium Grade 7 Corrosion Rates. Submittal date: 07/24/2007.

183485 SN0710PASZFTMA.003. Updated Saturated Zone 1-D Transport Model. Submittal date: 10/10/2007.

INTENTIONALLY LEFT BLANK